People's Democratic Republic of Algeria
Ministry of Higher Education and Scientific Research

University of Batna 2 – Mostefa Ben Boulaïd
Faculty of Technology
Department of Electronics

Dissertation

Prepared in LEA Laboratory

Presented in fulfillment of the requirement of the degree of
Doctor of Science in Electronics
Option: Microelectronics

Entitled:

Contribution to the modeling and optimization of new optoelectronic devices

---

Presented by:

FERHATI Hichem

Committee members:

Dr. Abdelhamid BENHAYA	Prof.	University of Batna 2	Chairman
Dr. Fayçal DJEFFAL	Prof.	University of Batna 2	Advisor
Dr. Ramdane MAHAMDI	Prof.	University of Batna 2	Examiner
Dr. Idris BOUCHAMA	Prof.	University of M'Sila	Examiner
Dr. Djamil RECHEM	Prof.	University of Oum El Bouaghi	Examiner
Dr. Fouad KERROUR	Prof.	University of Constantine 1	Examiner
Dr. Zohir DIBI	Prof.	University of Batna 2	Invited

April 2019

DEDICATION

This dissertation is dedicated to my lovely parents, my friends

and my brothers

Acknowledgments

First of all, I am deeply grateful to **The Almighty Allah (SWT)**, the Most High, the Most Compassionate, and the Most Merciful for all his giving and for the opportunity He gave me to study, to research and to write and finalizing this Ph.D. project. I Thank **Allah,** my outmost thanks, for providing me this opportunity and granting me the capability to proceed successfully. I must acknowledge my advisor **Professor Fayçal DJEFFAL**, the person to whom I wish to convey my solidest gratitude and profound respect and to whom I am indebted to for this whole thesis work. It was a great experience to work with him. He acquainted me with the world of advanced research. His mentorship has been tremendously helpful, and his vision and insight never cease to surprise me. His friendly guidance, suggestions and wholehearted supervision has made it possible for me to complete this thesis. I am grateful to him for his useful directions, continuous encouragement, consistent support and valuable remarks throughout the progress of this work. My completion of this work could not have been accomplished without his deepest expertise and the shrewder insight. I have really learned a lot from his comments and suggestions. I would like to thank **Professor Abdelhamid BENHAYA** from University of Batna-2- for being president of the examination committee. I thank my oral thesis committee members, **Professor Ramdane MAHAMDI** and **Professor Zohir DIBI** from University of Batna -2-, **Professor Idris BOUCHAMA** from University of M'Sila, **Professor Djamil RECHEM** from University of Oum El Bouaghi, and **Professor Fouad KERROUR** from University of Constantine 1, for accepting, taking time to serve as committee members, to review this dissertation and to give valuable comments.

I am really grateful to **all** my lab members and colleagues Dr. Toufik BENTRCIA, Mr. Elasaad Chebaki and Mrs. Kalinka KACHA for their advice and their willingness to share their bright thoughts with me, for shaping up my research.

Finally, I would like to take this opportunity to thank **all** my friends and colleagues and the staff at the Department of Electronics, University of Batna -2- who have given their support and helped **me in completing this work.**

If I did not mention someone's name here, it does not mean that I do not acknowledge your support and help. Again, I would like to thank **everyone** who supported and helped me during my Ph.D. study.

FERHATI HICHEM

Abstract

Optoelectronic devices are of vital technological importance because of their application in various fields including optical communication, environment monitoring and clean renewable energy sources. Integrated optoelectronic devices provide new opportunities toward dealing with the steady requirement of large bandwidth of next-generation optical interconnections technology. In spite of this tremendous success, there are many challenges associated with photoreceiver devices such as huge overhead in power consumption and relatively low sensitivity.

On the other hand, the advanced thin-film photovoltaic based on kesterite technology has been enabling great promise in meeting demands of carbon-neutral energy. However, the developed CZTS solar cell structures are still challenging and their efficiency remains far from that offered by the Silicon-based technology.

The work presented in this dissertation includes the development of new optoelectronic devices and their applications in advanced optical interconnects and photovoltaic. The discrepancy between the advanced nanoelectronic and photonic devices is investigated, with a focus on the photoreceiver that determines the power budget of optical interconnects. The goal of this thesis is also to explore the possibility to overcome the most critical problems of the CZTS solar cell with the aim of achieving superior conversion efficiencies.

Based upon these topics, the thesis is divided into the following parts

First, the state-of-the-art of the optoelectronic devices including photodetectors, phototransistors and kesterite solar cell will be presented. Afterwards, the basic photodetection mechanism and key device figure of merits are described. Finally, the recent progress in the CZTS solar cell and their advanced elaboration techniques are reviewed in detail. Next, metaheuristic techniques and their potential for treating many engineering problems are presented. An overview of various metaheuristic algorithms such as genetic algorithm (GA), particle swarm optimization (PSO) techniques and their derivatives are discussed in details, indicating its potential application for optimizing novel optoelectronic devices.

Thereafter, two novel UV photodetector designs are proposed and analytically investigated in order to achieve the dual-benefit of high-performance photoreceivers and reduced power consumption. The first one relies on combining front glass texturization to enhance the device performance. While the second design aims at developing self-powered photodetectors by using dual material aspect. The proposed designs are optimized using PSO-based approach, where improved device FoMs are achieved.

Afterwards, new CMOS compatible phototransistor designs are introduced in the second part of this thesis. We focus on improving the device sensitivity and reduce its fabrication cost by proposing a new design based on the junctionless aspect. The proposed structure is then optimized using GA technique, where it offers an outstanding capability to

achieve high-performance phototransistor. We also propose in this chapter a new optically controlled tunneling field effect transistor (OC-TFET) based on SiGe/Si/Ge Hetero-channel in order to enhance the optical commutation speed and reduce power consumption. The investigated phototransistor designs share the ultra-sensitivity and weak signal detection characteristics, which enables reducing the power from the emitter stage and thereby decreasing the power budget.

This thesis defines also a path to enable improved efficiency values of kesterite solar cell by appropriately engineering the absorber layer. Firstly, a graded band-gap aspect is introduced to avoid the recombination losses and enhance the carrier separation. Secondly, intermediate metallic sub-layers are introduced in the CZTS region to simultaneously achieving reduced optical losses and lower series resistance. PSO-based approach is conducted with the aim of maximizing the power efficiency. The physical reasons that govern the efficiency enhancement are also discussed.

Finally, the role of introducing an intermediate Indium Tin Oxide (ITO) thin-film in improving the Au/Si Schottky Barrier Diode (SBD) electrical and thermal stability performances is experimentally analyzed. The Au/ITO/Si/Au structures with different ITO thicknesses were fabricated using RF magnetron sputtering technique. The current-voltage (I-V) characteristics of the elaborated structures are studied. Moreover, the effect of the annealing process on the device performance is investigated. Our study shows that the annealed SBD allows avoiding the degradation related-heating effects.

Keywords: Optoelectronic; Photodetector; Self-powered, texturization, Phototransistor; Junctionless; Tunneling; Power consumption; Optical interconnects; Photovoltaic; CZTS; Recombination; Efficiency; Graded band-gap; Metallic sub-layers; ITO; Schottky Barrier Diode; thermal stability; annealing; GA; PSO.

Résumé

Les dispositifs optoélectroniques jouent un rôle très important dans divers domaines, tels que les liens optiques, la surveillance de l'environnement, et même l'énergie renouvelable. Le développement des ordinateurs à haute performance est crucial mais il est limité par la faible bande passante des interconnexions électriques. La communication optique peut faire face à ce problème en se basant sur les composants optoélectroniques pour concevoir des interconnexions à très haut débit. Néanmoins, cette évolution vers plus de débit cause de sérieux enjeux en ce qui concerne la puissance consommée par les photorécepteurs associés.

La technologie photovoltaïque en couches minces basée sur des matériaux à faibles coûts tell que le CZTS a permis de répondre aux besoins croissants en énergie. Cependant, les cellules solaires développées sont aujourd'hui principalement limitées par le faible rendement ce qui reste loin de celui offert par la technologie à base de silicium.

Dans ce manuscrit de thèse, nous proposons des nouveaux dispositifs optoélectroniques, qui pourront éventuellement améliorer les performances des systèmes de communication optique. Dans ce contexte, l'objectif majeur est d'adresser les pénalités en puissance consommée associées au lien de communication. Il s'agit également d'explorer la possibilité de surmonter les problèmes les plus critiques de la cellule solaire en couches minces afin d'atteindre des rendements supérieurs.

En se basant sur ces aspects, le manuscrit se compose de ces principaux chapitres

Tout d'abord, nous décrirons l'état de l'art des différents dispositifs optoélectroniques que nous allons étudier tels que les photodétecteurs, phototransistors et les cellules photovoltaïques CZTS. Les progrès récents concernant la cellule solaire CZTS et leurs procédés de fabrication sont illustrés et examinés en détail. Ensuite, on va présenter les techniques métaheuristiques et leur efficacité pour traiter de nombreux problèmes d'ingénierie. Un aperçu de divers algorithmes tels que l'algorithme génétique (GA), l'optimisation par essaims particulaires (OEP) est illustré.

Par la suite, deux nouvelles conceptions de photodétecteurs sont proposées et analysées analytiquement afin d'obtenir des photorécepteurs à haute performance et de réduire la consommation d'énergie. La première structure repose sur la texturation de la surface de substrat verre pour améliorer le comportement optique du composant. Alors que la deuxième conception vise à développer des photodétecteurs auto-alimentés en utilisant une couche active avec hétérojonction. En plus, les conceptions proposées sont optimisées en utilisant une approche basée sur l'OEP, où les structures optimisées présentent une excellente capacité à améliorer les performances optiques tout en réduisant la consommation d'énergie. De plus, de nouvelles structures de phototransistors compatibles à la technologie CMOS sont introduites dans la deuxième partie de cette thèse. Afin d'améliorer la sensibilité du dispositif et réduire son coût de fabrication, nous avons

proposés une nouvelle structure de phototransistor basée sur l'aspect sans jonction. Des modèles analytiques associés au photo-courant, aux paramètres de performance optique sont développés. La conception proposée est optimisée en utilisant les AGs, où le dispositif optimisé offre une capacité exceptionnelle pour réaliser un photorécepteur à haute performance. D'autre part, nous proposons un nouveau phototransistor basé sur l'effet tunnel afin d'améliorer la vitesse de commutation optique. Les conceptions de phototransistor étudiées partagent les caractéristiques de l'ultra-sensibilité ainsi que la capacité de détection des faibles signaux, ce qui permet de réduire la puissance optique de l'émetteur nécessaire pour parvenir à une réponse acceptable.

Ce travail de thèse porte aussi sur la conception des architectures alternatives basées sur l'ingénierie de la couche absorbante pour augmenter le rendement des cellules photovoltaïques CZTS. Premièrement, nous allons utiliser une couche absorbante avec une bande interdite graduée pour éviter les pertes de recombinaison et améliorer la capacité de séparation des pairs électrons/trous. Deuxièmement, des couches métalliques ultra-minces intermédiaires sont introduites dans la région CZTS pour simultanément diminuer les pertes optiques et la résistance série en bloquant la diffusion du soufre. Une approche basée sur l'OEP est menée dans le but d'optimiser le comportement optique des conceptions proposées en satisfaisant le but de maximiser le rendement de la cellule. Les phénomènes physiques qui régissent l'amélioration du rendement sont également discutés.

Enfin, nous nous intéresserons à l'élaboration d'une nouvelle structure d'une diode à barrière de Schottky Au/Si (DBS) basée sur l'introduction d'une couche mince intermédiaire d'ITO en utilisant la technique de pulvérisation cathodique magnétron RF. L'effet de l'épaisseur de la couche introduite sur les performances électriques et ainsi sur la stabilité thermique de la diode est étudié. En outre, l'influence du recuit sur la stabilité thermique du dispositif élaboré est également analysée. Notre étude montre que le recuit peut apporter de très bon résultats au niveau de la stabilité thermique de la diode.

Mots Clés: Optoelectronique; Photodétecteurs; Auto-alimenté, texturation, Phototransistor; Sans jonction; Effet Tunnel; consommation d'énergie; Interconnexion optique; Photovoltaïque; CZTS; Recombinaison; Rendement; bande interdite graduée; couches métalliques ultra-minces; diode à barrière de Schottky; stabilité thermique; ITO; AGs; OEP.

ملخص

للتجهيزات الكهروضوئية دورا هاما في مختلف الميادين، مثل الاتصالات الضوئية، مراقبة البيئة، وكذلك الطاقة المتجددة. إن تطوير أجهزة الكمبيوتر عالية الأداء يعد أمر بالغ الأهمية ولكن الطريق نحو ذلك تتخلله عدة مشاكل متعلقة بمحدودية عرض النطاق الترددي الذي يلازم الروابط الكهربائية. يمكن للروابط الضوئية التعامل مع هذه المشكلة عن طريق استخدام التقدم التكنولوجي في المركبات الكهروضوئية لتصميم اتصالات عالية السرعة. غير أن هذا التقدم نحو تدفق أكثر أثار تحديات جادة فيما يخص الطاقة المستهلكة من المستقبلات الضوئية.

تمكّن تقنية الألواح الضوئية ذات الأغشية الرقيقة القائمة على المواد منخفضة التكلفة مثل CZTS من تلبية احتياجات الطاقة المتزايدة.ومع ذلك، فإن بنية الخلايا الشمسية المتطورة تعد محدودة بشكل رئيسي من ناحية الكفاءة التي لا تزال بعيدة عما توفره التكنولوجيا المرتكزة على السليسيوم.

في هذه الأطروحة، نقترح مركبات كهروضوئية جديدة، التي تتيح إمكانية دمج الدوائر النانو الكترونية والضوئية على نفس الشريحة، والذي من شأنه أن يحسن أداء أنظمة الاتصال. في هذا السياق، نقترح مستقبلات ضوئية مستحدثة لمعالجة مشاكل استهلاك الطاقة في الاتصالات الضوئية.ومن ثمة فالهدف من هذه الأطروحة أيضا هو استكشاف إمكانية تخطي المشاكل الأكثر تعقيدا للخلايا الشمسية ذات الطبقات الرقيقة، حيث أن الهدف الأساسي هو الوصول إلى كفاءة قصوى.

بالاستناد على هذه المعطيات والأهداف، في هذه الأطروحة نقدم وصفا شاملا لمختلف التجهيزات الكهروضوئية التي سنقوم بدراستها بما في ذلك الكاشف الضوئي، الترانزستور الضوئي، والخلايا الشمسية على أساس CZTS. وتأسيسا على ذلك، اقترحنا تصميمين جديدين للكاشف الضوئي بغرض الحصول على مستقبلات ضوئية ذات أداء عالي وخفض الاستهلاك الطاقوي من جهة أخرى وفي الجزء الثاني من الأطروحة اقترحنا تصميمات جديدة متكاملة مع تكنولوجيا CMOS المتقدمة. المجهودات المبذولة لتحسين حساسية المستقبلات الضوئية ولتقليص تكلفة إنتاجها متمركزة حول تطوير بنية جديدة للترانزيستور الضوئي دون وصلات، كما تم تطوير نماذج تحليلية الخاصة بالتيار الضوئي. باستخدام الخوارزميات الجينية تم تحسين التصميم المقترح، فالترانزستور الضوئي المحسن يوفرا مكانية استثنائية لإنجاز مستقبل ضوئي ذو أداء عالي مع إجراء بسيط للتصنيع. من جهة أخرى نقترح ترانزيستور ضوئي جديد يستند على النفق الكموني بهدف رفع سرعة الاتصال الضوئي. تصاميم الترانزيستور الضوئي المدروسة تقدم مميزات عديدة كالحساسية العالية بالإضافة لإمكانية رصد الإشارات الضوئية الضعيفة، ما يسمح بتخفيض الطاقة الضوئية الخاصة بالمرسل للتحقيق استجابة مقبولة. في النهاية، ركزنا على تصميم طريقة بديلة تستند أساسا على هندسة الطبقة الممتصة لرفع كفاءة الخلايا الشمسية CZTS، وذلك باستعمال طبقة ممتصة ذات فجوة نطاق متدرجة لتفادي آثار ظاهرة عودة ارتباط ولتحسين الفصل بين زوج من الالكترونات المنتجة. من ناحية أخرى قد تم إدخال طبقات معدنية رقيقة جدًا في منطقة CZTSلتفادي الخسائر الناتجة من انعكاسات الأشعة الضوئية و تخفيض المقاومة عن طريق منع انتشار الكبريت. وبالإضافة إلى ذلك قد تم تطبيق طريقة قائمة أساسا علىOEP لتحسين السلوك الضوئي للتصاميم الخلايا الشمسية المقترحة من اجل تحقيق هدف زيادة كفاءة الخلية. وتناقش أيضا الظواهر الفيزيائية المسؤولة عن تحسين كفاءة الخلية الشمسية CZTS.

الكلمات المفتاحية: الكهروضوئية ،الاتصالات الضوئية، الطاقة المتجددة، الخلايا الشمسية، مستقبلات ضوئية، الكفاءة، الترانزستور الضوئي، تكنولوجيا CMOS، دون وصلات، الخوارزميات الجينية، النفق الكموني، انعكاسات الأشعة الضوئية.

Table of Contents

Chapter III: Metaheuristic Techniques

Chapter IV: New MSM-UV Photodetector Designs

Chapter V: Design and Optimization of Novel Ge-based Phototransistor Designs

Chapter VI: Boosting up the Efficiency of Thin-Film CZTS Solar Cells

Chapter VII: An Experimental Investigation of a New Au/ITO/Si Schottky Barrier Diode Design

Chapter VIII: Conclusion and Outlooks

List of Figures

List of Tables

List of Publications

The work in this thesis was mainly drawn from the following publications:

- H. Ferhati, F. Djeffal, "Role of Optimized Grooves Surface -Textured Front Glass in improving TiO_2 Thin Film UV Photodetector Performance," IEEE sensors journal, vol. 16, pp. 5618- 5624, 2016.
- H. Ferhati, F. Djeffal, "A novel high-performance self-powered ultraviolet photodetector: Concept, analytical modeling and analysis," Superlattices and Microstructures, vol. 112, pp.480-492, 2017.
- H. Ferhati, F. Djeffal, "Planar junctionless phototransistor: A potential high-performance and low-cost device for optical-communications," Optics & Laser Technology, vol.97, pp.29-35, 2017.
- H. Ferhati, F. Djeffal, "Boosting the optical performance and commutation speed of phototransistor using SiGe/Si/Ge tunneling structure," Materials Research Express, vol.5, pp. 065902, 2018.
- H. Ferhati and F. Djeffal, "Graded band-gap engineering for increased efficiency in CZTS solar cells," Optical materials, vol.76, pp. 393-399, 2018.
- H. Ferhati, F. Djeffal, "Role of intermediate metallic sub-layers in improving the efficiency of kesterite solar cells: concept and optimization," Materials Research Express, vol.5, pp. 036417, 2018.
- A. Benhaya, F. Djeffal, K. Kacha, H. Ferhati and A. Bendjerad, "Role of ITO ultra-thin layer in improving electrical performance and thermal reliability of Au/ITO/Si/Au structure: An experimental investigation," Superlattices and Microstructures, vol.120, pp. 419-426, 2018.

Chapter I

Introduction and Thesis Outlines

***Abstract:** This chapter is focused on presenting the underlying theme of this thesis, which is to address several optoelectronic devices, from a joint theory, modeling and global optimization standpoint. This chapter provides also the main motivation behind investigating several optoelectronic devices. Moreover, we present the photodetector and phototransistor challenges in current optical communication systems. On the other hand, this chapter presents the most pronounced problems associated with the CZTS thin-film solar cells. The proposed approaches and our contributions in this thesis are detailed. This chapter can be considered as an introductory platform of our work, where the thesis outlines are presented.*

I Introduction

Over the last few years, semiconductor-based devices have become an essential part of our daily life. In fact, the widespread proliferation of information exchange using the internet makes us immersed in a wider diversity of electronic services. Optoelectronic devices constitute an important part of electronic systems and could belong to our home appliances such as the mobile phone, cars, TV, computers or even carbon-neutral energy sources using photovoltaic systems. The main idea behind these devices resides on the interaction between photons and electrons, where materials with strong absorption/emission properties are suitable for optoelectronic applications. In this context, with the recent progress in optical technology, optoelectronic devices are expected to be exploited for chip-level communication applications [1]. In other words, the deficiencies associated with electrical wire links prevent achieving faster inter-chip communication and reduced power consumption [1-3]. For these reasons, optical links have begun to invade on areas that were once considered to be the exclusive dominion of electrical links [4-7]. Modern versions of optical communication have been well-developed thanks to the early progress regarding advanced photoreceivers (photodetectors, phototransistors and photodiodes) fabrication technologies and also to new radical ideas [5-7].

Optoelectronic devices were also emerged for different sensing applications such as: photovoltaic and environmental monitoring systems. Ultraviolet sensors analyze our environment, i.e. they detect the presence UV-radiations in our atmosphere [6-8]. The UV-photodetector as an optoelectronic device is considered of crucial importance for the control of our physical environment [8]. On the other hand, solar cell-based devices are forecasted to be the most strategically desirable solution for recording low cost and clean renewable energy resources [9]. As a matter of fact, the development of high-efficiency solar cells with low-cost to end the actual carbon economy is of fundamental significance in both economics and industrial sectors [10-13]. The main objective is therefore to make a good trade-off between both the elaboration cost and the conversion efficiency, which is unfortunately foreseen as a barrier for achieving low cost carbon neutral energy sources. To this extent, Chalcogenide-based solar cells are expected to be effective for providing an improved efficiency at low manufacturing cost [14]. However, practical challenges, such as structure complexity, efficiency losses and reliability, should also be taken into account [14-18].

I.1 Motivation

The continuous demand for low cost optoelectronic devices with high-performance is growing rapidly for diverse electronic applications such as optical communication, environmental monitoring, sensing and even photovoltaic energy. In this framework, the development of high-performance optoelectronic devices like phototransistors, photodetector and high efficiency solar cells is of paramount importance in nowadays industry requirement. In this regard, we have conducted a variety of studies to propose and develop novel design methodologies to address the most critical challenges associated with the current optoelectronic devices. Therefore, the enhancement of these devices seems of great importance which motivates us for investigating several optoelectronic devices including UV-photodetectors and NIR-phototransistors and thin-film solar cells in order to deal with the most pronounced issues faced by these devices.

I.2 The Gap Between Electronic and Photonic

The integration between photonics and electronics could improve CMOS capabilities and open up a new way toward continuing feature size shrinkage according to Moore's law. Following this direction, in chip-to-chip communication, shrinking the electrical wire interconnects size imposes several challenges mainly related to the increase in the resistivity, the total capacitance and power consumption, which results in an enormous reduction of the communication bandwidth [2-5]. Alternatively, integrated silicon photonics provide great promise in meeting the high bandwidth and low-energy demands since they offer the opportunity of optical communication technology [3-6]. In fact, optical interconnection technology offers the distance insensitivity property owing to the inherently low optical losses of fibers, enabling the prospect for new types of communications in modern digital systems and data-transfer centers. Three years ago, the first single-chip computer in which the connectivity was down by means of optical links based on monolithic integrated photonic technology is successfully demonstrated [5]. In spite of this achievement, there are still many challenges associated with silicon photonic interconnect that prevent the deployment of the optical links for the current nanoelectronic technology. As the industry moves towards the optical communications, their three essential stages namely, emitters, transmitters and photoreceivers should be improved in order to make the electronic-photonic integration very close. Therefore, it has become important to propose new insights in order the make the optical

communication technology more competitive with the electrical counterparts and to potentially improve the communication bandwidth.

I.3 Cost and Power Challenges

Power consumption is considered as the most pronounced problem of today's chip designers. Although the continuous downscaling has allowed a considerable increase in number of transistors and memory bits per chip, the power dissipation drawbacks prevent achieving high-performance designs at the upcoming technology nodes. Over the last few years, the recent progress regarding the optical wireless communication technology in chip-level communication has provided a new path toward achieving lower resistive losses and an enormous bandwidth [4-5]. However, this system consumes a huge amount of power due to the high energy dissipation of the photoreceiver circuit. In this perspective, the optical links technology faces the challenge of how to translate the photoreceiver devices into better performance under reduced power consumption. Moreover, the photoreceiver should be followed by Trans-Impedance Amplifier (TIA), to remove noise that gives digital transmission its high quality levels for optical communications systems. Moreover, amplifier stages are also used to convert the photoreceiver current to voltage signals that can be accepted by CMOS logic stages. These readout circuits consume a huge amount of power. In order to deal with this problem the optical receiver output capacitance should be minimized. On the other hand, several photoreceiver devices are exploited to develop the optical communication including photodetectors, photodiodes and phototransistors. The manufacturing cost of these structures is also considered a big issue, where it is of great importance to improve the photoreceiver performance with keeping the low cost property. Moreover, enhancing the optical receiver sensitivity, responsivity and optical commutation speed can be effective for reducing the light power intensity from the emitter which could decrease the overall energy consumption of the optical wireless communication systems. As a result, the second goal of this thesis is to get rid of power consumption issues and decrease the elaboration cost of the photoreceiver stage. Specifically, we will focus on improving the photodetectors and phototransistors performance and potentially suppressing leakage power.

I.4 CZTS ($Cu_2ZnSn(S,Se)_4$) Thin-Film Solar Cell Challenges

Several challenges still prohibit the implementation of CZTS-based technology as a compelling solution for achieving high-efficiency and low-cost photovoltaic device. In fact, the maximum achievable efficiency value associated with the Kesterite-based solar cell is reported to be approximately 30% [19]. Unfortunately, to date only 12.6% of conversion efficiency was recorded, which is considered very low and required further enhancement [20]. It is of great importance to understand the main reasons that prevent approaching the theoretical limit of the CZTS based solar cell. Accordingly, there are some problems regarding the solar cell design and the material quality and even experimental issues that can affect the device performance. Therefore, there are five essential effects that should be addressed in order to improve the solar cell performance:

- **V_{oc} deficit**: although an acceptable V_{oc} value about 0.7 V has been recently recorded [20], the open circuit voltage values are generally reported to be at the average of 550 mV. This indicates that there is a great deficit when compared to the theoretical limit of 1.23 V forecasted for CZTS-based thin-film photovoltaic technology. The V_{oc} deficit associated with the actual Kesterite solar cells can be attributed to two main factors namely the quality of the absorber layer and the degradation related-recombination effects.
- **Low diffusion length**: with minority carrier lifetime about 2.5ns, the CZTS compounds are considered extremely challenging for achieving superior values of the open circuit voltage. In this context, charge carrier transport parameters should be considerably improved. To do so, the good control of the CZTS compositional homogeneity as well as the phase purity can give wider possibilities for extending the carrier diffusion length and thereby enhancing the solar cell performance.
- **Intrinsic defects and stability issues:** the quality of the absorber layer CZTS plays a crucial role in determining the solar cell performance, where intrinsic defects can enormously degrade the device efficiency. Indeed, these defects can cause the electron-hole pair recombination phenomena, which are considered as major challenges that prohibit achieving favorable efficiency values. These effects are mainly due to the experimental conditions (fabrication processes) as well as the elaborated CZTS compositions. Therefore, the complexity associated

with different growth techniques and elaboration conditions constitute a major drawback for the better understanding of these experimental problems.

- **CZTS solar cell design:** engineering the device architecture appropriately can be beneficial for improving the conversion efficiency. The optimization of the absorber layer and the good choice of the buffer layer and contacts can offer the possibility to further increase the device efficiency. In fact, the actual Kesterite-based solar cell exhibits extensive limitations related to non-ohmic behavior of the back contact due to the formation of a potential barrier between the CZTS active region and the MoS_2 interfacial layer. This phenomenon can affect the device performance and causes significant degradation on the short-circuit current.
- **CZTS/Buffer layer interface quality:** the standard solar cell design adopted for CIGS is typically used for the CZTS-based photovoltaic device counterpart, where the material used as buffer layer is the CdS. This material has shown a good compatibility and improved interface quality for the CIGS technology, which is not the case for the Kesterite solar cells. In fact, the biggest problem is the band-alignment between CdS and CZTS, where the interfacial defects at the interface induces recombination losses. Moreover, the use of the CZTSSe absorber layer can give rise to possible enhancement regarding the solar cell absorption behavior, but with consequential increase of the interfacial defects. Thus, exploring suitable Cd-free buffer layers is obviously desirable not only from an environmental point of view, but also for improving the Kesterite solar cell performance.

In summary, a deep knowledge of the basic material properties, interfacial defects origin and the solar cell degradation reasons is certainly an important issue to identify both the appropriate buffer layer and the optimal CZTS absorber layer that enable improving the solar cell conversion efficiency. In this perspective, the third objective of the thesis work focuses on investigating the prospect for improving the Kesterite solar cell performance by taking into consideration the above-mentioned critical issues.

I.5 Our Approaches and Contributions

This section presents the approaches we use to bridge the gap between photonics and electronics as well as reducing both the fabrication cost and power consumption of

photoreceiver structures including photodetectors and phototransistors. New concepts for the eventual enhancement of the CZTS solar cell efficiency are also provided.

✓ Bridging the Gap Between Electronic and Photonic

Optical components used for the optical interconnections such as modulator, waveguide and (photodetector or phototransistors) should be integrated with advanced CMOS technology. One of the major objectives of the thesis is how to address the size mismatch between current electronic and photonic components, and achieve further promising improvements regarding the photoreceivers performance. For this purpose, we propose versatile Ge-phototransistor designs which are fully compatible with CMOS technology. The first one consists on a new junctionless Ge-phototransistor that provides substantial improvement regarding the device FoMs. The main objective is also to improve the photoreceiver performance and potentially bridge the gap between the advanced electronic technology and its silicon photonic counterpart. This benefit is achieved through using a suitable sensitive material that is effective in the near-infrared wavelength ranges and simultaneously compatible with silicon. In a similar manner, the second proposed Ge-phototransistor design suggests introducing a hetero-channel structure in order to generate the quantum band-to-band tunneling effect. The latter can provide small swing switch property which can enhance the phototransistor optical commutation speed. Moreover, the proposed design is suggested with SOI platform in order to make it potentially compatible with CMOS technology.

✓ Reducing Power Consumptions and Fabrication Costs

It is of great importance to reduce the photoreceiver power consumption. As a matter of fact, suppressing the leakage current of the photodetector and phototransistor could reduce the power dissipation. Moreover, taking lower applied voltages can also enormously decrease the power budget. Following this direction, the aim of this dissertation is to explore new design methodologies for removing the power issues. In this perspective, we propose a new self-powered photodetector that operates at zero bias conditions. A heterojunction channel is suggested to ensure the self-powered property. Moreover, we exploit metaheuristic techniques to achieve high-performance photodetector at zero voltage. Besides, the proposed design is suggested with earth abundant materials in order to reduce the fabrication cost.

The second approach is based on combining a new junctionless phototransistor design with metaheuristic techniques to potentially achieve the dual role of improved device performance and reduced power consumption. Moreover, we suggest the phototransistor without junctions at the source/drain regions in order to reduce the fabrication process and to avoid the thermal budget.

The third approach consists of proposing a new phototransistor design based on tunneling effect in order to suppress the leakage current that can subsequently reduce the power consumption. More importantly, using a phototransistor instead of photodetector as a photoreceiver in optical wireless communication systems could provide the receiver-less property that allows avoiding the use of amplification stages and thereby a considerable decrease in both energy consumption and cost challenges.

✓ Overcoming the CZTS Solar Cell Critical Challenges

The CZTS thin-film has drawn world-wide attention due to its outstanding photovoltaic performance and earth-abundant composition. However, nowadays CZTS-based solar cells efficiency values are still far from its theoretical limit. This is because of several limitations mainly associated with degradation-related recombination effects, optical losses and elaboration issues, which are above outlined. Thus, improved efficiency values are envisaged in order to make the CZTS solar cell technology competitive with its counterpart based on silicon. Accordingly, we focus our efforts on developing new approaches that enable improving the CZTS solar cell conversion efficiency. After the careful study of the CZTS-based solar cell working mechanisms, we have obtained three key insights that allows improving the solar cell performance

- Avoiding the degradation related-recombination effects
- The substantial reduce in the optical losses
- The series resistance modulation

These insights indicate that we can design the CZTS solar cell in an appropriate way that enables reaching these objectives. For this reason, we firstly propose a new design based on graded band-gap aspect to effectively suppress the recombination effects and hence improve the solar cell efficiency. The main idea behind it is to generate an electric field in the CZTS absorber layer that could efficiently derive the photogenerated carrier. We also use a metaheuristic technique to identify the favorable CZTS band-gap profile that provides the maximum possible efficiency value. The optimized design could open up the route not only for improving the minority carrier

life time but also for enhancing the absorbance behavior that can in turn offer superior efficiency values. The proposed CZTS solar cell design takes advantage from the electric field modulation aspect to provide the possibility to reduce the series resistance. Secondly, the CZTS solar cells have certain weakness mainly related to the high series resistance originated from the formation of the MoS_2 at the CZTS/Mo interface. The optical losses constitute also a serious problem that we should deal with. For this purpose, we propose a new design methodology based on coupling global optimization approach with a new solar cell structure with intermediate metallic layers. The latter are introduced in the CZTS absorber layer in order to achieve the dual benefit of preventing the sulfide diffusion and enhancing the absorption near the infrared spectrum range. We use various metallic sub-layers in order to identify the most favorable metal that provides the highest efficiency value. As a result, substantial improvements regarding the solar cell fill factor and photocurrent can be achieved by appropriately avoiding antireflection effects.

I.6 Thesis Outlines

The underlying theme of this thesis is to address several optoelectronic devices, from a joint theory, modeling and global optimization standpoints, with a focus on understanding the physical rules that governs their optical and electrical performances. This work is motivated in a part by the photodetector and phototransistor challenges in current optical communication systems and in another part by the search for new approaches to achieve improved conversion efficiency for the CZTS thin-film solar cells. The rest of this thesis is organized as follows:

The second chapter presents an overview of fundamental concepts concerning several optoelectronic devices. At the beginning, we define the conventional photoreceiver devices such as photodetectors and phototransistors, and we give a detailed description of their recent progress and future challenges. Then we define and describe the CZTS thin-film solar cells and their basic operating mechanisms. A detailed literature review on the CZTS solar cell deposition methods and record efficiencies is presented.

General concepts and description of metaheuristic techniques are presented in Chapter III. This chapter introduces the fundamentals of genetic algorithm (GA),

Particle Swarm Optimization (PSO) and its quantum derivative termed (QPSO). An overview of multi-objective optimization approaches in also presented.

In Chapter IV, we consider the enhancement of UV photodetectors (PD). In the first part, the impact of the surface-textured front glass on the absorption of TiO_2/glass Metal-Semiconductor-Metal (MSM) UV photodetector is investigated, in order to achieve the dual role of increasing the scattering path as well as reducing the refracting UV-light at the glass substrate. Moreover, semi-analytical modeling combined with PSO-based approach is carried out for studying and enhancing the MSM-UV photodetector optical and electrical performances. The second part of this chapter is devoted to the investigation of a new self-powered MSM-UV-photodetector based on dual wide band-gap material (DM) engineering aspect. Comprehensive analytical models for the proposed sensor photocurrent and the device properties are developed incorporating the impact of DM paradigm on the device photoelectrical behavior. A new hybrid approach based on analytical modeling and PSO approach is proposed to achieve improved photoelectric behavior at zero bias that can ensure favorable self-powered device.

Chapter V of this thesis investigates the prospect for improving the Ge-phototransistor performance by proposing two novel structures. The first one consists of a new junctionless optical controlled field effect transistor (JL-OCFET), where its comprehensive theoretical model is developed. The latter is exploited to formulate the objective functions to optimize the device performance using GAs. The optimized design offers high optical performance and low cost fabrication process. On the other hand, a new optically controlled tunneling field effect transistor (OC-TFET) based on SiGe/Si/Ge Hetero-channel is proposed to improve the optical commutation speed and reduce the power consumption. Importantly, a new FoM parameter called optical swing factor that describes the phototransistor commutation speed is proposed.

Chapter VI focuses on providing new insights for the potential improvement of the CZTS-solar cell conversion efficiency. The first idea relies on proposing a potential high efficiency design based on graded band-gap aspect that can offer the benefits of improved absorption behavior and reduced recombination effects. Analytical models for the proposed design are developed incorporating the impact of the graded band-gap profile on the solar cell photoelectrical behavior. A new design methodology based on

analytical modeling and PSO approach is proposed to determinate the better band-gap shape of the amended CZTS absorber layer. The second idea consists of investigating the role of intermediate metallic sub-layers (Au, Ti, and Ag) engineering coupled with metaheuristic techniques in enhancing light-scattering behavior and reducing recombination losses.

Finally, the last Chapter of this thesis explores the concept of using a new Au/p-Si SBD based on ITO intermediate thin-film to improve the diode electrical behavior. The device performances are experimentally investigated. The effect of the annealing temperature on the SBD electrical performance is also investigated. In order to show the role of the inserted ITO layer thickness on the device performance, we elaborated Au/ITO/p-Si structures with different ITO thicknesses by means of RF magnetron sputtering technique. The role of the annealing process in improving the SBD basic electrical parameters and thermal stability performance is also discussed. Finally, an overall performance comparison between the fabricated SBD structures with and without intermediate ITO layer is carried out.

Chapter II

Optoelectronic Devices: Concept and Recent Progress

Abstract: ***This chapter presents an overview of fundamental concepts associated with several optoelectronic devices. At the beginning, we define the conventional photoreceiver devices such as photodetectors and phototransistors, and we give their basic working principle. We thereafter provide a detailed description of their recent progress and future challenges. Then we describe and elucidate the main challenges of the CZTS thin-film solar cells and their basic operating mechanisms. A detailed literature review concerning the CZTS solar cell deposition methods and record efficiencies is finally presented.***

II.1.Chapter overview

Optoelectronic devices have been aggressively driven into several domains of application such as: optical communication, environmental monitoring and clean-renewable energy. In this work, we are mostly interested in optical photoreceivers (photodetectors and phototransistor) and photovoltaic devices based on CZTS material. In this chapter, we will briefly discuss the operating mechanisms associated with several optoelectronic devices. To beginning, we defining different photoreceiver devices, and we will give a global description of their potential applications. Then we will describe the CZTS-based solar cells technology and their advantages in comparison with other photovoltaic devices. The future challenges for developing high-efficiency solar cells are also presented. This chapter can be considered as an introductory platform for upcoming chapters.

II.2.Electrical interconnect

Eelectrical wiring has been considered as an efficient means of communication at various levels of electronic systems, and currently they still dominate the chip-to-chip and broad-to-broad interconnections. Microelectronic systems have offered a steady downscaling in accordance with Moore's law, which is the key towards achieving denser circuitry with high-performance chip and reduced power consumption [21]. Despite the fact that the continuous shrinking of transistors dimension is expected to eventually enhance chips performance, the Semiconductor Industry Association (SIA) has claimed that extensive limitations will be appeared in the future, which could prevent the good operating of the overall chip system [1], [21-22]. These concerns are mainly associated with metallic wires that connect chips to each other [2]. In this context, this problem is considered as one of the major issues in the future progress of integrated microelectronic circuits. The downscaling of the electrical wire increases the resistivity and thereby enlarges the total power consumption of the link, which degrades enormously the communication bandwidth. In order to avoid these problems, complicated signal processing techniques can be used to improve the information capacity, but in contrast, this can certainly further increase the overall cost of the communication system. For these reasons, alternative approaches should be developed in order to cope with the growing demand for larger communication bandwidth at chip level scale.

II.3.Optical interconnect as an alternative technique

Light is considered as electromagnetic (EM) waves for which the wavelengths are extended from Ultra-violet to Infrared range, where their ability to propagate at a very high-speed and for long distances constitute their main advantage. Indeed, optical communications came of age after the prestigious invention of the laser and photodetectors, which are an application of Einstein's theories in which a photon could stimulate an excited atom to emit another identical photon as well as the photoelectric effect that describes the UV-light detection phenomenon. Optical interconnects have been proposed as one of the promising candidates to replace traditional electrical wires due to their potential for overcoming the most pronounced challenges associated with the electrical links including the communication bandwidth [3-5]. The use of optical fibers or waveguides provides the opportunity for getting rid of the undesired resistive losses exhibited by the electrical wire. The deployment of interconnection systems with respect to the communication distance is presented in Figure II.1. Optical links technology not only dominates the long haul communications, but also it consistently pinpoints the way toward governing shorter distances. Meanwhile, till now inter chips and board connections are still done electrically [4-6].

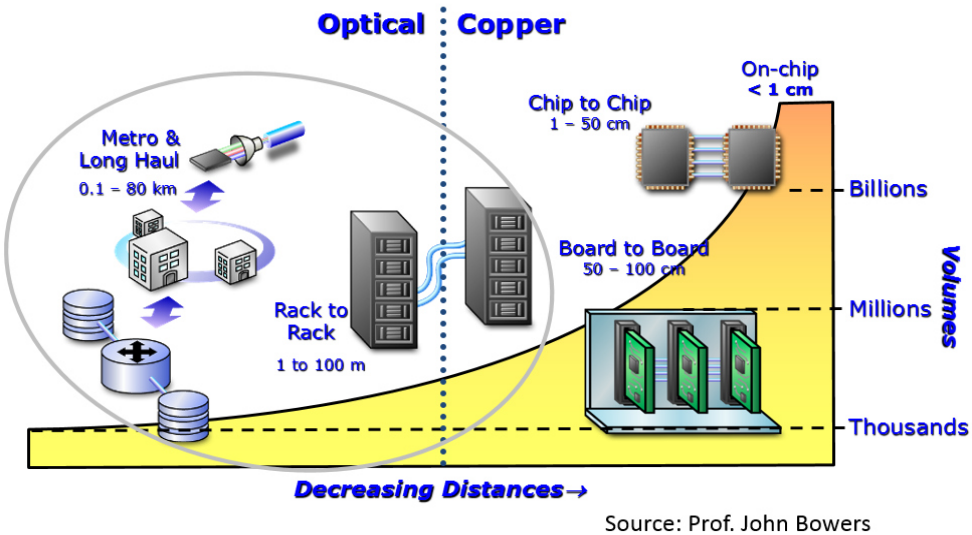

Figure II.1: Communication systems versus the length of the interconnection.

The major problem associated with the electrical connections technology is the huge overhead in energy consumption [6]. On the other hand, alternative approaches such as optical links should demonstrate reduced energy consumption. However,

although the large bandwidth offered by optical communication, transmitters and receivers typically, consume a considerable quantity of power, which makes the optical interconnects extremely challenging at short distance communication applications.

II.4.Optical interconnect challenges

There are many challenges for optical communication that should be addressed in order to make them competitive with electrical interconnections. In this context, typical optical interconnects require high-speed and low power electronics as well as optical components [5-6], [23]. Thus, the most pronounced problems for the optical links to become more efficient are described below.

- **Power consumption:** It is even desirable to run the receiving end of the link without amplification stages. In a traditional optical receiver, the optical signal is conveyed by an emitter through the waveguide to the receiving-end of the optical interconnects. Then, the optical signal will be converted into an electrical current by means of photodetectors. Finally, transimpedance amplifiers is used to convert current to an electrical voltage, which will be amplified using subsequent electronic circuitry to reach the logic level as it is illustrated in Figure II.2. This configuration can consume a huge amount of power, which constitutes a serious problem for the deployment of the optical links. Moreover, the high density of the receiver circuit can also prevent the use of the optical communication at short distance communication. Therefore, the main objective is to operate the photodetector "receiverless" i.e. avoiding all amplifications in the receiver readout circuit. In addition, to reduce the global power consumption of the optical links, it is important to reduce the light intensity at the emitter stage able to provide a tunable response. In summary, to eventually replace shorter electrical interconnects with the optical ones, the light source should be more efficient, and the optical receiver should be more sensitive.

- **Monolithic integration:** The VLSI technology (Very large scale integration) is considered as the mainstream for the actual microelectronics industry. This mature process is widely used to elaborate the widespread integrated circuit (IC), which is the result of investment and research over a number of decades. Admittedly, optical components associated with the optical links such as modulator, waveguide and the photodetector should be integrated

with advanced silicon transistor technology. Recent research has focused on overcoming this challenge with the aim of achieving highly integrated modulators, silicon-on-insulator (SOI) waveguide technology, and silicon-germanium based photodetectors [24-27]. Besides, using a suitable sensitive material that is effective in the ultraviolet and near-infrared wavelength ranges and simultaneously compatible with silicon is of vital importance to develop low-cost optical interconnects [13].

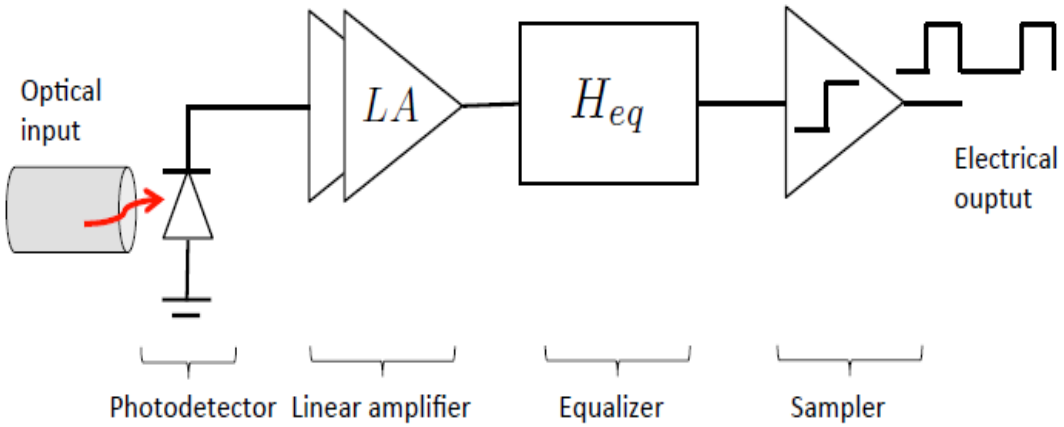

Figure II.2: Conventional optical interconnects receiver circuit.

The optical communication technology at short distances, particularly down to chip-levels, is still immature in comparison with its electrical counterpart [26-28]. Despite the above-outlined problems associated with the electrical wiring, they are still used for inter-chip connections. Consequently, although the long-distance optical communication technology is well developed, it cannot be readily applied to the actual downscaling technology since it has not proven a noticeable benefit over the electrical links regarding the power consumption or even the manufacturing cost. Therefore, it seems crucial to address the size mismatch between current electronic and photonic components, and achieve further promising improvements regarding the photoreceivers performance, and potentially lower energy consumption in order to build competitive optical interconnections.

II.5.Photoreceiver structures

II.5.1. Photodetectors

Photodetectors are typical optoelectronic devices and have now become the core of the optical wireless communication systems, which is the important foundation industry of the advanced electronic systems [8]. Basically, the same operating mechanism governs all solid-state photosensitive devices, where the incident photon with sufficient energy induces a temporarily change in the distribution of electron energies associated with the semiconductor. When the excited electron gets enough energy, it gains energetic conductive state and then it will be eventually free to move within the semiconductor. To this extent, an electron/hole pair will be generated for each absorbed incident photon. Ultimately, after a typical time described as the recombination lifetime (τ_r) that depends on the material properties, the electron/hole pair will recombine and give up the extra energy in the form of heat or light that corresponds to the material band-gap. However, the presence of an electric field through an external excitation can drift the electron and generate an electric current as it is illustrated in Figure II.3.

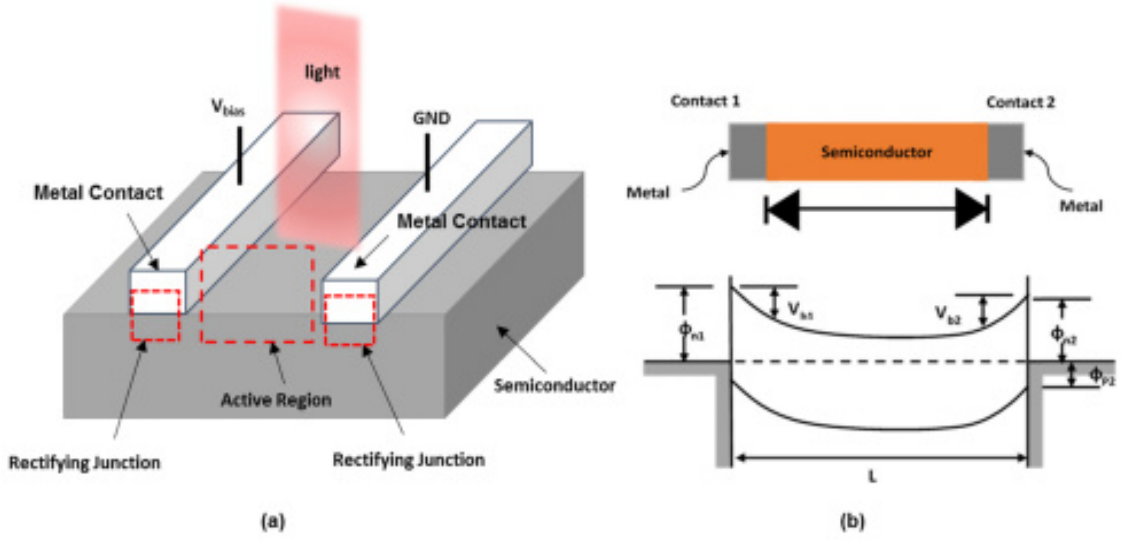

Figure II.3: Structure and band-diagram of the MSM photodetector.

II.5.1.1. Recent progress of UV-photodetectors

After more than a century of steady development, current versions of photodetectors share several exciting properties like high sensitivity, improved stability and reliability, high-speed, reduced noise, and suppressed power losses as it is shown in Figure II.4 [8-11]. These attractive characteristics have encouraged their potential

exploitation in numerous optoelectronic applications such as: communications and ozone-hole monitoring. In spite of the rapid progress of these devices, the growing demands and expectations from users are in fact going beyond the actual stage of maturity of the UV photodetectors. Accordingly, advanced UV sensors are required in health, optical communication, environment monitoring and so on. For this purpose, we will present some advanced technologies associated with the UV-photodetector devices.

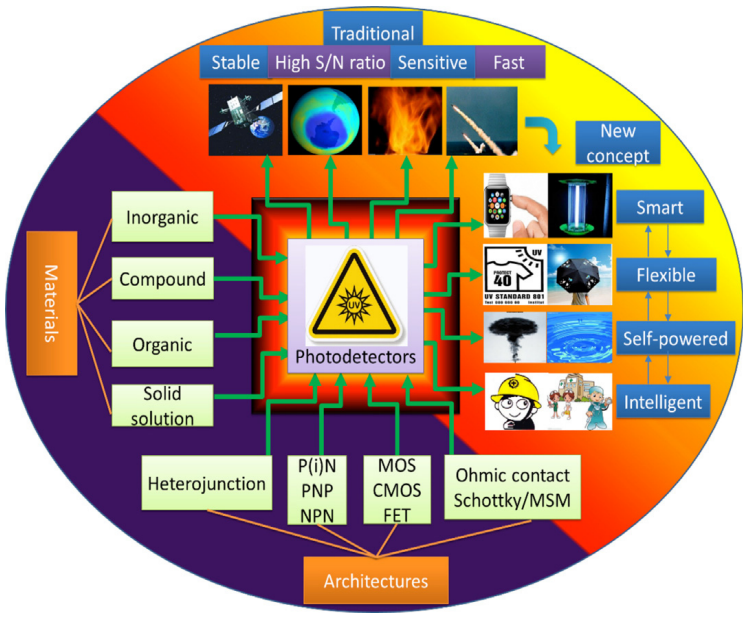

Figure II.4: A technology roadmap leading to next generational chip-scale photodetectors [19]

II.5.1.2. 2D material-based UV-photodetectors

Nowadays, 2D materials have attracted great interests in optoelectronic applications because of their numerous exceptional electrical and optical properties including ultrathin, lightweight, flexible, easy to fabricate and the compatibility with traditional elaboration techniques [29-31]. Graphene 2D material with zero band-gap and ultrahigh carrier mobility has proven its effectiveness for designing phototransistors and solar cells [30-33]. The emergence of Graphene material in UV-photodetectors provides a promising platform for achieving high-performance devices that can deal with the intrinsic limitations associated with the conventional sensors such as speed and flexibility issues [13] and [31-33]. Moreover, the Graphene material can serve as high performance electrodes because of its high conductivity as well as its improved transparency [32].

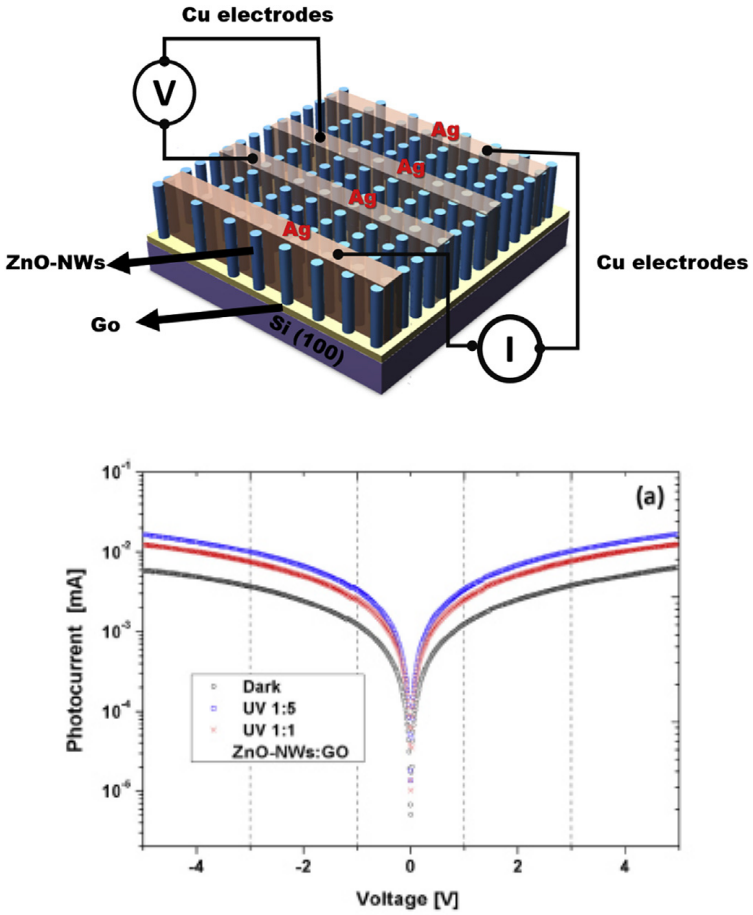

Figure II.5: **(a)** Schematic of UV-photodetector based on ZnO- Nanowires/graphene oxide /Si hybrid structure, **(b)** I-V characteristics of the device under dark and illumination conditions [32]

Firstly, Graphene/GaN-based Schottky UV-photodetector was recently elaborated, where graphene material was used as metal electrodes to suppress the reflection effects and avoid the contact resistive losses. Moreover, the built-in field at the interface between both graphene and GaN materials can be enlarged which leads to enhancing the carrier separation process [30].

In fact, wide band-gap semiconductors/graphene hybrid heterostructures are also used to elaborate UV-photodetector devices. For example, ZnO nano-materials have been integrated with graphene, where a new UV-photodetector based on ZnO-Nanowires (NW)/graphene oxide/Si have been elaborated with a good photoresponse as it is illustrated in Figure II.5 [32]. Besides, other nanostructures based on ZnO NW, ZnO nanoparticles (NPs), ZnO quantum dots (QDs) and ZnO/nanoribbons (NRs) graphene hybrid designs have been emerged to provide ultrasensitive photodetectors and higher photoconductive gain as compared to that exhibited by the conventional

devices [36] and [191-193]. This achievement can be explained by the presence of a high potential barrier between graphene and ZnO materials and the ultrahigh carrier mobility associated with the graphene 2D material. Moreover, a new photodetector based on Graphene/black phosphorus heterostructure has been proposed. Both device structure and SEM image are shown in Figure II.6 [13].

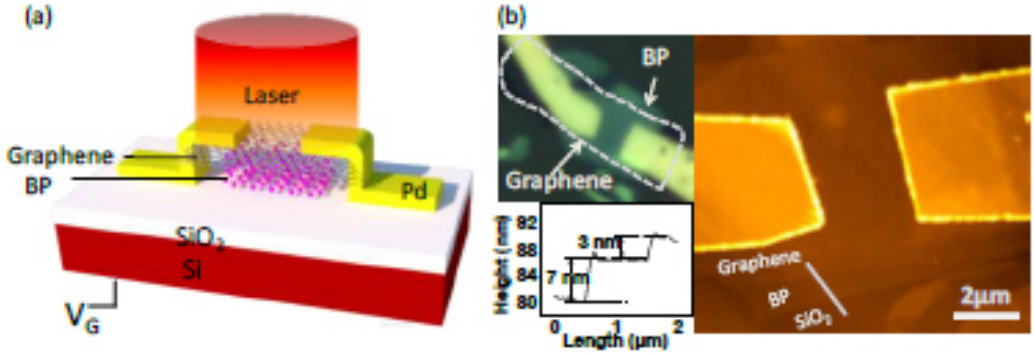

Figure II.6: (a) Schematic illustration of the graphene-BP photodetector. **(b)** Morphology of the graphene-BP heterostructured device: optical microscopy photograph [13].

II.5.1.3. Self-powered UV-photodetectors

One of the ultimate objectives of the developed semiconductor technology is to overcome the trade-off between high-performance optoelectronic devices and suppressed power consumption. To this extent, ultrasensitive UV photodetectors that can work at very low applied voltage are urgently required. Unfortunately, in order to achieve an acceptable detectivity, the majority of the developed UV-photodetectors require higher voltage bias. This makes the conventional designs extremely challenging from the power consumption viewpoint. For this reason, a new type of UV sensors called self-powered devices have been emerged with the aim to providing an effective solution to avoid the huge energy dissipation problem [12], [34-38]. The main idea behind this innovative device dwells on removing the supplied power without sacrificing the high responsivity and sensitivity properties [35]. Eventually, various techniques have been originated to satisfy the self-powered property. These approaches can be categorized into two major classes regarding the energy conversion aspect: the first class relies on using p-n junctions and heterojunctions-based photodetectors, where the device photoconductive behavior can be governed by the photovoltaic effect as it is illustrated in Figure II.7 [12]. On the other hand, there are also other approaches based on integrated power sources, which transform UV light into electrical power along with

mechanical energy or chemical energy [38-39]. In fact several design methodologies have been developed in order to achieve favorable self-powered devices. In this perspective, p-n junction p-ZnO/n-ZnO UV-based photodetector exhibits a small variation at zero bias voltage condition [12]. UV photodetectors based on n-ZnO/p-NiO core-shell heterojunction demonstrates also the potential for providing the self-powered property [40]. Besides, the use of asymmetric electrodes has also proven its effectiveness for developing self-powered photodetector [35].

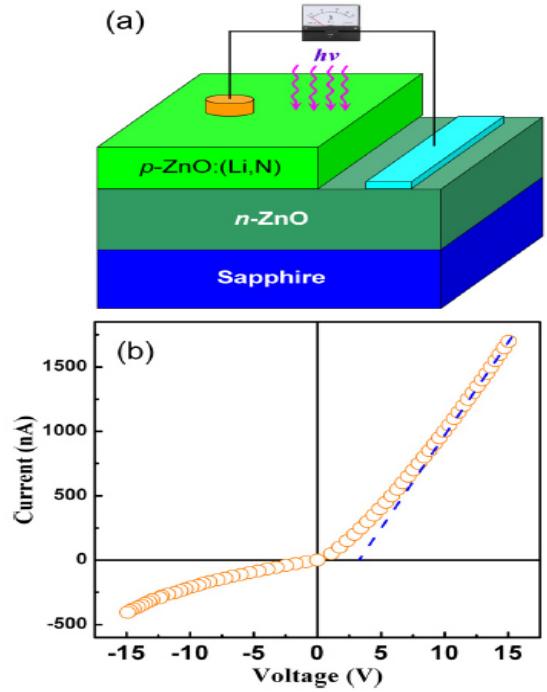

(a)

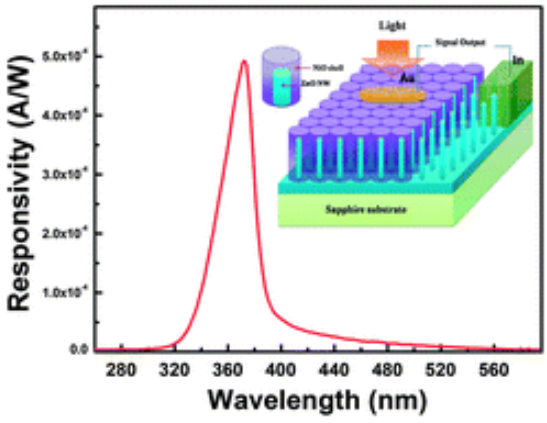

(b)

Figure II.7: **(a)** Schematic of the ZnO-based self-powered photodetector and its photoresponse [12], **(b)** UV photodetectors based on n-ZnO/p-NiO core-shell heterojunctions responsivity [40]

Even though the enormous advancement that has been made in this novel field of self-powered UV photodetectors, the deployment of these structures remains very far and needs much more efforts. This is because of the very low responsivity and sensitivity associated with the developed self-powered designs. Moreover, the elaboration of p-type ZnO is considered extremely challenging [12]. For these reasons, new efficient approaches should be proposed in order to enhance the device performance at zero bias conditions, which constitutes one of the objectives of the thesis work presented in latter chapters.

II.5.1.4. Plasmonics enhanced UV photodetectors

As it is above mentioned, integrating optoelectronic devices with the actual nanoscale electronic still face interconnection problems. In other words, the scale of silicon-based photonic devices with high data transfer speed is limited to micrometric scale. In this framework, it has been very difficult for nanoscale UV photodetectors to provide a tunable response. As a candidate technology, the introduction of metallic nanostructures can cause Surface Plasmon Resonance effect (SPR), which can eventually provide wider possibilities for bridging the gap between the worlds of nanoelectronics and microscale optoelectronics [41-43].

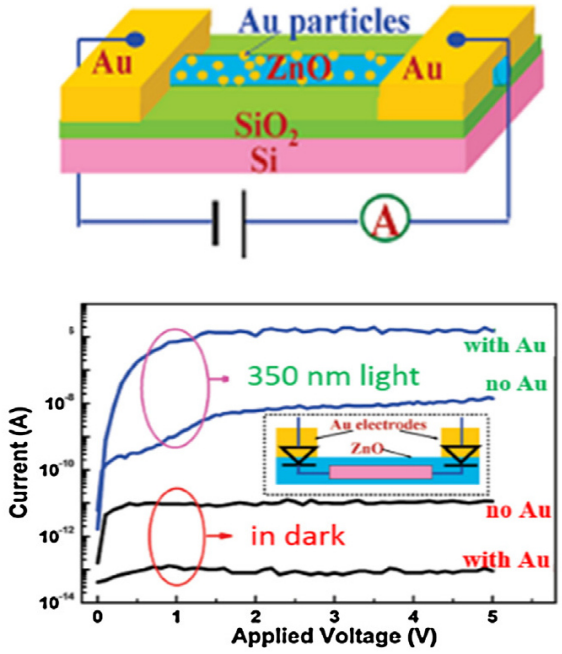

Figure II.8: High improvement of the performance of ZnO nanowire photodetectors by Au nanoparticles [44]

In fact, SPR is fundamentally described as oscillations of free electrons at the metal/semiconductor interface. The incident photons that are in resonance with the oscillation frequency associated with the free electrons can be absorbed and thereby accelerated. This provides the ability for enhancing the device performance. Figure II.8 describes a UV photodetector that includes metallic nanoparticles, where the photogenerated carriers can be increased. As a result, several researchers are focused on the performance enhancement of the photodetector responsivity by introducing metallic nanostructures. For example, a new ZnO nanowire based UV-photodetectors with gold nanoparticles was proposed, where great enhancements regarding response speed and dark current were achieved [44]. In a similar manner, GaN UV photodetectors with silver nanoparticles can provide favorable photoresponse as it is reported in [45].

II.5.2. Phototransistors

II.5.2.1. Why phototransistors?

Evidently, the substantial reduction of the capacitance associated with both photodetector and the followed transistor offers the possibility of decreasing the energy/bit ratio. The connecting wire between photodetector and first transistor plays an important role in determining the global photoreceiver capacitance, where increasing the wire length could increase the capacitance. Alternatively, getting rid of this wire can reduce enormously the capacitance. For this purpose, integrating the first stage photodetector with the second one can provide the opportunity for achieving high-performance photoreceivers with reduced capacitance. This task can be realized by using phototransistors, which is described by a monolithically integrated version of the photodetector and transistor.

On the other hand, monolithic co-fabrication of photonic and electronic devices is considered of paramount significance to realize high-performance chip-level communication. In fact, discrete components such as photodetectors and photodiodes cannot be integrated. This imposes the search for alternative platforms where photonic devices and CMOS electronics can be successfully integrated. Silicon photonics technology has confirmed its effectiveness for providing a good platform for optoelectronic devices monolithic integration [46]. The main idea behind this technology is to develop a diversity of photonic components elaborated on a SOI wafer that can be compatible with CMOS-based technology. This allows developing high-quality photonic chips for high-performance optical communication applications. In this

regard, phototransistors as photoreceivers devices are foreseen as alternative photonic components that can reproduce the function and performance of their discrete counterparts [47-50]. For this reason, phototransistors are expected to be suitable for building high-performance photoreceivers.

II.5.2.2. Operating mechanism of phototransistors

In a similar manner to photodetectors, phototransistors are defined as semiconductor devices that can receive an input optical signal, and convert it to an electrical current. However, the main deference between them resides on the fact that the phototransistor provides the amplification task by using transistor action which is not available with photodetectors. There are various phototransistor structures, which closely imitate the metaphor of the diverse designs of existing transistors: photo-JFETs [50-51], photo-MOSFETs [51-52] and bipolar phototransistors (BPTs) [53-54]. The basic working mechanisms associated with these different phototransistor designs is described in what follows.

II.5.2.3. Bipolar phototransistors

The bipolar-based phototransistor is not a new idea since it was proposed for the first time by Shockley in 1951 [55]. In this perspective, the first BP-phototransistor was elaborated using germanium material for infrared detection [56] and after that extended to heterojunction design by Kroemer [57]. These structures were previously considered to be very complex at the manufacturing level. However, the recent advances regarding fabrication technology coupled with the eventual integration of silicon photonics with industry-standard CMOS can pave the way for the elaboration of these devices, which makes them promising candidates for modern optical communication systems.

BP-phototransistors operate using the same mechanism associated with the electrical bipolar transistor. The only difference is that an additional optically induced current will be generated under illumination. Basically, for the electrical bipolar transistor, we reverse biased the base-collector junction and forward biased the emitter-base junction. The photocurrent occurs from the absorbed photons in the base-emitter depletion region, where electron/hole pairs will be generated and separated by the strong electric field as it is shown in Figure II.9. As long as the width of the base region is lower than the electrons diffusion length, electrons will diffuse through the base region and immediately swept to the collector region and create the photocurrent. Meanwhile, the photo-generated holes are accumulated at the emitter region. Since the

photocurrent generation in the BJ-based phototransistor is dominated by the photo-generation mechanism in the base-emitter junction, it is essential to take the emitter to base doping ratio as large as possible to achieve the dual role of superior gain and increased photogenerated electron/hole pairs.

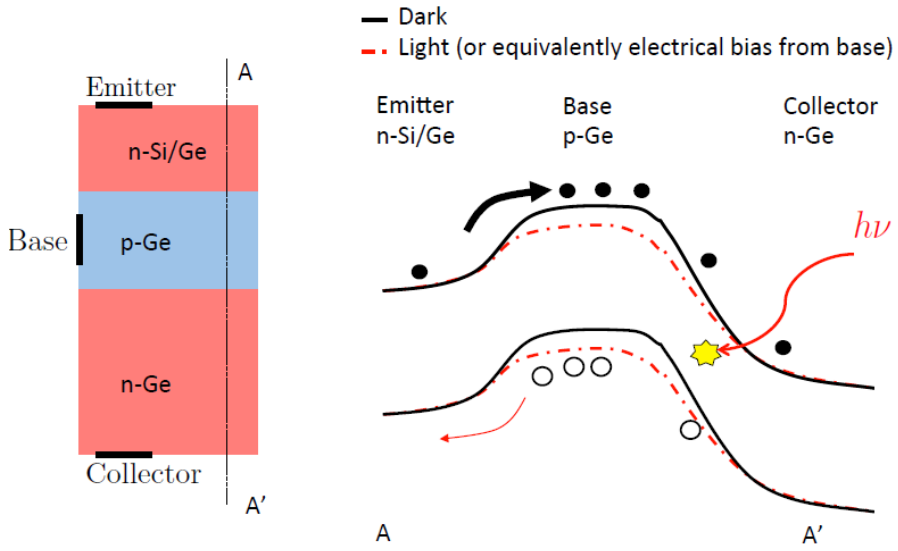

Figure II.9: BP-phototransistor schematic and its band diagram with and without illumination.

II.5.2.4. JFET-based phototransistor

The most common photo-JFET structure is presented in Figure II.10, it consists of a Ge/Si heterojunction photodiode integrated with a field-effect transistor. The device is made of a JFET and a floating photosensitive germanium gate, where near-infrared light can modulate the channel conductance behavior. In other words, the electrons created by the absorbed photons in the germanium gate can induce an optical voltage. The latter modulates the channel depletion region of the JFET, as shown in Figure II.10.

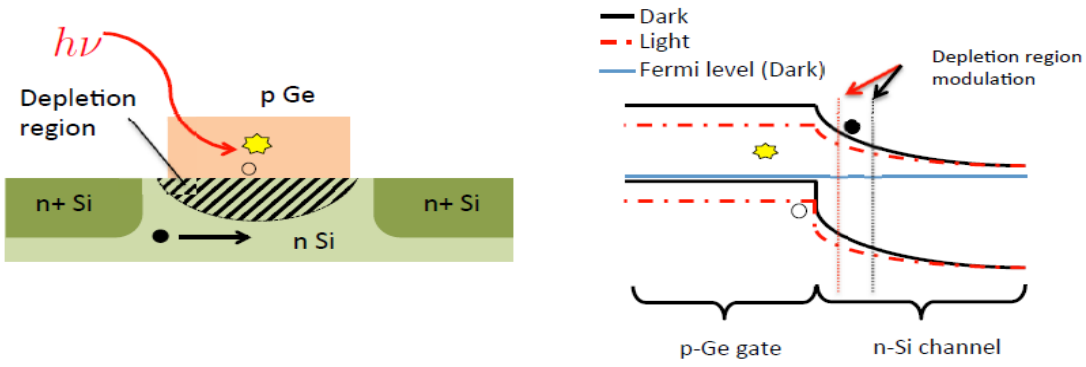

Figure II.10: Photo-JFET schematic and band diagram of a cross section of the device with and without illumination

Consequently, the JFET-phototransistor can turn on by simply illuminating the Ge photosensitive gate or turns back off through the recombination effect.

II.5.2.5. Photo-MOSFET photoreceivers

Basically, the photo MOSFET structure is another type of phototransistor design which was investigated during the last few years [51-52]. The FET-based phototransistor design involves the use of the conventional MOSFET structure combined with a Ge ultrasensitive layer as a gate contact instead of a metallic contact. In order to obtain an initial band bending between the Ge photosensitive layer and the silicon channel, the semiconductor in the gate should be doped with an opposite type of that of the channel. Moreover, the photo MOSFET design is illuminated at normal incidence with a monochromatic light at the wavelength value of 1.55µm. Figure II.11 depicts the photo-MOSFET device and the band-diagram with and without illumination. The operation principle of photo-MOSFETs dwells on modulating the channel conductivity using an optical excitation. The incident light creates electron/hole pairs in the Ge gate. These pairs will be separated by the electric field caused by the deference of the voltage applied at the gate terminal. The holes are accumulated at the Ge/SiO_2 interface which leads to modify the channel bending and thereby increasing the source to drain current. On the other hand, the device turns off as the photogenerated carriers recombine in the Ge photosensitive gate.

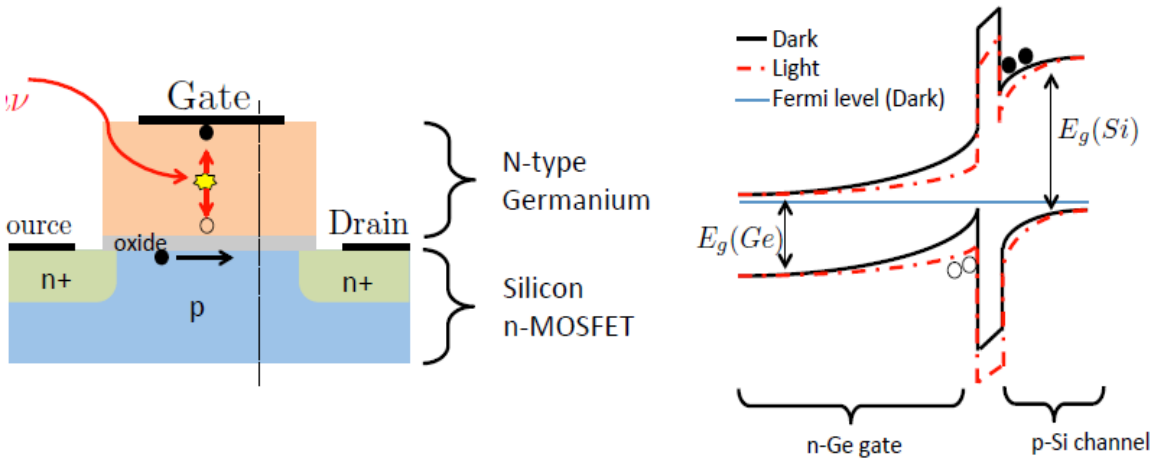

Figure II.11: Photo-MOSFET schematic and band diagram of a cross section of the device with and without illumination

II.6.Photovoltaic energy

Solar energy is gaining much attention in order to meet the world's increasing energy requirements and to displace fossil fuels as the dominant energy source [58]. In fact, the development and deployment of photovoltaic energy is found face to an essential problem mainly related to cost/efficiency ratio associated with the solar cell [59]. In order to make the solar cell energy competitive with other sources, photovoltaic technology should be able to produce lower electrical power cost or at least closely comparable to the actual energy resources. Fossil-fuel combustion and industrial processes induce global emissions of CO_2, which makes the search for alternative carbon-neutral sources such as photovoltaic renewable energy a primordial priority [60]. The first generation solar cell technology was based on conventional silicon material. In this perspective, silicon solar cells have dominated the market due to their relatively high conversion efficiency of 25.6%, which is approaching to the theoretical limit of 31% [61]. The second generation of the photovoltaic technology is mainly related to thin-film technology, where its efficiency is lower than that of first generation cells, but its cost-effectiveness property outweighs this weakness. In this regard, copper indium gallium selenide (CIGS) and cadmium telluride (CdTe) based thin-film technologies are gaining a considerable interest due to their improved efficiency of 21% [62-65]. One of the major drawbacks of CIGS technology is the use of rarer materials such as indium and Gallium. The economics of constituent elements have raised concerns about the scalability of CIGS-based solar cell to the terawatt intensities required for the world's energy consumption. On the other hand, Kesterite solar cells seems potential to avoid the above outlined issues associated with the CIGS technology by using earth abundant materials such as copper, zinc, tin, selenium and sulphur.

Following the continuous progress regarding the solar cell cost/efficiency ratio, researchers are looking for the third generation of the photovoltaic technology. The latter technology aims to recording superior efficiencies than that expected by the single-junction cells theoretical limit. This objective can be achieved by means of reducing the reflection effects, thermalization losses and recombination related degradations, while keeping up the cost-effective property. Numerous techniques like multi-junction solar cells [66], intermediate band solar cells [67], multiple carrier excitation [68], have been exploited to achieve the broadband absorption characteristic. However, achieving a good efficiency-cost trade-off seems challenging and requires

further efforts. Therefore, new approaches and design methodologies should be developed in order to achieve high performance solar cells at low elaboration cost.

It is to note that in our thesis work we have concerned at studying the thin-film solar cell technology.

II.6.1. Why thin-film solar cells?

Fundamentally, crystalline silicon based photovoltaic devices requires tens of microns thick absorber layer to achieve an acceptable conversion efficiency. On the other hand, solar cells with thinner absorber layer are in fact of great interest since they provide several benefits, however with the obvious drawback of lower light absorption. In fact, if the absorption losses associated with the thin-film solar cell can be avoided, this technology could subsequently offer the following advantages:

- ✓ **Cost reduction:** using thin-film technology can open up the route for decreasing the overall cost of the photovoltaic device. Furthermore, reducing the absorber region thickness could also decrease both the quantity of precursor gas required for the material growth and reactor run time for each device.
- ✓ **Flexibility:** thin-film materials can be flexible, however, a crystalline wafer is considered extremely fragile and can be broken or even fissured if it is used inappropriately. This pinpoint a new path toward numerous new applications that otherwise would not be practical with crystalline-based solar cells. For instance, a flexible module provides the opportunity for developing convenient charging station, where it can be rolled out or stored suitably as it required.
- ✓ **Enhanced V_{oc} and conversion efficiency:** bulk recombination effects are considered as the most pronounced issues that affects the crystalline solar cell efficiency. However, thin-film solar cell offers the possibility for reducing the recombination effects. This can in turn reduce also the dark current and subsequently increase the open circuit voltage. Thus, thin-film technology could reduce the total recombination within the device that can improve the solar cell conversion efficiency.

Therefore, several advantages can be gained by using the thin-film technology including cost-effectiveness and enhanced operating voltage. However, significant efforts should be devoted to this technology in order to maintain the photocurrent values associated with the first generation photovoltaic systems.

II.6.2. Basic operating mechanisms of thin-film based solar cells

Solar cells are basically considered as optoelectronic devices designed to convert energy captured from the incident light into electrical power. The majority of the conventional solar cells consist of conveying the sunlight to the moderately p-type doped base layer, designed to be the region in which the incident photons can be absorbed. Whereas, a thin heavily doped emitter at the front of the cell is considered to form a p/n junction with the base region. This junction behaves like an electron/hole pair's separator, where the built-in electrostatic field plays an important role in separating photogenerated carriers. Basically, the photovoltaic cell is mostly composed of two semiconducting layers with different doping types (n and p), where a potential difference can occur between both p-type and n-type semiconductors. This built-in potential induces a depletion region or a space-charge layer in which the photogeneration effect will takes place. There are four basic processes that govern the photocurrent generation and collection in the standard p-n junction solar cell:

- **Generation**: this process describes the absorption mechanism of the incident sunlight by taking advantage of the photovoltaic effect, where photons with energy above the material band-gap can be harvested inside the active region according to the Beer-Lambert law resulting in electron/hole pair's generation.
- **Diffusion:** Both generated electrons and holes carriers can diffuse respectively from the vicinity of the n-type and p-type regions towards the depletion region, where the built-in electric field sweeps them away. In an ideal solar cell, the diffusion length of minority carriers is large enough to achieve the space-charge region.
- **Drift mechanism**: the photogenerated carriers within the depletion region are separated and driven by the electric field, where electrons are accelerated towards the n-type layer, while holes are conducted to the p-type semiconductor.
- **Recombination**: this process illustrates the fact that photogenerated carriers can recombine near the surface, in the semiconductor bulk or even at the interface if there are interfacial defects, which is the case for heterostructure based solar cells.

These processes that contribute to the photocurrent generation are shown schematically in Figure II.12, where the electric field can be generated between both n-

type and p-type semiconducting layers or even between dissimilar materials if the solar cell is considered with a hetero-junction structure.

The conversion efficiency associated with the photovoltaic device constitutes the most important metric performance that determines the solar cell capability for providing electric power. In this regard, the solar cell efficiency is defined as the ratio between the generated power density and the optical incident one. In this context, Current-Voltage (I-V) characteristics which are typically representations of a diode under both dark and illuminated conditions can be described as it is shown in Figure II.12 (b). Under light, a power-producing region is clearly observed in this figure, where the maximum power operating point P_{max}, is calculated from the product of the photocurrent and voltage.

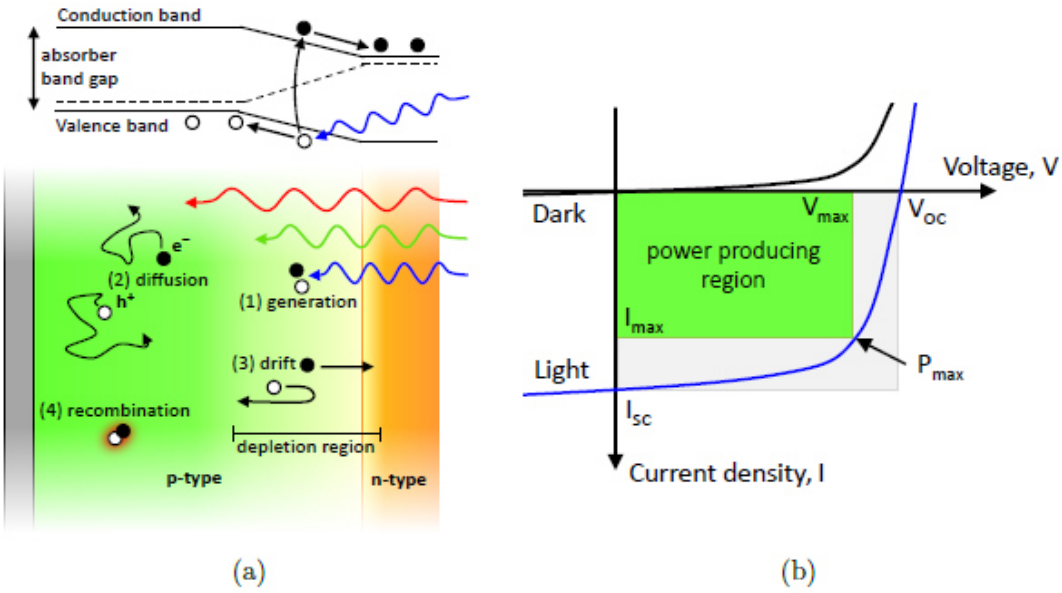

Figure II.12: **(a)** Illustration of the main charge carrier processes in a conventional p-n junction solar cell, **(b)** I-V characteristics of a p-n junction diode under both dark and illuminated conditions.

Besides, there are other performance parameters that can be extracted.

- The open-circuit voltage is the intercept of the I-V curve under illumination with the voltage axis. This parameter indicates the barrier height of the solar cell and enables evaluating the quality of the cell surface and interface, where voltage losses can be induced by severe recombination effects. In other words, a low V_{oc} is often indicative of low quality material or other defects at the interface or even at the solar cell surface.

- The short circuit current is described as the I-V characteristic intercept with the current axis as indicated in Figure II.12 (b), which describes the photovoltaic device ability for generating and collecting carriers. This performance parameter depends on the material band-gap and in large extent on the interface quality.
- Finally, the fill factor represents the ratio between both the maximum achievable power and the optically produced power. This parameter is affected by sources of loss such as series and shunt parasitic resistances.

Eventually, these performance parameters are detailed in latter chapters of this thesis in which they are used to evaluate the proposed thin-film solar cell designs.

II.6.3. Kesterite-based thin-film solar cells

Since this thesis focuses mainly on the enhancement of the CZTS thin-film solar cell, we describe the concepts regarding advantages and the recent progress associated with this photovoltaic technology. In this perspective, the idea behind the CZTS-based thin-film solar cells resides on the capability of the quaternary compound of copper-zinc-tin-sulfide to meet two essential aspects required for high efficiency solar cells [14]. The first one relies on the direct nature of the material band-gap with tunable value of 1.45eV and the other is associated with the high absorption coefficient of CZTS material [14-15]. This emphasizes that a thinner absorber layer less than few microns is able to suitably absorb the incident sun-light. A scheme of the typical CZTS solar cell stack is illustrated in Figure II.13. The solar cell back contact is made of soda lime glass (SLG) coated Molybdenum. At the front interface, a CdS (n-type) that acts as a buffer layer is deposited on the CZTS (p-type) absorber layer, which results in forming a p-n heterojunctions structure that enables efficient carrier separation. The top contact is performed by deposition of aluminum-doped ZnO (AZO) as a perfect Transparent Conductive Oxide (TCO). Finally, metal contact grid is deposited at the cell surface.

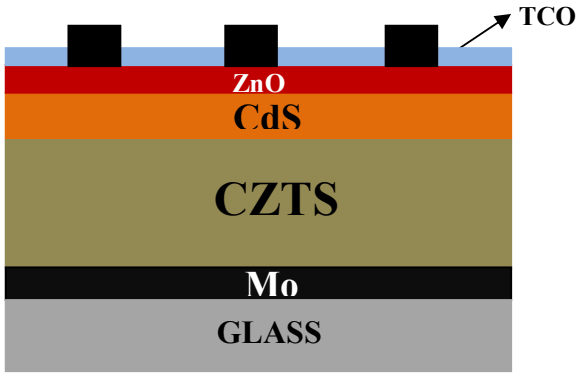

Figure II.13: Conventional CZTS-based solar cell architecture.

II.6.4. Recent progress of kesterite-based solar cells

As a matter of fact, the first evidence of the photovoltaic effect in CZTS heterojunctions was demonstrated in 1988 [16], where a CZTS thin-film was deposited by atom beam sputtering technique. This material has attracted a great deal of attention in order to develop effective absorber layers, which has led to huge progress regarding the CZTS-based solar cell technology. In 2008, a Japanese research group has proven that a conversion efficiency value of 6.7% can be reached by using a CZTS absorber layer deposited by co-sputtering technique [17]. After three years, IBM group has demonstrated a rapid enhancement, where co-evaporated CZTS thin-film can offer 8.4% of conversion efficiency [18]. In 2014, a relatively high conversion efficiency of 9.2% has been reported [69]. By May 2014, IBM has stroked the current world record regarding CZTS-based solar cell, achieving a 12.6% of conversion efficiency by using a S*e*-alloying structure [70]. In spite of this rapid improvement, reaching the CZTS-based solar cells theoretical limit (30%) remains still far and requires further improvements [19].

II.6.5. CZTS solar cell deposition methods and record efficiencies

As a matter of fact, in spite of the improved efficiency of the CZTS thin-film solar cell (12.6%), the low V_{oc} values is considered as the principal limiting factor for achieving further efficiency enhancement. The reported V_{oc} values remain still far from the theoretical limits, which is mainly due to several effects associated with the fabrication process [19]. In addition to the presence of states in the band-gap, the high density of defects can reduce the carrier lifetime which could affect the output voltage. Moreover, the inappropriate band-alignment between both buffer and absorber layer induces the formation of interfacial defects that cause huge recombination losses. The elaboration process therefore plays an important role in determining the CZTS solar cell efficiency [70]. The fabrication steps are illustrated in what follows, where the well-known 'sequential process' is widely used for preparing the CZTS solar cell [71]

- **Cutting and cleaning:** the standard substrate used for the kesetrite solar cell is soda lime glass with sputtered molybdenum as back contact. The substrate is first cut into smaller parts of 5cm × 5cm. After that the molybdenum surface is appropriately cleaned in order to avoid the formation of MoO_3 oxide.
- **Electron-beam deposition of metal precursors:** usually CZTS solar cell is elaborated using the so-called sequential process. The latter technique consists

on the sequential evaporation of metals onto the Mo surface. The stack of the deposited materials should be in the order presented in Figure II.14. The evaporation of the metals can be performed using the electron-beam deposition technique in a vacuum chamber at a pressure around 10^{-6} mbar.

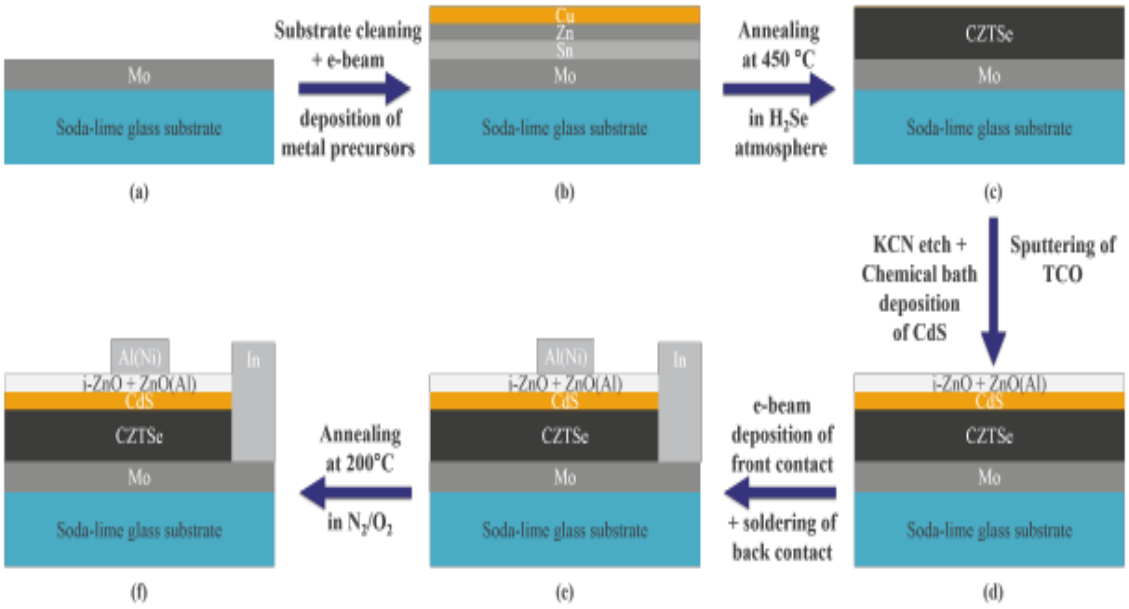

Figure II.14: Schematic representation of the general elaboration steps followed for the fabrication of the CZTS-based solar cell

- **Annealing in a Selenium atmosphere:** Substrates were then annealed at about 500°C in H_2Se gas atmosphere. A chemical reaction is done between the metals and H_2Se that results in the formation of $Cu2ZnSnSe_4$ material. A similar supply of H_2S is also useful for depositing $Cu2ZnSnS_4$ material.
- **KCN etch:** this step is used to remove undesired binary compounds formed at the surface during annealing in the H_2Se atmosphere.
- **Chemical bath deposition of CdS:** the deposition of the CdS n-type buffer layer can be carried out by means of the standard chemical bath deposition technique to get approximately 60 nm.
- **Sputtering of TCO layer:** combined ZnO and Al-doped ZnO are generally sputtered on top of the CdS layer. It should be noted that anti-reflection coating based on MgF_2 material could be also deposited on the top of the CZTS solar cells.

- **Front and back contacts:** the front and back contacts can be created using Ni /Al/Ni structure elaborated using e-beam deposition and shadow masks at the top, while the back contact is made of the molybdenum material.
- **Annealing of completed cells:** to finish, the CZTS solar cell will be annealed for the second time in an N_2 or O_2 atmosphere, where the main objective behind this step is to improve the quality of the deposited materials.

The right choice for the CZTS absorber layer deposition technique can be beneficial for improving the solar cell performance. As such, several deposition techniques are used to grow the CZTS active region, where hydrazine-based pure solution approach has demonstrated the ability for achieving the actual record efficiency. The cross-sectional view SEM images of a CZTSSe film to the 12.6% record device is shown in Figure II.15.

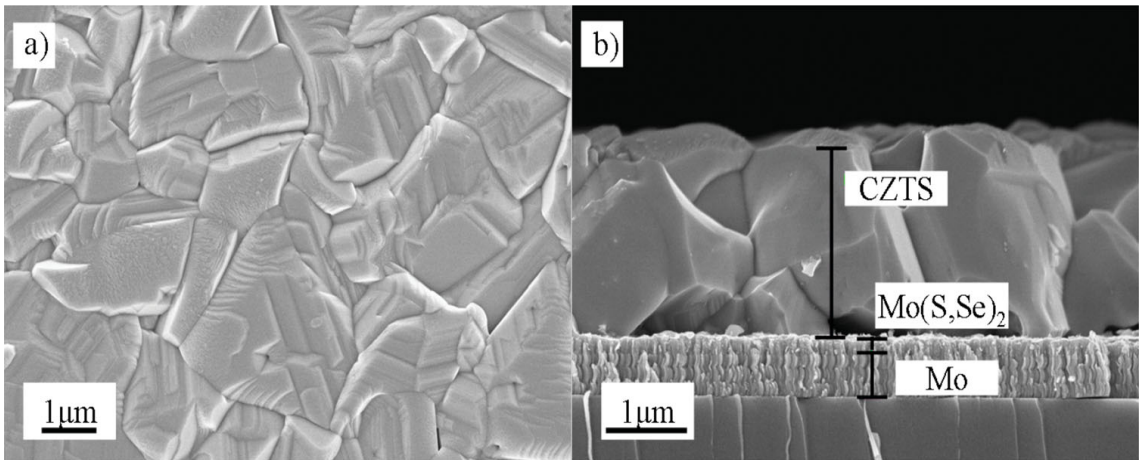

Figure II.15. Top-view and cross-sectional view SEM images of the CZTSSe-based solar cell device with 12.6% record efficiency [70].

Table II.1 Selection of top record efficiencies for CZTS based solar cell.

Material	Elaboration technique	Efficiency [%]	V_{oc}[mV]	J_{sc}[mA/cm^2]	FF [%]	Group
CZTS	Spin-coating	12.6	513.4	35.2	69.8	IBM [70]
	Spin-coating	12.3	471	37.1	70.3	IBM solar-frontier [72]
	Stacked metals	11	516	34.1	62.5	IBM solar-frontier [69]
	Spin-coating	10.5	480	35.7	61.5	EMPA [73]
	Co-evaporation	11.6	423	40.6	63.3	IBM [74]
	Ultrasonic spray	9.5	460	33.2	62.3	Hillhouse group [75]

In order to get a global idea about the impact of the deposition technique on the solar cell performance, Table. II.1 summarizes the state of the art of the word efficiency records and the deposition techniques used for the elaboration of the CZTS layer for each case.

II.7. Conclusion

In this chapter, different optoelectronic devices have been described and their operating mechanisms, advantages and challenges were briefly discussed. We have also presented a review of the actual photoreceiver structures based on various technologies (2D materials, self-powered designs and Plasmonic-based sensors). This has helped to identify some undesired effects and challenges related to the photorecievers optical behavior. On the other hand, thin-film solar cells based on CZTS compounds have been presented, where the recent progress and challenges associated with this technology are described. To conclude, we can emphasize that Kesterite solar cells are extremely interesting in spite of the cost-effectiveness property they offer, while the major problem resides on the optical and recombination losses that prohibit achieving promising efficiency values.

Chapter III

Metaheuristic Techniques

***Abstract:** this chapter focuses on presenting the general concepts and description of various metaheuristic techniques. The basic working of several optimization approaches such as genetic algorithm (GA), Particle Swarm Optimization (PSO) and its quantum derivative termed (QPSO) is exhaustively provided. An overview of multi-objective optimization approaches in also presented in this chapter. Finally, the latter explores the potential application of these metaheuristic techniques to boost up the performance of various optoelectronic devices.*

III.1 Introduction

Nowadays, extensive limitations have been encountered to solve many real-life global optimization problems in diverse fields such as engineering, industry, science, and economics [76]. As such, local optimization approaches face many difficulties in solving global optimization challenges [76-78]. The major reason behind the failure of classical optimization techniques dwells on the fact that they can easily be entrapped by local optima solutions [79]. Moreover, it seems to be very difficult to accurately solve the optimization issues within a reasonable amount of time. On the other hand, global optimization approaches can be effective to overcome these concerns [77-79]. In this context, a great deal of attention has been paid to emerge some innovative artificial intelligence tools in the field of the optimization [78-80]. For instance, metaheuristic-based techniques play a central role in treating many engineering problems, which contain usually multiple-conflict goals. For this purpose, these techniques have drawn much interest in order to deal with global optimization difficulties [79-81]. In this chapter, an overview of metaheuristic-based optimization methodes is presented. The chapter is organized as follows: firstly, we provide an overview of optimization techniques. Metaheuristic algorithms and their classification are also provided. In addition, a review of several metaheuristic approaches related to the thesis work and their basic concepts is outlined. Accordingly, genetic algorithm (GA) and particle swarm optimization (PSO) techniques and also quantum particle swarm optimization are discussed in details. The last section of this chapter is devoted to introducing some basic concepts about the application of these metaheuristic approaches in optimizing new optoelectronic devices, which constitutes one of the major objectives of this thesis.

III.2 Global optimization and heuristic algorithms

The global optimization approaches can be categorized into exact and heuristic. The main difference between them depends on the ability to guarantee an optimal solution. In exact methods, random factors are strongly involved, where they can converge toward a global optimum under specific conditions; however, the accurateness of the obtained solution may not be identified with precision [82]. Exact approaches need detailed access to the global information associated with the considered problem. In this context, these methods have confirmed their capability to find an optimal solution [83]. However, from a computational point of view, exact approaches are very expensive

regarding the computation time and alternative methods are in fact required in order to efficiently solve very complex optimization problems [81-83]. In computer science, there are two essential objectives, which algorithms have to achieve: solution quality whether good or optimal and provable short computational times [84]. In the last few years, heuristic methods have attracted more attention, where the major benefit of these techniques resides on sacrificing the identification of the optimal solution in order to obtain a good solution in a very short runtime [82-84]. In other words, these algorithms can easily find near-optimal solutions in a very short time, although without being able to guarantee either feasibility or optimality. The main advantage of heuristic methods is mainly associated with their strong ability to deal with complex problems. This makes them suitable to deal with difficult global optimization problems and even decision-making issues.

III.3 What is a metaheuristic technique?

As a matter of fact, heuristics are a problem-dependent technique, which means that they can solve the global optimization problem meanwhile they try to take benefits of the particularities of the treated problem [84]. However, they usually get trapped in a local optimum and thus don't succeed in obtaining a global optimum solution. On the other hand, metaheuristics are high-level problem-independent algorithmic frameworks that offer a set of guidelines or strategies to develop heuristic optimization algorithms [85-86]. In fact, the term metaheuristic was first proposed by Glover [87], which derives from the combination of two Greek words. In this context, heuristic originates from the term ''heuriskein'' which means to find, whereas the prefix ''meta'' means ''beyond''. Metaheuristic algorithms include well-known techniques, where some of them imitate successful mechanisms found in nature. There are several metaheuristic algorithms that have proven their effectiveness to deal with global optimization problems such as Genetic Algorithms evolutionary technique (GA) [88], particle swarm optimization (PSO) [89], Simulated Annealing (SA) [90], Tabu Search (TS) [91], Artificial immune system [92], Scatter Search (SS) [93], etc. In general, metaheuristic-based approaches are not problem specific and involve efficient strategies to effectively avoid being trapped on local optima. The main advantage of metaheuristic-based techniques dwells on making a good trade-off between intensification and diversification of the search mechanism. Intensification refers to focusing the search into certain regions of the search space to find out good quality solutions, whereas

diversification means the exploration of unvisited regions of the solution space. Bridging the gap between diversification and intensification seems of great importance in order to quickly identify regions with high-quality solutions.

III.4. Classification of Metaheuristic techniques

Metaheuristic approaches can be classified according to different aspects which are usually related to how these approaches operate over the multi-dimensional space during the search process [94-95]. Some of these aspects are discussed as follows:

- Nature-inspired techniques: The continuous increase in the size of the problems search space and the need of processing in short runtime has led to explore the potential for solving global optimization problems using nature-inspired metaheuristic techniques [96]. The latter approaches imitate the metaphor of natural processes such as evolutionary algorithms, artificial immune systems, particle swarm optimization and simulated annealing techniques.
- Deterministic or stochastic: the metaheuristic approaches that make deterministic decisions to deal with a global optimization problem are defined deterministic techniques (local search and tabu search approaches). On the other hand, the main idea behind stochastic metaheuristic techniques like, simulated annealing and evolutionary algorithms, relies on the randomization aspect, where random rules govern for the global search of the solution.
- Iterative or greedy techniques: Most of the metaheuristic approaches are iterative algorithms. Mainly, the initial population of solutions will go through some search operators, which reproduces for each subsequent iteration. While greedy algorithms counterparts start from an empty solution and make a decision at each step that depends on the considered problem until reaching a good solution.
- Single-solution or Population-based search approach: basically, this aspect constitutes the most commonly used concept for metaheuristic techniques classifications [97]. In single-solution based algorithms, the exploration of the search space is made by means of a single solution, which offers wider possibilities to focus the search in local regions. Simulated annealing and Tabu search are typical examples of single-solution based methods. These methods generally enable moving to worse solutions to be able to escape from local optima. On the other hand, a wide population of solutions is developed during

the search process in population-based algorithms, which leads to an outstanding capability for the diversification in the whole search space. The most common examples of population-based methods are genetic algorithms, particle swarm systems, cultural algorithms, etc.

As it is above outlined, the population-based metaheuristic techniques invoke a set of many solutions at the end of each iteration. In this context, in the thesis work, we have exploited this class of algorithms in order to optimize various optoelectronic devices. For this purpose, we highlight the principles of genetic algorithm and particle swarm optimization methods as an example of population-based metaheuristic techniques exploited in our work.

III.5. Genetic Algorithms

A genetic algorithm as a subfamily of evolutionary algorithms is defined as a stochastic global search method that seeks to mimic the species genetic evolution and the abstraction of Darwinian evolution [88]. Particularly, GA reproduces the natural selection of biological systems that enable the consecutive generations in a population to adapt to their environment. Basically, the population of potential solutions is generated using GA, in which the principle of survival of the fittest is applied in order to hopefully produce better approximations to a good solution. As it is aforementioned, GA categorizes in population-based metaheuristic technique class. Some research works go back to the middle of the 1960s in order to present the GA of Holland [88] in 1975. However, before the GA multipurpose presentation provided by Goldberg [98] in specific fields such as machine learning, GA was rarely applied. However, in the last few years, GA has become the most typically used metaheuristic technique to deal with global optimization problems [98-100]. The GA optimization does not require information or other internal knowledge of the treated problem, which constitutes their major advantage. This implies that these algorithms are typically black-box methods that use only fitness information, where the ultimate objective is to find the optimal solution, with respect to one or even more criteria.

Traditionally, chromosomes constitute the main elements of the GA population. The chromosome is constituted from variables, which are assigned as genes. Moreover, a fitness function describing the objective of the optimization procedure should be defined in order to evaluate and rank potential chromosomes in a population. Once the genetic representation and the objective function have been defined, GA proceeds to

initializing a random population. Selection, crossover and mutation operators should be then specified to build the complete structure of the GA procedure. These operators are repetitively applied to enhance the quality of solutions over numerous generations. Generally, the GA finishes when the optimization convergence conditions are satisfied, which are mainly related to the considered maximum number of generations or reaching a satisfactory desired fitness level. It should be noted that, if the condition of a maximum number of generations is adopted, the goodness of the solution cannot be ensured. In the following, more details about GA elements are appropriately discussed. The flowchart of the GA procedure is detailed in Figure III.1.

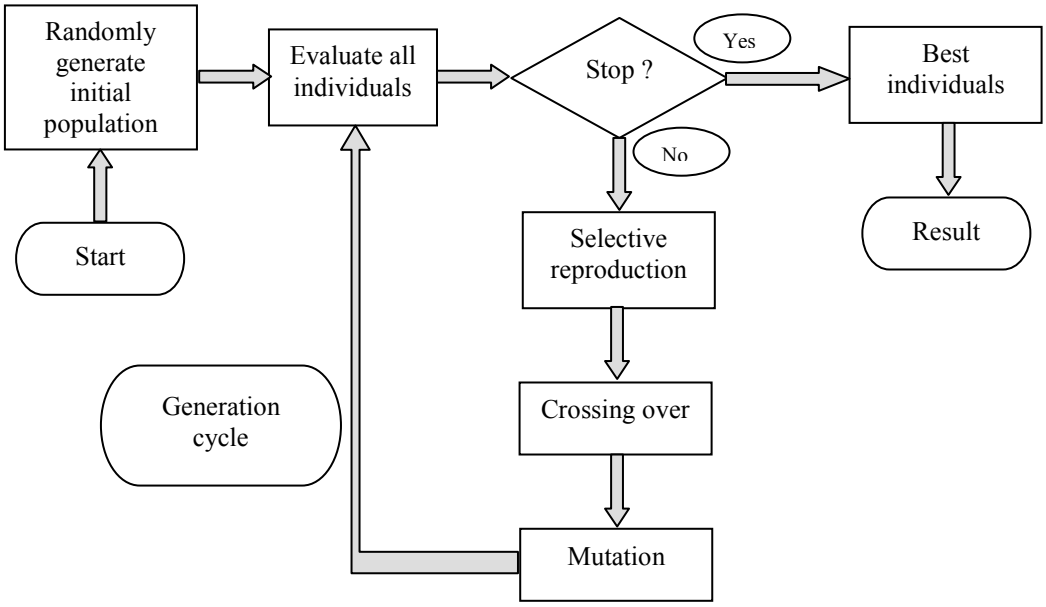

Figure III.1: Flow diagram of genetic algorithm [100]

III.5.1 Fitness Function

The fitness function plays an important role in determining the usefulness of the GA based metaheuristic technique for achieving the global optimum associated with the considered problem. Indeed, the objective function provides sufficient information about the physical problem and links it to the GA algorithm. Moreover, this function must be formed in an appropriate way in order to subserve higher potential solutions than the worse ones. Accordingly, the effectiveness of the genetic algorithm is governed by the fitness function definition and how it assesses the quality of the obtained solution with respect to the overall objectives of the considered optimization problem.

III.5.2 Coding

In the GA procedure, a chromosome includes the information about the optimization problem. In this context, chromosomes and genes are expressed in binary and real forms. This concept represents the coding step of the GA optimization technique. As a matter of fact, the binary form is considered as the ideal way of encoding in which the chromosome is expressed as a binary string. Consequently, the search space is constituted from binary strings through a coder mapping. After that, in order to calculate their objective function values associated with the optimization problem, a decoder mapping is applied to bring the binary gens back to their initial real form. On the other hand, the real coding is considered easy in programming.

III.5.3 Selection

The selection operator basically relies on the probability of selecting an individual in order to be used by the other operators; crossover and mutation. The main idea behind this process resides on giving wider possibilities to individuals with higher fitness function values to be selected over those with lower values. In this perspective, individuals can be chosen by using a fitness-based process, where solutions are probabilistically selected and better ones have greater chances. The success of the GA techniques requires an efficient selection process in which the adopted method is considered of great importance. To this extent, several methods are used to select which individuals should be chosen as parents. Therefore, the most popular selection schemes are given below

- Rank-based selection
- Roulette wheel selection (also known as the fitness proportional selection)
- Tournament selection.
- Elitist selection
- Steady-state selection
- Generational selection
- Hierarchical selection

III.5.4 Crossover

The concept of the crossover operator is based on exchanging the information between selected chromosomes. In this framework, parents are combined in an appropriate way in order to reproduce new children as it is described in Figure III.2. The new chromosome (offspring) may hopefully be better than its parents, where it can take

the best properties from the parents. Crossover operator can be applied with probability P_c, where the process is not typically applied to all individuals. Essentially, the crossover operator plays an important role in GA procedure, where defining a suitable crossover process is highly required in order to reach high-performance GA. Different types of crossover operator are reported [101-102], but the most popular methods are

- One-point crossover
- Two-point crossover
- Uniform crossover

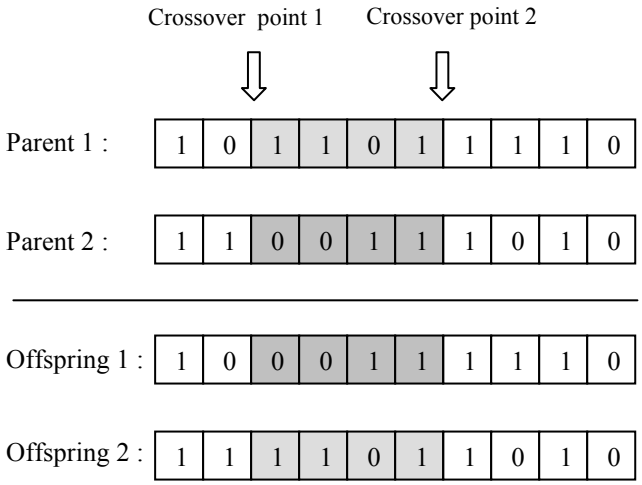

Figure III.2: Two-point crossover operator

III.5.5 Mutation

Basically, in a mutation genetic operator, a randomly chosen gene of the initial chromosome is altered, which leads to form entirely new gene values. This can provide the opportunity for increasing the population diversity, which can pave the way toward avoiding the probability to get trapped in local optima [103]. Moreover, a user-definable mutation probability should be taken into account, where its value is usually kept very low in the range of [0,1]. In binary chromosomes, it consists of flipping random bits of the chromosome as it is illustrated in Figure III.3.

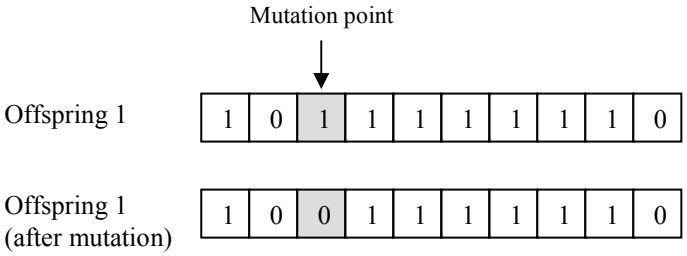

Figure III.3: Mutation Operator

III.5.6 Convergence criteria

As it is above outlined, the basic concept of the genetic algorithm is to repeatedly modify a population of individuals from a generation to another through the application of genetic operators. The stopping of this repetitive process is governed by the convergence criteria, which can be given as follows

- Maximum generations
- No change in fitness
- Stall time limit

III.6. Multiobjective Optimization

When an optimization problem involves more than one objective function, the task of searching one or more optimum solutions is called multi-objective optimization (MO). The MO-based optimization techniques have been exploited in a variety of disciplines to optimize a set of parameters that involve a multi-dimensional space and nonlinear functions [104-105]. Most of the optimization techniques provide one single solution, which explains the appropriateness use of the MO optimization techniques for achieving a population of solutions. It suggests addressing the problems that require the satisfaction of several criteria simultaneously. These criteria are sometimes complementary and sometimes conflicting [106]. One of the aspects characterizing the multi-objective optimization is that it can provide a set of solutions for identifying the best compromise between the considered objectives. In fact, we are usually interested in optimizing more than one metric such as in our thesis work, where the overall optical performance and leakage power concept are targeted. Generally, a weighted sum of the various design objectives, with the weights are based on the objective's significance, is exploited to carry out the global optimization procedure [107]. This approach relies on jointly improving a set of fitness functions by using a linear overall objective function presented as a weighted sum

$$F(x) = \sum_{i=1}^{i=n} w_i f_i \qquad \text{(III.1)}$$

where w_i represents the weight vector that is designed to illustrate the importance of each fitness function f_i.

If we consider each fitness function with a constant weight, the convergence of the global optimization algorithm will be performed by satisfying the objective functions

equally. Therefore, the direction of the optimization procedure in the search space can be fixed as it is illustrated in Figure III.4 (a).

The success of this method depends on the appropriateness of the weighting vector with respect to the desired solution targeted by the designer. However, it is really complex to find out the best weighting vector without knowing the non-dominated solutions. In this regard, the ultimate solution to deal with this problem is through Pareto rank [108]. Figure III.4 (b) shows the Pareto front representation of the MO-based optimization. The determination of Pareto optimum solutions is only the first phase in practical solving of MO optimization problems. An advantage for this technique is that it offers in a second time to the designer the choice to select a solution from Pareto fronts, where it enables making good trade-off between all considered objectives. Accordingly, the choice of a solution relative to another imposes high-level information about the problem and many factors concerning the treated problem inherent complexity.

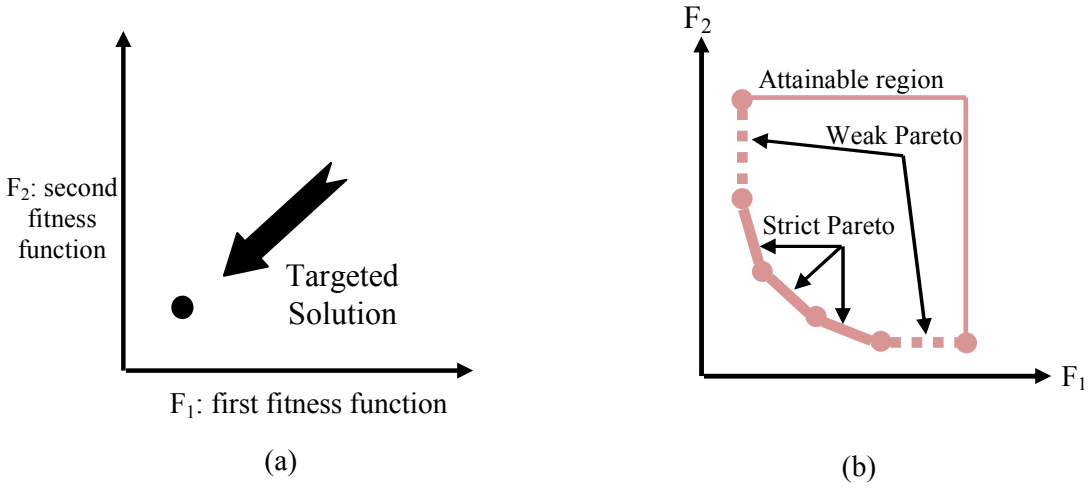

Figure III.4: (a) MO optimization using weighted sum approach. (b) Pareto front optimality

III.7. Particle swarm optimization (PSO)

Originally, PSO technique is a metaheuristic algorithm proposed by Eberhart and Kennedy [89]. Principally, this algorithm reproduces the metaphor of natural social behavior of bird flocking. In this regard, the major advantage offered by this approach relies on the simple mechanism and the capability for identifying optimal solutions

associated with various complex mathematical problems. These outlined characteristics prove the excellent ability and the usefulness of this technique to be adopted to study and optimize diverse of novel microelectronic and optoelectronic devices [109-111].

Basically, the PSO-based approach considers the use of random methods to minimize a well-defined fitness function which allows selecting the global solution of the analyzed problem. Furthermore, both best position of each particle in the swarm (p_{ij}^k) and the best position of the particles group (g_{ij}^k) affect the selection of candidate particles. In other words, The set of particles to which a particle is topologically connected is called neighborhood; defined as local best and global best particles. Thus, the particle in the swarm can interchange the information with every particle belongs to its neighborhood. Moreover, to adjust and update both position and velocity of the suggested particles, the equations inspired from bird flocking behavioral models can be used, which are given by the following equations

$$V_i^{k+1} = wV_i^k + c_1 r_1^k (p_{ij}^k - X_i^k) + c_2 r_2^k (g_{ij}^k - X_i^k) \quad \text{(III.2a)}$$

$$X_i^{k+1} = X_i^k + V_i^{k+1} \qquad \text{with } i = 1..n \quad \text{(III.2b)}$$

where n denotes to the swarm size, the particle position and velocity are presented by X_i^k and V_i^k, c_1 and c_2 represents the cognitive and social acceleration factors; r_1 and r_2 reveal the random numbers, which are picked from the range [0,1], w represents the inertia weight applied to balance the global exploration and X_i^k is the actual position of the particle in the swarm.

In fact, PSO executes searching through moving the particles around the well defined multidimensional search space, where a swarm of particles is updated from iteration to another with the main objective of minimizing the fitness function. In this regard, the swarm particle movement follows the same direction of the previous best (P_{ij}^k) position and the global best (g_{ij}^k) position experienced so far in the swarm. Moreover, the particle velocity given by Eq.2 (a) determines the swarm dynamic in the research space with the aim of constricting the particles velocities in order to limit their flying out of the defined research space. Likewise, there are three basic elements for the computation of the next position of the swarm particle: according to its own velocity, towards it best performance and the best performance of its best informant. The way in which these three vectors are combined linearly via confidence coefficients is the bases

of all the versions of the standard PSO. The three fat arrows represent such combination, which gives the next position of the particle as it is shown in Figure III.5.

The cognitive factors play an important role to control the particles magnitude of attraction toward their local best positions or global best position. In addition, the first part of Eq.2 (b) represents the inertia, which enables the opportunity to control efficiently the particle's momentum by simply weighting the impact of the preceding velocity. On the other hand, the last part of the equation acts as a cooperation component that involves information provided by other swarm particles which represents the particles collaborative effect to identify the global optimal solution.

The interaction of particles with their neighbors governs the effectiveness of the PSO-based metaheuristic technique. As one particle discovers an optimum, it becomes the best in the neighborhood and guides the other particles to itself.

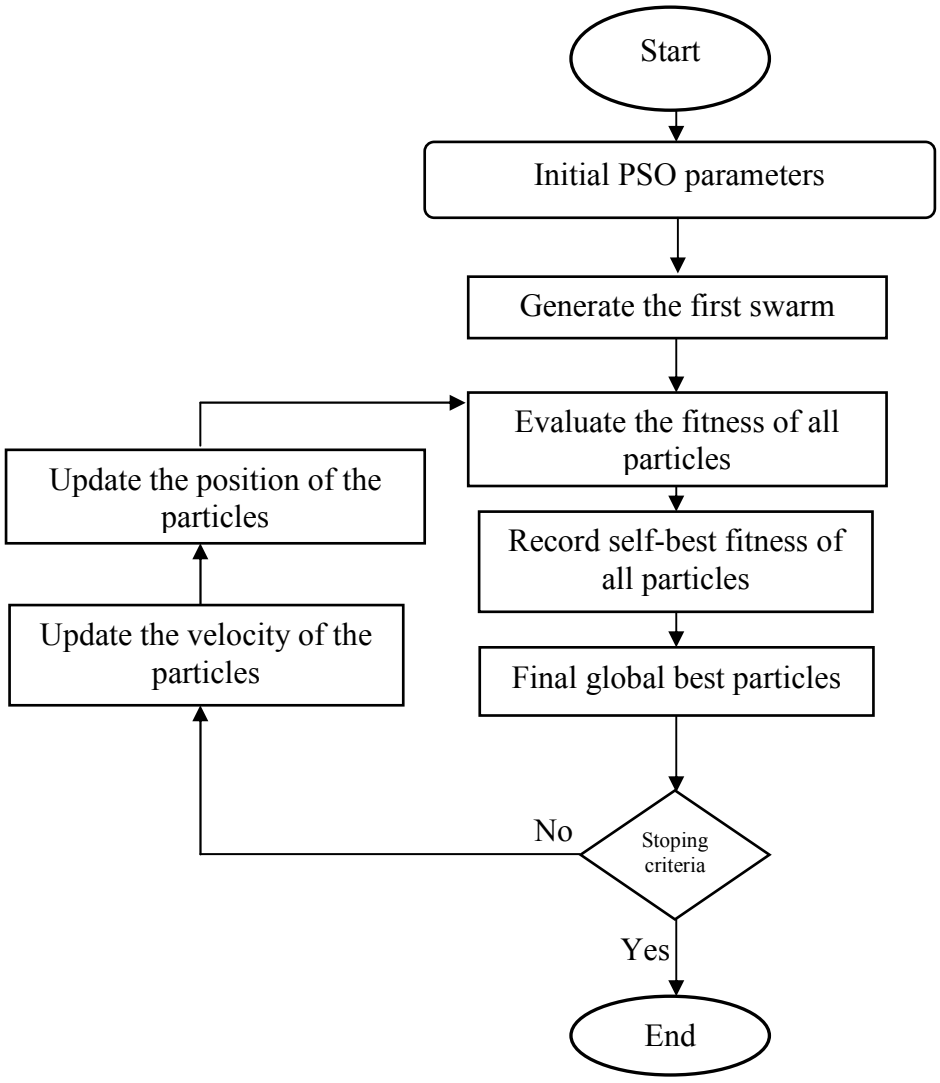

Figure III.5: The Standard flowchart of the PSO-based approach

III.7.1 Strength and weakness of the PSO-based approach

The main strength associated with the PSO metaheuristic technique are listed below

- PSO is considered as self-adaptive approach and not problem-dependent and easy to implement with few parameters to solve a global optimization problem. It can be effectively applied to deal with both simple and complex optimization problems with less computational difficulty.
- The PSO-based technique is considered as an intelligent technique, which implies that it does not require major amendments to adapt it to new problems. Besides, this metaheuristic technique does not need the gradient, continuity or differentiability of the problem to deal with.
- The PSO approach cannot be affected by initial solutions as well as problem dimensionality and can easily be parallelized for simultaneous processing. It provides the benefits of high ability of global search, good accurateness and fast searching speed.

The most pronounced problems of the PSO approach are given as follows

- Contrary to GA, there is no selection process in a PSO method. One of the weaknesses of the PSO-based approach is premature convergence problem and trapping in local optima, where all particles will quickly converge to the position of the global best particle found so far.
- Profound dependence on the settings of cognitive and social learning constants as well as inertia weight
- Blindness and computational inefficiency in the search process, where large weighting factors ranges that are randomly introduced could deviate the particles from the optimal solution regions.
- An increase in the required iterations for reaching the global solution may be induced by taking small weighting factors, which can increase the computational time.

In order to avoid the problems associated with the PSO-based metaheuristic technique, several research works focused on exploring other variants of PSO to improve its performance. In this perspective, Sun et al. [112] have combined the standard PSO algorithm with quantum mechanics resulting in the appearance of the Quantum behaved PSO algorithm called (QPSO).

III.8. Quantum Particle swarm optimization (PSO)

Motivated by the fact that the swarm social behavior is extremely complex to be represented by classical mechanics, researchers have proposed a new metaheuristic technique called QPSO [112]. The latter has modified and enhanced the search approach of the classical PSO by incorporating a new global point called the mean best position (mbest). This point is defined as the average of the particles self best positions. One of the drawbacks of PSO technique is the premature convergence, where each particle converges to the global best position directly. However, introducing the mbest new global point in QPSO, this problem can be avoided, where the swarm particles should consider their mates before converging to the global best position. In other words, particles that are close to the global best position will wait for the others that are far from the global best position. The flowchart associated with the QPSO technique is shown in Figure III.6. This will be done until they become closer to the global best position. This mechanism enables the capability of exploring globally the area around the global best position. Consequently, the QPSO-based technique is able to make a good trade-off between exploration and exploitation in the swarm, which allows avoiding premature convergence issue that is practically associated with the PSO approach. Sun et al. [105] suggests that the particle position involves two fundamental terms. The first one relies on attracting the particle, while the second term is associated with the gap between the particle's current position and the mean best performance of the whole swarm. Therefore, according to this new approach, the particle position at the i^{th} iteration is updated by using the following formulations [37]:

$$X_{ij}^{k+1} = Z_{ij}^{k} + \beta \left| mbest_{ij}^{k} - X_{ij}^{k} \right| \ln\left(\frac{1}{u_{ij}^{k}}\right) \tag{III.3}$$

where Z_{ij}^{k} denotes the local attractor which can be given by:

$$Z_{ji}^{k} = \upsilon p_{ij}^{k} + (1-\upsilon) g_{j}^{k} \tag{III.4}$$

The parameter β represents the Contraction Expansion coefficient (CE). It is the only tunable parameter of QPSO and plays a crucial role in controlling the algorithm convergence speed [37], mbest refers to the mean best position. Thus, this parameter describes the mean of sbest positions of all particles and it can be expressed as:

$$mbest_{ij}^{k} = \frac{1}{N}\sum_{i=1}^{N} p_{i}^{k} = \left(\frac{1}{N}\sum_{i=1}^{N} p_{i1}^{k}, \frac{1}{N}\sum_{i=1}^{N} p_{i2}^{k}, \frac{1}{N}\sum_{i=1}^{N} p_{i3}^{k}, \frac{1}{N}\sum_{i=1}^{N} p_{i4}^{k} \ldots\ldots, \frac{1}{N}\sum_{i=1}^{N} p_{iD}^{k} \right) \tag{III.5}$$

where N is the population size and D represents the global dimension of the optimization problem.

Basically, an efficient global optimization problem can be achieved by the effective exploration of search space with the aim of reaching high-quality solutions. As it aforementioned, GA-based metaheuristic technique uses genetic operators to perform the global optimization process. The GA develops through iterations by creating new subsequent populations from individuals in previous generations [13]. On the other hand, the evolutionary update equation is used to carry out the optimization process for the QPSO approach. Using this equation, the position of each particle of the swarm is updated with respect to the effect of the self-best performance, the global-best performance and the mean of the self-best positions of all particles.

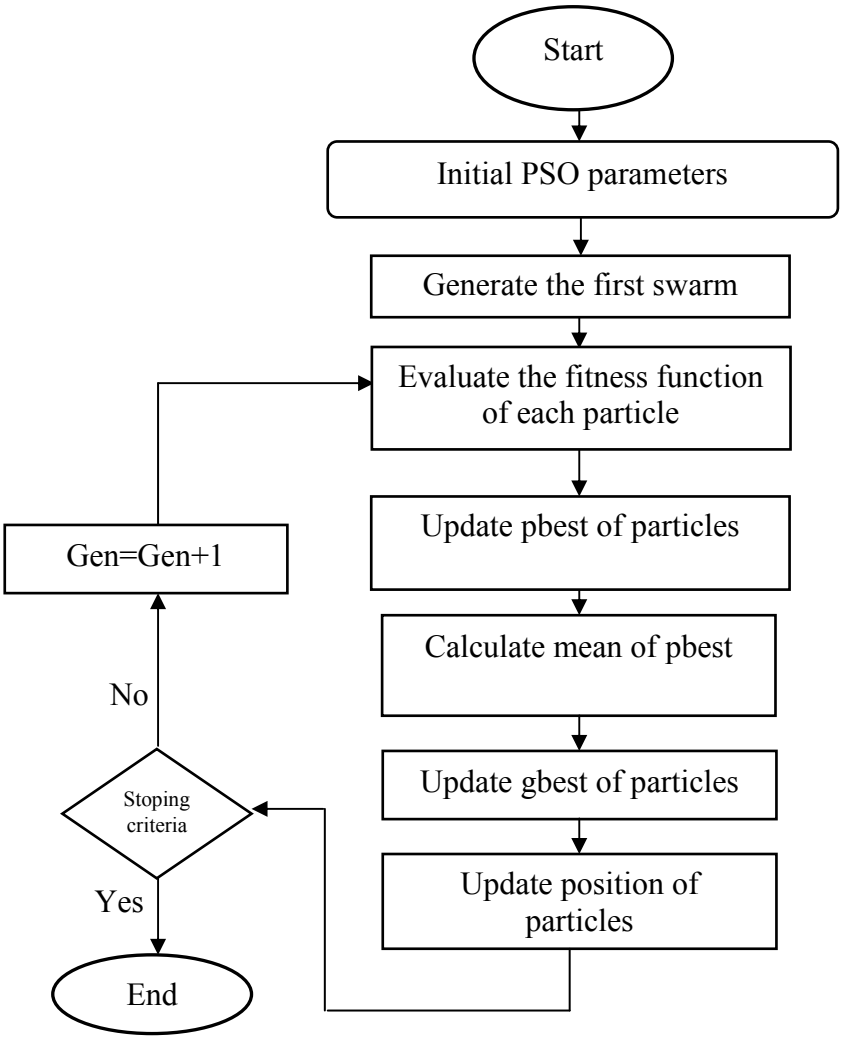

Figure III.6: The Standard flowchart of the QPSO-based metaheuristic technique

It is worth mentioning that the social behavior associated with the swarm is exploited to effectively update the QPSO population through following the best particle. Therefore, the basic mechanism of the QPSO-based metaheuristic technique provides the opportunity for enhancing the particles positions through generations.

III.9. Potential application of PSO and GA techniques to boost up the performance of various optoelectronic devices

As a matter of fact, solid-state electronic devices have become an important part of our daily life. Accordingly, the extensive propagation of information exchange by means of the internet makes us immersed in a wider diversity of electronic services. Optoelectronic devices are considered as an essential part of the modern systems, where they can be used to develop several appliances like the mobile phone, cars, TV, camera computers or even carbon-neutral energy sources using photovoltaic systems. Enhancing the optoelectronic device performance seems of paramount importance to reduce the appliances cost as well as their sizes and flexibility. In this context, the integration of the optoelectronic devices with the actual nanoelectronic technology still faces interconnection problems. The scale of silicon-based photonic devices with high data transfer speed is limited to micrometric scale because of the diffraction concept. It has been very difficult for the nanoscale optoelectronic technology to provide a satisfactory response at optical frequencies level. For this purpose, it seems vital to address the size mismatch between current electronic and photonic components through recording further improvements regarding the optoelectronic devices performance and power consumption.

Basically, the design parameters associated with various optoelectronic devices including photodetectors, phototransistors and solar cells determines in a great extent the overall device performances. In other words, the electrical and geometrical parameters have a profound implication in the optoelectronic device performance. The careful adjustment of the photonic components may lead to significant improvement regarding the devices optical behavior. On the other hand, the deep knowledge of the operating mechanism associated with different optoelectronic devices allows identifying the electrical parameter values that can improve the device performance. However, achieving a global optimal solution that enables achieving the highest possible device performance seems difficult because of the extreme complexity of the physical problem. Intuitively, metaheuristic techniques can be applied to solve global optimization

problems related to several domains. Indeed, the application of these approaches requires the definition of the fitness function and the search space. To do so, the accurate analytical modeling of the optoelectronic devices offer the possibility to formulate the objective function by taking into account the enhancement of the device FoMs. Therefore, the PSO and GA are exploited in the thesis work to outstandingly enhance the performance of several optoelectronic devices and to suppress some undesired effects such as the power dissipation and the device degradation related to several effects including recombination and reflective losses.

III.10. Conclusion

In this chapter, a review of metaheuristic-based optimization techniques and their classification are presented. Several global optimization approaches have been effectively defined. GA, PSO and QPSO-based metaheuristic algorithms are comprehensively discussed, where the basic concepts associated with these approaches has been given in details. Moreover, the advantages and weaknesses of several metaheuristic techniques are outlined. The last section of this chapter is devoted to exhaustively introducing some basic concepts about the application of these metaheuristic approaches for optimizing new optoelectronic devices, which constitutes one of the major objectives of this thesis. In spite of the versatility of the several metaheuristic techniques, in this modest dissertation the PSO-based approach is exploited to optimize photodetectors and solar cells in chapters IV and VI, respectively. On the other hand, GA is used as an individual tool in chapter V to boost up the phototransistor performance.

Chapter IV

New MSM-UV Photodetector Designs

***Abstract:** In this chapter, we propose a new MSM-UV photodetector designs. In the first part, the impact of the surface-textured front glass on the absorption of TiO2/Glass MSM UV photodetector is investigated, in order to achieve the dual role of increasing the scattering of UV-light as well as reducing the refracting UV-light in the glass. Moreover, semi-analytical modeling combined with PSO-based approach is carried out for studying and enhancing the MSM-UV photodetector optical and electrical performances. The second part of this chapter is devoted to the investigation of a new self-powered MSM-UV-photodetector based on dual wide band-gap material (DM) engineering aspect. Comprehensive analytical models for the proposed sensor photocurrent and the device properties are developed incorporating the impact of DM aspect on the device photoelectrical behavior. A new hybrid approach based on analytical modeling and PSO approach is also proposed to achieve improved photoelectric behavior at zero bias that can ensure favorable self-powered device.*

IV. 1. Introduction

Recently, new challenges are arisen when incorporating the traditional copper electrical interconnects in chip-level communication, including resistive loss, signal attenuation, distortion and the overhead cost [1-2]. Alternatively, optical wireless communication systems (OWCS) are becoming increasingly attractive and can potentially improve the computation speed and decrease the power consumption in long distance communication [7]. However, at very short length scales, the energy consumption of the optical links should be drastically improved in order to make them competitive with their electrical counterparts [4-6]. In this perspective, the OWCS are believed to face an upward change in the future to overcome the difficulty for reducing the huge amount of the power consumed by the optical receivers [6]. For this purpose, numerous research works have focused on the performance improvement of several photoreceivers' designs based on PN and Schottky barrier photodiode, phototransistors and MSM-UV photodetectors (PDs) [113-117]. The latter can pave the way to achieve powerful and practical optical links owing to its several advantages namely faster response, low fabrication cost and low dark noise. Indeed, MSM-UV-PDs-demonstrates high-quality structural and optical characteristics [118]. However, despite the actual stage of maturity of MSM-based UV sensors, the high power dissipation and the low responsivity are considered as major challenges to deal with. These limitations adversely affect the device performance for optical interconnections and environment monitoring applications. In such situation, the photodetector should be followed by Trans-Impedance Amplifier, to remove noise that gives digital transmission its high quality levels for optical communications systems. In this context, several numerical and experimental researches have been recently published with the aim of improving the MSM-based UV-PDs performance in terms of responsivity and reducing the high density of photonic circuits [36], [118-119]. Unfortunately, the obtained responsivity remains low and cannot meet the growing demands of the OWCS technology. This is closely related to a low derived photocurrent and the poor photoconductive behavior [35-37], [120-122]. This can seriously complicate the use of these devices for photoreceiver systems applications. Obviously, it is important to explore how to surmount the trade-off between the energy dissipation and the derived photocurrent capability. Therefore, alternative designs are in fact required and remain inevitable to enhance the MSM-based UV-PDs optical and electrical performances.

The aim of the work presented in this chapter is to propose new design methodologies in order to deal with the most pronounced issues associated with UV sensors. For this purpose, the chapter is divided into two parts. The first part focuses on investigating the impact of the periodic grating aspect in enhancing the TiO_2 based-MSM-UV-PDs performance. The influence of the surface-textured front glass on the absorption of TiO_2/glass thin-film UV photodetector is investigated in order to achieve the dual role of increasing the light scattering as well as reducing the refracting UV-light at the glass substrate. To consolidate this viewpoint, combined semi-analytical modeling and PSO-based optimization approaches are carried out for boosting up the TiO_2 based-MSM-UV-PDs performance. In the second part, we will describe the potential of using a lateral hetero-junction with DM aspect to ensure the device asymmetry, which can in turn offer exciting opportunities for reaching high-responsivity self-powered devices. In this context, a new hybrid approach based on analytical modeling of the proposed DM-MSM-UV-PDs assisted with PSO-based metaheuristic technique is proposed to address the challenges associated with the device photoconductive behavior at self-powered conditions.

IV. 2. Part (1): Role of Optimized Grooves Surface-Textured Front Glass in Improving TiO_2 Thin-Film UV Photodetector Performance

IV.2.1 Motivation

The quality of OWCS depends mainly on the performance of the devices used in conversions electrical/optical (LED or laser emitters) and optical/electrical (photodetectors or phototransistors receivers). The MSM UV photodetector is considered more appropriate due to its simple structural design and low elaboration cost. Moreover, materials with large band-gap such as TiO_2 exhibit an acceptable UV absorption rate, operation stability and blindness in visible and infrared regions, which enables a low rejection rate. Although the actual stage of maturity of TiO_2 based-MSM-UV-PDs for UV sensing applications, the device shows many problems such as: extensive optical losses, low responsivity and high power dissipation [121-122]. These persistent problems adversely affect the device performance, especially for chip-level communication applications. Thus, further UV absorption improvement may yet be required for TiO_2 based-MSM-UV-PDs to become a substantial part of the optical

communication systems. This work shows the impact of the surface-textured front glass in improving the TiO_2 based-MSM-UV-PDs absorption behavior. The efficient control of the introduced texture may lead to more electric field confinement and UV-light trapping in TiO_2 absorber layer. Moreover, we describe a new design methodology to further improve the device electrical and optical performances. Finally, we perform an overall performance comparison between the optimized design and the conventional TiO_2 based-MSM-UV-PDs.

IV.2.2 Modeling framework

The MSM structure for UV sensing is a lateral structure consisting of back-to-back Schottky contacts, separated by a thin-film wide band-gap semiconductor. Figure IV.1 schematically describes the investigated MSM UV-photodetector structure, where (a) depicts the conventional flat structure, while (b) shows the photodetector design including periodic grooves morphology. In these structures, a thin-film of TiO_2 deposited on glass substrate is used for the absorption of UV radiation. In addition, platinum contact fingers are deposited on the TiO_2 layer. The key advantage of the proposed design with grooves resides in the simplicity of manufacturing, where a simple etching of the glass substrate with high precision is sufficient. For our semi-analytical modeling, d represents the TiO_2 thickness, h is the grooves height and W is the grooves width.

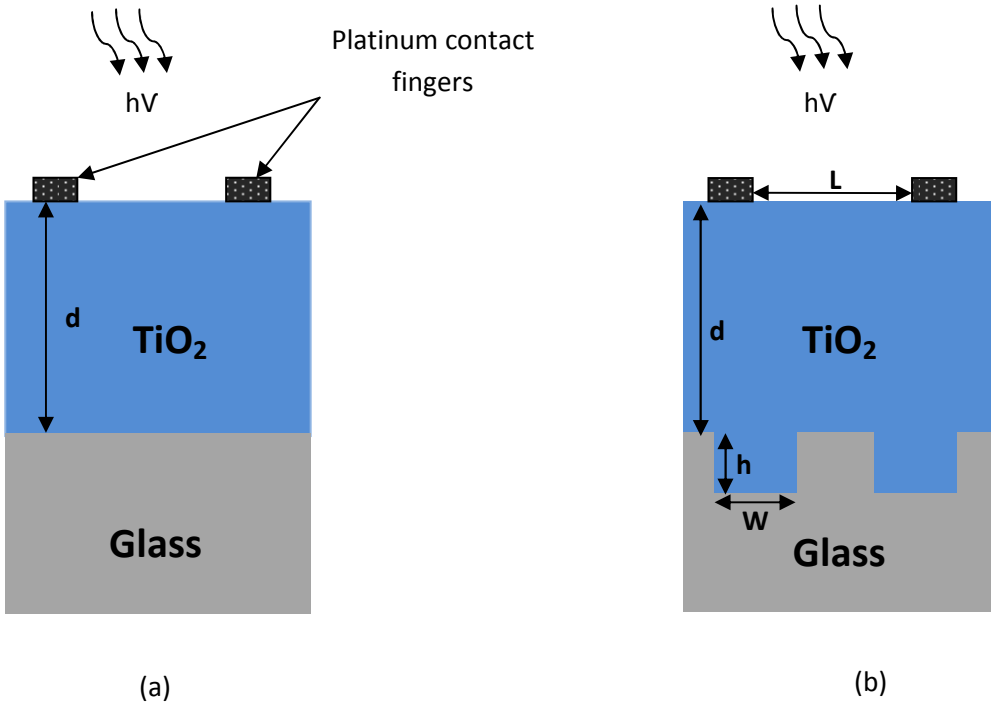

Figure IV.1: Cross-sectional view of **(a)** conventional TiO_2 based UV photodetector, **(b)** proposed UV photodetector with grooves.

For the modeling procedure, a two-dimensional (2-D) finite element method using numerical simulations has been adopted for numerically modeling the optical behavior of the proposed device including the diffraction grating aspect. The extracted absorbance and the total reflection will be employed in our analytical development for modeling the MSM photodetector current and the FoMs parameters under UV-illumination. The optical behavior modeling of the proposed design involves the accurate solving of Maxwell's equations. As a consequence of these equations, we obtain the Helmholtz equations as follows

$$\nabla^2 E + \mu\varepsilon\omega^2 E = 0 \quad \text{(IV.1a)}$$

$$\nabla^2 H + \mu\varepsilon\omega^2 H = 0 \quad \text{(IV.1b)}$$

where E and H are the Electric and Magnetic fields intensities, μ is the TiO_2 permeability and ε represents the material permittivity.

In our numerical study, we assume a plane wave conveyed in air at normal incidence and diffracted at the MSM structure. In addition, transverse electric field (TE) mode of the incident wave is considered. In the developed model, periodic boundary conditions are used to describe the periodicity for tow grooves morphology. While at the top and bottom of the proposed structure, perfect boundary conditions are assumed. Thus, the Helmholtz equations are reduced to only one equation as follows

$$\nabla^2 E_z + \mu\varepsilon\omega^2 E_z = 0 \quad \text{(IV.2)}$$

To evaluate the overall optical performance of the proposed design with periodic diffraction grating aspect over a wide wavelength range, we should numerically estimate the integral absorption and the total reflection of the device. However, when electromagnetic wave strikes the investigated MSM photodetector we can deduce three dissimilar components of the incident wave. The first component of the incident wave is related to the reflection from the device surface, whereas the second is attached to the absorbance and the last component is linked to the transmitted portion of the wave. In this context, the device absorbance can be defined as the ratio between the power loss in the TiO_2 layer and the incident power; while the reflected radiation is defined as the ratio between the incident power and the reflected power at the structure surface. Therefore, we can calculate the reflected power by integrating the poynting vector with respect to the device surface.

On the other hand, we can estimate the absorbed power by integrating the time-averaged Poynting vector in the TiO_2 volume. The final formulation of the device absorbance can be expressed as [122]

$$A(\lambda)=\frac{\int_V \frac{1}{2}\left|\vec{E}_z(\vec{r})\right|^2 \omega\varepsilon_0\varepsilon''(\lambda)dV}{\int_S \frac{1}{2}\mathrm{Re}\left\{\vec{E}_z(\vec{r})\times\vec{H}^*(\vec{r})\right\}dS}=\frac{Absorbed\ \ power[W]}{Incident\ \ power[W]} \quad \text{(IV.3)}$$

where $\vec{H}^*$ denotes the complex Magnetic field conjugate, σ represents the TiO_2 conductivity calculated from $\sigma=\omega\varepsilon_0\varepsilon''(\lambda)$, with ε_0 is the vacuum permittivity and ε'' represents the imaginary part of the complex TiO_2 dielectric constant. The TiO_2 material optical parameters namely the refractive index (n) and the extinction coefficient (k) describing the device reflection and absorption respectively, are taken from the SOPRA database.

To determine the total reflection, we principally need to define the scattering parameter S-parameter in term of the electric field, which is given at the top by

$$S_{11}=\frac{\int_{port1}(E_c-E_1)E_1^*dA_1}{\int_{port1}\left(E_1E_1^*\right)dA_1}=\frac{reflected\ \ power[W]}{Incident\ \ power[W]} \quad \text{(IV.4)}$$

where E_c is the computed electric field on the port which consists of the excitation added to the reflected field and E_1 is the electric pattern on port 1 [122-123].

IV.2.2.1 Analytical model of the photocurrent

In order to analyze the impact of our proposed structure on the device optical and electrical performances, we basically need to develop the generated photocurrent model. This task can be achieved through the knowledge of the absorption coefficient, which is calculated using Beer–Lambert's law as follows [124]

$$\alpha=\frac{2.303}{d}A(\lambda) \quad \text{(IV.5)}$$

Based on the thermionic emission model, the analytical current expression of the illuminated MSM photodetector is given by [125]

$$I=I_s\exp\left(\frac{q(V-R_sI)}{nKT}-1\right)+I_{ph} \quad \text{(IV.6)}$$

where q represents the electron charge, V is the applied voltage, T and K are respectively the absolute temperature and the Boltzmann constant, R_s is the series

resistance, n is the ideality factor and I_s denotes the saturation current, which is well represented by the thermionic-emission relation provided by

$$I_s = SA_n^* T^2 \exp\left(\frac{-q\phi_{Bn}}{KT}\right) + SA_p^* T^2 \exp\left(\frac{-q\phi_{Bp}}{KT}\right) \quad \text{(IV.7)}$$

where A_n^* represents the effective Richardson constant, S refers to the contact area, ϕ_{Bp} and ϕ_{Bn} are respectively the Schottky barrier heights of Platinum/TiO_2 contacts expressed as

$$\phi_{Bn} = \phi_{MS} + V_t \ln\left(\frac{N_c}{N_d}\right) \quad \text{(IV.8a)}$$

$$\phi_{Bp} = \phi_{MS} + V_t \ln\left(\frac{N_v}{N_d}\right) \quad \text{(IV.8b)}$$

with Φ_{MS} represents the difference between the Platinum and TiO_2 workfunction values, V_t is the thermal voltage, N_d is the TiO_2 doping concentration and N_c, N_v are respectively the effective densities of states in the TiO_2 valence and conduction bands.

After illuminating the device with a given incident power P_i, an additional current will be produced from the photogenerated carriers. This current is dominated by the generation of electron/hole pair within the depletion regions and it can be computed from

$$I_{ph} = \left[q\phi(1-R)(1-\exp(-\alpha W_d))\right] \quad \text{(IV.9)}$$

where ϕ is the number of the incident photons mainly depending on the incident power and W_d represents the space charge width expressed as

$$W_d = \sqrt{\frac{2\varepsilon_s(\phi_{MS}+V)}{qN_d}} \quad \text{(IV.10)}$$

with ε_s represents the TiO_2 permittivity.

It is noteworthy that as the applied voltage increases the depletion region reaches its limit which corresponds to W_d=L, with L the spacing between electrodes. In this situation, the photocurrent will be saturated and the flat energy band regime is recorded. Hence, the flat band voltage can be estimated by

$$V_{fb} = \frac{qN_d}{2\varepsilon_s} L^2 \quad \text{(IV.11)}$$

IV.2.3 Results and discussions

In order to show the particular strengths of our proposed design with grooves over the flat conventional structure for UV sensing applications, this section is mainly dedicated to the investigation and comparison of the optical and the electrical performances of both conventional and proposed devices.

Figure IV.2 depicts the integral absorbance evolution versus the free space wavelength of both conventional flat design and the proposed design involving glass texturization with grooves morphology.

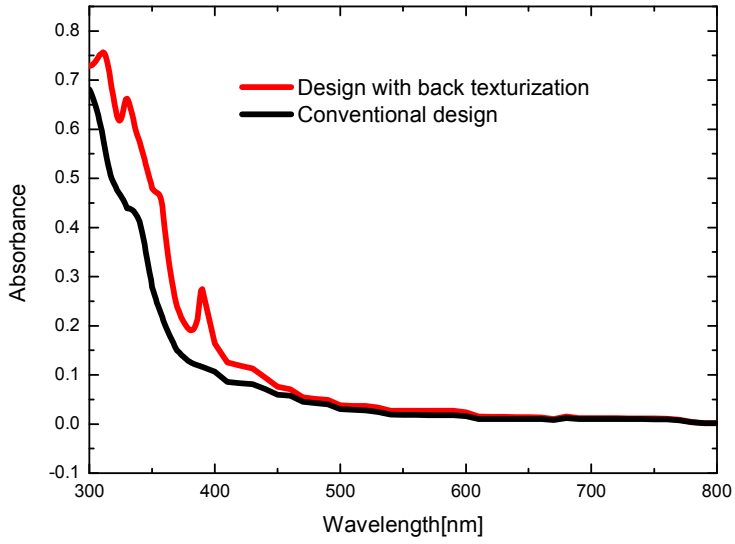

(a)

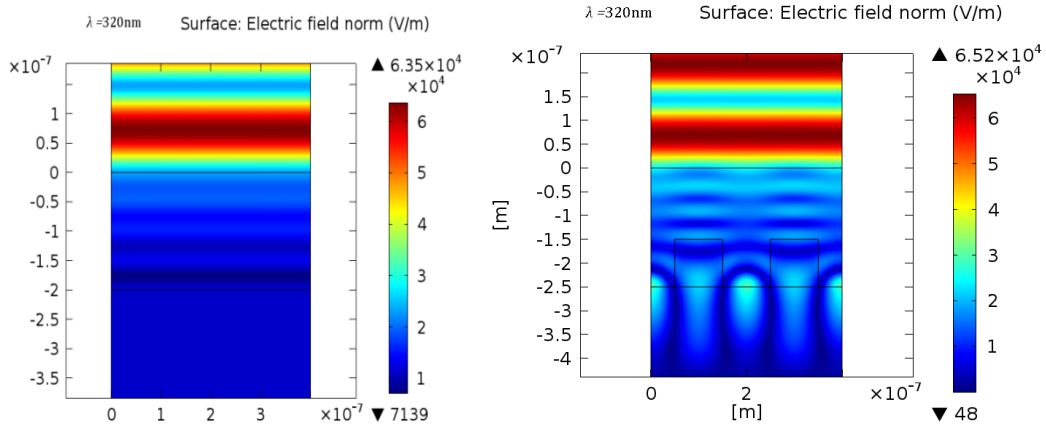

(b)

Figure IV.2: (a) Absorbance versus the free space wavelength for both planar and back textured structures. **(b)** Electric field profile for both planar and periodic back textured structures for two different wavelength (λ =320nm), with d=200 nm, W=100nm, h = 100nm.

From Figure IV.2 (a), it is clearly observed that the proposed design shows better optical behavior exhibiting higher absorbance values compared to that provided by the conventional planar structure. Moreover, a relative improvement of (20%) over the flat design can be achieved by including the diffraction grating aspect. This enhancement is mainly due to the optical confinement effect induced by the glass texturization. In addition, the grooves morphology extends the optical path of the incident wave through the improvement in the light trapping capability leading to a substantial decrease in the structure optical losses.

In order to explore the origin of such enhancement and to understand the physics behind the integral absorption behavior of the proposed design, the electric field profile inside both planar structure and design with periodic diffraction grating for a specific wavelength value is examined in Figure IV.2 (b). From this figure, we can notice strong electric fields are mainly confined in the TiO_2 thin-film as compared to the planar design, which can be attributed to the superior light trapping capability. These important enhancing results of the device absorbance suggest the possibility to modulate the electric field behavior using the adopted diffraction grating aspect, which leads to highly improved optical performance. Figure IV.3 shows the I-V characteristic of the proposed photodetector with grooves compared to the conventional structure [113].

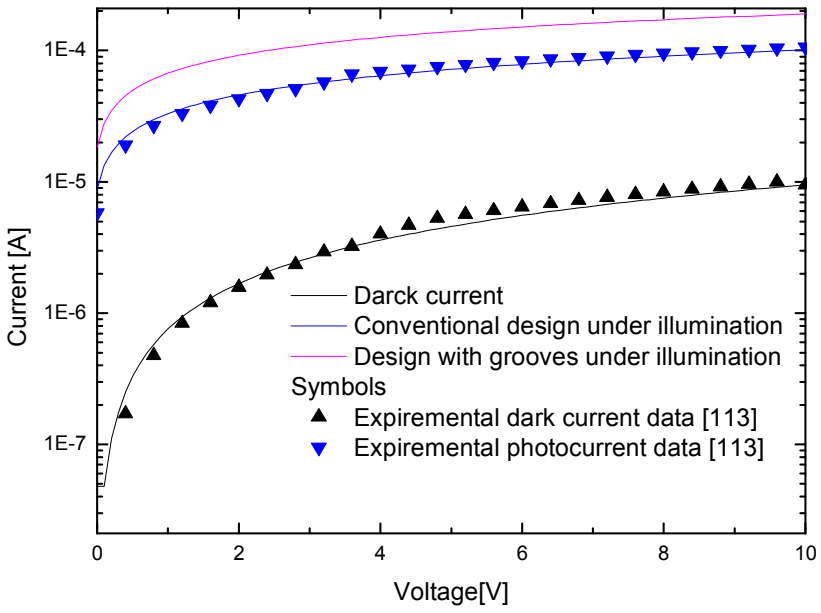

Figure IV.3: I-V characteristics of the proposed design with grooves compared with that of the conventional planar design with and without illumination, with d=200 nm, W=100nm, h = 100nm, $N_d=1\times10^{15}cm^{-3}$.

As shown in this figure, a good agreement is clearly observable between our semi-analytical results and those of experiment characteristic. It has been found that an enhancement in the derived current for the proposed design with diffraction grating aspect is obtained. This improvement in the photodetector derived current is explained by the increase of UV-light scattering in the TiO_2 absorbent layer. Hence, there is an enhanced light trapping capability resulting from the high optical confinement located at texture grooves.

IV.2.3.1 Optical parameters (FoMs) analysis

In order to evaluate the impact of the proposed design on the electrical and optical performances, critical parameters such as the device responsivity should be estimated. In this context, the responsivity can be defined by the ratio between the obtained photocurrent and the incident power as given below

$$R = \frac{I_{ph}}{P_{incident}} \tag{IV.12}$$

Another important parameter for evaluating the device electrical performance is the optical gain. This latter can be computed as follows

$$G = \frac{I_{ph}}{I} \tag{IV.13}$$

Out of the most significant figures of merit of a photodetector for optical interconnections applications, we can cite the device detectivity D and sensitivity S as key criteria. These latter are expressed as

$$D = R\sqrt{\frac{A_s}{2qI_{Dark}}} \tag{IV.14}$$

$$S = \frac{I_{ph} - I}{I} \times 100 \tag{IV.15}$$

where I_{dark} represents the dark current.

The other two figures of merit characterizing the undesired power dissipation effect are the signal to noise ratio SN and the $I_{ON\ (light)}/I_{OFF\ (Dark)}$ current ratio. The SN can be given by the following relation

$$SN = \frac{I_{ON}(light) - I_{OFF}(dark)}{I_{OFF}(dark)} \tag{IV.16}$$

It is to highlight that for better optical performance and for achieving lower power dissipation, the above defined parameters should be as high as possible.

Figure IV.4 illustrates the device responsivity against the wavelength for both structures with diffraction grating and conventional planar design for an applied voltage of V=5V. A similar tendency of the absorbance variation is observed. As expected, the peak responsivity of the proposed device in the UV spectrum is greater than the one provided by the planar design, where a maximum responsivity of (19 mA/W) with (21%) relative improvement has been reached by including grooves texture. This enhancement can be firstly ascribed to the improved integral absorbance induced by the optical confinement effects and secondly to the enormous decrease in the total reflection caused by the introduced grooves texture.

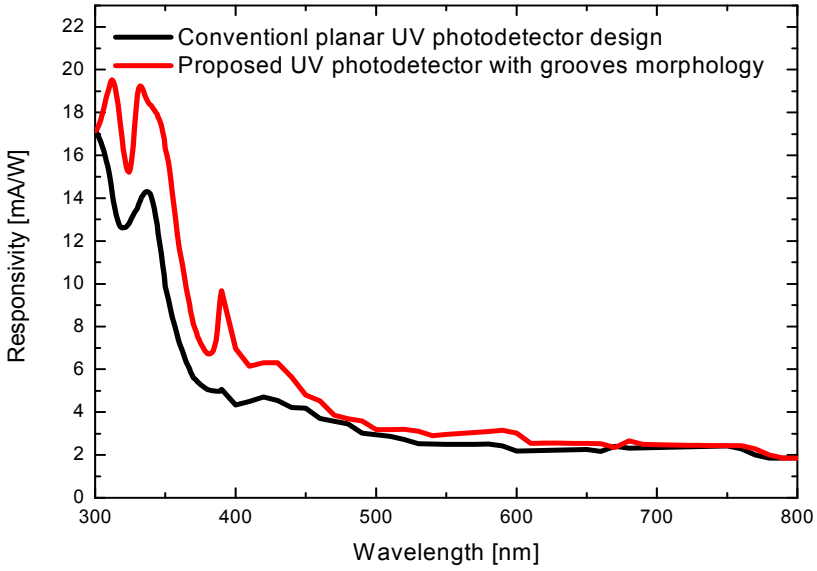

Figure IV.4: Device responsivity against the free space wavelength for both planar and back textured structures with d=200 nm, W=100nm, h = 100nm, $N_d=1\times10^{16}cm^{-3}$, V=5V.

There are also a few other features of interest characterizing optical communication systems, which should be examined carefully. In this context, the proposed design exhibits superior FoMs with relative improvement of optical gain 18.1%, sensitivity 23%, detectivity 19%, signal to noise ratio 24% and $I_{ON\ (light)}/I_{OFF\ (Dark)}$ current ratio 13.5% over the conventional planar design. These satisfactory results in improving the device optical and electrical performances suggest the possibility of proposing a new insight to optimize the device overall performances, which constitute the main objective of the next subsection.

IV.2.3.2 Optimization of MSM-TiO_2 UV photodetector performance

The usefulness of the proposed diffraction grating aspect depends on the ability to design the periodic grooves morphology by choosing well-defined dimensions for boosting up the structure light trapping capability. In this perspective, we focus in the present subsection on optimizing the electrical, physical and geometrical parameters of the proposed design to achieve the highest possible optical and electrical performances. To do this task, we exploit a new metaheuristic technique based on PSO approach.

In order to optimize the proposed MSM-TiO_2 UV photodetector including diffraction grating aspect, the key FoMs characterizing the device optical behavior are used to formulate the fitness function. Hence, we have to satisfy to following set of goals

- Maximizing the responsivity
- Maximizing the sensitivity
- Maximizing the derived current
- Maximizing the detectivity
- Maximizing signal to noise ratio
- Maximizing the I_{on}/I_{off} ratio

To this extent, based on the "weighted sum approach method", the overall objective functions above listed can be represented by only one equation including weighting coefficients as follows

$$F(X) = w_1(\mathrm{I_{ON}} / I_{OFF}) + w_2 R_{ph} + w_3 SN + w_4 \mathrm{I_{max}} + w_5 S + w_6 D \qquad \text{(IV.17)}$$

where X represents the design variables vector incorporating geometrical, electrical and optical parameters given by: X= (N_d, ϕ_m, d, H,W, d_{glass}, λ, V), w_i (i = 1-6) is a weighting coefficient equals to 1/6.

The constraints allow defining the conditions to be respected by the design variables in the search space. In our case, the constraints are given by:

$g_1(x) : x \in [x_{i\min}, x_{i\max}]$, $x_i \in X$ (each design variable should be confined within a given range).

- $g_2(x) : \mathrm{d_{glass}} > H$.
- $g_3(x) : d < 200\,nm$.

In the optimization process, the number of particles in the swarm is considered to be equal to 50 and the stall generation for the global optimization process is equal to 200, for which the fitness function stabilization was achieved and the optimization error for the stopping criterion is considered infinitesimal.

As expected, using the global optimization procedure based on PSO gives rise to highly improved device optical and electrical performances. In this regard, we present in Figure IV.5 (a) the device integral absorbance for both conventional planar structure and the optimized design with diffraction grating aspect. To a significant extent, the integral absorption is greatly boosted, where the maximum peak absorbance provided by the optimized design is equal to 98% for a specific wavelength near 320nm. Moreover, a 52 percent of the relative improvement in the integral absorbance over the conventional planar device is reached.

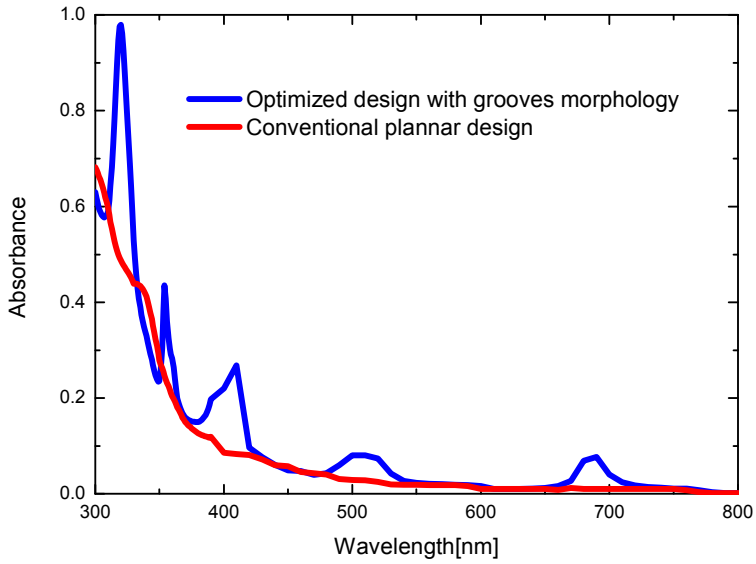

(a)

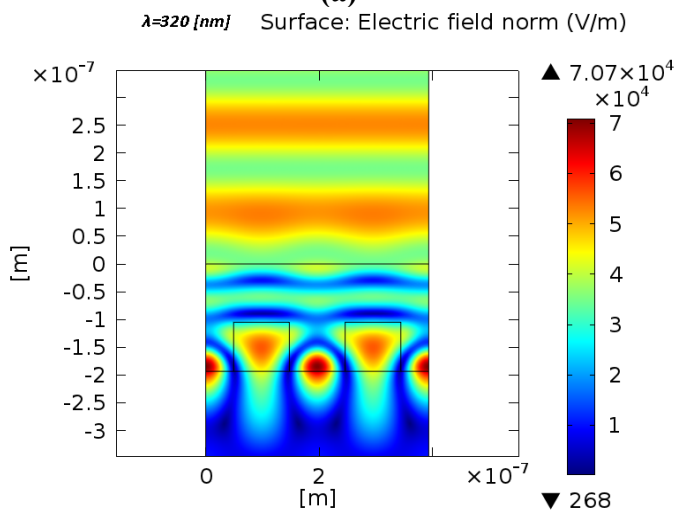

(b)

Figure IV.5: (a) Absorbance as function of the free space wavelength for the optimized TiO_2 UV-Photodetector with grooves morphology, **(b)** Electric field profile for the optimized TiO_2 UV-Photodetector with back texturization structure.

Therefore, such satisfactory enhancement confirms the ability of the global optimization approach for achieving the maximum possible of light trapping efficiency. However, for understanding the main basis behind this adequate optical behavior, it is important to examine the electric field distribution of the optimized design in the TiO_2 layer absorbance. Accordingly, Figure IV.5 (b) shows the electric field profile of the optimized MSM-TiO_2 UV photodetector including grooves texture at the free space wavelength value of 320nm. It is clearly shown that an important improvement of the electric field profile is exhibited by enormously dense and high value electric field in the textured region, which leads to longer lifetime of the photons trapped in the TiO_2 absorbent layer enabled by the high optical confinement. These good results suggest the high ability associated with the proposed glass texturization paradigm to modulate the electric field in the absorbent layer. Therefore, the overall device optical and electrical performances for optoelectronic applications may be consolidated by introducing such UV photodetector design. Figure IV.6 compares the optimized I-V output characteristic with its counterpart of the conventional design and the photodetector including the diffraction grating aspect without optimization. It is found that the optimized design demonstrates superior derived current compared to that exhibited by the planar conventional photodetector. The obtained improvement can be explained by the important increase in the device absorbance gained from the high light trapping capability recorded using joint adopting aspects of diffraction grating and PSO-based optimization. The obtained results indicate the outstanding capability of the optimized device for improving the photocurrent, which makes it a very promising design for avoiding the undesired power dissipation effects.

Eventually, it is of great significance to address the impact of our new insight for optimizing the proposed design on the optical and electrical parameters (FoMs). In this perspective, Table IV.1 illustrates an overall performance comparison between the optimized design and the flat conventional counterpart. From this table, it is clearly demonstrated that the optimized device offers better optical and electrical performances in comparison with the conventional planar one. Moreover, the optimized TiO_2-based UV photodetector enables achieving a maximum responsivity of 75mA/W, emphasizing the effectiveness of the global optimization technique. This makes it as a potential alternative for developing high-performance optical links for chip-level optical communication applications.

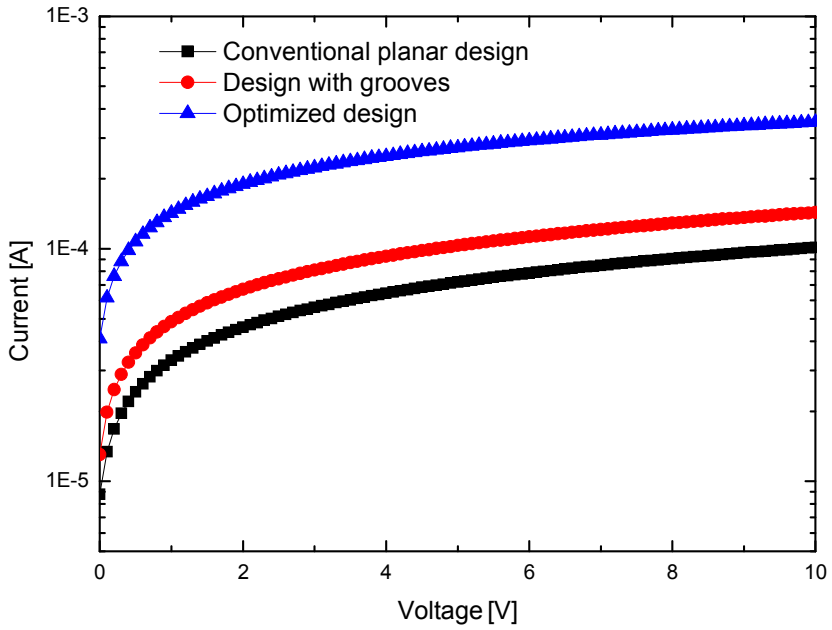

Figure IV.6: I-V characteristics of the optimized design with grooves compared to both conventional planar design and the proposed structure without optimization.

Table IV.1: Comparison of optical and electrical performance obtained from our optimized device with back texturization with that of the conventional (planar) structure for UV optical communication applications.

Symbol	Conventional planar design	Optimized design with grooves
Design variables		
Wavelength λ (nm)	300	320
Applied voltage V(V)	5	5
Contact work function (eV)	5.4	5.1
TiO_2 doping concentration (cm^{-3})	1×10^{15}	6×10^{16}
Spacing length L(cm)	1	1
Grooves height h(nm)	-	90
Grooves width W(nm)	-	98
Titanium dioxide thickness d (nm)	200	105
Glass thickness d_1 (nm)	200	200
Objective functions		
Optical gain(G)	11	36.5
ON-OFF Current Ratio (I_{ON}/I_{OFF}) (dB)	45	68
Detectivity (Jones)	1.66×10^{10}	5.57×10^{10}
Responsivity (mA/W)	17	75
Sensitivity (S)	1000	3550
SN	9	35.48

In summary, the introduced grooves texturization has an important impact on the optical behavior of TiO_2 based-MSM-UV-PDs. Moreover, high improvement in the device figure of merits parameters has been recorded. The grooves realized in the glass

substrate provide the ability for modulating the electric field behavior in the TiO_2 thin-film, while the main objective is to achieve a significant optical confinement and thereby a superior light trapping capability. Furthermore, the usefulness of the global optimization using PSO approach to boost the device optical and electrical performance has been successfully demonstrated, where the optimized design outperforms greatly the conventional design. The obtained results indicate that the optimized TiO_2 based-MSM-UV-PDs design can be considered as a potential candidate to address the most challenging problems associated with the low and delay responsivity for UV sensing applications.

IV. 3. Part (2): A Novel High-Performance Self-powered UV Photodetector: Concept, Analytical Modeling and Analysis

IV.3.1 Motivation

As a matter of fact, MSM-UV-PDs-based on ZnO material with direct wide band-gap (3.3eV), exhibits high-quality structural and optical properties [118]. In spite of these benefits, the high power dissipation and the low responsivity are considered as major challenges that prevent achieving high-performance optical links. In this context, several pioneering works focused on reducing the device power consumption by proposing new self-powered structures based on various design amendments such as: asymmetric electrodes, ZnO nanowires and nanorod, in order to push the limits of the ZnO based-MSM-UV-PDs performance [35-37]. However, the investigated structures still suffer from some problems mainly related to low responsivity and sensitivity at zero bias [35-37], [119]. Therefore, more improvements regarding the device responsivity at self-powered conditions are in fact of great importance to reduce the photoreceiver's energy consumption. In this regard, this work describes the possibility of achieving this objective through proposing a new design methodology. In this framework, ZnTe is an important p-type semiconducting material of the II-VI family possessing a band-gap of 2.26eV, which is suitable for the design of a variety of novel optoelectronic devices [126-128]. Introducing this material with the aim of designing a lateral hetero-junction appears to be helpful to ensure the device asymmetry, which can in turn offer the self-powered property. The built-in electric field induced at the ZnO/ZnTe interface can also efficiently separate electrons/holes pairs at zero bias, leading to a substantial decrease in the device power consumption. Besides, the use of ZnO/ZnTe can be beneficial from another aspect regarding the dark conditions, where

the potential barrier induced at this interface enables a considerable reduction in the dark current. In this part of the chapter, we will investigate the role of a new hybrid approach based on analytical modeling of the proposed DM-MSM-UV-PDs and PSO-based metaheuristic technique in avoiding extensive challenges associated with the device photoconductive behavior at self-powered conditions. Moreover, we will perform a new comparison of the performance metrics obtained from the optimized MSM-based DM-UV-PDs designs with that of the experimental results of a ZnO-based MSM-UV-PD self-powered design based on asymmetric electrodes aspect [35].

IV.3.2 Analytical modeling methodology

Principally, the key idea behind the proposed ZnO-based MSM-UV-PDs basically resides on a lateral structure with back-to-back Schottky contacts separated by a thin-film wide band-gap material. In the proposed design, the design amendment is made in the MSM-UV-PDs active layer level by assuming two regions with different wide band-gap compounds in order to form a lateral heterojunction, where L_1 and L_2 are the first and the second region lengths, respectively. Thus, the total thin-films length, which corresponds to the spacing between both Schottky contacts is equal to $L= L_1+ L_2$.

Figure IV.7 (a) illustrates the schema of the proposed ZnO-based MSM-UV-PDs including DM aspect. In this figure, d and d_{glass} represent the active layer and the glass substrate thicknesses, respectively. Basically, the proposed MSM-based DM-UV-PDs can be in fact represented using an equivalent circuit as it is shown in Figure IV.7 (b), where the investigated design is assumed with a series combination of two MSM-based UV-PDs with a dissimilar material in the active layer. Hence, a systematic analytical modeling of the proposed design incorporation the impact of the DM aspect is of great importance to understand the device photoconductive behavior associated with different optical and electrical design parameters.

It is important to note that the investigated design is considered technologically feasible, where the chemical vapor deposition technique has confirmed its effectiveness for developing good crystalline quality of ZnO/ZnTe and without interfacial defects [126-128].

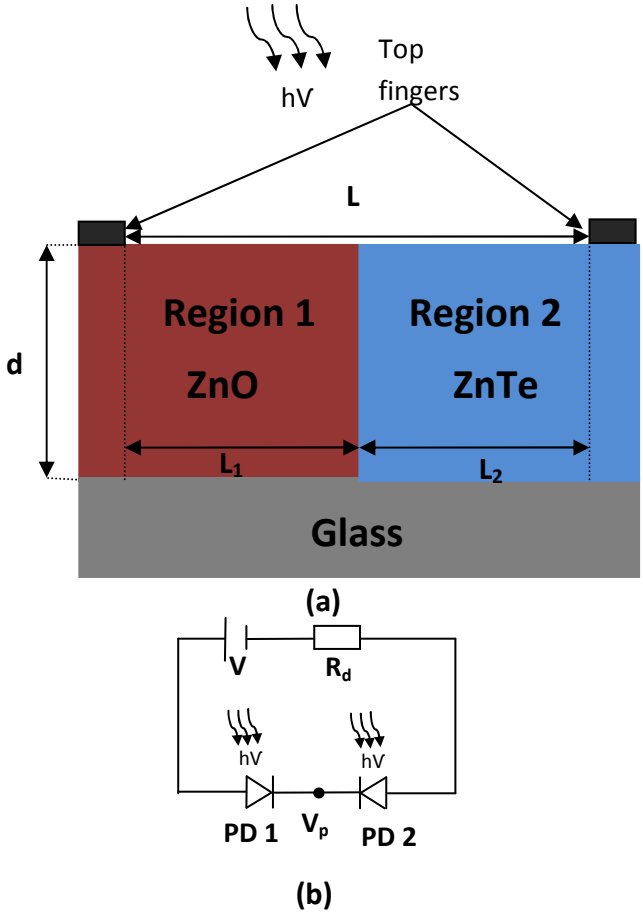

Figure IV.7: (a) Cross-sectional view of the investigated MSM-based DM-UV-PDs, **(b)** equivalent circuit representation of the photocurrent modeling with PD1 corresponds to the first ZnO sub-photodetector, PD2 represents the second sub-device with ZnTe material, V_p is the interfacial potential and R_d is the load resistance.

IV.3.2.1 Analytical model of the photocurrent

In order to accurately model the proposed structure, we assume that the device is equivalent to two dissimilar sub-photodetectors related in series, each having its own spacing length L_1 and L_2 as it is above outlined. In this perspective, the applied voltage between both electrodes will be different for each region and can be given by $V_1 = V_p$ and $V_2 = V - V_p$. In these equations, V_1 and V_2 represent the modified applied voltages for both regions assumed with different wide band-gap thin-film materials, V is the applied voltage and V_p denotes the unknown interface potential as it is shown in Figure IV.7 (b).

Therefore, by using the thermionic emission model of the MSM-based UV-PDs structure, the analytical current expression of the suggested sub-devices under illumination can be given by the following expressions [113], [124] and [129]

$$\begin{cases} I_1 = I_{s1}\exp\left(\dfrac{q\left(V_p - R_{s1}I_1\right)}{n_1 KT} - 1\right) + I_{ph1} \\ I_2 = I_{s2}\exp\left(\dfrac{q\left(\left(V - V_p\right) - R_{s2}I_2\right)}{nKT} - 1\right) + I_{ph2} \end{cases} \quad \text{(IV.18)}$$

where R_{s1} and R_{s2} represent the series resistance for both introduced wide band-gap materials, n_1 and n_2 are the ideality factors for both suggested active layers.

The saturation currents for both sub-photodetectors (I_{s1}, I_{s2}) are well represented by the thermionic-emission relation [113], [124] and [129] and can be given by

$$\begin{cases} I_{s1} = S\ A_n^* T^2 \exp\left(\dfrac{-q\phi_{B_1}}{KT}\right) \\ I_{s2} = S\ A_n^* T^2 \exp\left(\dfrac{-q\phi_{B2}}{KT}\right) \end{cases} \quad \text{(IV.19)}$$

where A_n^* is the effective Richardson constant, S is the contact area, ϕ_{B1} and ϕ_{B2} represent the Schottky barrier height for both contacts expressed as

$$\phi_{B1} = \phi_{MS1} + V_t \ln\left(\frac{N_c}{N_d}\right) \quad \text{(IV.20a)}$$

$$\phi_{B2} = -\phi_{MS2} + V_t \ln\left(\frac{N_v}{N_a}\right) \quad \text{(IV.21b)}$$

with Φ_{MS1} and Φ_{MS2} are the difference between the metal and the semiconductor workfunctions for both suggested regions, respectively. N_d is the ZnO doping concentration while N_a denotes the donor doping level of the ZnTe material.

The photocurrent produced by the generation of electron/hole when the device is under illumination can be computed for both sub-photodetectors using the following equations

$$\begin{cases} I_{ph1} = \left[q\phi(1 - R_1)(1 - \exp(-\alpha_1 W_{d1}))\right] \\ I_{ph2} = \left[q\phi(1 - R_2)(1 - \exp(-\alpha_2 W_{d2}))\right] \end{cases} \quad \text{(IV.22)}$$

where α_1 and α_2 are the absorption coefficient associated with the first and the second region, R_1 and R_2 are the reflection coefficient of the ZnTe and ZnO materials, respectively. All these optical parameters are estimated using the same modeling methodology given in the first part of this chapter (Equation IV.1, 2, 3, 4 and 5).

It should be noted that the materials (ZnTe, ZnO and TiO_2) optical constants (n, K) used in the FDTD modeling technique are normally wavelength dependent and are extracted from the experimental results and the SOPRA database [130] and [131].

The space charge width W_{di} for each sub-device can be calculated from the following expresions

$$W_{d1} = \sqrt{\frac{2\varepsilon_{s1}\left(\Phi_{MS1} + V_p\right)}{qN_d}} \quad \text{(IV.23a)}$$

$$W_{d2} = \sqrt{\frac{2\varepsilon_{s2}\left(\Phi_{MS2} + \left(V - V_p\right)\right)}{qN_a}} \quad \text{(IV.23b)}$$

with ε_{s1} and ε_{s2} are the ZnO and ZnTe materials permittivity, respectively.

In fact, we suggest in our analytical modeling that the proposed design can be modeled as two elementary sub-devices connected in series with different materials in the active layer [132]. Thus, the investigated MSM-based DM-UV-PDs can be considered as two photodetectors as aforementioned which implies applying the continuity of the current at the junction of the suggested materials to calculate the interfacial potential V_p by using the following equality

$$I_1 = I_2 \quad \text{(IV.24)}$$

Using this condition, a complex and implicit function is resulted, which requires using numerical technique to estimate the interfacial potential V_p. Accordingly, Newton algorithm is used to solve the obtained implicit function numerically.

After calculating the potential V_p between the assumed sub-devices, the proposed device photocurrent which includes the effect of the DM engineering aspect can be estimated using the current equation (Equation IV.18).

IV.3.3 Results and discussions

In this section, we have versatile objectives. Firstly, it is important to provide a comparison between different architectures including experimental results and using dissimilar materials by exploiting the developed analytical models of the optical device properties. Secondly, we propose a new effective shape optimization approach using PSO-based metaheuristic technique for achieving high-responsivity self-powered device to be implemented as a component for building high-performance photorecievers.

In order to assess the photoconductive behavior of the proposed design including DM engineering aspect, Figure IV.8 compares the I-V characteristics of the proposed

MSM-based DM-UV-PDs and the experimental results of the MSM-UV-PD based on TiO_2 nanorod [113], under illumination with the optical power value of P_i=2.3mW/cm^2 and for an appropriate wavelength value of 365nm. From this figure, we can see that the proposed design exhibits superior photocurrent in reverse bias conditions as compared to that of the TiO_2 nanorod structure [113]. This photoconductive behavior can be explained by the built-in electric field induced by the potential shift in the interface between both ZnO and ZnTe materials leading to effective electron/holes pair separation. Notably, it is clearly observed from Figure IV.8 that the I-V characteristic associated with the proposed MSM-based DM-UV-PDs design shows an asymmetric behavior for both reverse and forward conditions. This behavior suggests achieving an acceptable photocurrent (I=20µA) at the self-powered condition, which enables enormously reducing the photoreceiver systems power consumption. The obtained results confirm the fact that the band-bending occurred at the ZnO/ZnTe interface acts like an electric field modulator that enables the opportunity for achieving a good photoconductive aspect at zero voltage. It is important to note that the investigated design provides an extremely low dark current (below 10^{-3} nA) which is mainly due to the potential barrier induced at the ZnO/ZnTe interface.

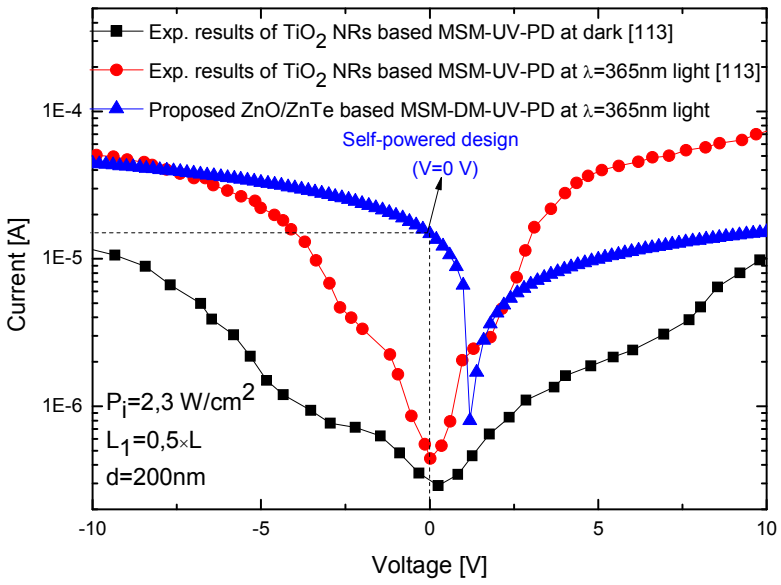

Figure IV.8: I-V characteristics of both the proposed ZnO/ZnTe MSM-based DM-UV-PDs design and the experimental results of MSM-UV-PD based on TiO_2 nanorod structure with and without illumination, N_a=10^{18} cm^{-3}, N_d=10^{18}cm^{-3}, P_i=2.3W/cm^2.

To further reveal the optical and electrical performances of the investigated MSM-based DM-UV-PDs structure, we propose to study how I-V curves of the proposed device are altered by introducing different materials in the second region (ZnO, ZnTe and TiO_2). Figure IV.9 depicts I-V characteristics of both proposed designs with ZnO/ZnTe and ZnO/TiO_2 lateral heterojunctions compared with that of the conventional design with uniform ZnO active layer. We can notice from this figure the good agreement between our analytical results and those obtained from TCAD simulations. Moreover, it is clearly demonstrated that the proposed designs incorporating the DM engineering paradigm greatly outperform the conventional ZnO-based MSM-UV-PD counterpart. Obviously, the use of dual thin-films based on ZnO/ZnTe and ZnO/TiO_2 interfaces bring the opportunity for achieving the asymmetrical property leading to reach superior photoresponses at V=0V as compared with that provided by the conventional design. Moreover, unlike the ZnO/ZnTe-based DM-UV-PD I-V curve, we can see from Figure IV.9 that the I-V characteristic of the ZnO/TiO_2 lateral heterojunction structure demonstrates higher photocurrent in forwarding bias conditions. In this case, the asymmetric behavior is changed as compared to that of ZnO/ZnTe interface. This phenomenon can be explained by the nature of the suggested heterojunctions (n/p or n/n), where the depletion regions induced in the interface play a crucial role in determining the asymmetrical behavior of the proposed design.

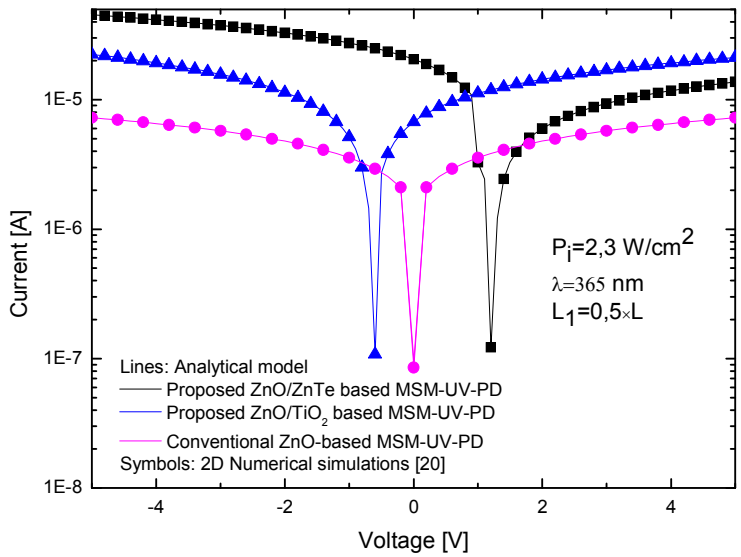

Figure IV.9: I-V characteristic of the conventional design compared with that of both proposed designs based on ZnO/ZnTe and ZnO/TiO_2 lateral heterojunctions under illumination with $N_a=10^{18}$ cm^{-3}, $N_d=10^{18}cm^{-3}$.

The encouraging results obtained for the distinctive photoconductive behavior of the proposed design at zero bias inspire subsequent investigations in order to achieve further improvements regarding the device self-powered property. The latter can be achieved by analyzing the impact of the materials engineering on the optical device properties such as the sensitivity and detectivity. Figure IV.10 (a) plots both device detectivity and sensitivity as a function of the normalized first region length position.

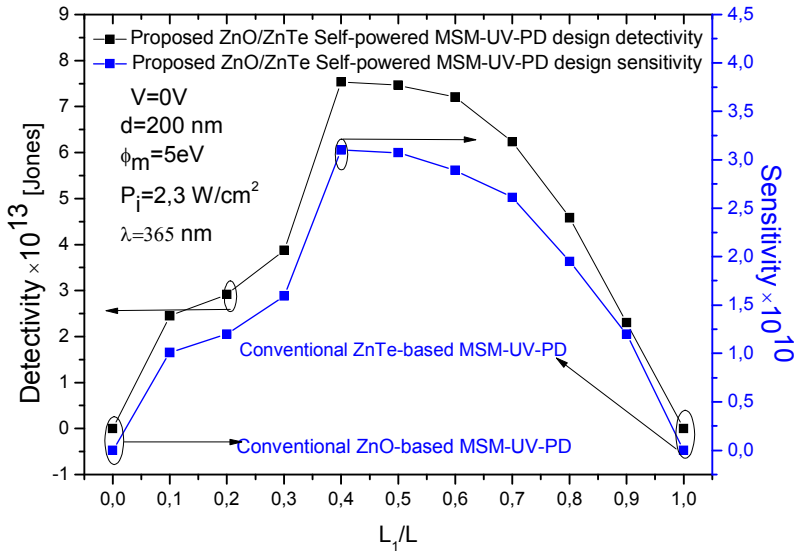

(a)

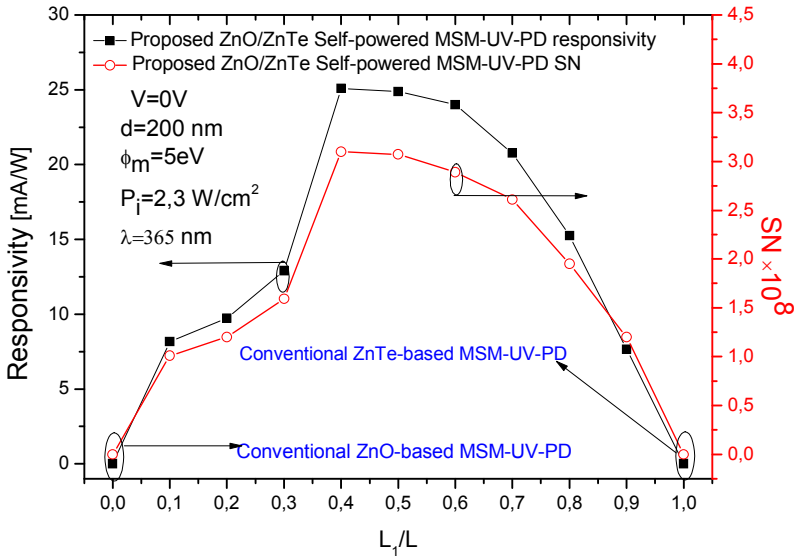

(b)

Figure IV.10: (a) Device detectivity and sensitivity against the normalized spacing length position for the proposed ZnO/ZnTe MSM-based DM-UV-PDs. **(b)** Variation of the Device responsivity and SN ratio against the normalized first region length with $N_a=10^{18}$ cm^{-3}, $N_d=10^{18}cm^{-3}$

While, Figure IV.10 (b) depicts the variation of both the device responsivity and the signal to noise ratio as a function of the normalized first region length. In a similar manner to the device detectivity, it is clearly observed that the proposed design enables improved performance as compared to the conventional design, where a high responsivity of 26 mA/W and superior SN ratio of 6×10^{8} can be achieved with taking $L_1=0.4\times L$. This is because of the improved derived current capability at self-powered conditions allowed by the proposed structure with DM aspect. Moreover, the potential barrier at the interface between both suggested materials can greatly reduce the dark current (I_{Dark}=0.5 nA), which leads to a substantial improvement regarding the signal to noise ratio.

In fact, using two different metals for a Schottky contact can indeed ensure the asymmetrical behavior of the device, which can in turn provide the self-powered characteristic as it is presented in [34], where it suggests a slight differences between the Schottky barriers height at both metal contacts. However, the obtained ON-current is very small, leading to reduced device properties at self-powered condition (I=50nA and R_{esp}=0.106 mA/W). Materials with high work-function values (Pt, Pd and Au) are in fact needed to enhance the derived current capability as well as the device responsivity, which can impose the high fabrication cost. Conversely, the proposed design suggests the opportunity for achieving superior performance through modulating the electric field behavior at the ZnO/ZnTe interface and achieving better photo-generated carrier separation. Moreover, the proposed design requires only the use of n-type doped polysilicon material as metal contact, which leads to significantly decrease the fabrication cost of the investigated UV sensor.

Despite the obtained results in improving the device performance at self-powered conditions, the design parameters like the geometrical configuration of the proposed DM thin-film, the metal work-function, the materials doping levels and the thin-film thickness have a profound implication in the device optical behavior and determine in a large extent the MSM-UV-PD performance. Moreover, although the good photocurrent recorded at zero bias for the proposed design, the device remains challenging for chip-level communication applications and requires more enhancements regarding the device power consumption as well as the device derived current capability. Therefore, it seems to be of great significance to identify the better design parameters that offer the

maximum device properties without neglecting the fabrication cost aspect. Hence, new insight based on an efficient shape optimization technique using PSO-based approach can intuitively be effective for achieving high-responsivity self-powered device at low cost, which constitutes the main objective of the next subsection.

IV.3.4 Optimization of the proposed self-powered photodetector design

In order to address important issues related to both global power consumption and the device optical performance at self-powered conditions, it seems crucial to develop an efficient optimization scheme by exploiting the accurate analytical models of the device properties. In this perspective, our proposed hybrid approach is based on developing a new methodology that would enable systematic improvement of the proposed design regarding three essential aspects. Firstly, achieving the desired optical and electrical performances by maximizing the device properties, secondly, performing the optimization procedure at self-powered conditions to ensure the low energy consumption property. Finally, reducing the elaboration cost through avoiding the use of noble materials with high work-function values (Au, Pt, Pd,…) to reach a low dark current.

Therefore, the proposed MSM-based DM-UV-PDs design will be optimized by satisfying the following objectives:

- Maximizing the normalized detectivity ΔD
- Maximizing the normalized responsivity ΔR_{esp}
- Maximizing the normalized derived current $\Delta I_{\max}$
- Maximizing the normalized sensitivity ΔS
- Maximizing the normalized $\Delta I_{ON} / I_{OFF}$
- Maximizing the normalized signal to noise ratio ΔSN
- Minimizing the normalized dark current ΔI_{OFF}

In our proposed design approach, we are interested in optimizing more than one metric as it is aforementioned. The weighted sum approach systematically brings the possibility to find an appropriate design configuration that leads to achieve our objectives. Thus, by using a mono-objective global optimization scheme which counts on weighting coefficients, the fitness function is given as follows

$$Fitness(X) = w_1(\Delta \mathrm{I}_{\mathrm{ON}} / I_{OFF}) + w_2 \Delta R_{esp} + w_3 \frac{1}{\Delta I_{OFF}} + w_4 \Delta SN + w_5 \Delta \mathrm{I} + w_6 \Delta S + w_7 \Delta D \quad \text{(IV.25)}$$

where w_n (n = 1-7) are weighting coefficients considered to be equal to 1/7.

In the global optimization procedure, the device properties (sensitivity, detectivity, I_{ON}/I_{OFF} ratio, SN and responsivity) are normalized with respect to their maximum theoretical values in order to avoid the domination of the detectivity parameter in the fitness function. In other words, the device properties are confined within the range of [0,1], which enables the possibility to take into account all the device properties equally. In this regard, the fitness function will also be maximized in the same range [0,1].

Clearly, a global optimization problem is mainly illustrated by a candidate solution in a well defined search space and a set of constraints that should be respected. In our case, the constraints used in the mono-objective optimization are imposed to achieve high-performance self-powered device. In fact, the idea behind is that the optimization procedure should be performed at zero bias, which means without an external applied voltage. Moreover, lower work-function value is imposed in order to ensure the low fabrication cost. The constraints can be given in our case by the following conditions

- $x \in [x_{m\min}, x_{m\max}]$, $x_i \in X$
- $V = 0$ (self-powered photodetector constraints)
- $\Phi_M = 4.8$ corresponds to n-doped polysilicon (for low-cost applications).

The flowchart of the proposed design methodology based on both analytical modeling and metaheuristic technique used to optimize the proposed MSM-based DM-UV-PDs is detailed in Figure IV.11.

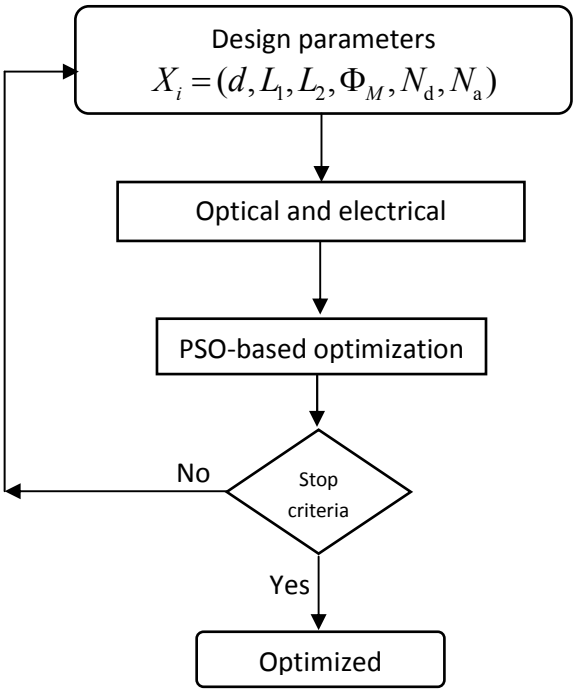

Figure IV.11: Flowchart of the proposed PSO-based optimization approach.

After performing the optimization procedure, the evolution of the fitness function versus the generation number is depicted in Figure IV.12, where it is obvious that with increasing the generation the fitness function is maximized, which can prove the outstanding capability of the proposed design approach to improve the device performance. We can also notice that the stabilization of the objective function can be achieved nearly after 450 iterations.

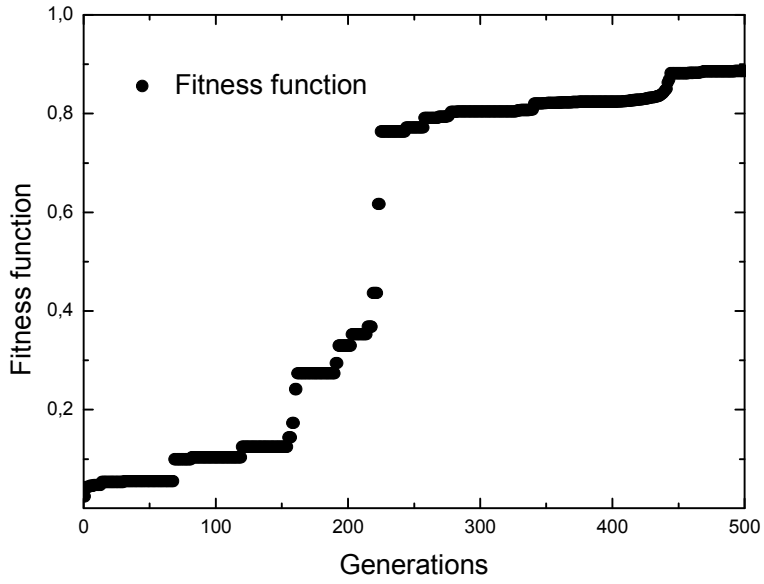

Figure IV.12: Evolution of the normalized overall objective functions versus the number of generation.

As expected, the proposed hybrid approach can give rise to significant improvements in the MSM-based DM-UV-PDs photoconductive behavior at self-powered conditions. Moreover, the adopted design methodology has succeeded in selecting the better and the most favorable design parameters associated with superior device properties and low power consumption.

For the completeness of this work, it appears important to evaluate the optimized MSM-based DM-UV-PDs for low power photoreceiver system applications. In this perspective, Table IV.2 summarizes a comparison of the performance metrics obtained from the optimized MSM-based DM-UV-PDs designs with that of the experimental results of a ZnO-based MSM-UV-PD self-powered design [35]. From this table, it is clearly demonstrated that our optimized designs using both ZnO/TiO_2 and ZnO/ZnTe lateral heterojunctions exhibit superior device properties in comparison with that of the

ZnO-based self-powered design reported in [35]. In this framework, it can be noticed that an enhancement of 485% in the device responsivity is recorded as compared to the experimental results of the ZnO-based self-powered. The optimized design with ZnO/ZnTe yields higher photocurrent value of 1.1 mA, in addition to an extremely low dark current value of 5.2×10^{-5} nA. To this extent, it is evidently confirmed that the global optimization significantly improves the device performance through identifying the best design configuration of the proposed sensor parameters that enables maximizing the objective function. Thus, the optimized design offers superior device properties over the conventional design at self-powered conditions, which is mainly ascribed to a mixture of two effects; firstly, the enhanced optical behavior of the investigated design offered by the geometrical optimization by carefully tailoring the device dimensions for maximizing the absorbance and minimizing the total reflectance. Secondly, the global optimization enables the opportunity for achieving the maximum possible electric field at the ZnO/ZnTe interface, which leads to an efficient separation of the photogenerated electron/hole pairs in addition to an effective reduce in the dark current due to the high potential barrier provided by the optimized design. Therefore, these remarkable results prove the outstanding capability of the optimized MSM-based DM-UV-PDs structure for improving the device performance at self-powered conditions. The proposed hybrid approach offers the possibility for modulating the electric field behavior at the ZnO/ZnTe junction that opens up the route to record distinctive electron/hole pairs separation. Moreover, it can be deduced that the optimized design can give wider possibilities to meet the limitations imposed by the OWCS progress regarding the requirement of high responsivity self-powered devices with low fabrication cost. Likewise, the optimized MSM-based DM-UV-PDs structure illustrates an ultimate advantage described by achieving ultra-low dark current without using noble materials as Schottky electrodes, emphasizing the reduced power consumption at a low elaboration cost.

In summary, it is evidently confirmed that the adopted mixture approach based on the analytical modeling of the proposed MSM-based DM-UV-PDs design and metaheuristic investigation can dramatically improve the device photoconductive behavior, not only enables the benefit for achieving the self-powered property, but also leading to improving the device optical performance. This allows developing high-performance photodetectors with low power consumption.

Table IV.2: Overall performance metrics comparison obtained from the optimized MSM-based DM-UV-PDs designs with that of the experimental results of ZnO-based self-powered design for optical communication applications.

Symbol	ZnO-based Self-powered MSM-UV-PD [35]	ZnO/TiO_2-based self-powered MSM-DM-UV-PD design	ZnO/ZnTe-based self-powered MSM-DM-UV-PD design
Design variables:			
Wavelength λ (nm)	365	365	365
Incident power P (mW/cm^2)	2.3	2.3	2.3
Applied voltage V(V)	0	0	0
Contact work function (eV)	5.1	4.8	4.8
ZnO doping concentration (cm^{-3})	-	N type 1×10^{16}	N type 3×10^{16}
TiO_2 doping concentration (cm^{-3})	-	N type 5×10^{17}	-
ZnTe doping concentration (cm^{-3})	-	-	P type 6×10^{17}
Spacing length L(µm)	10	11	12.5
First region length L_1(µm)	-	5	5.2
Second region length L_2(µm)	-	6	7.3
Film thickness d (nm)	-	154	137
Performance parameters:			
OFF current (I_{OFF}) (nA)	-	1.65	**5.2×10^{-5}**
ON-OFF Ratio (I_{ON}/I_{OFF}) (dB)	-	242.21	**479**
Sensitivity (S)	-	1.8×10^{7}	**2.6×10^{12}**
Signal to Noise ratio (SN)	-	1.8×10^{5}	**2.6×10^{10}**
Derived current I_{MAX} (mA)	1.2×10^{-2}	0.36	**1.1**
Detectivity (Jones)	1.9×10^{10}	1.7×10^{13}	**4.4×10^{13}**
Responsivity (mA/W)	20	41.2	**97.5**

IV. 4. Conclusion

In this chapter, two promising features are proposed to improve the MSM-based UV-PDs optical and electrical performances. Firstly, a new TiO_2-based MSM UV-PD with diffraction grating aspect has been proposed and semi-analytically investigated using accurate solutions of Maxwell's equations and coupled Poisson-continuity equations. Furthermore, it has been found that the grooves texturization aspect has an important impact on the device optical behavior. The introduced grooves can offer the opportunity for modulating the electric field behavior inside the TiO_2 absorber layer. The proposed PSO-based approach has succeeded in improving the device performance, where the UV sensor FoMs are significantly improved using the optimized design.

Secondly, the role of dual-material engineering aspect in improving the self-powered MSM-based UV-PDs performance has been analytically investigated. Our study reveals that the adopted design amendment behaves electrically as an electric field modulator, which enables the possibility to enhance the transport efficiency of the photo-generated carriers without an external applied voltage. Moreover, a new hybrid approach that combines analytical modeling and PSO-based metaheuristic technique has

been proposed with the aim to achieve favorable self-powered device. Promising results have been obtained with respect to the device properties, where the optimized structure offers superior derived photocurrent, responsivity, high-sensitivity, low power consumption and improved detectivity as compared to the conventional counterpart. Finally, the obtained results indicate that the proposed designs provide wider possibilities for bridging the gap between high-performance photodetectors with low power consumption and reduced fabrication cost. This makes them potential alternatives for providing low energy consumption devices for high-performance communication and monitoring applications. However, the extreme requirement of low capacitance photoreceivers for chip-level communication applications imposes the search for alternative devices. Using phototransistors instead of photodetectors can be a promising solution for achieving high-performance optical links but unfortunately with sacrificing the elaboration cost aspect.

The next chapter will discuss the prospect of improving phototransistors performance through proposing innovative low-cost designs with improved sensitivity in order to develop high-performance photoreceivers for chip-level communication applications.

Chapter V

Design and Optimization of Novel Ge-based Phototransistor Designs

***Abstract:** Chapter V of this thesis investigates the prospect for improving the Ge-phototransistor performance by proposing two novel structures. The first one consists of a new junctionless optical controlled field effect transistor (JL-OCFET), where its comprehensive theoretical model is developed. The latter is exploited to formulate the objective functions to optimize the device performance using Genetic Algorithms (GAs). The optimized design offers high optical performance with low elaboration cost. On the other hand, a new optically controlled tunneling field effect transistor (OC-TFET) based on SiGe/Si/Ge Hetero-channel is proposed to improve the optical commutation speed and reduce the power consumption. Importantly, a new Figure of Merit (FoM) parameter called optical swing factor that describes the phototransistor commutation speed is also proposed.*

V. 1. Introduction

The resistive loss of the electric wire in inter-chip data communication originates electric signal attenuation and distortion, which imposes the use of signal processing to maximize the emitted information [1-6]. Recently, condensed efforts and attentions have been paid to optical interconnects due to the lower resistive losses and the enormous bandwidth achieved by OWCS [3-6]. The high energy consumed by the optical links is the most pronounced problem that should be addressed for the eventual replacement of electrical wires. Obviously, the total power consumption associated with the OWCS is greatly determined by the photoreceivers for which the optical power levels required for the communication can be estimated. In this context, several optical receiver structures based on Schottky barrier photodiode, MSM photodetectors and FET-based phototransistors have been investigated during the last few years in order to improve the OWCS performance [113-116]. In this framework, small capacitance photoreceivers are required in order to reach high sensitivity and faster response [34], [132-134]. Despite this, the incapability to reduce the photoreceivers capacitance still persists and prevents achieving competitive optical links at chip-level communication applications. On the other hand, the high circuit density constraint associated with the readout stage can increase also the dissipated power. In this context, decreasing the photoreceiver capacitance and getting rid of TIA could reduce enormously the total power consumption of the optical links [34], [132-134]. Obviously, the FET-based phototransistor is regarded as the most common device to open up the possibility for avoiding the high density of the optoelectronic readout circuits. Moreover, Ge-based phototransistors, monolithically integrated to silicon electronics, combines impedance amplifier with NIR photodetector, which can pave the way to reach high optical gain phototransistors with receiver-less detection property [132-135]. Unfortunately, the Ge-based OCFET operating at λ=1.55µm has revealed excellent performance but only with individual tenability that is, low power and cost devices or high-performance and ultrasensitive phototransistors. Moreover, the use of highly doped Ge gate can exacerbate the dark current and hence degrade enormously the device FoMs. Further, the thermionic limit of the swing factor (60mV/decade) associated with the conventional MOSFET design can prevent achieving improved optical commutation speed, which is considered as an essential issue for designing high-performance OWCS. Accordingly, Ge-based OC-FET designs are believed to face an upward amendment to

meet the above-outlined requirements. In this perspective, alternative approaches and design methodologies remain inevitable to achieve ultrasensitive photoreceivers at low elaboration cost and with lower energy consumption.

The main goal of this chapter is to propose new design methodologies in order to overcome the abovementioned challenges associated with the Ge-based phototransistor. For this purpose, two approaches have been pursued. The first one has focused on proposing a novel Junctionless architecture in order to reduce the manufacturing cost and achieve ultrasensitive phototransistor. To analyze the proposed device performance, accurate analytical models describing the device photoconductive behavior are developed. The results showed that the analytical models are in good agreement with the 2-D numerical simulation over a wide range of device parameters [123]. Moreover, an overall performance comparison between both conventional Inversion Mode (IM) and the proposed JL devices is carried out. Further, new insight based on global optimization is proposed to improve the device performance. The obtained results indicate the crucial role of the JL architecture for overcoming the trade-off between the high sensitivity and power consumption.

To consolidate this perspective, the second part of this chapter is devoted to the improvement of the Ge-based phototransistor regarding both optical commutation speed and the total power consumption. To do so, a new optically controlled tunneling field effect transistor based on SiGe/Si/Ge Hetero-channel is proposed. Moreover, a new FoM parameter called optical swing factor that describes the phototransistor optical commutation speed is proposed. We demonstrate that the band-to-band tunneling effect can be beneficial for improving the device optical commutation speed. The impact of the Ge mole fraction of the SiGe source region on the device FoMs is investigated. Besides, an overall performance metric comparison between the proposed OC-TFET device and the conventional structures is performed, where the investigated design greatly outperforms the conventional counterparts.

V. 2. Part (1): Planar Junctionless Phototransistor: A Potential High-Performance and Low-Cost Device for Optical Communications

V. 2.1 Motivation

The Junctionless aspect used for designing the transistors has been aggressively driven into deep submicron scales to achieve the desired improvement regarding the device fabrication cost. In this perspective, the main advantage offered by this design

principally resides on avoiding the elaboration of the S/D regions (n^{++}) and hence the establishment of junctions that seems to be not a trivial task. This constitutes a serious problem that imposes the high manufacturing cost for the IM design namely the high thermal budget. Device structures that do not have any junctions in the S–channel–D path will hence be of interest for low-cost optoelectronic applications. Several experimental studies have confirmed the low fabrication cost of the JL structure in comparison with the conventional IM design [136-140]. Intuitively, assuming the Ge-based phototransistor with JL architecture not only enables achieving the desired improvement concerning the phototransistor elaboration cost, but also provides the opportunity for enhancing the device sensitivity. To this extent, this work presents the potential of a new JL-OCFET design for achieving photoreceivers with both ultrasensitive and low power dissipation characteristics. The impact of different design parameters on the phototransistor performance is analytically investigated. Finally, the developed analytical expressions are exploited to formulate the objective functions to optimize the Ge-based phototransistor regarding both ultrasensitive and low power consumption aspects using GAs approach described in the third chapter.

V. 2.2 Modeling methodology

The junctionless design basically relies on the fact that the silicon channel and the source/drain regions are uniformly and highly doped regions, which are indicated by n+/n+/n+. Figure V.1 describes schematically the investigated JL-OCFET design, where the germanium gate is deposited on the oxide/n-Si structure. In order to acquire an initial band bending between the photosensitive gate and the silicon body, we consider the Ge gate with p-type doping concentration illuminated at normal incidence with a monochromatic light at the wavelength value of $\lambda = 1.55\mu m$. For our analytical modeling, t_{Ge} and t_{Si} are the photosensitive Ge layer and the silicon thicknesses, respectively. L represents the channel length; N_d and N_a denote the doping of the silicon channel and the Ge gate, respectively.

In our analytical modeling procedure, the investigated JL-OCFET design is assumed as a long channel device, which allows us to reduce the Poisson's equation to a 1-D problem. Likewise, for achieving an excellent light controllability of the phototransistor channel conductivity, in our analytical modeling, the silicon body is considered very thin (<40 nm). On the other hand, in order to avoid the quantum confinement effects the minimum channel thickness value is restricted by a limiting value equals to 10nm (larger

than 5nm). Hence the silicon body is taken as (10nm<t_{Si}<40 nm).

It is important to note that for the fabrication viewpoint, the proposed JL design involves a simple manufacturing process, where a simple epitaxial growth of the Ge on the oxide/n^+-Si structure is sufficient to develop the JL-OCFET design. Moreover, source, drain and gate contacts can be also deposited on the top of the investigated JL-based phototransistor.

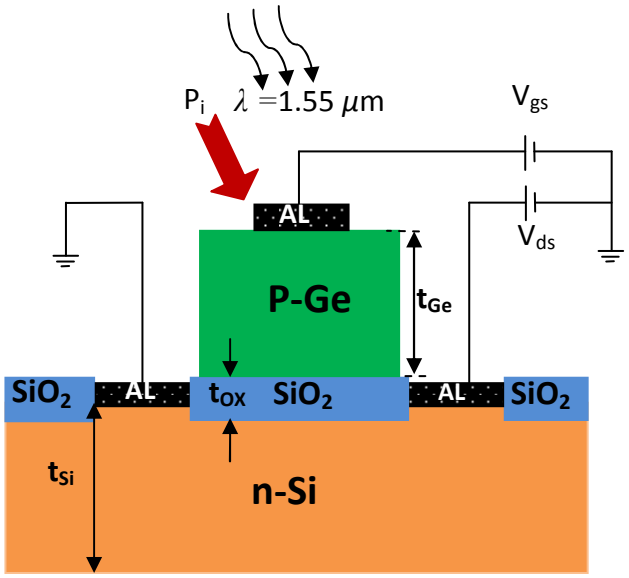

Figure V.1: Cross-sectional view of the proposed JL-OCFET phototransistor.

IV.2.2.1 Drain current model

Poisson equation for an N-type device, with donor doping impurities is given by

$$\frac{d^2\Phi}{dx^2} = \frac{qN_d}{\varepsilon_{si}}\left(\exp\left(\frac{\Phi(x)-V}{V_t}\right)-1\right) \qquad \text{(V.1)}$$

where q represents the electron charge, $\Phi(x)$ is the electrostatic potential, V_t is the thermal voltage which is equal to $\frac{KT}{q}$, V reveals to the potential shift across the silicon body, from source V_S (0)= 0 V to drain V_D(L) and ε_{si} represents the silicon permittivity.

Under the condition of zero electric field at the end of the semiconductor film (x=t_{si}) that describes the fully depletion mode, the boundary conditions for determining the potential $\Phi(x)$ in our investigated structure can be given by

$$\Phi(0) = \Phi_s \qquad \text{(V.2a)}$$

$$\left.\frac{d\Phi}{dx}\right|_{x=t_{si}} = 0 \qquad \text{(V.2b)}$$

$$V(0) = 0 \qquad \text{(V.2c)}$$

$$V(L) = V_{ds} \qquad \text{(V.2d)}$$

where Φ_s reveals the surface potential, V_{ds} is the applied drain-source voltage.

By integrating Eq.(V.1) from x=0 to x=t_{si} and using the appropriate boundary conditions we can find the following equation

$$\left[\frac{d\Phi}{dx}\right]^2 = \frac{qN_d\, V_t}{\varepsilon_{si}}\left(\exp\left(\frac{\Phi_s - V}{V_t}\right) - \exp\left(\frac{\Phi_0 - V}{V_t}\right) - \frac{\Phi_s - \Phi_0}{V_t}\right) \qquad \text{(V.3)}$$

where Φ_0 represents the potential at x=t_{si} and Φ_s is the surface potential.

Obviously, the gate voltage V_{gs} is divided between the insulator and the Si film; hence using the continuity of the electric flux at the Oxide/n-Si interface, we can find the surface potential as follows

$$\Phi_s = V_{gs}^* - V_{FB} - \frac{Q_m - Q_{fix}}{C_{ox}} \qquad \text{(V.4)}$$

where Q_m and Q_{fix} refer to the mobile and the fixed charges respectively, the fixed charge can be estimated from $Q_{fix} = qN_d t_{si}$. The oxide capacitance C_{ox} can be calculated from $C_{ox} = \varepsilon_{ox} / t_{ox}$, with ε_{ox} and t_{ox} are the oxide permittivity and the oxide thickness, respectively. V_{FB} represents the flat band voltage which is principally related to both Ge and Si workfunctions and can be given as [115-117] and [132]

$$V_{FB} = \varphi_{Ge} - \varphi_{Si} + V_t \ln\left(\frac{N_d}{n_i}\right) \qquad \text{(V.5)}$$

where, φ_{Ge} and φ_{Si} are Ge and Si workfunctions, respectively, V_{gs}^* represents the optically modified gate voltage which is in our case mainly depending on the optically induced voltage V_{ph} and can be calculated from $V_{gs}^* = V_{gs} + V_{ph}$.

In order to estimate analytically the optically controlled voltage, it is essential to understand the operation mechanism of the proposed design. In this framework, under illumination with an appropriate input light power P_i, charge carriers will be photogenerated in the Ge photosensitive gate that can change the band bending in the Si

channel which leads to an increase in the channel conductivity. This physical mechanism behaves like the gate voltage control and suggests the opportunity for modulating the device output current by simply modifying the input power P_i. To this extent, it seems more accurately to exploit the similar modeling approach used for estimating the open circuit voltage for the solar cell devices [115-117], [125]. Therefore, the optically controlled voltage can be given as

$$V_{ph} = V_t \ln\left(\frac{J_{ph}}{J_S}\right) \tag{V.6}$$

with, J_S is the saturation current density expressed as

$$J_S = \left(\frac{qN_cN_v}{N_a}\right)\sqrt{\frac{D_n}{\tau_n}}\exp\left(\frac{-Eg_{ge}}{KT}\right) \tag{V.7}$$

where, N_c and N_v are effective densities of states in the Ge valence and conduction bands, respectively, τ_n represents the free carrier life time, D_n is diffusion coefficient and Eg_{Ge} reveals the Ge bandgap.

For estimating the optically controlled voltage, we need to calculate the photocurrent density J_{ph} generated in the Ge active layer. To do that, we solve the continuity equation by applying the appropriate boundary conditions given as

- At x=- (t_{ox}+t_{Ge}) we calculate the recombination velocity (S_p) using the following formulation $D_P\frac{d(P_n - P_{n0})}{dx} = S_P(P_n - P_{n0})$.
- At the x=-t_{ox} which refers to the interface between the germanium gate and the oxide, we assume that the excess carrier density can be neglected ($P_n - P_{n0} = 0$).

Therefore, after some mathematical manipulations we can express the photocurrent density in the Ge gate as

$$J_{ph} = \left[\frac{q\eta(1-R)\alpha L_P}{(L_P{}^2\alpha^2 - 1)}\right] \times \left[\frac{\left(\frac{S_PL_P}{D_P} + \alpha L_P\right) - \exp(-\alpha t_{Ge})\left(\frac{S_PL_P}{D_P}ch\left(\frac{t_{Ge}}{L_P}\right) + sh\left(\frac{t_{Ge}}{L_P}\right)\right)}{\left(\frac{S_PL_P}{D_P}\right)sh\left(\frac{t_{Ge}}{L_P}\right) + ch\left(\frac{t_{Ge}}{L_P}\right)} - \alpha L_P\exp(-\alpha d)\right] \tag{V.8}$$

where L_n represents the diffusion length calculated from $L_n = \sqrt{D_n \tau_n}$, R is the reflection coefficient and η is the number of the incident photons related to the incident power P_i, α represents the absorption coefficient, which defined by $\alpha(\lambda) = \frac{C}{E(\lambda)}\left(E(\lambda) - E_{gGe}\right)^{\frac{1}{2}}$ with C a fitting parameter [141]. It is important to note that this formula is mainly depending on the material band-gap, where it can be applied to investigate the optoelectronic devices with different materials. It is also worth mentioning that the generation of carriers in the silicon film is ignored due to the high band gap of the silicon material.

To calculate the electrostatic potential for both depletion and accumulation modes, we assume that the potential shape along the channel has a parabolic profile which appears to be an accurate presentation in full depletion and accumulation modes [139-140]. Thus, by applying the appropriate boundary conditions given by Equation (2), and under the hypothesis that the electric field at the end of the silicon body is equal to zero we can find the electrostatic potential as follows

$$\Phi(x) = \frac{\Phi_s - \Phi_0}{t_{si}^{\,2}}\left(x - t_{si}\right)^2 + \Phi_0 \tag{V.9}$$

To estimate the mobile charge density in the silicon body, we need to apply Gauss theorem at the Si/SiO_2 interface. Therefore, the relationship between the potential and the mobile charge is given by

$$\left.\frac{d\Phi(x)}{dx}\right|_{x=0} = \frac{Q_m - Q_{fix}}{\varepsilon_{si}} \tag{V.10}$$

In the depletion mode, we assume that the mobile charge in the silicon channel is governed by the Boltzmann distribution and using Equations (3, 9 and 10), we can find an implicit form of the mobile charge for both accumulation and depletion modes as

$$Q_m = Q_{fix} Q_i \frac{1 - M\exp\left(\frac{t_{si}\left(Q_m - Q_{fix}\right)}{\varepsilon_{si} V_t}\right)}{\left(Q_m - Q_{fix}\right) - \frac{\varepsilon_{si} V_t}{t_{si}}\ln(M)} \exp\left(\frac{\Phi_s - V}{V_t}\right) \tag{V.11}$$

with $Q_i = \varepsilon_{si} V_t / t_{si}$ and $M = 1 + \sqrt{\pi \frac{Q_{fix}}{2Q_i}}\frac{1}{2}\exp\left(-\frac{t_{si}\left(Q_m - Q_{fix}\right)}{\varepsilon_{si} V_t}\right)$.

In order to calculate the drain current using the charge based modeling methodology, it is of great significance to develop an explicit formulation of the mobile charge density. This can be achieved using the Lambert function LW(z) [142]

$$LW(z)=\ln(1+z)\left(1-\frac{\ln(1+\ln(1+z))}{2+\ln(1+z)}\right) \tag{V.12}$$

Therefore, using the Lambert function approximation and after some mathematical manipulations, we can find the mobile charge density as follows

$$Q_m(V)=Q_e LW\left[\frac{KM}{Q_e}\frac{\exp-\left(\frac{Q_{fix}-MQ_{m1}(V)}{Q_i}\right)}{Q_{m1}(V)-Q_{fix}-Q_i\ln(M)}\exp(\psi(V))\right] \tag{V.13a}$$

with

$$Q_{m1}(V)=\mathrm{C_{ox}}V_t LW\left[\frac{K\exp(\psi(V))}{\mathrm{C_{ox}}V_t}\frac{1-\exp\left(\frac{Q_{fix}-\mathrm{C_{ox}}V}{Q_i}\ln(\exp(\psi(V))+1)\right)}{\mathrm{C_{ox}}V_t\ln(\exp(\psi(V))+1)-Q_{fix}}\right] \tag{V.13b}$$

with $K=Q_{fix}Q_i$, $Q_e=\frac{Q_i\mathrm{C_{ox}}V_t}{Q_i+\mathrm{C_{ox}}V_t}$ and $\psi(V)=\left(V_{gs}+V_{FB}+\frac{Q_i}{\mathrm{C_{ox}}}+V\right)/V_t$.

In our case, we consider a long channel structure, therefore only the drift-diffusion model is used to calculate the drain current for different values of the applied gate voltage V_{gs}. Thus, the drain current can be estimated by the integration of the mobile charge between the two values of drain and source bias $V_2= V_{ds}$ and $V_1= 0$, respectively.

$$I_{ds}=\frac{W\mu_n V_t}{L}\int_0^{V_{ds}}Q_m dV \tag{V.14}$$

where μ_n reveals the electron mobility in the silicon channel region, which can be affected by the high channel doping profile. The latter plays a crucial role in our proposed junctionless device. Hence, the mobility is inversely proportional to the channel doping and it can be given as

$$\mu_n=\mu_{min}+\left(\frac{\mu_{max}-\mu_{min}}{1+\left(\frac{N_d}{N}\right)^{\alpha}}\right) \tag{V.15}$$

with $\mu_{max} = 1400\,cm^2/V.s, \mu_{min} = 68.8cm^2/V.s$ are fit parameters related to the maximum and the minimum silicon mobility, respectively, α =0.71 and N =10^{18}cm^{-3} [143], [144]. It is to note that these fit parameters are function of temperature and this formula can be applied at near room temperature and low electric fields.

Based on the calculation methodology presented in [140], we can calculate the integral given in (Equation (14)). Thus, we can find the drain current with a compact accurate analytical form as follows

$$I_{ds} = \frac{W\mu_n V_t}{L}\left(F(0) - F(V_{ds})\right) \tag{V.16}$$

where $F(0)$ and $F(V_{ds})$ are estimated by substituting V =0 and V= V_{ds} , respectively, in the following analytical formulation

$$F(V) = \frac{Q_m(V)^2}{Q_e} + 2Q_m(V) - Q_m(V)\ln\left(1+\exp\left(\frac{Q_m(V)-Q_{fix}}{MQ_i}\right)\right)$$
$$+\frac{Q_{fix}}{2}\ln\left[\frac{Q_m(V)-Q_{fix}}{2Q_i\left(\exp\left(\frac{Q_m(V)-Q_{fix}}{2Q_i}\right)-1\right)}\right] \tag{V.17}$$

V. 2.3 Results and discussions

To assess the most important characteristic of OCFET that describes the device capability for controlling the channel conductivity, we need first to show the optical modulation behavior of the drain current. This enables us to independently evaluate our proposed junctionless design regarding this aspect. For this purpose, we illustrate in Figure V.2 the transfer characteristics of the proposed JL-OCFET design for different incident power intensities and with an appropriate gate voltage value of (V_{gs}=-0.3V). From this figure, we can notice the good agreement between our analytical results and those obtained from numerical simulations. Moreover, we can see also the simple and the excellent operating behavior of the JL design for an appropriate wavelength value of 1.55µm, where by increasing the incident power intensity we can raise the drain current that describes the excellent fluctuation from the OFF to ON state. The obtained optical behavior confirms the fact that the optically induced voltage acts like an additional gate voltage bias that modify the band-bending and hence achieve the photoconductive aspect of the channel. Furthermore, the proposed design can provide an acceptable ON

current value of (8µA). While, the JL-OCFET presents extremely low dark current (below 10^{-3} nA) which can be attributed to the fully depletion of the channel under dark condition with the appropriate gate voltage value of V_{gs}=-0.3V. In contrast, the conventional IM-OCFET exhibits higher drain current in darkness (I_{dark}=50nA) [117], which proves the superior switching behavior of the JL design over the conventional IM-OCFET structure.

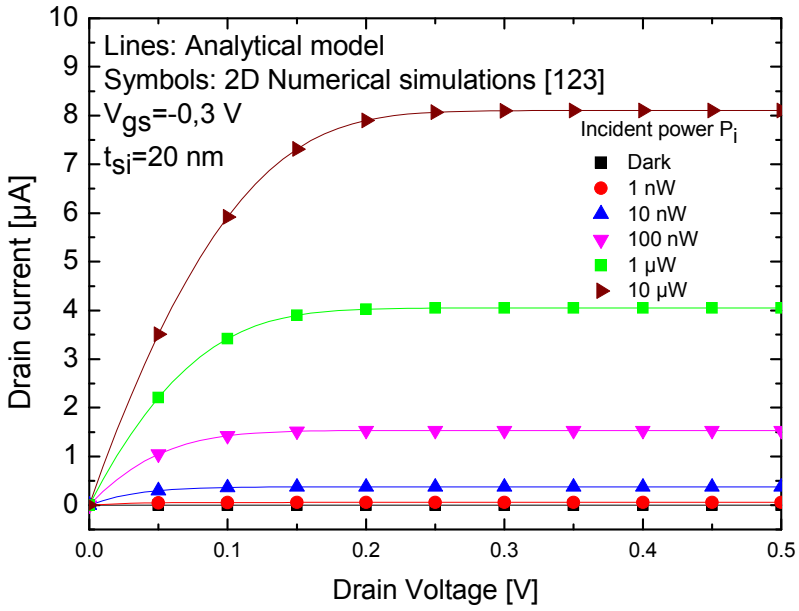

Figure V.2: I-V characteristics of the proposed JL-OCFET for different optical powers, with N_a=5.10^{18} cm^{-3}, N_d=1.$10^{19}$$cm^{-3}$, applied gate voltage V_{gs}=-0.3 V and drain voltage V_{ds}=0.2 V.

The encouraging results obtained for the excellent optical controllability of our proposed design inspire further studies using other performance parameters such as the on-state to off-state current ratio (I_{ON}/I_{OFF}). In this framework, Figure V.3 depicts the variation of the I_{ON}/I_{OFF} ratio as a function of the Ge gate doping concentration for both proposed JL and conventional IM designs. It is important to note that for achieving a good optical switching performance, the applied gate voltages should be approximately equal to the threshold voltage for each design. This can induce higher electric field in the Ge film, which can in turn enhance the charge separation and the energy bending in the Si film. It is clearly observed from this figure that the proposed design provides superior electrical performance in comparison with the IM-OCFET design especially for the high doping concentration values. Otherwise, the results from the published work [117], show a decrease in the I_{ON}/I_{OFF} ratio behavior for the case of larger Ge-gate

doping as compared to the Si channel doping that results in increasing the potential drops in the Ge gate. This can greatly affect and reduce the bend-banding in the Si channel and hence damage the modulation of the channel conductivity. While, the high potential drops across the Ge gate can improve the electron-hole pair's dissociation offering excellent device sensitivity. In contrast, for our proposed design this problem is completely not pronounced owing to the high doping concentration of the channel in the JL design, which gives the opportunity for achieving both characteristics namely the improved charge separation and the good channel conductivity modulation benefit. Moreover, the limited silicon thickness sets the depletion-mode nature of the phototransistor especially in dark condition leading to very low dark current and enhance the I_{ON}/I_{OFF} ratio.

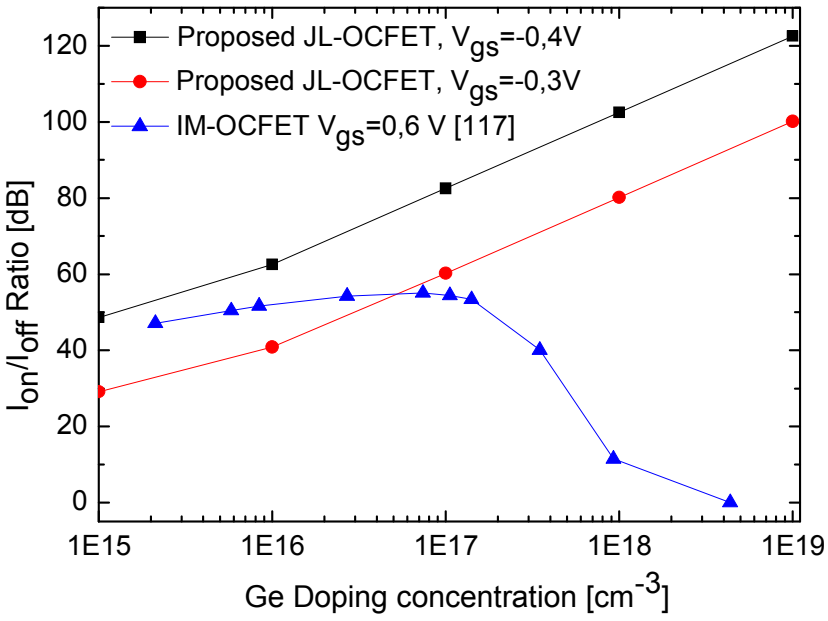

Figure V.3: Variation of the I_{ON}/I_{OFF} ratio against the Ge-gate doping concentration of the proposed JL-OCFET design for dissimilar applied gate voltage compared with that of the conventional IM-OCFET with V_{gs} = 0.6 V.

To further reveal the optical and electrical properties of our proposed JL design, we show in Figure V.4 the device detectivity versus the incident optical power intensity for both proposed JL-OCFET and conventional IM-OCFET structures for a fixed applied gate and drain voltages, V_{gs} = -0.3 V and V_{ds} =0.25V. As expected, the peak detectivity of the proposed design is much higher than that provided by the IM-OCFET structure, where a maximum detectivity of (5×10^{14} Jones) with (2100%) relative improvement has

been achieved by using the JL aspect, which proves the high optical-to-electrical conversion efficiency enabled by the analyzed JL-based phototransistor. In addition, we can notice also from this figure that the proposed JL-OCFET exhibits a high detectivity performance for weak optical signals in comparison to that provided by the conventional IM counterpart, where the device detectivity reaches its maximum for a very low light power value of (~4nW). This improvement can be ascribed to a combination of two effects: firstly, the increased potential drops in the Ge gate offers an excellent and effective charge separation in the photosensitive layer. Secondly, the small thickness of the silicon film leads to the achievement of a full depletion mode in darkness, which opens up the way for acquiring a good light control of the transport mechanism in the channel.

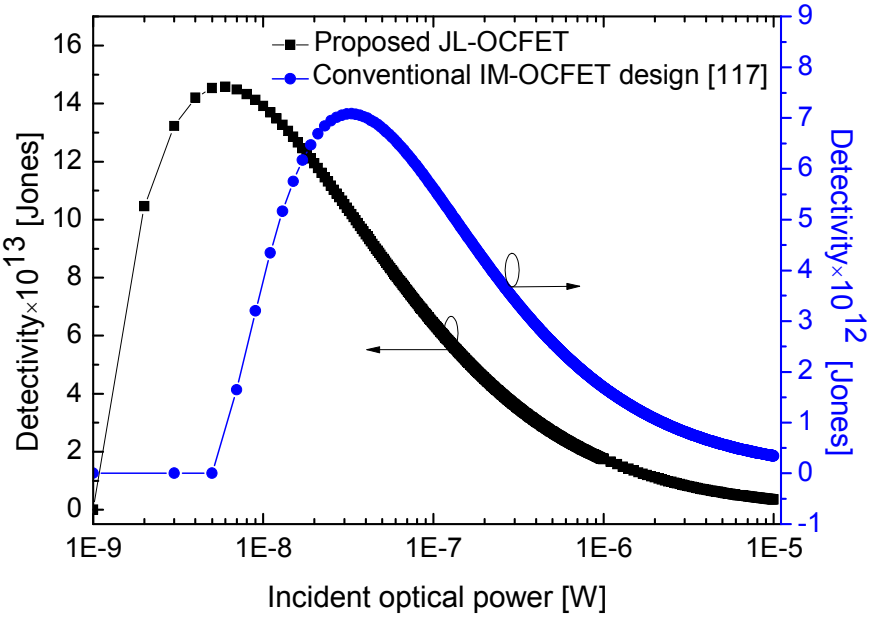

Figure V.4: Device detectivity versus the applied optical powers for different designs (conventional IM-OCFET, proposed JL-OCFET).

Basically, there are also more other FoMs that characterize the optical communication systems in terms of power consumption, which should be carefully analyzed. To this extent, in order to get a qualitative idea about the impact of the gate voltage on the device optical performance, Figure V.5 depicts both device sensitivity and signal to noise ratio parameters with respect to the applied gate voltage. This figure illustrates the steep decrease of the phototransistor sensitivity and the SN ratio with the increase in the applied gate voltage. This phenomenon can be explained by the strong

dependence between the gate voltage and the depletion width, where the critical gate voltage is strongly correlated with depletion width that is related in turn to the channel thickness. Besides, increasing further V_{gs}, the device sensitivity will be degraded because of the larger dark current when the gate voltage approaching to the threshold voltage that describes the accumulation mode of the JL-OCFET. In the other side, it is evident that the proposed JL-OCFET design exhibits high optical sensitivity and SN ratio. This substantial result can be related to the efficient charge separation in the Ge gate in addition to the superior threshold voltage sensitivity of the JL technology in comparison to the IM design.

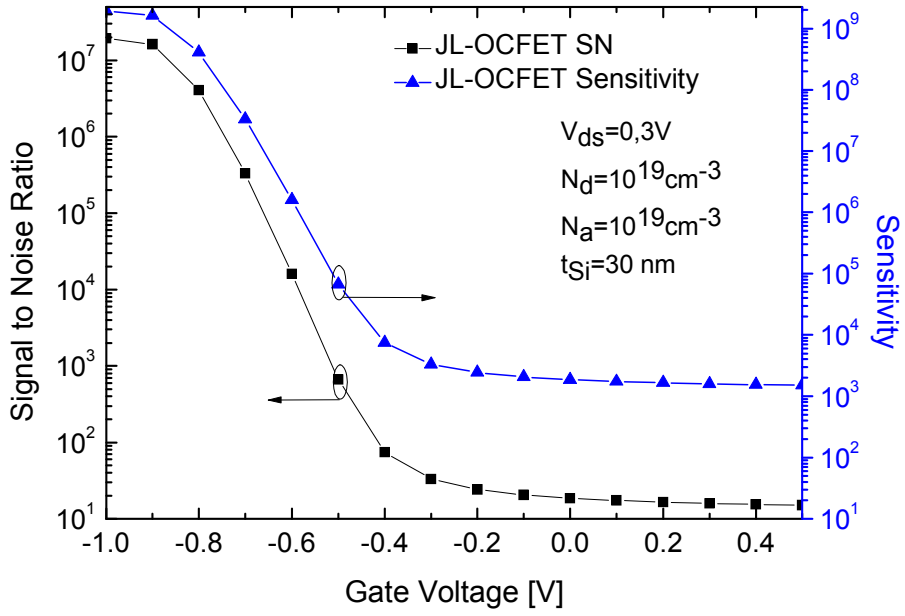

Figure V.5: Variation of the device sensitivity and the signal-to-noise ratio as function of the applied gate voltage with $N_a=5.10^{18}$ cm^{-3}, $N_d=1.10^{19}cm^{-3}$, t_{Si}=30nm, t_{ox}=4nm, t_{Ge}=200nm and V_{ds}=0.3V.

Therefore, two promising features are simultaneously achieved with respect to the device optical and electrical performance. First, superior optical control of the switching behavior is obtained which leads to high commutation performance for digital data processing. Second, the advantage of a simple fabrication process and reduced power dissipation compared to the conventional IM devices. These remarkable results and the complex behavior regarding the high dependence between the electrical and physical design parameters motivate us to conduct new computation methodology for optimizing the device performance, which constitutes the main objective of the next subsection.

V. 2.3.1 Device performance optimization

To a great extent, the Junctionless design can highly improve the optical performance of the OCFET through achieving better optical and electrical responses. However, it seems possible to reach further improvements concerning the phototransistor FoMs, where adjusting the design parameters of the proposed JL-OCFET can offer the opportunity for modulating the device photoconductive behavior. In this framework, we focus on optimizing the electrical, physical and geometrical design parameters of our proposed JL structure with the aim of reaching the greatest possible of device FoMs. For this purpose, we exploit one of the most known metaheuristic techniques known as genetic algorithm approach. In fact, GA-based approach can be appropriate for investigating and optimizing the proposed JL-OCFET design through mono-objective global optimization. The latter can be useful also for bridging the gap between both aspects namely low power consumption and the high detectivity. In other words, the JL design physical and geometrical parameters have a profound implication in the device photoconductive behavior and determine greatly the device performance particularly for optical communication applications. Thus, it is of great significance to identify the best configuration of these parameters that offers the maximum achievable device FoMs. Accordingly, the proposed JL-OCFET will be optimized satisfying the following targets:

- Maximizing the detectivity D
- Maximizing the derived current I_{DMAX}
- Maximizing the sensitivity S
- Maximizing the I_{ON}/I_{OFF} ratio
- Maximizing the signal to noise ratio SN
- Minimizing the dark current I_{OFF}

Typically, based on the "weighted sum approach method", the overall objective functions mentioned above can be expressed by only one equation counting weighting coefficients as follows

$$Fitness(X) = w_1(I_{ON}/I_{OFF}) + w_2\frac{1}{I_{OFF}} + w_3 SN + w_4 I_{dmax} + w_5 S + w_6 D \qquad (V.18)$$

where X denotes the design physical and geometrical vector presented by: X= (λ ,P_i, t_{Si}, t_{Ge}, t_{ox}, L, N_d,N_a, V_{ds}, V_{gs}), w_i (i = 1-6) are weighting coefficients considered to be equal to 1/6.

Evidently, a global optimization problem based on mono-objective procedure is mainly illustrated by a candidate solution in well defined search space and a set of constraints that should be respected. These constraints can be given in our case by the following conditions

- $x \in [x_{i\min}, x_{i\max}]$, $x_i \in X$ (each design variable should be confined within a given range).
- $40\,nm > t_{Si} > 5\,nm$.

In our optimization procedure, the binary coding method is used for the representation of chromosomes, tournament selection is chosen and for the crossover stage, scattered method is applied in which the formation of the vector is used randomly. Besides, we consider 30 individuals to formulate the initial population, the stall generation for our optimization process is equal to 400, for which a quick stabilization of the objective function can be achieved, where the estimated error is extremely small.

Outstandingly, using the GA-based metaheuristic technique can give rise to an enormous enhancement in the OCFET photoconductive mechanism and boost the device FoMs by efficiently selecting the better design parameters. Therefore, for the completeness of this work, we need to evaluate the optimized JL-OCFET for optical communication applications. Consequently, we summarize in Table V.1, a new performance comparison between both the optimized JL-OCFET design and the conventional IM-OCFET structure in terms of the device FoMs, which seems to be effective especially regarding both power consumption and optical performance aspects. From this table, it is evidently demonstrated that our optimized JL structure exhibits better device FoMs in comparison with the conventional IM-OCFET counterpart [117], where an enhancement of 180% in the device I_{ON}/I_{OFF} ratio is recorded. Besides, the optimized design yields 790% improvement in the device sensitivity, an enhancement of 2500% in device detectivity. In addition, the optimized design demonstrates an extremely low dark current, which could significantly reduce the dissipated energy. Hence, these outstanding results emphasize the exciting ability of the exploited global optimization approach-based on GAs metaheuristic algorithm for improving the phototransistor electrical and optical performances.

Table V.1: Overall performance metrics comparison obtained from our optimized JL-OCFET device with that of the conventional IM-OCFET for optical communication applications.

Symbol	Conventional IM-OCFET design [117]	Optimized JL-OCFET design
Design variables:		
Wavelength λ (μm)	1.55	1.55
Incident power P (μW)	10	10
Drain voltage V_{ds}(V)	1	0.22
Gate voltage V_{gs}(V)	0.6	-0.68
Ge doping concentration (cm^{-3})	P type 1×10^{17}	P type 7×10^{17}
Si doping concentration (cm^{-3})	N type 1×10^{17}	N type 1×10^{19}
Channel length L(nm)	180	180
Ge thickness t_{Ge}(nm)	200	180
Si thickness t_{Si}(nm)	190	28
D/S doping concentration (cm^{-3})	P type 1×10^{20}	/
Performance parameters:		
OFF current (I_{OFF}) (A)	5×10^{-8}	1×10^{-13}
ON-OFF Current Ratio (I_{ON}/I_{OFF}) (dB)	60	168
Sensitivity (S)	1200	9.5×10^{7}
Signal to Noise ratio (SN)	12	12×10^{3}
Derived Drain current I_{DMAX} (μA)	11.8	9
Detectivity (Jones)	3×10^{11}	8.4×10^{13}

Eventually, it can be deduced from the obtained results that the proposed OCFET design with the JL paradigm can overcome the limitations imposed by OWCS regarding the requirement of ultrasensitive phototransistors with low elaboration cost. In addition, the proposed JL structure illustrates an ultimate advantage described on the weak signal detection property. More importantly, the adopted mixture approach based on the analytical modeling supported by metaheuristic investigation demonstrates its great capability for achieving the desired high-performance optical receivers with low power dissipation. This makes the optimized JL Ge-based phototransistor potentially suitable for high-performance and low-cost chip-level communication applications.

V. 3. Part (2): Boosting the Optical Performance and Commutation Speed of Phototransistor by Using SiGe/Si/Ge Tunneling Structure

V. 3.1 Motivation

Small swing switch devices such as TFETs are gaining much attention because of their good subthreshold characteristics, high scalability and ultra-low OFF current [145-149]. The main idea behind this innovative device is the use of a gated p-i-n diode, where its operating mechanism is based on quantum band-to-band tunneling effect. This makes it more immune against the undesired short-channel effects and enables

achieving better commutation speed [147-149]. In spite of these advantages, the low ON-state current has become one of the greatest challenges of the TFET design [149]. To this extent, researchers have been focused on enhancing the TFET derived current capability by proposing new designs based on hetero-channel, gate engineering and high-k dielectric materials [150-152]. Thus, it is envisaged that these attractive properties of the TFET transistor can be exploited to effectively design a new tunneling FET-based Ge-gate phototransistor, in order to meet the delay challenges faced by the conventional structures. The basic idea behind our approach resides on the fact that the input light can modulate the channel conductivity by optically reducing the quantum tunneling barrier. This approach can be advantageous for enhancing the optical receiver's characteristics and achieving high-performance optical interconnections.

The second part of this chapter demonstrates a new SiGe/Si/Ge-based OC-TFET to achieve the dual-role of ultra-low power consumption and improved optical commutation speed. In addition, an overall performance comparison between the investigated OC-TFET, the conventional IM and JL (investigated in the first part of this chapter) designs is performed.

V. 3.2 Device structure and simulation

In this section, we firstly present the investigated SiGe/Si/Ge-based OC-TFET design incorporating the impact of the Ge content associated with the SiGe-source region on the phototransistor electrical and optical performances. Secondly, we illustrate the numerical modeling frameworks used for evaluating the proposed photoreceiver design regarding both leakage power and optical commutation speed properties.

V. 3.2.1 Device design

The proposed FET-based phototransistor design consists of a TFET transistor with hetero-channel (SiGe/Si/Ge) and a Ge ultrasensitive gate deposited on the HfO_2 dielectric material. In this context, we consider the Ge gate with p-type doping concentration in order to obtain an initial band bending between the Ge photosensitive layer and the silicon channel. Moreover, the investigated design is illuminated at normal incidence with a monochromatic light at a specific wavelength value of $\lambda = 1.55$ µm. Figure V.6 describes a cross-sectional view of the proposed SiGe/Si/Ge-based OC-TFET design.

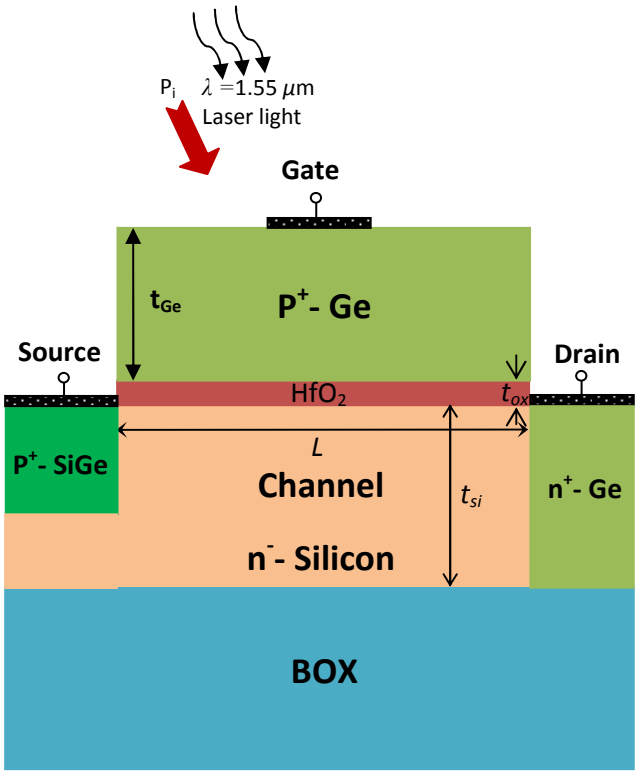

Figure V.6: Cross-sectional view of the investigated OC-TFET with SiGe/Si/Ge hetero-channel aspect.

The key idea of the investigated phototransistor is to modulate the channel conductivity by minimizing the quantum tunneling barrier at the source/channel interface. In other words, the incident light induces a band bending in the Si channel that enables generating the band-to-band tunneling effect. In addition, the proposed phototransistor involves an HfO_2 gate dielectric, which could ensure the good electrostatic control of the channel, where t_{ox} represents its thickness.

From Figure V.6, t_{Ge} and t_{Si} are the photosensitive Ge layer and the silicon thicknesses, L represents the channel length, L_s denotes the source and drain extensions length, N_{ch} and N_{Ge} are the doping of the silicon channel and the Ge gate. The source and drain regions are considered with high doping level and with different doping type P^+ and N^+, respectively. For the numerical investigation, the design parameters values associated with the proposed photoreceiver are listed in Table V.2.

Table V.2: Device design parameters used in our simulation.

Parameter name	Symbol	Value
Drain voltage	V_{ds}(V)	1
Gate voltage	V_{gs}(V)	0.4
Source side doping level (P^+-type)	N_s (cm^{-3})	5×10^{19}
Drain side doping level (N^+-type)	N_d (cm^{-3})	10^{19}
Channel side intrinsic doping level	N_{ch} (cm^{-3})	10^{17}
Ge-gate doping level (P-type)	N_a (cm^{-3})	5×10^{17}
Channel length	L(nm)	100
Source/drain extensions length	L_s(nm)	40
Ge-gate thickness	t_{Ge}(nm)	200
Si Channel thickness	t_{Si}(nm)	20
Ge mole fraction	x_{Ge}(%)	50
Oxide thickness	t_{ox}(nm)	3
HfO_2 dielectric permittivity	ε_{HfO2}	25

V. 3.2.2 Simulation models

Basically, the accurate modeling of the investigated SiGe/Si/Ge-based OC-TFET phototransistor requires taking into account the quantum mechanical effects, which leads to some modeling bottlenecks associated with the complicated systems of equations resulting from the necessity of considering the band-to-band quantum tunneling mechanism. These nonlinear equations can impose several mathematical difficulties. The outlined limitations complicate the analytical modeling of the phototransistor optical performance with hetero-channel aspect. As a consequence, numerical approaches are considered as the ultimate resort to deal with the above mentioned critical problems. These techniques provide the opportunity for the effective and the accurate modeling of the photoreceivers electrical and optical performances. In this regard, ATLAS 2D device simulator using S-PISCES module has emerged recently as a useful and realistic tool for modeling the electrostatic behavior of transistors [123]. For the numerical modeling procedure, the investigated phototransistor electrostatic behavior including the tunnel effect is involved using the nonlocal-BTBT command in the models statement. This enables the possibility to take into consideration the nonlocal band to-band quantum tunneling model. The tunnel current is generated near the source/channel junction and can be characterized by electrons and holes transfer across this junction. Hence, the tunneling current for an electron with longitudinal energy E and transverse energy E_T can be expressed as follow [123]

$$J(E)=\frac{q}{\pi h}\iint T(E)\left[f_l(E+E_T)-f_r(E+E_T)\right]\frac{\sqrt{m_e m_h}}{2\pi h^2} \quad \text{(V.19)}$$

where, $T(E)$ represents the electrons tunneling probability, q is the electron charge, m_e and m_h are the effective electrons and holes masses, respectively, f_l and f_r are the Fermi-Dirac functions on the left and the right sides of the source/channel junction, respectively, and can be given by

$$\begin{cases} f_l(E) = \left(1 + \exp\left[\left(E + E_T - E_{fSiGe}\right)/KT\right]\right)^{-1} \\ f_r(E) = \left(1 + \exp\left[\left(E + E_T - E_{fSi}\right)/KT\right]\right)^{-1} \end{cases} \quad \text{(V.20)}$$

where, E_{fSiGe} and E_{fSi} are the Fermi levels at the SiGe source and Si channel regions, respectively.

Models for carriers recombination effect (Shockley–Read–Hall (SRH), Auger and surface recombination) are also adopted [153]. In fact, the carriers' mobility is mainly dependent on three effects (transverse and parallel electric Field dependence, doping and temperature effect) combined using Matthiessen's formula. Accordingly, the Lombardi model (CVT) is used to express the carriers' mobility in the channel [154].

In order to model the absorption behavior of the considered photosensitive Ge gate, we need to exploit the FDTD method provided by Luminous Module [123], which allows us to accurately model the electromagnetic wave propagation within the Ge-gate photosensitive layer. The major benefit of the FDTD method resides on the estimation of the reflected, transmitted and absorbed light fractions by using the materials optical constant. In this framework, this method offers the direct solution of Maxwell's equations by considering both diffraction and interference effects. Therefore, the FDTD technique involves the finite difference numerical method as a good approximation in order to effectively solve the spatial and temporal derivatives illustrated in the following equations

$$\frac{\partial H_x}{\partial t} = \frac{1}{\mu}\left[\frac{\partial E_z}{\partial y} - \left(M_s + \sigma^* H_x\right)\right] \quad \text{(V.21a)}$$

$$\frac{\partial H_y}{\partial t} = \frac{1}{\mu}\left[\frac{\partial E_z}{\partial x} - \left(M_s + \sigma^* H_y\right)\right] \quad \text{(V.21b)}$$

$$\frac{\partial E_z}{\partial t} = \frac{1}{\mu}\left[\frac{\partial H_y}{\partial x} - \frac{\partial H_x}{\partial y}\left(J_s + \sigma E_z\right)\right] \quad \text{(V.21c)}$$

where, E_z represents the electric field in the z direction, H_x and H_y are the magnetic fields in the x and y directions, respectively, μ denotes the Ge material permeability, M_s is the equivalent magnetic current density, J_s represents the electric current density, σ is the electric conductivity, and σ^* is the equivalent magnetic loss.

It should be noted that the Ge mole fraction is varied between 0 and 70%, which corresponds to the experimental SiGe growing limit for avoiding the interfacial defects when the adopted SiGe source well thickness value is taken to be equal to t_{SiGe}=8nm [155].

V. 3.3 Results and discussion

In order to evaluate the proposed OC-TFET regarding the ability for optically controlling the channel conductivity, it seems to be of great importance to illustrate the optical modulation behavior of the device drain current. In this context, the photoconductive characteristic of the investigated phototransistor is analyzed. To do so, different material configurations at the source, drain and channel regions are investigated in order to distinguish which hetero-channel design offers the better optical modulation behavior. Accordingly, Figure V.7 (a) depicts I_{ds}-P_i characteristics of the proposed OC-TFET design with different hetero-channel material configurations compared to that of the conventional structure using a uniform Si channel with L=100nm, L_s=40nm and $N_{ch}=10^{17}cm^{-3}$. It is clearly observed from this figure that the investigated designs exhibit a good optical modulation behavior. Likewise, the increase of the NIR-light power intensity leads to appropriately raise the drain current to reach an acceptable value of 3µA for an applied optical power of 1µW. Moreover, the proposed designs show a very low dark current. This can underline the excellent optical commutation from the OFF to the ON-state associated with the proposed structure. In fact, the incident light generates an optically induced voltage at the Ge-gate that modifies the band-bending in the device channel. The latter can decrease the quantum tunneling barrier and give rise to superior possibilities of the electron transfer at the source/channel interface as it is shown in Figure V.7 (b). The latter figure depicts the variation of the band diagram associated with the proposed Si/Si/Si OC-TFET design with the change in the incident optical power, which allows us to understand the physical rules governing the optical behavior of the investigated photoreceiver.

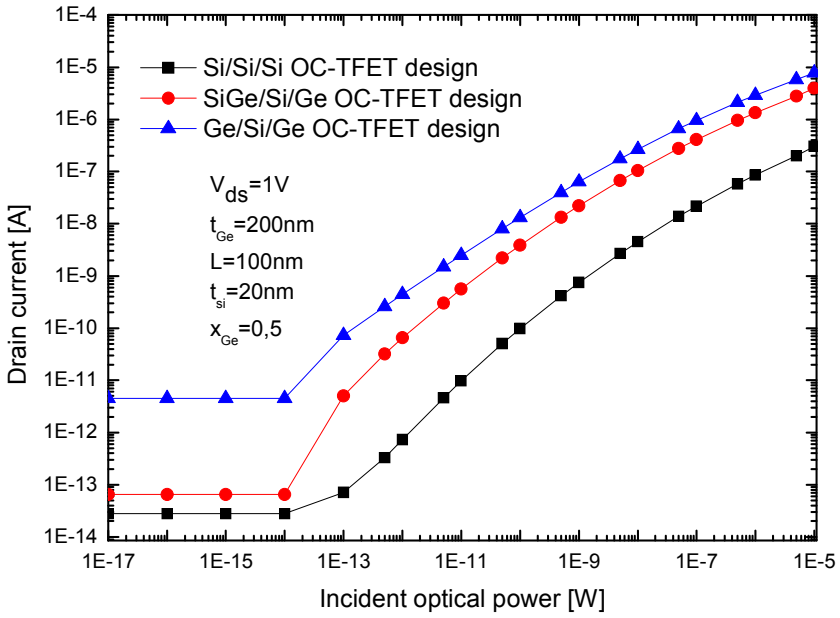

(a)

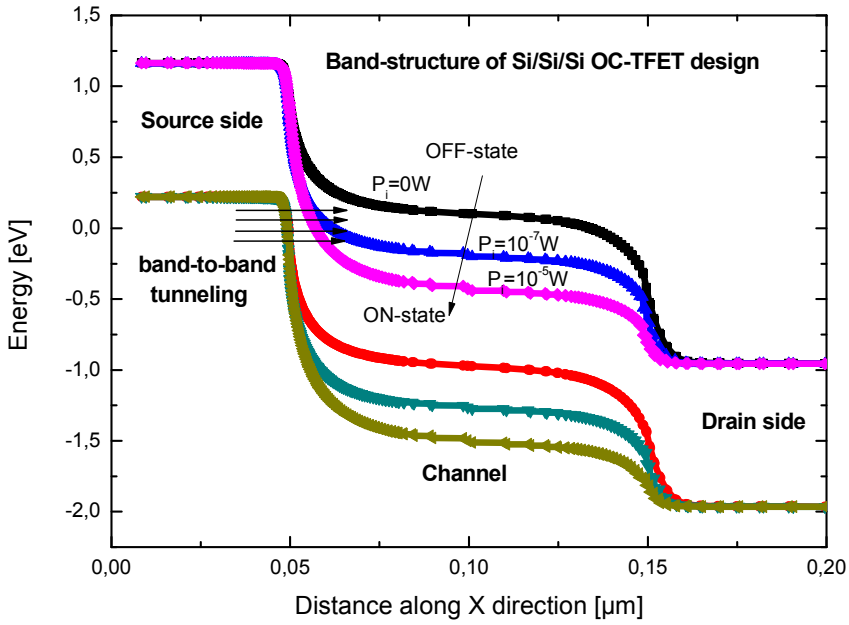

(b)

Figure V.7: (a) I-P_i characteristics of the proposed Ge-based OC-TFET with different hetero-channel configurations with $N_{ch}=10^{17}$ cm^{-3}, $N_s=5\times10^{19}cm^{-3}$, x_{Ge}=50%, fixed gate voltage V_{gs} = 0.4 V and drain voltage V_{ds} = 1 V. **(b)** comparison of Band diagrams associated with the proposed OC-TFET design with uniform Si channel for different applied optical power intensities.

Figure V.7 (b) reveals that as the incident power intensity is increased, the tunneling barrier at the source-channel junction decreases, and when the band alignment at the source/channel junction is satisfied, the tunneling current starts to take place. This confirms the excellent capability of the proposed design for optically controlling the channel conductivity. It can be also seen from Figure V.7 (a) that the investigated designs with the hetero-channel aspect exhibit superior ON-state current as compared to the conventional design with uniform Si channel. This can be attributed to the enhanced tunneling current resulted from the tunneling barrier modulation property. This characteristic is offered by the inserted hetero-channel paradigm. On the other hand, we can notice that the proposed design with SiGe source demonstrates a lower OFF-current as compared to that of the investigated structure with Ge material at the source side. The obtained behavior indicates that making a good trade-off between channel material configurations can offer the opportunity of enhancing the I_{ON}/I_{OFF} ratio. Therefore, varying the Ge concentration associated with the SiGe source region can be useful for modulating the quantum tunneling barrier width at the source/channel interface.

The comprehensive study of the phototransistor switching behavior plays an important role in evaluating the proposed photoreceiver optical performance. In this perspective, it seems crucial to introduce a new Figure of Merit called optical swing factor (SS_{op}) that describes the phototransistor optical commutation speed capability, which can be given by the following formula

$$SS_{op} = \frac{\partial P_i}{\partial \log 10(I_{ds})}[mW/dec] \tag{V.22}$$

In order to simplify this new FoM and make it very similar to the electrical swing factor, the incident power can be described by an induced optical voltage. To this extent, the phototransistor output current is modulated by simply modifying the optical induced voltage V_{ph} that behaves like the gate voltage control. Therefore, the optically controlled voltage can be given as [113-116]

$$V_{ph} = V_t \ln\left(\frac{J_{ph}}{J_S}\right) \tag{V.23}$$

where, J_{ph} is the photogenerated current in the Ge gate, J_s represents the saturation current and V_t denotes the thermal voltage.

Thus, the simplified optical swing factor can be calculated by considering the

optical induced voltage instead of the light power and can be estimated by using the following equation

$$SS_{op} = \frac{\partial V_{ph}}{\partial \log 10(I_{ds})}[mV/dec] \quad \text{(V.24)}$$

It is to note that for high-commutation speed of the phototransistor, the optical swing factor should be minimized.

Aiming at elucidating the impact of the proposed SiGe/Si/Ge-based OC-TFET structure on the photoreceiver optical commutation speed, Figure V.8 shows the variation of both the optical swing factor and the I_{ON}/I_{OFF} ratio as a function of the Ge content associated with the SiGe material at the source side region. It is clearly seen from this figure that by increasing the Ge concentration, the I_{ON}/I_{OFF} ratio significantly increases to reach its maximum for the Ge mole fraction value of 40% and decreases slowly after this optimal value. Furthermore, we can notice that the proposed SiGe/Si/Ge-based OC-TFET structure provides superior I_{ON}/I_{OFF} ratio as compared to the conventional design with uniform Si channel. This behavior can be ascribed to the tunneling barrier modulation aspect that brings wider possibilities for achieving an enhanced electrostatic behavior. On the other hand, we can see from this figure that the better optical swing factor value can be achieved by taking the SiGe-source with 60% of Ge content. This can underline the complex optical behavior of the proposed design with SiGe/Si/Ge hetero-channel, where the Ge mole fraction induces a highly non-linear behavior of both the optical swing factor and I_{ON}/I_{OFF} ratio. This phenomenon can be ascribed to the quantum nature of the band-to-band tunneling effects, where identifying the Ge concentration that provides the better tunneling barrier for achieving an enhanced optical switching behavior seems to be extremely complex. Accordingly, taking the SiGe source region with 40% of Ge content enables making a good trade-off between both the low power consumption aspect and superior optical commutation speed. In this context, the optimized SiGe/Si/Ge-based OC-TFET design exhibits a superior I_{ON}/I_{OFF} ratio value of 155dB, and a lower optical swing factor value of 48mV/dec. The latter value is considered much lower as compared to the thermal limit associated with the conventional Ge-OCFET design (60mV/dec). Thus, the obtained results prove the unique characteristic of the optimized SiGe/Si/Ge-based OC-TFET to jointly offering both high optical commutation speed and low power consumption merits.

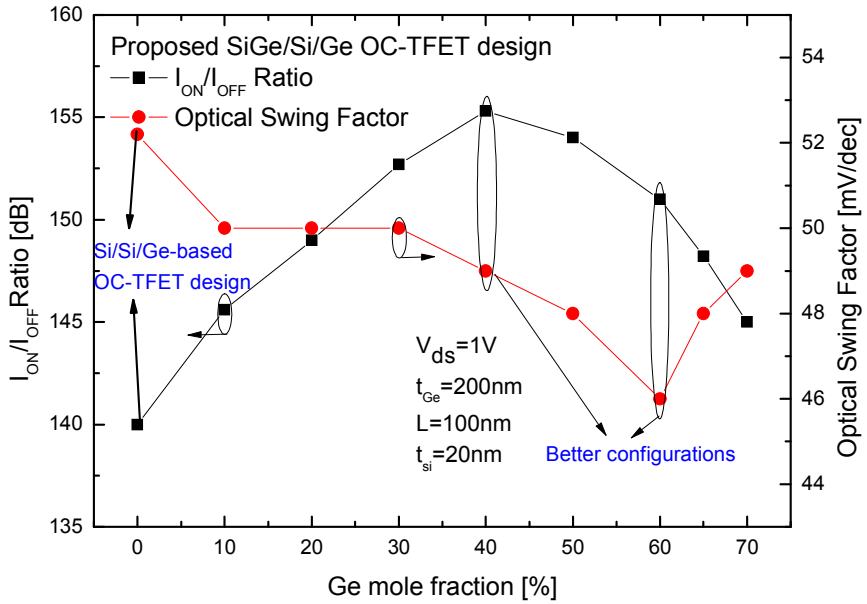

Figure V.8: Variation of the optical swing factor and the I_{ON}/I_{OFF} ratio against the SiGe source Ge mole fraction for the investigated SiGe/Si/Ge-based OC-TFET structure with L=100nm, t_{Si}=20nm $N_{ch}=10^{17}cm^{-3}$, $N_s=5\times10^{19}cm^{-3}$, fixed gate voltage V_{gs}=0.4V and drain voltage V_{ds}=1V.

To further assess the optical characteristics of the proposed SiGe/Si/Ge-based OC-TFET design, Figure V.9 depicts the device detectivity versus the incident power intensity for the investigated phototransistor design and the conventional JL and IM-OCFET counterparts for a fixed applied gate and drain voltages values of V_{gs} = 0.4 V and V_{ds} =1V, respectively. As expected, the proposed SiGe/Si/Ge-based OC-TFET design exhibits much higher peak detectivity as compared to that provided by the IM and JL-OCFET conventional technologies, where a maximum detectivity value of $D^*=5\times10^{14}$ Jones can be achieved by considering the band-to-band tunneling transport mechanism. Besides, it can be also observed that the proposed structure opens up the route for achieving the weak optical signal detection property. In other words, the device detectivity reaches its maximum for a much lower incident power intensity value of $P_i\sim2\times10^{-3}$ nW as compared to the conventional designs. This achievement can be attributed to a mixture of two effects: firstly, the effective separation of the photogenerated carrier in the photosensitive Ge-gate layer enabled by the increased potential drops in the gate region. Secondly, the transport mechanism of the proposed design is based on the band-to-band tunneling effect, which gives the opportunity for

achieving a good light control of the channel conductivity with a very low dark current about (I_{OFF}= 2×10^{-5} nA).

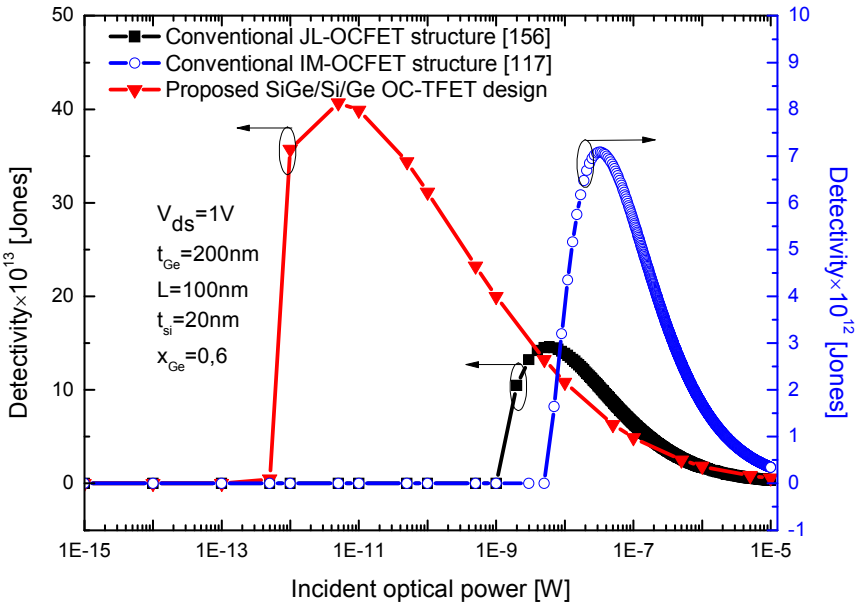

Figure V.9: Device detectivity versus the applied optical power for the proposed SiGe/Si/Ge-based OC-TFET compared to that of the conventional designs based on IM and JL technologies.

Basically, there are also more other FoMs that characterize the photoreceivers performance in terms of the device photo-responsivity which should be investigated carefully. In this framework, Figure V.10 illustrates the variation of both responsivity and sensitivity as a function of the device channel thickness with L=100nm, x=0.4 and N_{ch}=10^{17} cm^{-3}. Observing this figure, we can notice that increasing the device thickness leads to increase the device sensitivity and responsivity. This is because of the enhanced tunneling effect at the source/channel junction when the channel thickness is increased. In addition, the channel thickness increase can cause the drain current enhancement, which leads to improve the derived current capability of the investigated OCTFET phototransistor. This phenomenon can in turn allow substantial improvements concerning the device responsivity. Moreover, the proposed design offers superior responsivity and sensitivity as compared to the conventional designs based on JL and IM-OCFET technologies [9-10]. This indicates the enhanced optical performance enabled by the proposed NIR phototransistor based on SiGe/Si/Ge OC-TFET design with an optimized Ge content.

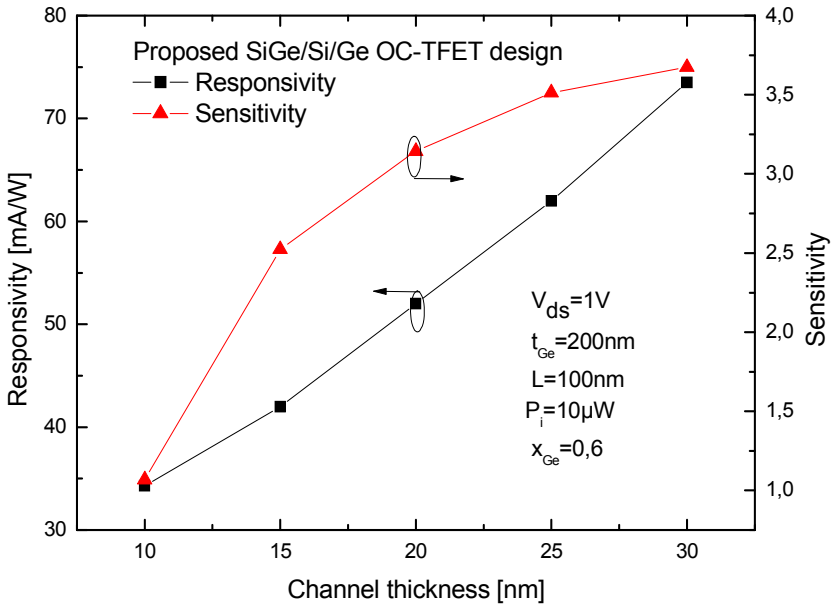

Figure V.10: Variation of the device sensitivity and responsivity as function of the channel thickness with L=100 nm, $N_{ch}=10^{17}$ cm^{-3}, $N_d=10^{19}cm^{-3}$, x_{Ge}=40%, fixed gate voltage V_{gs} = 0.4 V and drain voltage V_{ds} = 1 V.

Importantly, it appears to be valuable to assess the strength of the proposed TFET-based phototransistor design over the conventional designs regarding the optical and electrical performances. To do so, Table V.3 summarizes an overall optical and electrical metrics comparison between the investigated SiGe/Si/Ge-based OC-TFET design and the conventional structures based on IM and JL technologies. This table demonstrates that the proposed design with band-to-band tunneling transport mechanism and hetero-channel aspect considerably outperforms the conventional IM and JL-OCFET counterparts, where it yields 2150% of relative improvement regarding the device sensitivity, 2000% enhancement regarding the device detectivity and 140% of relative improvement in terms of the I_{ON}/I_{OFF} ratio with respect to the conventional devices [117] and [156]. Moreover, the proposed design provides a very low optical swing factor, which indicates the superior optical commutation speed capability as compared to that of the conventional designs (>60mV/dec). In addition, the investigated photoreceiver exhibits an acceptable responsivity value of 70mA/W.

Table V.3: Overall electrical and optical FoMs comparison between the proposed SiGe/Si/Ge-based Ge-OC-TFET and both conventional designs with IM and JL technologies.

Symbol	Conventional IM-OCFET design [117]	Conventional JL-OCFET design [156]	Proposed SiGe/Si/Ge OC-TFET design
Design variables:			
Wavelength λ (μm)	1.55	1.55	1.55
Incident power P (μW)	10	10	10
Drain voltage V_{ds}(V)	1	1	1
Gate voltage V_{gs}(V)	0.6	-0.3	0.4
Ge-gate doping concentration (cm^{-3})	P type 1×10^{17}	N type 1×10^{17}	P type 1×10^{17}
Si doping concentration (cm^{-3})	N type 1×10^{17}	P type 1×10^{19}	N type 1×10^{17}
Channel length L(nm)	180	180	180
Ge thickness t_{Ge}(nm)	200	200	200
Si thickness t_{Si}(nm)	190	20	20
Source doping concentration (cm^{-3})	N type 1×10^{20}	/	P^{+} type 5×10^{19}
Drain doping concentration (cm^{-3})	N type 1×10^{20}	/	N^{+} type 1×10^{19}
Ge mole fraction (%)	/	/	0.4
Performance parameters:			
OFF current (I_{OFF}) (A)	5×10^{-8}	4×10^{-11}	1.6×10^{-13}
ON-OFF Current Ratio (I_{ON}/I_{OFF}) (dB)	60	101	156
Responsivity (mA/W)	118	80	67
Sensitivity (S)	1200	9.5×10^{4}	3.5×10^{9}
Signal to Noise ratio (SN)	12	1.2×10^{2}	3.5×10^{7}
Detectivity (Jones)	3×10^{11}	12×10^{13}	43×10^{13}
Optical swing factor (mV/dec)	>60	>60	48.5
Optical commutation speed	low	low	high

Substantially, it is evidently demonstrated that the optimized SiGe/Si/Ge-based OC-TFET design can noticeably improve the phototransistor optical performance, not only by achieving an effective optical commutation speed, but also leading to basically an effective reduction of the undesired power dissipation. It was found also that the proposed design exhibits the ultra-low optical power detection property (sub-1pW), which infers that it requires less light power from the optical emitter to reach an acceptable photo-response as compared to the conventional designs. Therefore, the proposed OC-TFET structure pinpoints a new path toward achieving high optical commutation speed with reduced power dissipation, which makes it a potential alternative for providing high-performance chip-level optical communications applications.

V. 4. Conclusion

In summary, versatile Ge-based phototransistor designs were proposed in order to improve the photoreceiver performance. Firstly, we have investigated a new optimized planar JL phototransistor using both mathematical modeling and metaheuristic

optimization. Further, the device performance has been compared with conventional IM-OCFET design and its enhancement has been discussed, where the proposed JL Ge-based phototransistor provides superior signal to noise ratio, low power consumption, high I_{ON}/I_{OFF} ratio and high-detectivity as compared to the IM-OCFET counterpart. Moreover, compared with previous IM-OCFET devices, our device has the benefit of the simple fabrication process and is fully compatible with the CMOS technology.

On the other hand, we have proposed a new SiGe/Si/Ge-based OC-TFET design based on a hetero-channel (SiGe/Si/Ge) aspect. Moreover, we have proposed a new FoM parameter called optical swing factor that illustrates the photoreceiver optical commutation speed. Moreover, the impact of the Ge content on the device FoMs has been also analyzed. It has been demonstrated that the adopted band-to-band tunneling transport mechanism can be effective for improving the device optical commutation speed. It has been deduced also that the optimized design with 40% of Ge concentration offers an enhanced commutation performance, where it provides 48mV/dec of optical swing factor and 3×10^{9} of sensitivity. It was found also that the proposed design exhibits the ultra-low optical power detection property (sub-1pW), which infers that it requires less light power from the optical emitter to reach an acceptable photo-response as compared to the conventional designs.

Therefore, the proposed Ge-based phototransistors open up a new path toward developing low-cost devices with high optical commutation speed and reduced power dissipation, making them potential alternatives for providing high-performance optical receivers.

Chapter VI

Boosting up the Efficiency of Thin-Film CZTS Solar Cells

Abstract: ***This Chapter focuses on providing new insights for the potential improvement of the CZTS-solar cell conversion efficiency. The first idea relies on proposing a potential high-efficiency CZTS solar cell design based on graded band-gap aspect that can offer the benefits of improved absorption behavior and reduced recombination effects. Moreover, analytical models for the proposed design are developed incorporating the impact of the graded band-gap profile on the solar cell photoelectrical behavior. A new design methodology based on analytical modeling and PSO approach is proposed to determinate the better band-gap profile of the amended CZTS absorber layer. The second idea consists of investigating the role of intermediate metallic sub-layers (Au, Ti, and Ag) engineering coupled with metaheuristic techniques in enhancing light-scattering behavior and reducing recombination losses.***

VI.1. Introduction

In today's energy production, the deployment of photovoltaic systems with larger affordability is expected to be an economically advantageous technique for providing carbon neutral clean energy [157]. Despite this, to effectively meet the actual energy resources, it seems to be of vital importance to enhance the solar cell performance for achieving low-cost photovoltaic energy [61], [157]. Principally, the c-Si-based technology provides higher efficiency value of 26.6%, while it exhibits several problems mainly associated with the high manufacturing cost that arises from the purification, crystallization, and processing steps [61], [157-185]. Otherwise, cost-effective technologies based on organic/inorganic, perovskite and dye-sensitized designs still suffer from the low conversion efficiency, reliability and stability issues [158-160]. Alternatively, thin-film chalcogenide $CuIn_xGa_{(1-x)}Se_2$ (CGIS)-based solar cell has certainty attracted a great interest due to its high stability as well as its superior efficiency value of 22% [161-162]. However, the use of rare metals or toxic materials like: arsenic, germanium, indium, cadmium and tellurium can prevent achieving high efficiency/cost ratio. In this regard, for the continuous progress of the thin-film solar cells, kesterite CZTS material is believed to be an alternative and substitutional earth-abundant, inexpensive and nontoxic material with distinctive optical properties [62-64]. In fact, this absorber material exhibits a high absorption coefficient ($>10^4$ cm^{-1}) and enables the opportunity for appropriately adjusting the band-gap energy [65]. To this extent, CZTS is typically considered as an important chalcogenide p-type semiconducting material having a tunable direct optical band-gap of 1.52 eV, which makes it suitable for the design of a variety of novel optoelectronic devices [163-165]. These advantages make it as a prospective candidate to overcome the trade-off between both high-efficiency and low fabrication cost. For this purpose, a great deal of attention has been paid to CZTS-based photovoltaic technology in order to improve the thin-film solar cell properties, where 9.5% efficiency for the conventional CZTS structure, 12.6% for Se-alloying kesterite-based design, and 11.2% for CZCTS solar cell with Cd-containing have been recorded [70], [164] and [166-167]. However, the power efficiency of the CZTS solar cell is considered still far from that offered by CIGS-based technology (22%). This is mainly due to the extensive limitations typically observed for kesterite solar cells, which are associated with the short minority carrier lifetime and the high series resistance imposed by the contact barrier induced by the formation of the

MoS_2 layer at the CZTS/Mo interface [164]. In this context, several published works are focused on addressing these problems in order to achieve high-efficiency CZTS solar cells through proposing new designs based on rear passivation layer, In/Cd hybrid buffers and CZTS/CeO_2 solar cell design [164], [168-169]. Yet, the incapability to remove the effect of the high recombination rate as well as the high series resistance still persist and prohibit achieving competitive efficiencies. Consequently, alternative approaches remain inevitable to deal with the above mentioned challenges and to target over than 16% efficiency values for high-performance photovoltaic application.

The major objective of this chapter is to investigate the possibility of moving forward from the abovementioned efficiency achievements associated with CZTS solar cells. For this purpose, promising designs are proposed in this chapter in order to enhance the CZTS solar cells performance. The first design relies on the use of graded band-gap aspect that can offer the benefits of improved absorption behavior and reduced recombination effects. While, the second one aims to introducing intermediate metallic sub-layers (Au, Ti, and Ag) engineering aspect for enhancing light-scattering behavior and reducing recombination losses at the Mo/CZTS interface.

VI.2. Part (1): Graded Band-Gap Engineering for Increased Efficiency in CZTS Solar Cells

VI.2.1 Motivation

In fact, CZTS material not only offers the benefit of substituting rare metals with earth abundant ones, but also exhibits a quite high absorption coefficient [165]. However, recombination effects are considered also as a serious problem, where the short carrier life time of the CZTS material prevents achieving favorable efficiencies. Intuitively, the use of graded band-gap engineering for the CZTS absorber layer can be beneficial for improving the carrier collection as well as the optical absorption behavior. In other words, linearly increasing the CZTS band-gap through varying the Se content can be a substantial solution to modulate the electric field in the absorber layer and enhance the transport mechanism of the photogenerated carriers [170]. Furthermore, this approach can be advantageous for enhancing the solar cell resistive behavior by modulating the shunt and series resistances. In this perspective, we present in this chapter part a new hybrid approach based on the analytical modeling of the proposed CZTS-based solar cell structure including graded band-gap profile and PSO-based metaheuristic computation with the aim of recording better efficiency values. The merit

of this hybrid approach is to determinate the global optimized graded band-gap profile that enables getting rid of recombination losses and enhancing the solar cell absorption.

VI.2.2 Analytical modeling methodology

Basically, the cornerstone of the proposed CZTS-based solar cell design dwells on engineering the absorber layer by using a graded-band gap profile. In this perspective, the Se content is increased with the CZTS layer thickness increase to reach its maximum at the CZTS/Mo interface as it is shown in Figure VI.1 (a).

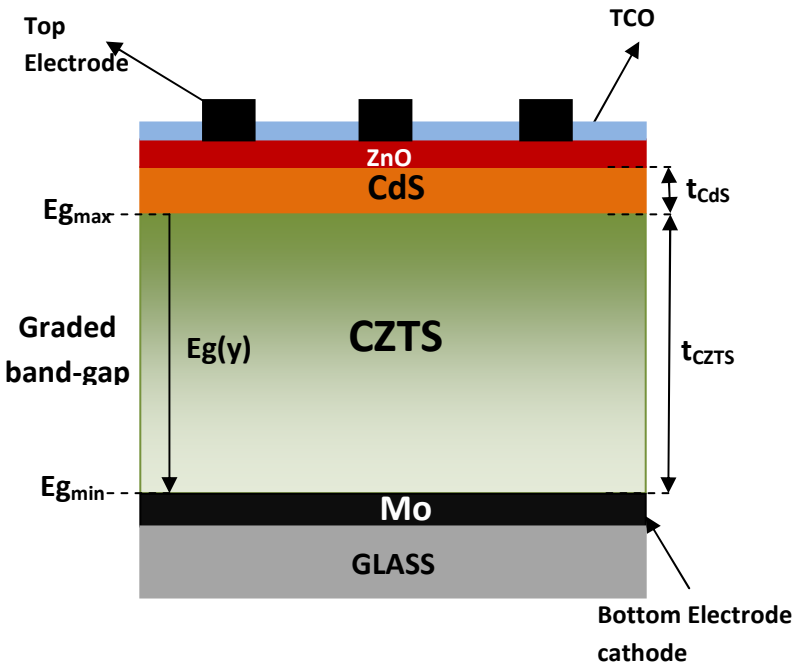

(a)

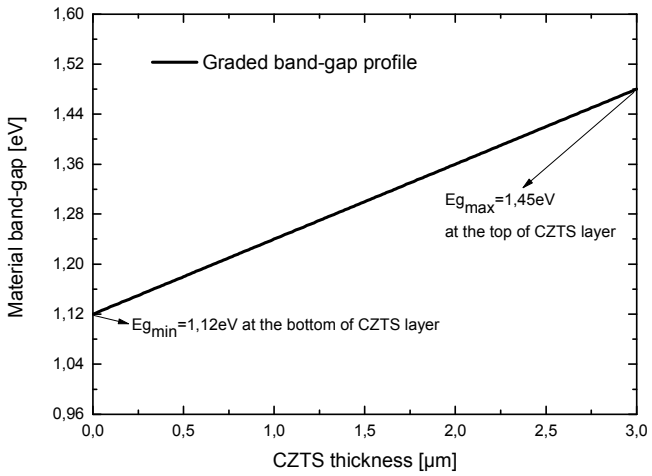

(b)

Figure VI.1: (a) Cross-sectional view of the proposed CZTS-based solar cell with graded band-bap aspect, **(b)** graded band-gap profile in the CZTS absorber layer.

This figure depicts the cross-sectional view of the proposed structure with an amended CZTS layer, where $E_g(y)$ is the gradual band-gap profile in the y direction. Besides, the graded band-gap shape is suggested with a linear profile, as it is illustrated in Figure VI.1 (b). It is to note that numerous experimental studies have proved the possibility to change the CZTS material band-gap in the range of 1.5eV and 1eV by increasing the Se mole fraction from x=0 to x=1 [170].

The investigated design is considered with P-N heterojunction chalcogenide thin-film design, where the CdS layer acts as buffer layer at the top of the analyzed design. While, at the solar cell bottom, a glass coated Mo is used, where the rear contact can be realized by the Mo metal, whereas at the top of the solar cell the front finger contacts can be formed on the AZO film, which behaves as a good TCO.

For our analytical modeling, the parameter t_{CZTS} represents the P-CZTS absorber region thickness, t_{CdS} is the n-CdS layer thickness and $E_g(y)$ refers to the material band-gap variation as a function of the thickness, where Eg_{min} and Eg_{max} are the CZTS material band-gap values at the top and bottom of the amended absorber layer, respectively.

VI.2.2.1 Analytical model of the solar cell photocurrent

The analytical current-voltage formulation of the investigated CZTS-based solar cell under illumination can be given by the following expressions [125]

$$I(V) = I_{ph} - I_s\left[e^{\frac{V-IR_s}{nV_{th}}} - 1\right] - \frac{V - IR_s}{R_{sh}} \qquad \text{(VI.1)}$$

where, q is the electron charge, V_{th} represents the thermal voltage, R_s and R_{sh} are the series and shunt resistances, respectively, n is the ideality factor, I_s is the saturation current and I_{ph} refers to the photogenerated current which is wavelength dependent.

In order to estimate the photocurrent we need to calculate the proposed CZTS-based solar cell optical parameters including the suggested graded band-gap profile. In this perspective, we exploit a well-known expression of the absorption coefficient as a function of wavelength for un-polarized light provided by Tauc et al. model [172], which is considered as a good approximation that reproduces the experimental results associated with chalcogenide materials for direct band–gap transitions. The materials absorption coefficient can be estimated from the following expression [172-176]

$$\alpha_c(\lambda)=\begin{cases}0 & \dfrac{hc}{\lambda}<E_g \\ \dfrac{B\lambda}{hc}\left(\dfrac{hc}{\lambda}-E_g\right)^{1/2} & \dfrac{hc}{\lambda}>E_g\end{cases} \qquad \text{(VI.2)}$$

where h is the blanck's constant, c represents the speed of light, B is a constant mainly depending on the semiconductor intrinsic properties and λ is the optical wavelength.

For the proposed design with graded band-gap aspect, the material absorption coefficient can be estimated by exploiting the equivalent model reported in [174-175], which suggest using a modified absorption coefficient represented as follows

$$\alpha_p(\lambda)=\begin{cases}0 \ \ for \quad 0<\dfrac{hc}{\lambda}<E_{g\min} \\ \dfrac{2}{3}\alpha_c(\lambda)\left(\dfrac{\left(\dfrac{hc}{\lambda}-E_{g\min}\right)}{\left(E_{g\max}-E_{g\min}\right)}-E_g\right)^{1/2} \quad for \quad E_{g\min}<\dfrac{hc}{\lambda}<\dfrac{3E_{g\max}-E_{g\min}}{2} \\ \alpha_c(\lambda) \qquad for \quad \dfrac{hc}{\lambda}>\dfrac{3E_{g\max}-E_{g\min}}{2}\end{cases} \qquad \text{(VI.3)}$$

After estimating the absorption coefficient of the modified design with graded band-gap profile, we can calculate the photogenerated current by solving the Poisson's equation combined with the continuity equation. In this context, the photocurrent can be described by the following equation [125]

$$I_{ph}=\int_{\lambda_{\min}}^{\lambda_{\max}} I_d(\lambda)+I_b(\lambda)+I_a(\lambda) \qquad \text{(VI.4)}$$

where I_d, I_b and I_a are photocurrents associated with the depletion, base and emitter regions, respectively.

The photogenerated current within the depletion region is considered as the dominant current for the kesterite solar cell and can be expressed by

$$I_d(\lambda)=q\phi(\lambda)(1-R(\lambda))\exp(-\alpha_{CdS}(\lambda)W_n)\left[1-\left(\exp(\alpha_{CdS}(\lambda)W_n-\alpha_p(\lambda)W_p)\right)\right] \qquad \text{(VI.5)}$$

where W_n and W_p are the depletion widths extended in the CdS and P-CZTS region respectively, $\alpha_{CdS}(\lambda)$ and $\alpha_p(\lambda)$ are the absorption coefficients of both CdS and CZTS materials calculated from Eq. VI.2 and VI.3, respectively. $R(\lambda)$ represents the reflection coefficient, which is mainly depending on the incident wavelength values and $\phi(\lambda)$ is the number of the incident photons. The latter is given by $\phi(\lambda)=\dfrac{P_i(\lambda)}{qE(\lambda)}$, with

$E(\lambda)=\frac{1.24[eV.\mu m]}{\lambda}$ and $P_i(\lambda)$ is the solar spectral irradiance which can be approximated by a well known non linear function [177].

It is to highlight that the final formulation of the photocurrents associated with the neutral regions (I_b and I_a) can be found in [115] and [132]. However, we introduce for the proposed design a new effective recombination velocity for minority carrier in the engineered CZTS layer (S_{neff}), which can be estimated from

$$S_{neff} = S_n - \mu_n \xi \tag{VI.6}$$

where μ_n is the electron mobility, S_n represents recombination velocity of the conventional design and ξ is the electric field occurred from the use of graded band-gap profile given by [174]

$$\xi = \frac{dE_g}{dx} \tag{VI.7}$$

Obviously, engineering the band-gap in the CZTS absorber layer requires introducing the effect of the resulted electric field on the material diffusion length. In this context, a drift-diffusion length should be taken into account to describe the carrier moving by using the drift-diffusion mechanism. Thus, the modified diffusion length for the proposed design can be estimated using the following expression [174-175]

$$L_{neff} = \frac{L_n}{\sqrt{1+\left(\frac{L_n\xi}{2V_{th}}\right)^2}-\frac{L_n\xi}{2V_{th}}} \tag{VI.8}$$

with $L_n=\sqrt{D_n\tau_n}$ where D_n and τ_n respectively represent the diffusion constant and the effective minority carrier lifetime of the CZTS material.

The saturation current is mainly depending on the materials intrinsic properties, where the suggested graded band-gap profile has a significant impact on the current at dark conditions. Hence, the saturation current for the proposed CZTS-based solar cell can be estimated by exploiting this formula [174-175]

$$I_{Seff} = I_s\left(\frac{2V_{th}}{E_{g\max}-E_{g\min}}\right) \tag{VI.9}$$

It is important to note that the diffusion length and coefficient of the absorber regions are mainly depending on the effective minority carrier life time which can be given as follows [176]

$$\frac{1}{\tau_n}=\frac{1}{\tau_{ib}}+\frac{1}{\tau_{is}}+\frac{1}{\tau_{iau}} \quad \text{(VI.10)}$$

where τ_{ib}, τ_{ib} and τ_{iAu} are the bulk, surface, and Auger time of recombination associated with the simulated solar cell, respectively.

As it is above-outlined, large output voltage deficit associated with kesterite technology is considered as the most pronounced loss mechanism that prohibit achieving favorable efficiency values although the theoretical value of the V_{oc} of the CZTS-based solar cell is assumed to be around 1V. This phenomenon is mainly due to the interface recombination effects imposed by the electrical and structural discrepancies between buffer and absorber materials, which give rise to lattice mismatch problem, inducing defects at the buffer/absorber interface. Therefore, it is of great significance to take into consideration the degradation related-interface recombination effects in the developed model in order to be closer to the realistic behavior of the kesterite solar cell. For this purpose, the carrier lifetime is affected by the interface recombination effects and depends on the interface density of defects D_i, and can be calculated using the following equation [176]

$$\frac{1}{\tau_{is}}=\frac{2D_i\delta V_{th}}{t_{ib}} \quad \text{(VI.11)}$$

where V_{th} and σ represent respectively the capture coefficient and the carrier thermal velocity.

Afterward, the recombination current is introduced in the developed analytical model and can be given by [176]

$$I_{ir}=\frac{1}{2}qD_i\delta V_{th}n_i \quad \text{(VI.12)}$$

where n_i refers to the intrinsic carrier concentration of the absorber material.

The saturation current-density of the heterojunction solar cell taking into account the conduction band offset can be expressed as follows [176]

$$I_{DE}=q\frac{D_p}{L_p}\Delta p\frac{\frac{S_pL_p}{D_p}\cosh\left(\frac{t_{ie}}{L_p}\right)+\sinh\left(\frac{t_{ie}}{L_p}\right)}{\cosh\left(\frac{t_{ie}}{L_p}\right)+\frac{S_pL_p}{D_p}\sinh\left(\frac{t_{ie}}{L_p}\right)} \quad \text{(VI.12a)}$$

$$I_{DB}=q\frac{D_n}{L_n}\Delta n\frac{\frac{S_nL_n}{D_n}\cosh\left(\frac{t_{ib}}{L_n}\right)+\sinh\left(\frac{t_{ib}}{L_n}\right)}{\cosh\left(\frac{t_{ib}}{L_n}\right)+\frac{S_nL_n}{D_n}\sinh\left(\frac{t_{ib}}{L_n}\right)} \quad \text{(VI.12b)}$$

$$I_S = I_{DE} + I_{DB} \tag{VI.12c}$$

where Δn and Δp are respectively, the minority carrier densities in both absorber and buffer regions, which can be calculated from the following equations

$$\Delta n = N_{ai} \exp\left(\frac{V_{bi} + \Delta E_{ci}}{V_t}\right) \tag{VI.13a}$$

$$\Delta p = N_{di} \exp\left(\frac{V_{bi} - \Delta E_{vi}}{V_t}\right) \tag{VI.13b}$$

where ΔE_{ci} and ΔE_{vi} denote the conduction and valence band offsets and V_{bi} represents the potential barrier at the CdS/CZTS junction, N_{ai} and N_{di} are respectively the absorber and buffer doping concentrations.

Afterward the current voltage characteristics of the CZTS solar cell including the degradation related-recombination effects can be carried out using this equation

$$I\ (V) = I_{ph} - I_s\left[e^{\frac{V - I\ R_s}{nV_{th}}} - 1\right] - I_{ir}\left[e^{\frac{V - I\ R_s}{2V_{th}}} - 1\right] - \frac{V - I\ R_s}{R_{sh}} \tag{VI.14}$$

The open circuit voltage is given by

$$V_{oc} = V_{th} \ln\left(\frac{I_{ph}}{I_{Seff}} - 1\right) \tag{VI.15}$$

The conversion efficiency and the fill factor can be expressed as

$$FF = \frac{P_m}{I_{SC} V_{OC}} \tag{VI.16}$$

$$\eta = \frac{P_m}{P_i} \tag{VI.17}$$

In order to validate the developed model, we compare in Figure VI.2 the obtained I-V characteristics from the developed analytical model of the conventional kesterite-based solar cell with that of the experimental data reported in [166]. The materials properties used in the analytical investigation are taken from [178]. It is clearly observed from this figure that the analytical results are found to be in close agreement with the experimental results emphasizing the good accuracy of the developed model. Moreover, the obtained results indicate that our model is able to reproduce the CZTS solar cell I-V characteristics, typical to that of the experimental results associated with the conventional design inferring the accurateness of the adopted approach for estimating the absorption coefficient.

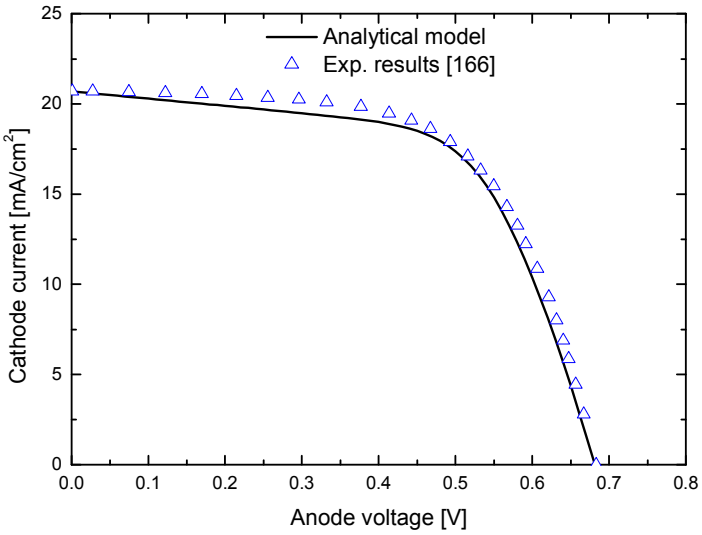

Figure VI.2: I-V characteristics comparison between the experimental data and the developed model of the conventional CZTS-based solar cell.

VI.2.3 Results and discussion

The most important motivation behind the use of an amended CZTS absorber layer with graded band-gap profile is to potentially enhance the kesterite-based solar cell performance. In this framework, it seems to be of great importance to show the impact of the adopted design modification on the thin-film solar cell characteristics. To this extent, Figure VI.3 illustrates the I-V curves associated with the conventional CZTS solar cell and the proposed structure with different graded band-gap profiles.

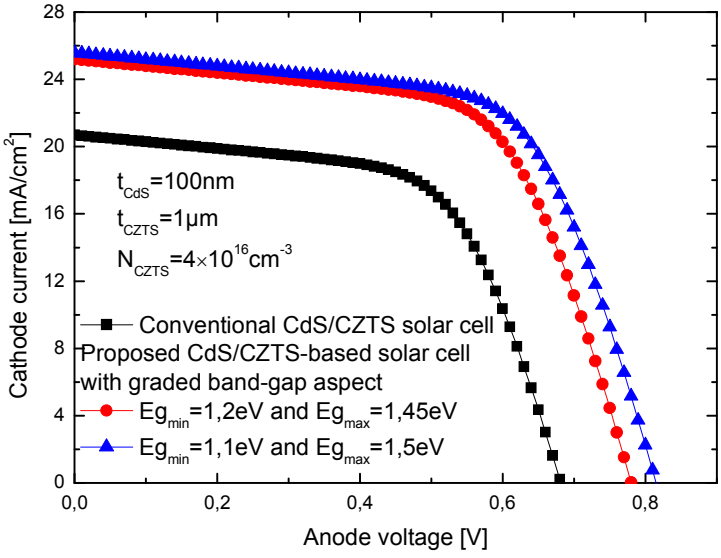

Figure VI.3: I-V curves of the conventional CZTS-based solar cell compared to that of the proposed design including the graded band-gap paradigm.

Observing this figure, it is clearly demonstrated that the proposed design exhibits an improved short-circuit current (about 23mA/cm^2) and open circuit voltage (about 690mV) in comparison with that of the conventional counterpart. Moreover, the proposed design enables higher efficiency of 11.8% as compared to the conventional design (8.7%). This enhancement can be attributed to the superior photocurrent provided by the enhanced absorption behavior in the whole solar spectrum. Moreover, the graded band-gap paradigm generates an electric field within the CZTS absorber layer, which leads to achieving an effective electron/holes pair separation and an improved carrier life time. The promising results obtained for the distinctive photoelectric behavior of the proposed CZTS solar cell inspire further analysis to record more enhancements with respect to the solar cell efficiency. In this perspective, Figure VI.4 shows the conversion efficiency and the V_{oc} as a function of the CZTS layer thickness for both proposed and conventional designs with E_{gmin}=1.2eV and E_{gmax}=1.52eV. It can be deduced from this figure that the proposed structure with a graded band-gap aspect provides superior efficiency and V_{oc} as compared to the conventional design. This behavior can be explained by the enhanced carrier collection and the higher absorbance provided by lowering the material band-gap. In addition, the superior open circuit voltage can be attributed to the decreased saturation current indicating the distinctive reduction of the recombination losses, which can be explained by the enhanced carrier life time allowed by the graded band-gap aspect.

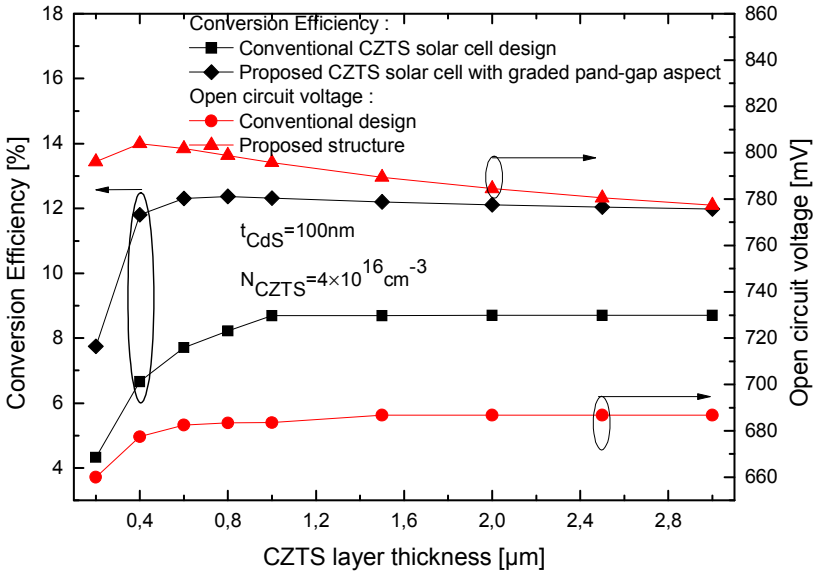

Figure VI.4: The conversion efficiency and the open circuit voltage as a function of the CZTS absorber layer thickness for both proposed and conventional CZTS solar cell.

Otherwise, we can notice from this figure that the total efficiency associated with the conventional design increases as a function of the absorber thickness increase to reach its maximum at t_{CZTS}=900nm, and after that saturates with the CZTS thickness enlargement. In contrast, for the proposed design the conversion efficiency decreases slowly when the absorber layer thickness exceeds an optimum value of t_{CZTS}=500nm indicating the complex photoelectrical behavior of the proposed design. This efficiency reduction is mainly due to the V_{oc} deficit for large CZTS thicknesses as it is illustrated in Figure VI.4, which can be ascribed to the band-gap reduction in the absorber layer and to the high recombination rate originated for thicker absorber layers.

Although the good characteristics recorded for the proposed design, the obtained CZTS solar cell efficiency remains unsatisfactory behind that provided by c-Si and CIGS-based solar cells and requires substantial enhancement. To this extent, the obtained complex electrical behavior of the proposed structure with graded band-gap CZTS layer signifies that the design parameters like the solar cell geometrical configuration, the graded band-gap profile, n-CdS and P-CZTS materials doping levels have a profound implication and play an important role in determining the CZTS photovoltaic cell performance. This indicates that there are wider opportunities for achieving further efficiency improvements by engineering the band-gap profile of the CZTS absorber layer and selecting the better configuration of the above-mentioned design parameters. Intuitively, a new insight based on an efficient global optimization approach using PSO-based metaheuristic technique (detailed in Chapter III) can be in fact helpful for achieving the highest possible efficiency for the proposed CZTS-based thin-film solar cell, which constitutes the main objective of the next section.

VI.2.4 The hybrid approach used for improving the conversion efficiency

Ultimately, to address the fundamental challenges associated with the CZTS-based solar cell performance namely the high recombination rate as well as the relatively low carrier life time; new approaches are in fact required to achieve superior efficiencies. For this purpose, it seems to be valuable to systematically shape a global optimization of the investigated design using the developed analytical models with an appropriate way to enhance the thin-film solar cell properties. For this purpose, our proposed hybrid approach involves engineering the proposed CZTS absorber layer with a graded band-gap profile to achieve further enhancement of the proposed solar cell conversion efficiency. In this context, the proposed CZTS-based solar cell will be optimized by

satisfying the objective of maximizing the total efficiency, which implies the maximization of the solar cell characteristics namely the short-circuit current, the open circuit voltage and the fill factor. To this extent, the fitness function adopted in our global optimization is given as follows

$$Fitness(X) = \frac{1}{\eta(X)} \tag{VI.18}$$

It is worth mentioning that for our global optimization procedure, the proposed CZTS-based solar cell design parameters is described by vector $X_i = (E_{g\min}, E_{g\max}, t_{CdS}, t_{CZTS}, N_{\mathrm{CZTS}}, N_{\mathrm{CdS}})$ of the i^{th} particle in the swarm.

Obviously, as it is outlined in Chapter III, a global optimization problem is principally presented by candidate solutions in a well defined search space and a set of constraints that should be considerably taken into account. In our case, the condition used in our global optimization is imposed by the possible band-gap values of the CZTS material. In this context, numerous experimental studies of this material indicate that band-gap values can be varied by increasing the Se content gradually from 1.52eV to 1eV [69-71]. Accordingly, the band-gap values at the top and bottom of the CZTS absorber layer should be confined in a given range according to the experimental data presented in [170]. Therefore, the constraints can be given by the following conditions

- $x \in [x_{m\min}, x_{m\max}]$, $x_i \in X$ (each design variable should be confined within a given range).
- $E_{g\max}, E_{g\max} \in [1, 1.54]$, which corresponds to the Se content variation in the CZTS material from 0 to 1.

In the PSO-based computation, the swarm is suggested with 20 particles and the stall generation for the mono-objective optimization of the investigated design is taken to be equal to 1000. Furthermore, a quick stabilization of the fitness function is reached and the optimization error for the stopping criteria is found infinitesimal.

Aiming at evaluating the impact of the proposed hybrid approach on the investigated CZTS-based solar cell performance, Figure VI.5 compares the I-V characteristics of the optimized design, the proposed structure with random configuration and the conventional solar cell counterparts. It can observed from this figure that the proposed hybrid approach can give rise to significant improvements regarding the solar cell photoelectric behavior, where the optimized design outperforms greatly the conventional one in terms of the photocurrent and the open circuit voltage.

This enhancement can be attributed to the effective engineering of the CZTS absorber region offered by the proposed approach. In other words, the adopted design methodology plays an important role for identifying the best graded band-gap profile that enables bridging the gap between avoiding the recombination losses and enhancing the absorption behavior of the investigated design.

More importantly, exploring the origin of such enhancement of the CZTS-based photovoltaic cell performance is crucial to understand the physical reasons behind the obtained favorable results. In this perspective, the external quantum efficiency (EQE) of both optimized and conventional designs is examined in Figure VI.6. From this figure, it is evidently demonstrated that the optimized design exhibits better optical behavior illustrated in the enhanced absorption efficiency in the whole spectrum. This is because the advantageous light-scattering improvement suggested by the effective absorber layer engineering enabled by the adopted PSO technique. Specifically, we can notice also the enhanced spectral absorption in the near infrared range [800, 1050] nm, which may be explained by the band-gap modulation offered by the proposed hybrid approach. Hence, the obtained EQE behavior can underline the substantial enhancing results recorded for the optimized design.

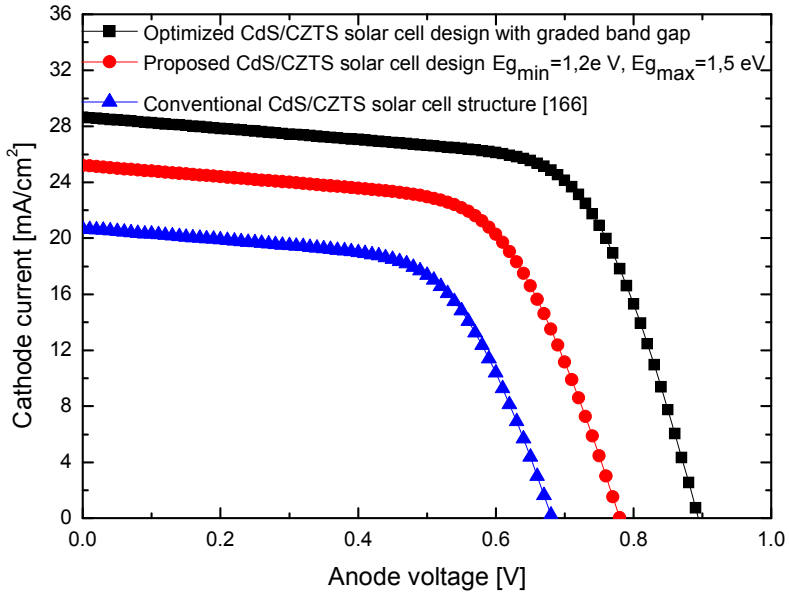

Figure VI.5: I-V characteristics of the optimized design compared to that of both the proposed design with a random band-gap profile and the conventional solar cell counterparts.

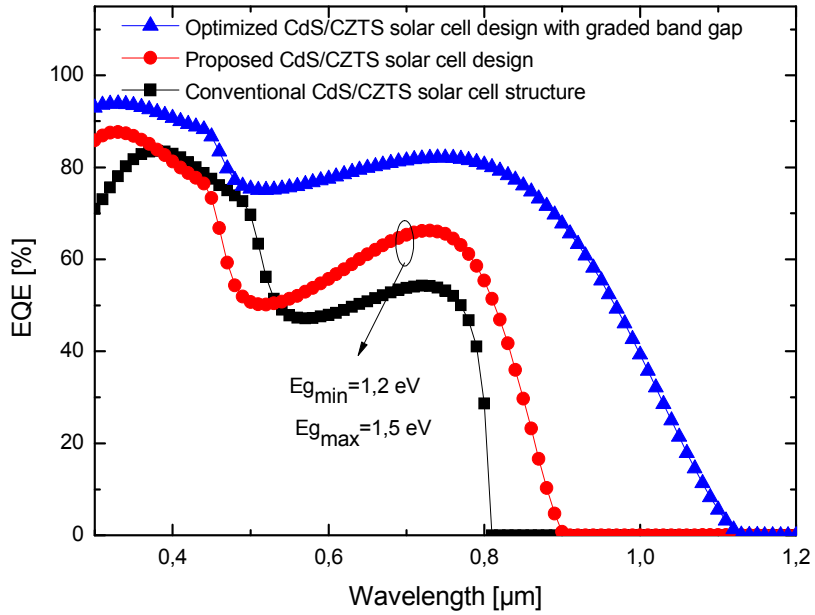

Figure VI.6: EQE curves associated with the conventional design compared to that of the optimized CZTS-based solar cell with.

For the completeness of this work, it appears to be essential to assess the optimized CZTS solar cell performance for high-performance photovoltaic applications. In this context, Table VI.1 summarizes a comparison of the performance metrics obtained from the optimized CZTS solar cell design with that of the experimental results of the conventional CdS/CZTS-based heterojunctions solar cell [166].

Table VI.1: Overall performance metrics obtained from the proposed design with and without optimization compared with that of the experimental results of the conventional CdS/CZTS-based solar cell.

Symbols	**Conventional CdS/CZTS-based solar cell Exp. results [166]**	**Proposed CdS/CZTS solar cell with graded band-gap aspect**	**Optimized CdS/CZTS solar cell with graded band-gap aspect**
Design variables:			
CdS (n+) region thickness t_{CdS} (nm)	80	80	50
CZTS (P) region thickness t_{CZTS} (µm)	1	1	1.15
ZnO thickness t_{ZnO} (nm)	60	60	60
CdS (n^+) region doping N_{CdS} (cm^{-3})	4.4×10^{16}	4.4×10^{16}	3×10^{17}
CZTS (P) region doping N_{CZTS} (cm^{-3})	1.4×10^{16}	1.4×10^{16}	6.5×10^{16}
Maximum band-gap value Eg_{max}(eV)	-	1.5	1.45
Minimum band-gap value Eg_{min} (eV)	-	1.2	1.05
Performance parameters:			
Short-circuit current (I_{sc}) (mA)	20.5	24.3	28.5
Open-circuit voltage (V_{oc}) (mV)	683	800	889
Fill factor (%)	62.5	63.1	65.9
Conversion Efficiency (%)	8.8	12.3	16.9

From this table, it is clearly demonstrated that our optimized design exhibits superior solar cell characteristics in comparison with that of the photovoltaic cell reported in [166]. To this extent, a high efficiency of 16.9% is recorded for the optimized design with a relative improvement of 105% as compared to the experimental results associated with the conventional design. Likewise, the optimized design with a graded band-gap aspect enables achieving higher fill factor value of 66% in comparison with that of the conventional counterpart. This improvement can be attributed to the total resistance modulation aspect, where the adopted hybrid approach brings the opportunity for reducing the series resistance through modulating the electric field in the CZTS absorber layer. It can be noticed also that the optimized design is considered technologically feasible, where the obtained band-gap values at the top and bottom of the CZTS absorber layer corresponds to the Se content of 0.15 and 0.94, respectively, according to the experimental data reported in [170].

In summary, we can conclude that it is evidently confirmed that the adopted hybrid approach based on the analytical modeling of the proposed chalcogenide solar cell and the metaheuristic analysis can considerably enhance the solar cells performance by reducing the recombination losses and increasing the absorption behavior as compared to that of the conventional structure. The proposed design methodology opens up a new way toward achieving promising conversion efficiency for photovoltaic applications.

VI.3. Part (2): Role of Intermediate Metallic Sub-Layers in Improving the Efficiency of Kesterite Solar Cells: Concept and Optimization

VI.3.1 Motivation

The CZTS solar cells are unable to reach the upper limit of conversion efficiency achievable with the more mature CGIS-based technology. In this perspective, new conceptions should be developed in order to overcome the reflective losses associated with the solar cell structure. As a matter of fact, increasing the light trapping capability by appropriately designing nanotexture morphologies has proved its effectiveness for suppressing reflection and can improve the solar cell optical behavior [179-181]. However, these techniques are found very complex at the manufacturing level and induce surface defects, which leads to extremely severe degradation related-recombination effects. In this context, introducing metallic sub-layers in the CZTS absorber region can be useful for providing the dual-benefit of reduced recombination

rate and enhanced absorbance behavior by creating resonant optical micro-cavity effects. This technique enables achieving promising improvements in terms of the solar cell light management without increasing the elaboration cost. In this perspective, we propose in the second part of this chapter a new hybrid approach that combines 2-D numerical analysis of a novel proposed design involving ultra-thin metal layers and PSO-based metaheuristic computation to enhance the CZTS solar cell electrical and optical performances. Our main objective is to select the global optimized design that provides improved absorbance over a broadband spectral range by achieving superior light trapping capability. Moreover, the proposed design methodology can enable reducing the series resistance by blocking the Sulfur diffusion at CZTS/Mo interface.

VI.3.2 Solar cell designing methodology

Principally, the cornerstone of the proposed CZTS-based solar cell design dwells on engineering the absorber layer by introducing intermediate metallic sub-layers. In this context, Figure VI.7 depicts the schematic of the investigated kesterite solar cell, where the first thin-film metallic layer is deposited on the Mo back contact that behaves as a blocking layer to the Sulfur diffusion for the eventual reduction of the series resistance. While, the second sub-layer is introduced in the CZTS absorber region in order to achieve favorable anti-reflection effects.

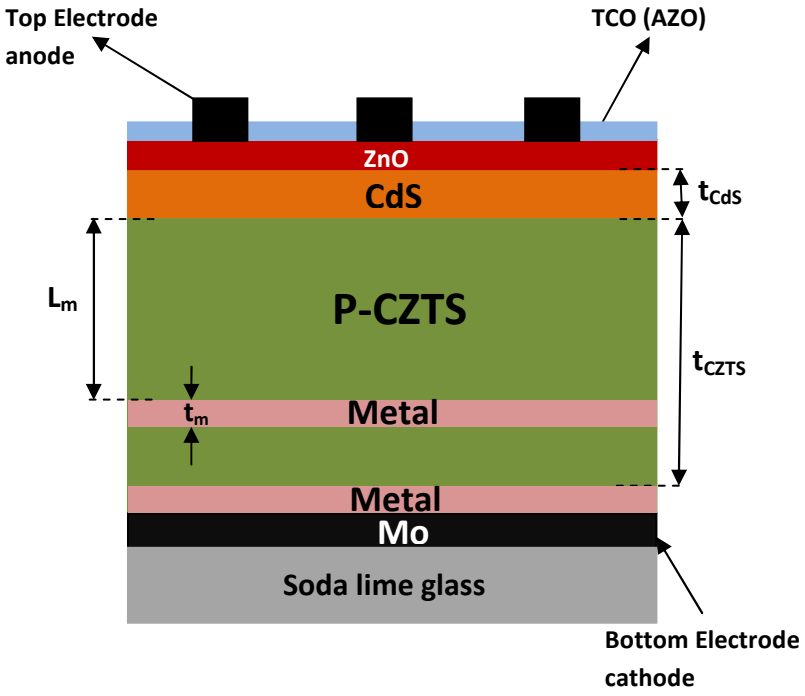

Figure VI.7: Cross-sectional view of the proposed CZTS-based solar cell with intermediate metallic sub-layers.

The parameters t_m and L_m refer to the metal sub-layer thickness and position with respect to CZTS/CdS interface, respectively, as it is illustrated in Figure VI.7. It is to not that, the impact of metallic sub-layers on the solar cell performance is carried out by considering three different metals namely Ag, Au and Ti.

The absorption coefficient and reflection factor are the most important parameters that play a crucial role in evaluating the optical behavior of the investigated CZTS-based solar cell. In this context, these optical parameters should be calculated accurately in order to model the solar cell optical behavior including intermediate metallic sub-layers. In this context, the discretization of Maxwell's equations is carried out by using the FDTD method provided by the ATLAS-2D device simulator using 2-D LUMINOUS module, which is considered as a powerful tool for modeling and investigating the thin-film solar cell optical behavior [123]. To this extent, the both absorbance and reflectance are estimated using the same modeling methodology presented in chapter IV.

In order to quantitatively evaluate the CZTS solar cell optical performance incorporating the impact of the metallic thin-film over the entire solar spectrum, it is important to calculate the total absorption efficiency (TAE). This parameter is considered as an essential figure of merit to assess the solar cell optical behavior. Thus, the TAE is given by the following equation

$$TAE = \frac{\int_{\lambda_{\min}}^{\lambda_{\max}} \frac{\lambda}{hc} A_i(\lambda) P_i(\lambda) d\lambda}{\int_{\lambda_{\min}}^{\lambda_{\max}} \frac{\lambda}{hc} P_i(\lambda) d\lambda} \quad \text{(VI.19)}$$

In order to estimate the delivered photocurrent for the proposed design including the adopted design amendment, we need to calculate the absorption coefficient in the visible to near infrared wavelength range. This can be achieved by using the Beer-Lambert's law given by the following equation [114]

$$\alpha_i = \frac{2.303}{t_{CZTS}} A_i(\lambda) \quad \text{(VI.20)}$$

It is worth mentioning that the materials, (CdS, AZO, Ag, Au, Ti and CZTS), optical constants (n,K) used in the developed FDTD modeling procedure are wavelength dependent and are extracted from SOPRA database and the experimental results [131] and [182-183].

VI.3.3 Results and discussion

Figure VI.8 depicts the absorption and reflection spectra of the conventional CZTS solar cell compared to that of the investigated designs including intermediate metallic sub-layers. It is clearly shown from this figure that the proposed designs provide better absorbance behavior, especially in the near infrared range as compared to that of the conventional structure. Moreover, the proposed design with Ti offers superior TAE value of 75% in comparison with the investigated structures with Ag (70%) and Au (71%) metallic sub-layers. Such advantageous absorption behavior could raise the number of generated electron/hole pairs, which are able to contribute in the photocurrent density and subsequently enables achieving superior efficiencies. The obtained achievements can be attributed to the optical confinement effect offered by the optical micro-cavity aspect generated in the CZTS absorber layer. The latter effect can increase the light trapping capability, which can be beneficial for promoting the optical path and improving photon forward scattering. In other words, the introduced intermediate metallic thin-film facilitates field penetration inside the CZTS absorber region, which can in turn greatly reduce the total reflection over a large wavelength range by avoiding the undesired interference effect as it is shown in Figure VI.8.

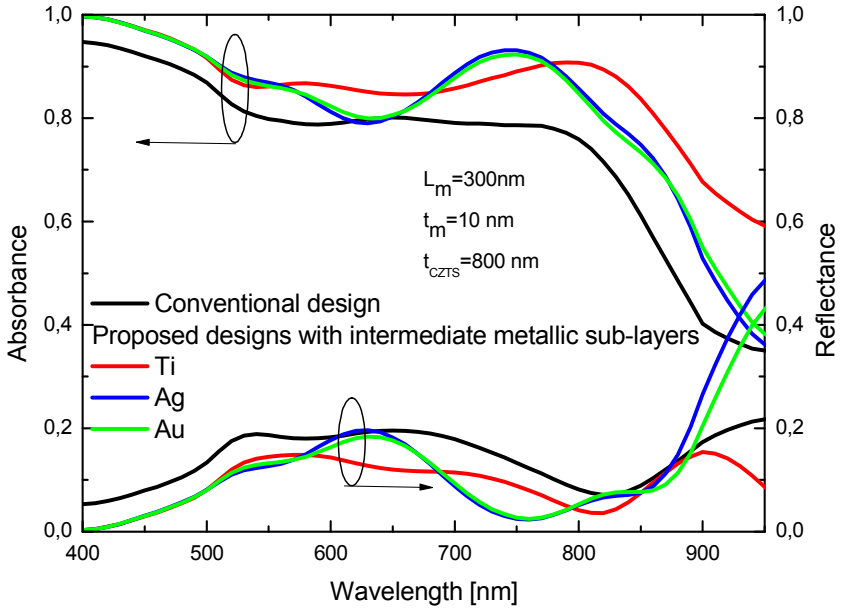

Figure VI.8: Absorbance and reflectance versus the free space wavelength for the conventional design compared to the proposed designs including metallic sub-layer (Ti, Au and Ag), with t_m=10 nm, L_m=350 nm and t_{CZTS}=800nm.

This figure demonstrates also that the proposed designs allow manipulating the light scattering to achieve better antireflection effects thereby reduced optical losses. This confirms the effectiveness of the proposed design amendment in enhancing the CZTS solar cell optical behavior.

In order to comprehensively illustrate the impact of the enhanced absorbance behavior on the solar cell characteristic, Figure VI.9 illustrates the I-V curves associated with the conventional structure and the proposed CZTS solar cell designs with different intermediate metallic sub-layers (Au, Ag, and Ti) under standard AM1.5 illumination. It is clearly observed from this figure that the proposed structures exhibit an improved short-circuit current as compared to that provided by the conventional counterpart. Moreover, the proposed structure with Ti sub-layer provides superior short circuit current (about 23.8 mA/cm^2) in comparison with that offered by the conventional design (about 21mA/cm^2). This improvement can be ascribed to the enhanced absorbance behavior as well as the reduced total reflection suggested by the optical micro-cavity effect as it is above outlined.

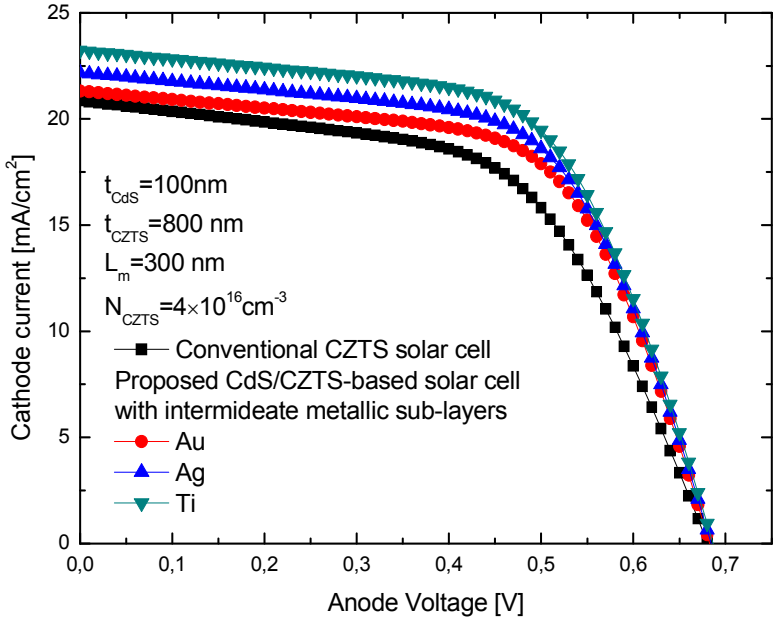

Figure VI.9: I-V curves of the conventional CZTS solar cell compared to that of the proposed designs including with dissimilar metallic sub-layer (Ti, Au and Ag) with t_{CZTS}=800m, N_{CZTS}=1.4×10^{16}cm^{-3} and N_{CdS}=10^{17}cm^{-3}.

It can be noticed also from this figure that an enhanced fill factor behavior (about 15%) can be achieved by introducing metallic sub-layers in the CZTS absorber region. This phenomenon can be explained by the total resistance modulation effect, where Au,

Ag, and Ti thin-films act as blocking layers for the Sulfur diffusion leading to a substantial decrease in the solar cell series resistance. Moreover, the adopted sub-layers offer the possibility for improving the carrier life time through inducing an electric field modulation at the metal/CZTS interfaces, which leads to reduce the recombination losses. Besides, the introduced metallic sub-layers (Ag, Au and Ti) have a relatively high work-function, resulting in the formation of small depletion regions in the CZTS absorber layer. This can enhance carrier separation and further reduce recombination effects. Thus, the proposed design with Ti metallic sub-layers outperforms the conventional design in terms of the photogenerated photocurrent.

The observed enhancement motivates us for conducting further investigations concerning the impact of the ultra-thin metallic layer position on the solar cell performance. Figure VI.10 displays the variation of the conversion efficiency of the investigated designs as a function of the sub-layer position with respect to the top of the absorber region. It can be seen from this figure that a maximum efficiency value of 11.85% can be achieved for an optimum metal position of L_m=400nm. Over this optimal value, the power efficiency is slowly decreased to achieve its minimum when the inserted metal sub-layer is localized near the CZTS/Mo interface. This behavior can be explained by the electric field modulation aspect, where appropriately adjusting the metal position can be effective for increasing the light trapping capability.

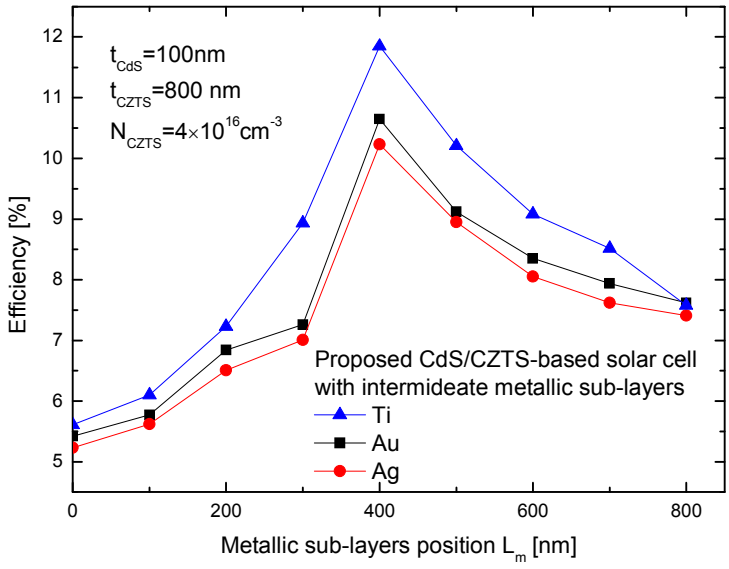

Figure VI.10: The conversion efficiency as a function of the metallic sub-layer position for the proposed structures including different metallic sub-layers (Ti, Au and Ag) with t_m=10 nm and t_{CZTS}=800nm.

It can be also deduced that the proposed design with Ti thin-films provides the better conversion efficiency as compared to that offered by the investigated solar cells using Au and Ag metallic sub-layers. Accordingly, these observations can also underline the complex optical behavior of the analyzed CZTS solar cell including Au, Ag, and Ti sub-layers engineering paradigm.

Therefore, the carful adjustment of the geometrical parameters plays an important role to reach further improvement in terms of antireflecting effects and photogeneration rate, claiming that there are wider opportunities for recording superior efficiencies. In this framework, a new insight based on an efficient global optimization approach by using the PSO-based metaheuristic technique can be helpful for boosting up the efficiency of the investigated CZTS solar cell including metallic sub-layers, which constitutes the main purpose of the next section.

VI.3.4 The proposed design methodology to boost the conversion efficiency

The proposed designs with Au, Ag, and Ti ultrathin metallic layers only decrease the total reflectance in a narrow wavelength range, indicating that they are not perfect options in this condition for the CZTS-based technology that requires reduced reflection effects over a wide solar spectrum. In this framework, it seems to be valuable to perform a global optimization of the proposed design considering the objective of improving the absorbance and reducing the reflectance over the entire solar spectrum. For this purpose, our proposed approach involves engineering the adopted metallic sub-layers to achieve further enhancement regarding the solar cell efficiency. The flowchart of the proposed design methodology based on PSO metaheuristic technique used to optimize the investigated CZTS solar cell performance is detailed in Figure VI.11. In this context, the proposed designs will be optimized by maximizing the solar cell power efficiency. Thus, the objective function considered in our global optimization approach is given as follows

$$Fitness(X) = \frac{1}{\eta(X)} \tag{VI.21}$$

where $X_i = (L_m, t_m, t_{ZnO}, t_{CdS}, t_{CZTS}, N_{\mathrm{CZTS}}, N_{\mathrm{CdS}})$ of the i^{th} particle in the swarm represents the investigated CZTS solar cell design parameters.

The design parameters should be confined in a given range in order to get appropriate values regarding the physical and geometrical parameters considered in our investigation. In our global optimization procedure, we have introduced a constraint that

should be considerably taken into account, where the idea is to introduce the design parameter ranges as a set of constraints, which are given by the following conditions

- $x \in [x_{m\,\min}, x_{m\,\max}]$, $x_i \in X$ (each design variable should be confined within a given range).

It is worth mentioning that the swarm is suggested with 20 particles and the stall generation for the optimization procedure is taken to be equal to 200. These considered values for the swarm particles and the stall generation are optimized carefully in order to achieve the better possible of the conversion efficiency.

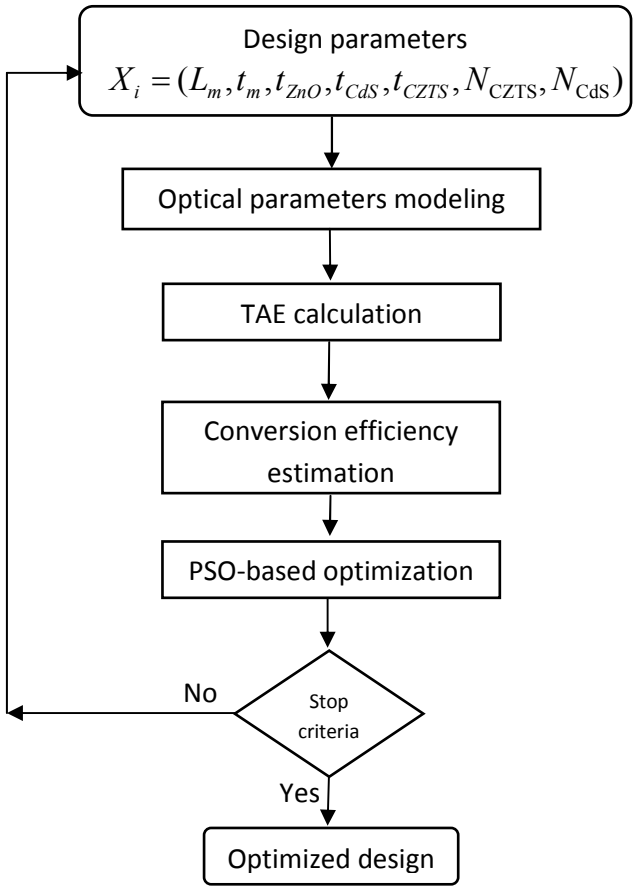

Figure VI.11: Flowchart of the proposed PSO-based optimization approach.

In order to elucidate the impact of the proposed hybrid approach on the investigated CZTS solar cell optical performance, Figure VI.12 (a) compares the absorbance and reflectance spectra of the optimized structures with different (Au, Ag, and Ti) intermediate metallic sub-layers and the conventional counterpart. It can be observed from this figure that the proposed hybrid approach can give rise to significant improvements regarding the solar cell optical behavior, where the optimized designs

provide superior absorbance and near zero reflection over a broad solar spectrum. In fact, the introduction of metallic sub-layers in the CZTS absorber layer induces a complex optical behavior. This figure also reveals that the optimized design with Ti offers superior total absorption efficiency value of 92% as compared to that provided by the conventional structure (65%) and solar cells with Au (86%) and Ag (85%). Thus, the Ti sub-layers have the potential for providing superior optical behavior especially in the near infrared part of the solar spectrum. This is because of the superior compatibility of the materials (Ti and CZTS) optical properties for providing an enhanced optical behavior as compared to other metals (Ag and Au). Moreover, the Ti metal exhibits superior absorption efficiency as compared to the Ag and Au metals. On the other hand, the experimental study given in [184] demonstrates that the introduction of an ultrathin Ti intermediate layer prevents the Sulfide diffusion into Mo and thereby reduces the MoS_2 layer thickness. In addition, this study reveals that the CdS buffer can grow more uniformly and therefore enable the formation of a better p-n junction with the CZTS film, which leads to increase the crystallinity and therefore reduces recombination effects. This proves the excellent compatibility of both Ti and CZTS in terms of the materials optical properties for achieving an enhanced photovoltaic performance. Moreover, the obtained optical behavior of the optimized designs can be attributed to the effective engineering of the CZTS absorber layer offered by the proposed hybrid approach that allows the potential for selecting the best thickness and position of the introduced metallic sub-layers.

Based on the optimized solar cell structure, we have further investigated the electric field distribution in order to understand the physical rules governing the obtained adequate optical behavior. In this perspective, Figure VI.12 (b) depicts the electric field profile associated with both optimized CZTS-based solar cell with Ti intermediate thin-film and the conventional design for the free space wavelength value of 800 nm. It is clearly observed that the optimized design shows an extremely dense electric field inside the CZTS absorber layer in comparison with that of the conventional one, indicating its superior light trapping capability. This allows achieving longer lifetime of the photons trapped in the CZTS absorbent layer through the high optical confinement effect, which leads to improve the absorption near the infrared range of the solar spectrum. These results confirm the ability of the proposed design methodology for improving the solar cell absorbance in the entire spectrum.

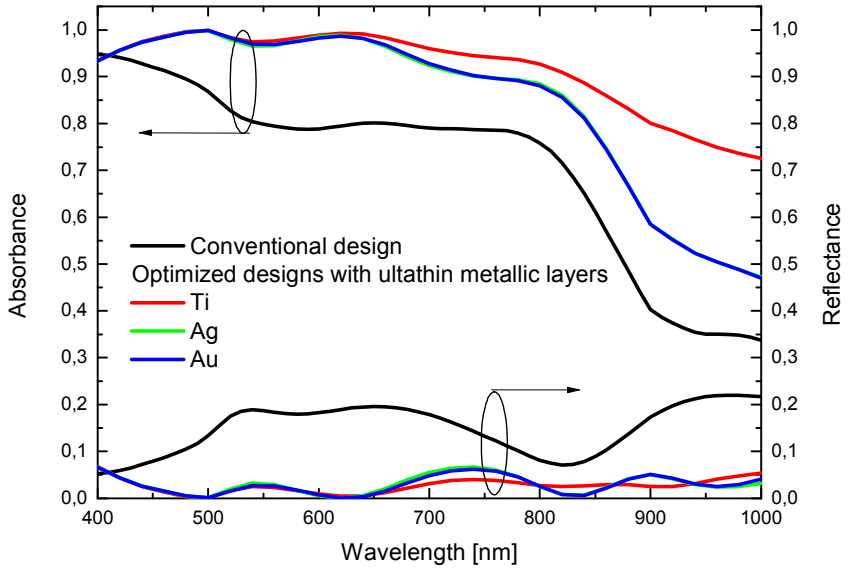

(a)

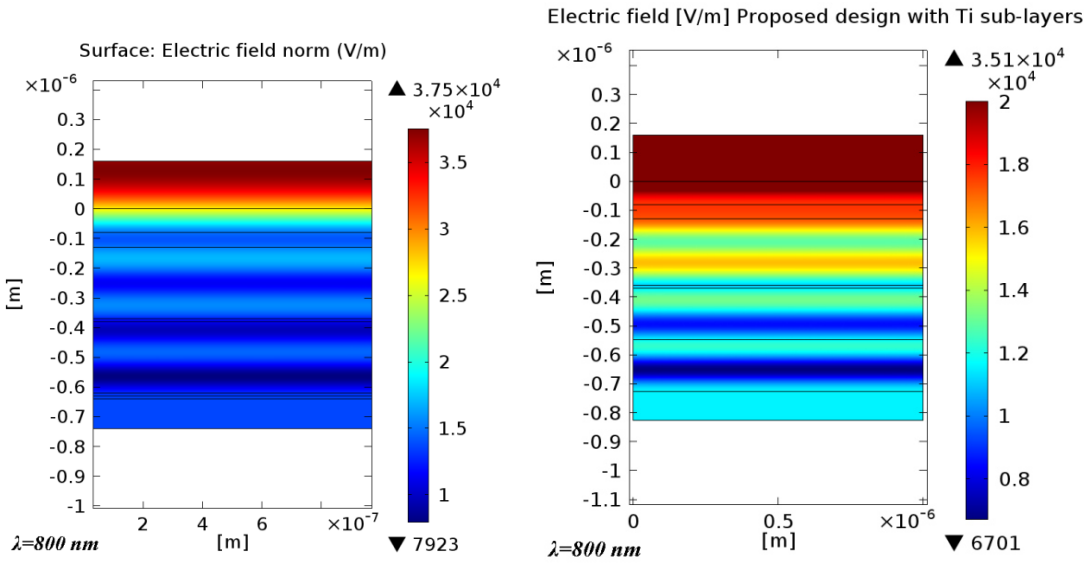

(b)

Figure VI.12: (a) Absorbance versus the free space wavelength for conventional design and the optimized structures with intermediate metallic sub-layers aspect. **(b)** Electric field distribution associated with both the conventional CZTS solar cell and the optimized design with Ti intermediate metallic thin-films.

It is advantageous to consolidate the investigation of the CZTS solar cell by analyzing the effect of the adopted approach on its electrical behavior. In this context, Figure VI.13 illustrates the I-V characteristic of the optimized design with Ti intermediate metallic thin-film compared to that of the conventional kesterite solar cell.

The design parameters associated with the optimized structure $X_i = (L_m, t_m, t_{ZnO}, t_{CdS}, t_{CZTS}, N_{CZTS}, N_{CdS})$ are illustrated in Table VI.2.

It is clearly demonstrated that the optimized design showcases superior short-circuit current compared to that offered by conventional structure. This can be explained by the improvements concerning the solar cell optical behavior gained from the optical confinement effect, which is achieved using joint adopting aspects of metallic sub-layer engineering and PSO-based optimization. In other words, the adopted design methodology offers the possibility for achieving a broadband absorption behavior and near zero reflection as it is shown in Figure VI.12.

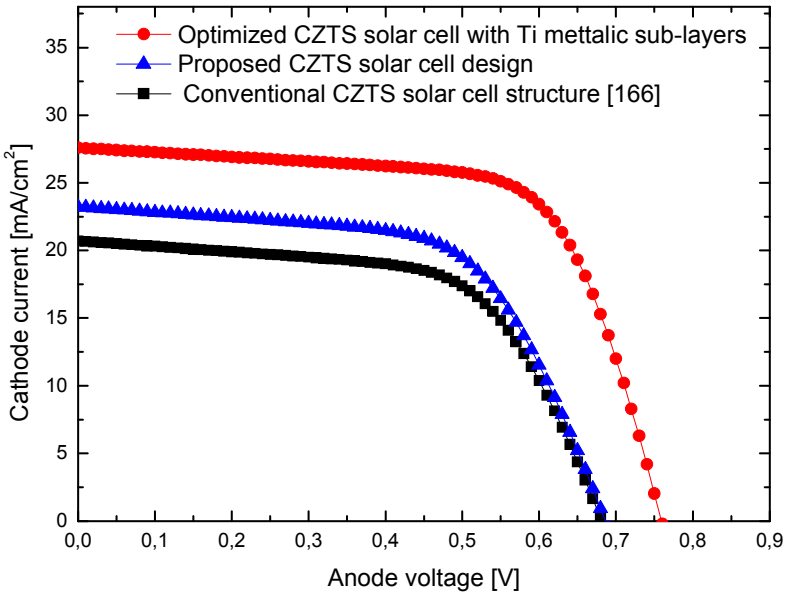

Figure VI.13: I-V characteristics of the optimized design with Ti ultrathin metal layers compared to that of both the proposed design with a random geometrical configuration and the conventional CZTS solar cell counterparts.

It can be also seen from this figure that the optimized design with Ti ultra-thin layer provides superior open circuit voltage (770mV) in comparison with that exhibited by the conventional one (680mV), which is due to the enhanced optical behavior enabled by the global optimization and the reduced recombination effects offered by the improved carrier life time. Moreover, the optimized designs allow us improving the photocurrent without sacrificing the V_{oc}, which is mainly due to the adopted hybrid approach. In summary, the proposed design methodology has succeeded in identifying the best design configuration that provides higher power conversion efficiency.

Notably, it appears to be important to assess the optimized CZTS solar cell characteristics for high-performance photovoltaic applications. In this context, Table VI.2 illustrates the overall performance metrics obtained from the optimized structures with dissimilar (Au, Ag, and Ti) metal ultrathin layers compared to that of the experimental results of the conventional CdS/CZTS-based heterojunctions solar cell. From this table, it is obviously confirmed that our optimized designs offers superior solar cell properties over the conventional design reported in [166]. In this regard, it is clearly demonstrated that the optimized structure with Ti metallic ultrathin-film yields an improvement of 60% concerning the conversion efficiency, 31% in the short circuit current, 20% in the open circuit voltage and 10% with respect to the fill factor over the conventional design. These enhancing results underline the effectiveness of the proposed approach that pinpoints a new path toward recording high-efficiency kesterite solar cell (14.1%), through achieving favorable antireflection effects and reduced recombination losses.

Table.VI.2: Overall performance metrics obtained from the optimized designs with dissimilar metallic sub-layers (Ti, Au and Ag) compared with that of the experimental results of the conventional CdS/CZTS-based solar cell.

Symbol	**Conventional CZTS design, Experimental results [166]**	**Optimized CZTS solar cell designs with intermediate metallic sub-layers**		
		Au	**Ag**	**Ti**
Design variables :				
CdS (n+) region thickness t_{CdS} (nm)	80	80	73	45
CZTS (P) region thickness t_{CZTS} (nm)	800	510	480	580
ZnO thickness t_{ZnO} (nm)	60	100	80	70
CdS (n^+) region doping N_{CdS} (cm^{-3})	4.4×10^{16}	6×10^{18}	2×10^{18}	5×10^{18}
CZTS (P) region doping N_{CZTS} (cm^{-3})	1.4×10^{16}	1×10^{17}	1.5×10^{17}	1×10^{17}
Metallic sub-layer thickness t_m (nm)	/	5	7	6
Metallic sub-layer position L_m(nm)	/	440	265	410
Objective functions :				
Total absorbance efficiency (TAE) (%)	68	88	86.4	92
Short-circuit current (I_{sc}) (mA)	20.5	26.6	25	27.5
Open-circuit voltage (V_{oc}) (mV)	683	770	783	766
Fill factor (%)	62.5	67	66.3	67.5
Conversion Efficiency (%)	8.8	13.8	13.5	14.1

It should be noted that from the fabrication view point, the experimental investigation reported in [184] provides an easy and cost-effective approach to overcome limitations in CZTS solar cells related to defects in the interface between the CZTS and Mo layers by introducing an ultrathin Ti intermediate layer. The latter thin-films can be

deposited on Mo-coated soda-lime glass substrate by radio frequency magnetron sputtering. Then the CZTS thin-film can be prepared on the Ti sub-layer by co-sputtering with three different targets Cu, Sn and ZnS. This confirms the feasibility of the optimized design with intermediate metallic sub layers, where it can be elaborated with a good cristallinity, decreased surface roughness and better p-n junction.

Eventually, the optimized versatile CZTS solar cell designs based on intermediate metallic sub-layers (Au, Ti, and Ag) engineering aspect provide promising effectiveness for enhancing light-scattering behavior and reducing recombination losses. The introduced feature generates optical confinement regions in the CZTS absorber layer to achieve an improved absorption and appropriate antireflection effects. Therefore, the optimized designs offer the opportunity for bridging the gap between improved optical behavior and reduced recombination losses, which makes them potential alternatives for providing high-performance kesterite solar cells.

VI.4. Conclusion

Overall, this chapter has provided useful quantitative insights about the prospect of enhancing the CZTS-based solar cell efficiency. It was concluded that amended CZTS absorber layer with graded band-gap aspect behaves like an electric field modulator, which leads to enhance the carrier life time and reduce the recombination losses. Moreover, the proposed design suggests the ability for improving the solar cell absorbance behavior through effectively engineering the band-gap profile. It is found that by using a new approach based on analytical modeling supported by metaheuristic techniques, exciting opportunities for further efficiency enhancement are indeed possible. It was revealed also that the adopted approach opens up the route for distinctively engineering the CZTS absorber layer, which enables improving the overall characteristics of the solar cell. In this regard, promising results have been recorded according to the solar cell photoelectric behavior, where the optimized design can provide superior efficiency, photocurrent, V_{oc} and higher FF. Therefore, the proposed design methodology offers a new insight toward reducing recombination effects and enhancing the absorbance efficiency.

In another way, a novel CZTS-based solar cell design based on intermediate metallic sub-layers engineering aspect has been proposed and investigated. Our analysis indicates that the amended CZTS absorber layer occurs optical resonant micro-cavity effects, which leads to improve light trapping capability. It was revealed that the adopted hybrid

approach offers a new path toward reaching broadband absorption and near zero reflection. The obtained results indicate also that the optimized design enables reducing the series resistance, where the introduced metallic sub-layers acts as a blocking layer for the Sulfur diffusion. Therefore, the proposed design methodology provides a new insight toward improving the total absorbance efficiency and reducing the recombination losses, where the design with Ti sub-layers provides the highest efficiency value of 14.1%.

Therefore, the obtained results make the optimized designs potential alternatives for developing high-efficiency thin-film solar cells for high-performance photovoltaic applications.

Chapter VII

An Experimental Investigation of a New Au/ITO/Si Schottky Barrier Diode Design

***Abstract:** the last Chapter of this thesis explores the concept of using a new Au/p-Si SBD based on ITO intermediate thin-film to improve the diode electrical behavior. The device performances are experimentally investigated. The effect of the annealing temperature on the SBD electrical performance is also investigated. In order to show the role of the inserted ITO layer thickness on the device performance, we elaborated Au/ITO/p-Si structures with different ITO thicknesses by means of RF magnetron sputtering technique. The role of the annealing process in improving the SBD basic electrical parameters and thermal stability performance is also discussed. Finally, an overall performance comparison between the fabricated SBD structures with and without intermediate ITO layer is carried out.*

VII. 1. Introduction

In the last few years, metal oxides semiconducting transparent thin-films have strategically attracted an enormous deal of attention owing to their excellent transparency, relatively high workfunction and good semiconducting properties [185-187]. As a matter of fact, metal oxide thin-layers such as ITO, vanadium pentoxide (V_2O_5), zinc oxide (ZnO) and tungsten trioxide (WO_3) provide the opportunity for making a good trade-off between both electrical and optical material characteristics [186-199]. This makes them effective for designing different microelectronic and sensing devices like organic light emitting diodes (OLED), solar cells and Schottky barrier diode SBDs [187-190]. The latter is considered as the preferred rectifying device due to its high derived current capability. Moreover, Schottky diodes consisting of metal–semiconductor (MS) junction can pave the way to avoid the degradation-related recombination effect as compared to the PN heterojunction-based diodes [191]. Even though Schottky barrier diodes have been well-developed, they still suffer from other bottlenecks mainly associated with the high series resistance and high density of the interfacial states arisen from the poor quality of the MS interface [190-192]. Moreover, the relatively low Schottky barrier height and the high leakage current of the Au/Si SBD constitute the most pronounced critical problems that should be addressed. In this perspective, the good control of the MS interface plays a crucial role in developing high-performance SBDs for microelectronics and photovoltaic applications [193]. In this context, much attention has been paid to improve the device performance by introducing suitable thin-films at the MS interface such as polymers, organic materials and metal oxides [194-198]. In fact, the developed SBD designs have demonstrated a good electrical performance, but in contrast, they exhibit a high degradation related to heating effects that can adversely affect the device performance. Despite the numerous investigations regarding the Au/Si SBDs electrical performance there is surprisingly a lack of information regarding their reliability against thermal variation effects. These effects can prevent achieving high-performance SBDs with improved thermal stability, which is considered as an essential issue for different sensing applications. Consequently, analyzing the impact of the temperature variation on the device performance is of great importance for acquiring a global insight about its thermal stability.

Numerous processes are used for growing high-quality films of ITO material such as: sputtering from oxide targets, chemical vapor deposition, and plasma deposition method [199-200]. The ITO thin-film with distinctive transparency and improved electrical conductivity has been extensively exploited as an optical window for thermally stable solar cell application [200]. In this regard, the prospect to reach Au/Si SBD with both enhanced electrical performance and thermal stability behavior through introducing ITO thin-layers with an appropriate thickness appear motivating and deserves advance analysis. Therefore, it is envisaged that these attractive properties can be exploited to effectively design a new SBDs with ITO interface layer, in order to improve the device electrical performance and to get rid of thermal stability issues faced by the conventional Au/Si junction design. To the best of our knowledge, no design approach based on an experimental investigation of the Au/Si SBD with ITO thin intermediate layer was conducted to enhance the diode electrical performance and thermal stability behavior. For this purpose, in the last chapter of this thesis, we investigate the impact of introducing ITO thin-films with different thicknesses on the Au/Si SBD electrical performance. Accordingly, we fabricated Au/ITO/Si hetero-structures by using RF magnetron sputtering technique. Moreover, I-V characteristics associated with the investigated designs are analyzed. The Au/Si SBD performance parameters such as barrier height (ϕ_{bn}), ideality factor, interfacial state density and series resistance were extracted. Besides, the merit of the introduced ITO thin layer at the MS interface and the annealing process on the Au/Si SBD thermal stability is successfully presented, where the proposed design with an appropriate ITO thickness provides improved electrical and thermal stability properties. This makes the proposed Au/ITO/Si structure suitable for designing high-performance SBDs for thermally reliable microelectronics and photovoltaic applications.

VII. 2. Experimental detail

Basically, the cornerstone of the proposed Au/ITO/Si/Au structure resides on introducing the ITO thin layer between both Si and gold contact materials. In this regard, the ITO thickness is varied from 5 to 15nm in order to reveal the impact of the material thickness on the device electrical and thermal stability characteristics. In this context, Figure VII.1 (a) depicts a cross-sectional view of the investigated Au/ITO/Si/Au structure, where t_{ITO} represents the ITO thickness. It is noteworthy that

the N^+ local regions illustrated in this figure are generated through the minority carrier injection effect at the metal/semiconductor interface.

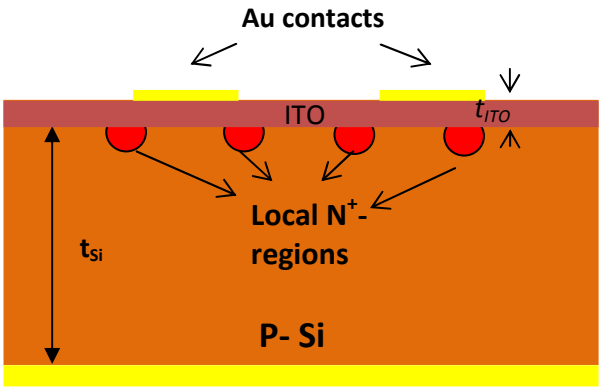

(a)

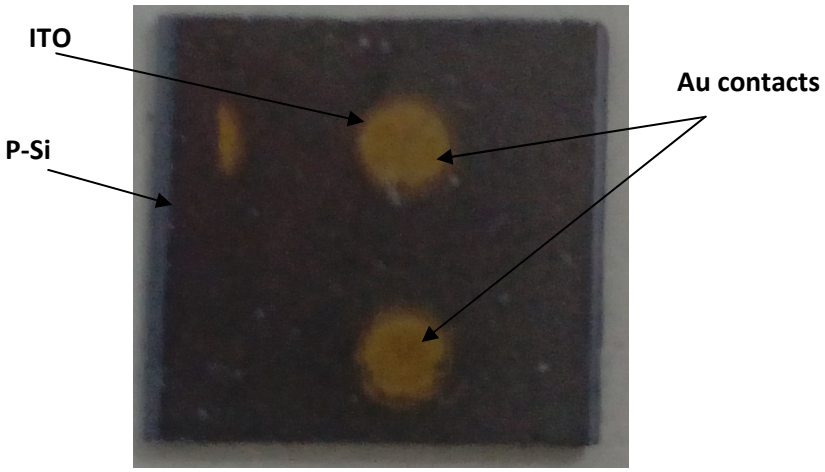

(b)

Figure VII.1: (a) Cross-sectional view of the investigated Au/Si SBD with ITO intermediate thin layer. **(b)** The camera image of the elaborated Au/ITO/Si/Au structure.

Au/ITO/Si/Au thin films were deposited on glass substrates using the cathodic RF magnetron sputtering technique (MOORFIELD MiniLab 060). Resistivity and thickness of the P-Si wafer were 10Ωcm and 500µm, respectively. Firstly, the substrates, with size dimensions of $1cm^2$, were cleaned in the commercial detergent and then passed through an ultrasonic bath in the following sequence: 25 min in ethanol then rinsed in deionized water heated at 90°C, and after that quipped for 25 min in acetone and subsequently rinsed with demineralized water for native oxide removal. The last step consists of drying under a nitrogen jet. The Au/Si SBD structure was fabricated on the top of the P-Si wafer with high quality gold deposited by means of RF magnetron sputtering

technique. While for the investigated structures, different ITO thin-films (5, 10 and 15nm) were deposited by using RF magnetron sputtering technique. Moreover, the thin layers uniformity and homogeneity are controlled by optimizing both the target-substrate distance and the power of the sputtering target. The camera image of the fabricated Au/ITO/Si/Au structure is illustrated in Figure VII.1 (b). It should be noted that the substrate holder was keeping in rotation during spraying in order to achieve a good homogeneity of the deposited thin films.

VII.2.1 RF sputtering technique

The sputtering phenomenon was observed for the first time in 1852 by Grove then in 1858 by Plucker. They have found that when an electric discharge is applied between two electrodes in the presence of an inert gas under reduced pressure, a thin layer of the material constituting the cathode is formed on the surface of the anode. This laboratory observation has remained an untapped century without realization because of the technological difficulties related to this process. In the 1950s, the experimental conditions of sputtering began to be defined, which has paved the way in 1965 to elaborate films. Afterword, it was in 1972 that the true spray development began to sprout thanks to the invention of the magnetron cathode [201].

The vaporization of the source material is carried out under vacuum in order to ensure the development of high quality thin-layers. Moreover, the working pressure associated with the sputtering technique plays an important role in determining the quality of the deposited films, where the lower the pressure (<10 Pa) is, the more the trajectories of the vaporized particles will be straight and efficient. In this case, only parts of the substrate directly facing the material source will be covered. On the other hand, the sputtering technique is basically consisting on applying an electrical voltage between the two considered electrodes. When this voltage is sufficient, the ionization of the atmosphere (generally composed of argon) takes place and thereby the creation of plasma with luminescent discharge is achieved. The ionized charges are then accelerated to the cathode (in which the target or source of the material to be deposited is located). The vapor phase is then done according to a wholly mechanical process, by transfer of the kinetic energy of the ions to the atoms of the target.

In general, the synthesis of coatings by sputtering takes place according to three main stages [202]:

- Creating a metal vapor from a solid source (or target)

- Transporting the vapor to the substrate to be coated in a rarefied atmosphere
- Condensation of this vapor on the surface of the substrate, resulting in the formation one layer by germination and growth.

In order to obtain a lower pressure discharge with a higher ion density and higher energy incident species, but at the same time to increase the deposition rate, it is essential to equip the cathode with a magnetron device. The latter is composed of permanent magnets of inverse polarities installed at the rear of the cathode [202]. These magnets create a magnetic field ($\vec{B}$) parallel to the surface of the target, perpendicular to the electric field ($\vec{E}$). The electrons emitted by the cathode and present in the gas are then trapped by the magnetic field. This phenomenon also makes possible confinement of the electrons in the vicinity of the cathode. The electrons wrap around the magnetic field lines (Figure VII.2), greatly increasing the probability of ionizing a gas molecule which increases the ionization rate of the gas.

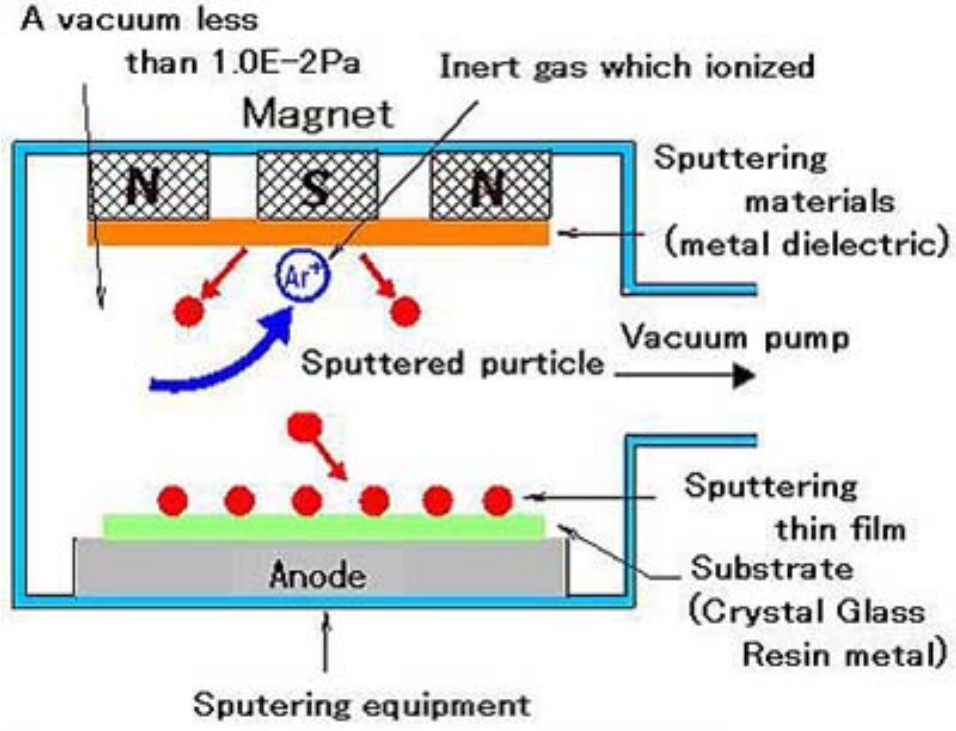

Figure VII.2: The basic working mechanism associated with the RF sputtering technique.

As a matter of fact, the main parameters influencing the quality of the deposition are the pressure, the nature of the gas, the power of the supply and the temperature of the substrate.

Fortunately, the clean room of the University of Batna-2 is equipped with Moor feld's MiniLab systems, which could provide superior quality coating films, with the flexibility to meet a wide range of research requirements. The MiniLab consists of several platforms. Each platform is usually associated with a specific vacuum chamber size, while, all rooms are built to the same standards and allow operating in high-level vacuum conditions. Moreover, larger rooms enable more flexibility than their smaller counterparts.

MiniLab 060 systems (Figure VII.3) are vacuum systems based on a flat bottom exploited for metal, dielectric and thin organic films deposition. All systems involve a box-type stainless steel chamber with front door. The chamber is cubic and ideally suited to magnetron cathode sputtering. A turbo-molecular pumping system is standard, for basic pressures at high vacuum level superior to 5×10^{-7} mbar.

Figure VII.3: The RF sputtering MiniLab 060.

VII. 3. Results and discussion

The measured current-voltage (I-V) characteristics of the elaborated Au/ITO/Si/Au structure design with different ITO thicknesses are shown in Figure VII.4. It is clearly observed from this figure that by introducing the ITO thin layer, the derived current is increased as compared to the conventional Au/Si SBD design. Moreover, we can also see that by increasing the interface thin layer thickness, the current is also increased.

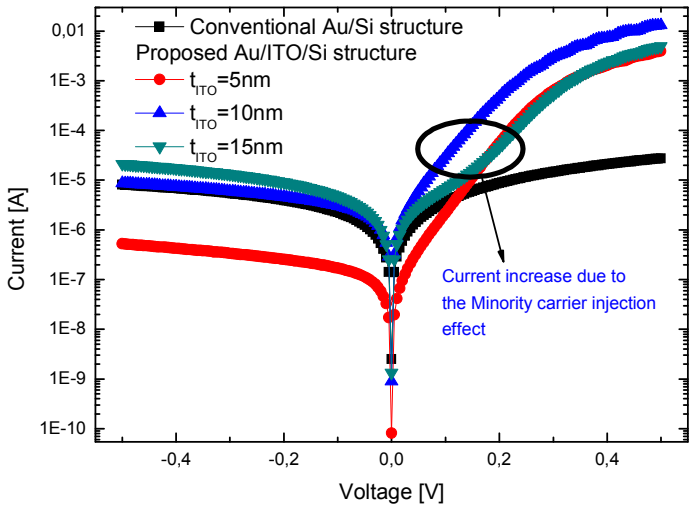

Figure VII.4: The semi-logarithmic current-voltage (I-V) characteristics associated with the conventional Au/Si SBD design and the proposed Au/ITO/Si/Au structures with different ITO thicknesses at room temperature.

The current enhancement can be attributed to a mixture of effects; firstly, the effective Schottky barrier height modulation induced by the use of ITO thin-films as an interface layer. Secondly, the latter layer acts as a passivation layer and can provide also the possibility for decreasing the structure series resistance, which leads to enhancing the device conductance behavior and thereby increasing the derived current capability. More importantly, the Schottky barrier raise causes the minority carrier injection effect at the MS interface, which leads to the current enlargement in comparison with the conventional structure. In other words, the injected minority carriers create local N^+ regions at the ITO/Si interface as it is shown in Figure VII.1 that can form forward-biased p–n junctions. The latter injects minority carriers into the base of the Au/ITO/Si/Au structure and as a result, the current increases [203]. It can be also

noticed from Figure VII.4 the asymmetrical behavior of the I-V characteristics associated with the proposed design including ITO thin-films for both reverse and forward conditions. This behavior indicates that there is a slight non-uniformity of the deposited ITO thickness on the silicon.

The comprehensive study of the Au/Si SBD performance parameters plays an important role in evaluating the impact of the introduced ITO thin-film on the device electrical behavior. In this perspective, it seems crucial to estimate the electrical parameters such as Schottky barrier height (ϕ_{bn}), ideality factor (n), interfacial state density (N_{ss}) and series resistance (R_s) by means of an effective electrical characterization in order to get a global idea about the effect of the introduced ITO thin-layers on the device performance. Thus, by using the thermionic emission model of the MS-based SBDs, the current-voltage formulation at forward and reverse bias with taking into account the effect of the series resistance can be given by the following expressions [125], [204-205]

$$I = I_s \exp\left(\frac{q\left(V - R_s I\right)}{n\, KT} - 1\right) \quad \text{(VII.1)}$$

where, q is the electron charge, T and K are the absolute temperature and the Boltzmann constant, respectively.

The saturation current is well represented by the thermionic-emission model and can be expressed as [125], [205]

$$I_s = S\, A_n^* T^2 \exp\left(\frac{-q\phi_{B_n}}{KT}\right) \quad \text{(VII.2)}$$

where, A_n^* is the effective Richardson constant for the silicon material and S denotes the gold contact area.

In order to extract the device electrical parameters, we exploit the ln(I)=f(V) characteristic [205]. In this context, this characteristic illustrates two linear regions, where the slope of the first linear part enables estimating the ideality factor. While, the second part slope provides the possibility for calculating the series resistance. On the other hand, the saturation current can be estimated from the intersection between the current axis and the interpolated line associated with the first linear region. Besides, by using Equation (VII.2), we can determine Schottky barrier height values. The interface state density can be calculated by using the following formula [204]

$$N_{ss} = \frac{1}{q}\left[\frac{\varepsilon_i}{\delta}(n-1) - \frac{\varepsilon_s}{W}\right] \quad \text{(VII.3)}$$

where, ε_i, ε_s are the interfacial layer and silicon permittivity, respectively, δ denotes the ITO interfacial layer thickness and W the depletion layer width, which is calculated using the experimental C(V) curves.

The ideality factor is mainly depending on the applied voltage and can be calculated from the following formula [204]

$$n(V) = \frac{q}{kT}\left[\frac{(V - IR_i)}{\ln(I / I_s)}\right] \quad \text{(VII.4)}$$

After calculating the density of states, the energy dependent value of the N_{ss} with respect to the top of the conduction band (E_c) at the MS interface can be calculated from the following equation

$$(E_{ss} - E_c) = \phi_{b0} + \left(1 - \frac{1}{n(V)}\right)(V - R_s I) \quad \text{(VII.5)}$$

Aiming at elucidating the impact of the introduced ITO thin-films on the device electrical performance, Figure VII.5 shows the variation of the electrical parameters (ϕ_{bn}, n, N_{ss} and R_s) associated with the proposed Au/ITO/Si/Au SBD design as a function of the ITO interface thin layer thickness. It is clearly shown from Figure VII.5 (a) that by increasing the ITO thin-film thickness, the ideality factor significantly decreases to reach its minimum (n=1.25) for the ITO thickness value of 5nm and after that increases slowly. Moreover, we can notice that the proposed Au/ITO/Si/Au structure with 5nm of ITO interface layer thickness provides superior Schottky barrier height (ϕ_{B_n}=0.7V) and reduced interfacial state density (N_{ss}=1.5×$10^{12}$$cm^{-2}$) as compared to the conventional Au/Si design. This behavior can be ascribed to the enhanced structural quality of MS interface associated with the proposed structure, where introducing the ITO material can reduce the interfacial defects and improve the device conductivity behavior. Moreover, the ITO thin-film induces a substantial shift in the metal workfunction as well as in the silicon electron affinity, which leads to modify the space charge region width and hence increase the Schottky barrier height. Therefore, the unique feature of the prepared SBD dwells on the tenability of barrier height through the introduction of the ITO thin-films at the MS interface, which enables the potential to appropriately design and alter the I-V characteristics of the investigated Au/Si SBD.

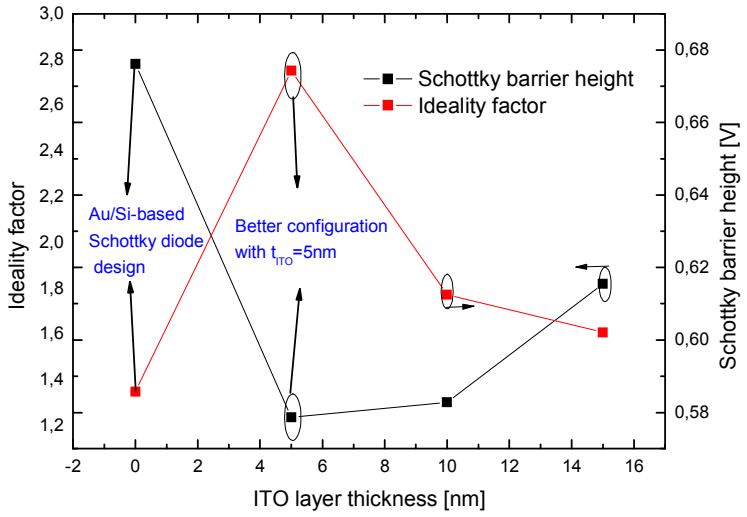

(a)

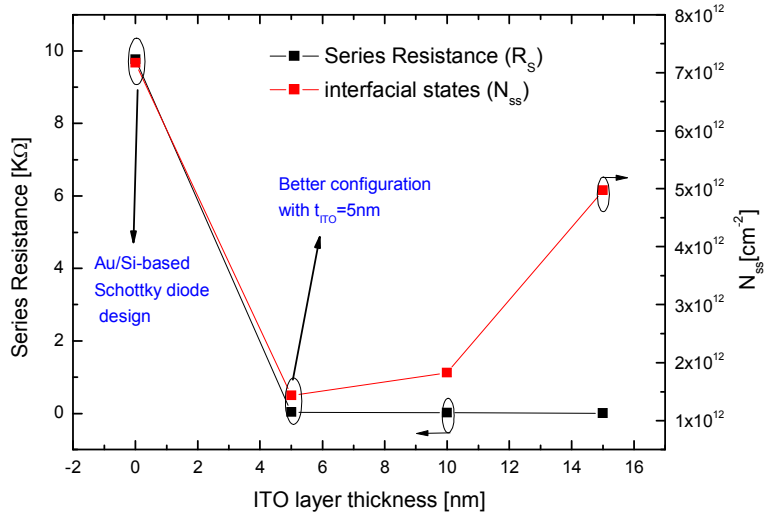

(b)

Figure VII.5: (a) Variation of the investigated structure Au/ITO/Si/Au ideality factor and Schottky barrier height as a function of the intermediate ITO layer thickness. **(b)** Series resistance and interfacial density of states versus the introduced ITO thin-film thickness.

Figure VII.5 (b) shows that the series resistance decreases with the ITO thickness increase, which is mainly due to the enhanced conductivity behavior of the Schottky contact as well as the minority carrier injection at the Si/ITO junction [203]. On the other hand, it can be noticed that the better electrical behavior of the proposed design can be achieved by taking the ITO thin layer thickness with 5nm. This can underline the

complex electrical behavior of the proposed design with Au/ITO/Si/Au structure, where the introduced ITO thin-film causes a highly non-linear behavior of the device electrical performance. This phenomenon can be explained by the quantum nature associated with the proposed Au/ITO/Si/Au structure, where identifying the ITO material thickness that provides the better diffusion of charge carrier across the MS interface by tunneling effect seems to be extremely complex. Accordingly, introducing a very thin ITO layer between the Si and the Au materials enables making a good trade-off between both the improved interface quality with superior conductance and enhanced current flow through the metal-semiconductor junction.

Aiming at evaluating the impact of the introduced ITO thin-film on the performance enhancement of the Au/Si interface quality, it seems important to quantify the density of states for both investigated designs with and without intermediate layer aspect. In this context, Figure VII.6 depicts the variation of the density of states against the energy difference between both interface state energy (E_{ss}) and the conduction band edge (E_c) for the investigated structures with t_{ITO}=5nm. It is clearly observed from this figure that the N_{SS} increases from the mid-gap to the bottom of the conduction band for both designs with and without ITO thin-film. It can be seen that N_{SS} are varied from 5×10^{13} to 1×10^{13} $cm^{-2}eV^{-1}$ for the Au/p-Si SBD, while, for the proposed Au/ITO/p-Si structure the interfacial states are found in the range of 6×10^{12} to $1\times10^{12}cm^{-2}eV^{-1}$. This observation underlines the effectiveness of the introduced ITO intermediate thin-layer for improving the Au/Si interface quality, where reduced defects can be reached by adopting the proposed structure. It can be also noticed from Figure VII.6 that the proposed design exhibits an exponential variation of the N_{ss} as a function of E_c-E_{ss} energy difference. Conversely, for the conventional design, the density of states increases linearly to reach its maximum at the E_c bottom. This dissimilarity indicates that the interface properties associated with the proposed Au/p-Si SBD are strongly modified and it is mainly depending on ITO intermediate thin-film inserted between the metal and the silicon layer. Accordingly, the introduced ITO interlayer acts as a passivation layer and induce significant reduction in the interfacial defects. Besides, this can decrease the leakage current and suitably improve the effective Schottky barrier height.

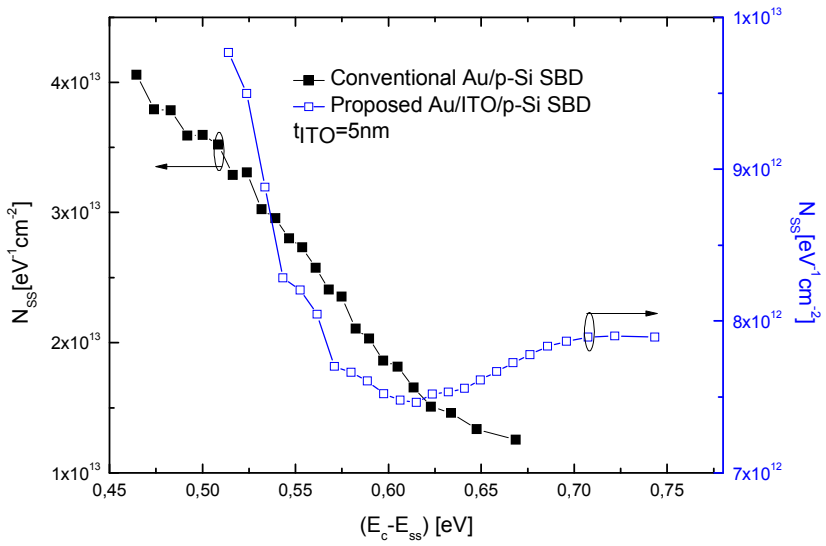

Figure VII.6: The energy distribution profiles of interface density of states for both conventional and proposed designs.

As far as the structure thermal stability is concerned, the heating effect is regarded as the main reason of the Au/Si SBD performance degradation for power electronics and even photovoltaic applications. In this context, the study of device thermal stability behavior remains crucial and complementary to their electrical performance. Following this direction, it is important to investigate the impact of the introduced ITO thin-films on the Au/Si SBD thermal stability. In this perspective, Figure VII.7 depicts the variation of the device electrical parameters as a function of the working temperature for both conventional and proposed Au/ITO/Si/Au structures with t_{ITO}=5nm. It is clearly observed from this figure that a great increase in the ideality factor and the interfacial state density can be induced by increasing the temperature. This phenomenon confirms that the heating effect can affect greatly the device electrical performance. In this regard, the thermal effect has a profound implication on the device reliability behavior, where it induces significant damage in the MS interface as well as a substantial rise in the carrier's temperature. On the other hand, the proposed Au/ITO/Si/Au structure offers an improved immunity against heating effects, where it provides an enhanced thermal stability as compared to the conventional counterpart. In this context, Figure VII.7 (a) demonstrates that the ideality factor associated with the proposed design exhibits a very slow increasing tendency as a function of the working temperature in comparison with the conventional Au/Si structure. This observation confirms the improved thermal

stability and reliability of the proposed design including the effect of temperature compared to that of the conventional one.

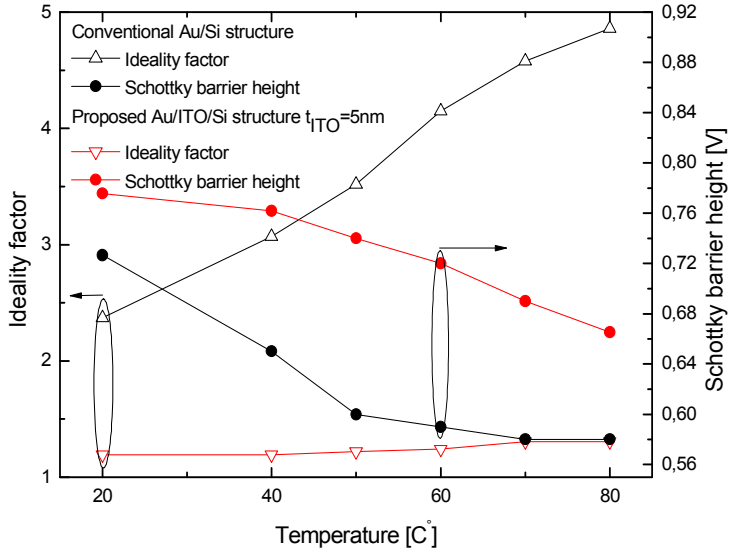

(a)

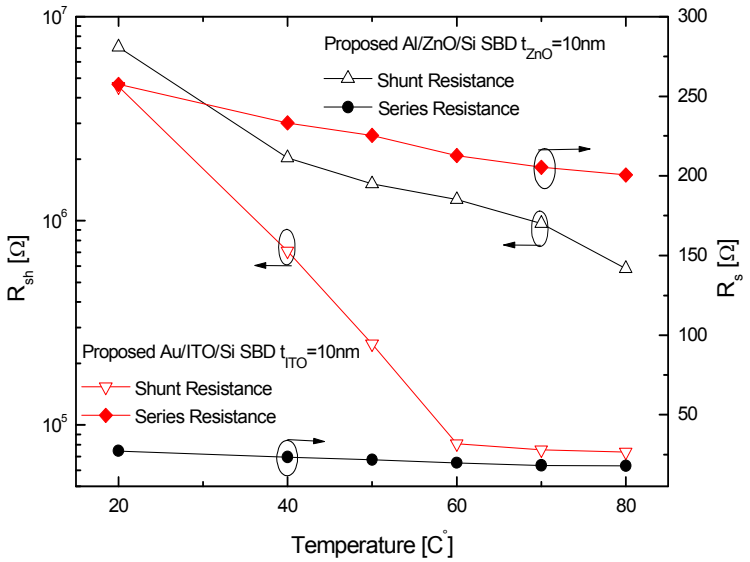

(b)

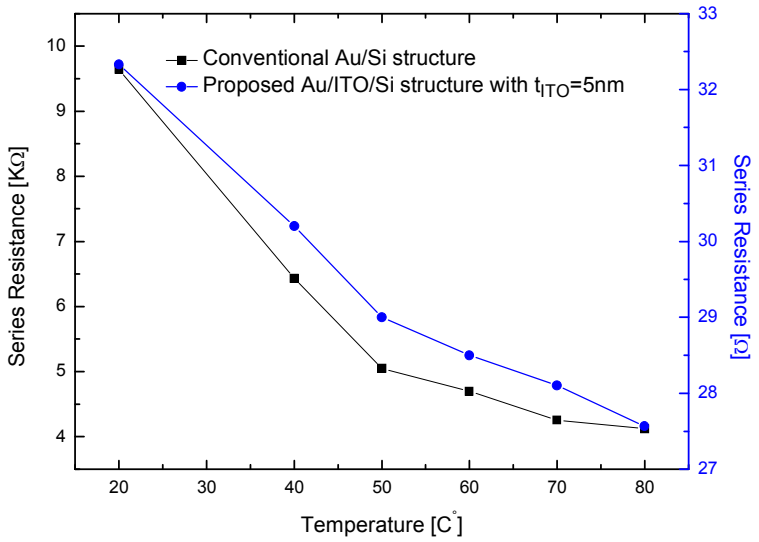

(c)

Figure VII.7: Temperature dependence of **(a)** ideality factor and Schottky barrier height, **(b)** interfacial density of states and saturation current, **(c)** Series resistance associated with the proposed Au/ITO/Si/Au structure and the conventional Au/Si SBD design with t_{ITO}=5nm.

Besides, it is obvious from Figure VII.7 (b) that the proposed structure enables also a better stability behavior regarding the saturation current with the thermal variation in comparison with that of the conventional structure. This phenomenon offers the possibility of reducing the leakage current under high-temperature working conditions. The improved thermal stability of the Au/ITO/Si/Au structure can be in fact attributed to the reduced damage at the MS interface suggested by incorporating the effect of the inserted ITO thin-film. Moreover, the superior thermal stability of the included ITO thin-layers contributes also in avoiding the degradation related heating effects. Figure VII.7 (c) depicts the variation of the series resistance against the temperature for both conventional and proposed structures. Observing this figure, the series resistance associated with the proposed design is much lower than that exhibited by the conventional Au/Si SBD counterpart. Moreover, we can notice that the series resistance decreases with the temperature increase for both designs. This behavior can be explained by the enhanced homogeneity of the MS interface caused by the effect of the temperature increase. Moreover, the series resistance decrease can be ascribed to the improved conductivity of Si substrate induced by the thermal variation effect. To this

extent, the obtained resistive behavior inspires further investigation by exploring the impact of the annealing effect on the proposed Au/ITO/Si/Au structure thermal stability behavior. In this context, Figure VII.8 compares the Temperature-dependent I-V characteristics associated with the investigated designs after annealing effect at 400°C with and without ITO intermediate layer.

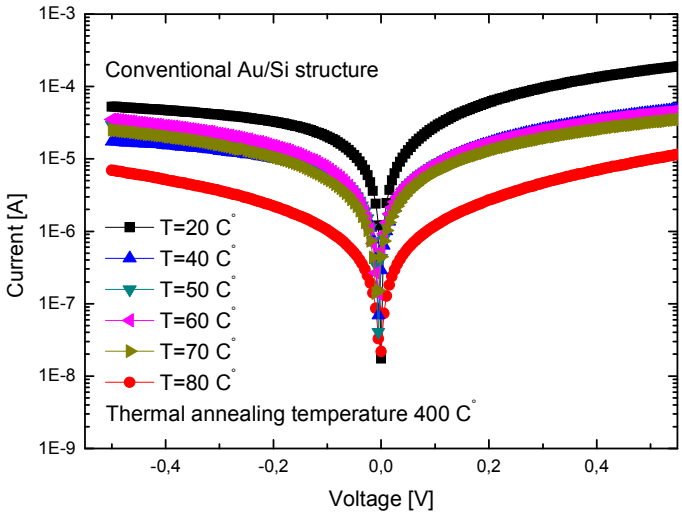

(a)

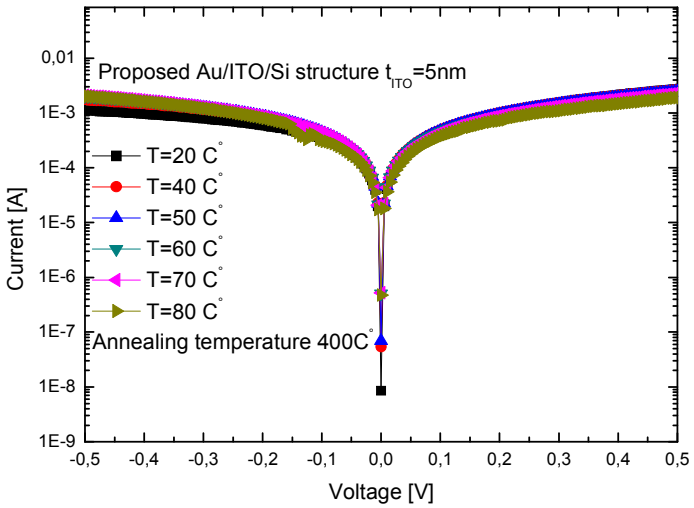

(b)

Figure VII.8: I-V characteristics associated with the conventional Au/Si SBD design and the proposed Au/ITO/Si/Au structure including thermal annealing at T=400°C in the temperature range of 20°C-80°C with t_{ITO}=5nm.

It is evidently demonstrated from Figure VII.8 (b) that the annealing effect induces an improved thermal stability as compared to the investigated designs before annealing effect, where it can be seen from this figure that there is no change in I-V curves with increasing the temperature for the proposed design with ITO thin layer and after annealing effect. This observation proves the improved thermal stability associated with the proposed design including the annealing at T=400°C. This improvement regarding the device reliability behavior can be ascribed to the enhanced homogeneity and the reduced defects at the MS interface provided by the annealing process and the ITO thin-film that acts as a perfect passivation layer. In addition, as it is above outlined, the proposed Au/ITO/Si/Au structure shows an asymmetrical behavior of the I-V curves. However, it can be observed from Figure VII.8 (b) that the I-V characteristics become quite symmetrical after annealing in both reverse and forward conditions. This indicates that the deposited ITO thickness becomes uniform after the annealing process at 400°C.

Ultimately, it is evidently confirmed that the introduced ITO thin-layer can considerably enhance the SBD electrical performance not only enables reducing the series resistance and the interfacial traps, but also leads to basically an advantageous thermally stable device suitable for developing high-performance sensing and microelectronic applications.

VII. 4. Conclusion

In this work, the introduction of ITO thin-films as an intermediate layer between both Si and Au materials is proposed as a new way to achieve the dual role of improved interface quality and enhanced electrical performance. The investigated Au/ITO/Si/Au structures with different ITO thicknesses were elaborated using RF magnetron sputtering technique. Moreover, I-V curves associated with the investigated designs are analyzed, where the device electrical parameters (ϕ_{bn}, n, N_{ss} and R_s) are extracted. It was revealed that the introduced ITO thin-films play an important role in achieving ideality factor close to the unit (n=1.25), much less defects, a very low series resistance and superior Schottky barrier height as compared to the conventional Au/Si structure. In addition, the impact of the proposed feature on the device thermal stability behavior is investigated, where the proposed Au/ITO/Si/Au structure offers the possibility for outstandingly avoiding the degradation related-heating effects. Besides, the influence of

the annealing process on the device thermal stability is analyzed. It was demonstrated that the elaborated structure with ITO intermediate layer shows the potential for achieving high-performance and thermally stable devices. Therefore, the proposed Au/ITO/Si/Au structure pinpoint a new path toward bridging the gap between high electrical performance devices and improved thermal stability behavior, which makes it a potential alternative for high-performance sensing and microelectronic applications.

Chapter VIII

Conclusion and Outlooks

Abstract: the concluding Chapter of this thesis presents comprehensive review regarding the performed work. It provides also the main contributions of the dissertation concerning advanced optoelectronic devices such as photodetectors, phototransistors, Si-based Schottky barrier diodes and even thin-film solar cells. Lastly, this chapter presents some future perspectives regarding the prospect for achieving further improvements of the analyzed optoelectronic devices.

VIII.1 Conclusion

The various threads of this thesis are all focused on the design, modeling, optimization and elaboration of novel optoelectronic devices. Moreover, this thesis has explored various aspects for enhancing photodetectors and phototransistor for optical communication and environmental monitoring applications. This is motivated primarily by the sense that reducing the power consumption of the optical receiver is highly valuable for developing high-performance optical links. In another sense, the deployment of optical communication systems requires high-performance and effectiveness from every aspect of the optical system's design, in this case, the photoreceivers are envisaged and high responsivity and ultra-sensitive phototransistor and photodetectors are of almost importance. This dissertation develops several novel CZTS-based solar cell designs through the appropriate engineering the absorber layer. Those devices exhibit significantly improved conversion efficiencies due to the enhanced carrier separation and the reduced optical losses. On the other hand, this thesis was also focused on the elaboration of a new Si-based SBD based on inserting an ITO thin-film at the MS interface. The prepared SBD structures have allowed exciting properties concerning the electrical and thermal stability performances.

VIII.2 High-Performance Photodetectors with Reduced Power Consumption

After the background introduction dedicated to several photodetector designs given in Chapter II which includes a brief review of the theory, the recent progress and the various applications of UV-photodetectors, we firstly present in Chapter III a motivation for achieving high-performance MSM TiO_2 photodetector based on front glass texturization. Semi-analytically models using accurate solutions of Maxwell's equations and coupled Poisson-continuity equations are developed. Our investigation has been focused on studying the device overall performance for optical interconnections' and environment monitoring applications. We discussed the key factors for the proposed design that allows high improvement in the device figures of merit parameters. The diffraction grating aspect opens up the route for modulating the electric field behavior in the TiO_2 active layer. Furthermore, the usefulness of global optimization using PSO approach to boost the device sensitivity as well as responsivity

has been successfully demonstrated, where the optimized design outperforms greatly the conventional flat design.

To further jointly assess the photodetector optical performance and the power consumption challenge, we have proposed a scheme to reduce the leakage power of MSM photodetectors by exploring the prospect of getting rid of the applied voltage. In Chapter IV, we developed a new self-powered UV-photodetector based on dual material aspect. Our study reveals that the adopted design amendment behaves electrically as an electric field modulator which leads to enhance the transport efficiency of the photo-generated carriers without the need of an external applied voltage. Moreover, a new hybrid approach that combines analytical modeling and PSO-based metaheuristic technique has been proposed with the aim to achieve favorable self-powered device. Promising results have been obtained with respect to the device FoMs. The obtained results indicate that the proposed design methodology pinpoint a new path toward reaching high-performance self-powered device with low power consumption.

VIII.3 Bridging the Gap between Nanoelectronic and Silicon Photonics Technologies

The goals of this study are to develop novel photoreceiver structures, push the performance limits and explore new architectures for achieving high-speed optical interconnects. This investigation took the prospect of reducing the size mismatch between electronic and photonic technologies and addressed the major design challenges from optical systems power consumption and sensitivity levels. Built upon the achievements of other researchers, new phototransistor architectures and models have been proposed. In Chapter V, we identified two powerful approaches for replacing conventional photoreceiver designs with CMOS compatible devices to enable continued technology scaling.

First, we have investigated a new optimized planar Junctionless phototransistor using both mathematical modeling and metaheuristic optimization. The proposed JL-phototransistor offers improved device FoMs as compared to the conventional design. Moreover, our device has the advantage of a simple and low fabrication cost process over the conventional structure and is fully compatible with the CMOS technology. It has also been concluded that the proposed design provides the weak signal detection

benefit. Moreover, we exploited GAs method not only to boost the device performance but also to reduce the power consumption, where favorable results have been achieved by the optimized phototransistor structure.

The second half of the chapter was devoted to proposing a new SiGe/Si/Ge-based OC-TFET design based on a hetero-channel (SiGe/Si/Ge) aspect. The proposed design provides a new way to achieve the dual-role of enhanced optical switching behavior and reduced power consumption. We have proposed a new FoM parameter called optical swing factor that describes the photoreceiver optical commutation speed. It has been demonstrated that the adopted band-to-band tunneling transport mechanism can be effective for improving the device optical commutation speed, where only 48mV/dec of optical swing factor is achieved by considering the proposed design. It was deduced also that the proposed design offers the ultra-low optical power detection property (sub-1pW), which implies that it requires less light power from the optical emitter to reach an acceptable photo-response.

VIII.4 Boosting the Efficiency of CZTS Solar Cells

The recent progress in kesterite thin-film solar cell technology has opened the door to a wide range of research topics to record high-efficiencies at low fabrication cost. At the same time, this photovoltaic technology presents new challenges for researchers such as the recombination losses and reflection effects. Solving these challenges requires the deep knowledge about the two critical issues that have limited performance in previous devices. The final step in our work which is presented in Chapter VI was to study the CZTS solar cell properties, where the ultimate objective was to record superior efficiency values. Two promising designs based on engineering the CZTS absorber layer have been proposed and investigated. The first one relies on altering the band gap profile of the CZTS material in order to improve the transport mechanism in the absorber layer. Analytical models for the proposed solar cell design were also developed. Our analysis demonstrates that the engineered CZTS absorber layer acts as an electric field modulator. This has allowed significant improvements regarding the carrier life time and thereby reducing the degradation related recombination effects. More importantly, a new hybrid approach based on analytical modeling supported by PSO technique has been conducted, where new opportunities for further efficiency enhancement are possible. It was revealed that this methodology could open up the

route for effectively engineering the CZTS absorber layer. Promising enhancements regarding the CZTS solar cell conversion efficiency have been achieved, where close to 17% efficiency was recorded. Therefore, the proposed design methodology offers a new insight toward reducing recombination effects and enhancing the absorbance efficiency.

Thereafter, in the second part of Chapter IV, we have introduced a novel CZTS solar cell based on intermediate metallic sub-layers engineering aspect. It was revealed that optical resonant micro-cavity effects are generated, which leads to enormously decrease the optical losses. It was confirmed that the optimized design enables achieving broadband absorption and near zero reflection over a wide spectrum range. Moreover, the inserted metallic sub-layers behave like a blocking layer for the Sulfur diffusion, which offers the opportunity for reducing the series resistance. These benefits jointly contribute in achieving superior conversion efficiency value of 14% with using the Ti material as intermediate thin-layers.

VIII.5 Improving Au/Si SBD Electrical and Thermal Reliability Performances

In the last chapter of this thesis, we have proposed a new SBD deign based on inserting ITO thin-films as an intermediate layer between both Si and Au materials to achieve the dual role of improved interface quality and enhanced electrical performance. The investigated Au/ITO/Si/Au structures with different ITO thicknesses were elaborated using RF magnetron sputtering technique. Moreover, an effective electrical characterization has been carried out in order to assess the impact of the introduced ITO thin-film on the derived current capability of the Si-based SBD. It is found that the by inserting an ultrathin ITO layer of 5nm thickness, we were able to achieve exciting opportunities for enhancing the SBD electrical performance, where the elaborated structure demonstrates close to the unit ideality factor of n=1.25, reduced defects, lower series resistance and higher Schottky barrier height as compared to the conventional Au/Si SBD counterpart. In addition, the role of the proposed SBD architecture in enhancing the device thermal stability properties is demonstrated, where the prepared Au/ITO/Si/Au structure provides the opportunity for suppressing the degradation related-thermal effects. Furthermore, the impact of the heat treatment on the SBD thermal stability characteristics is investigated, where the annealed sample paves the way for elaborating a highly stable device against the thermal effects.

VIII.6 Outlooks

The different concepts of the work presented in this dissertation have contributed considerably to basic understanding of various novel optoelectronic devices. We have also evaluated these new designs for the potential use in several applications. The results of these evaluations could be useful for researchers in order to explore new ways for achieving improved optoelectronic devices. There remain significant opportunities to continue the development of more advanced optoelectronic devices which would take into account other aspects such as the time response, the manufacturing cost and further reduce concerning the power budget. The significant improvement regarding the optoelectronic devices performance promotes their continued development for achieving high-performance nanoelectronic-photonic co-design technology. The following topics underline the possible future direction that might focus on the further development of high-performance optoelectronic devices.

First, extending the investigation of the proposed MSM UV photodetectors to include the response time paradigm, which constitutes one of the main parameters that characterizes the optical response speed. Moreover, the exploration of new possibilities to incorporate novel 2-D materials such as graphene, black phosphorous and silicene in order to achieve flexible self-powered MSM photodetectors with keeping the ultrahigh sensitivity characteristic is in fact of paramount importance. These 2-D materials can provide the prospect for bridging the gap between nanoelectronic and nanophotonic technologies. For this purpose, the silicon channel in Ge-based phototransistor designs can also be replaced by graphene material in order to improve derived current capability and hence the phototransistor FoM.

Second, improving the light trapping capability by appropriately designing nanotexture morphologies has confirmed its effectiveness for suppressing refection and can enhance several solar cell technologies. The performed investigation of the CZTS solar cell can be extended by proposing new designs based on introducing several texture morphologies in order to reduce the reflection effects. Moreover, introducing new nanomaterials to generate the plasmonic effects could be effective for enhancing the conversion efficiency. The CZTS/Buffer interface quality plays an important role in reducing the recombination effects. The exploration of new defect-free buffer layers technologically compatible with the CZTS absorber seems essential to develop defect free interfaces.

References

References

[1] S. Manipatruni, M. Lipson, and I. A. Young, "Device Scaling Considerations for Nanophotonic CMOS Global Interconnects," IEEE Journal of Selected Topics in Quantum Electronics, vol. 19, pp. 1077-1086 , 2013.

[2] N. Kannan and M. J. Kumar, "Technology and reliability constrained future copper interconnects," IEEE Trans. Electron Devices, vol. 49, pp. 590-597, 2002.

[3] D. A. B. Miller, "Optical interconnects to silicon," IEEE Journal of Selected Topics in Quantum Electronics, vol. 6, pp. 1312-1317, 2000.

[4] A. V. Krishnamoorthy, D. A. B. Miller, "Firehose architectures for free-space optically interconnected VLSI circuits," Journal of Parallel and Distributed Computing, vol. 41, pp. 109-114, 1997.

[5] C. Sun, M. T. Wade, Y. Lee, J. S. Orcutt, L. Alloatti, M. S. Georgas, A. S. Waterman, J. M. Shainline, R. R. Avizienis, S. Lin, B. R. Moss, R. Kumar, F. Pavanello, A. H. Atabaki, H. M. Cook, A. J. Ou, J. C. Leu, Y.-H. Chen, K. Asanovic, R. J. Ram, M. Popovic, and V. M. Stojanovic, "Single-chip microprocessor that communicates directly using light," Nature, vol. 528, pp. 534-538, 2015.

[6] C. Kachris and I. Tomkos. "A survey on optical interconnects for data centers," In: IEEE Communications Surveys & Tutorials, vol. 14, pp. 1021–1036, 2012.

[7] D. A. B. Miller, "Physical reasons for optical interconnection," International Journal of Optoelectronics, vol. 11, pp. 155-68, 1997.

[8] S. Ghanbarzadeh, S. Abbaszadeh, and K. S. Karim, "Low Dark Current Amorphous Silicon Metal-Semiconductor-Metal Photodetector for Digital Imaging Applications," IEEE Electron Device Letters, vol. 35, pp. 235-37, 2014.

[9] Z. Zheng, L. Gan, H. Li, Y. Ma, Y. Bando, D. Golberg, and T. Zhai, "A Fully Transparent and Flexible Ultraviolet-Visible Photodetector Based on Controlled Electrospun ZnO-CdO Heterojunction Nanofiber Arrays," Advanced Functional Materials, vol. 25, pp. 5885-5894, 2015.

[10] G. Maculan, A. D. Sheikh, A. L. Abdelhady, M. I. Saidaminov, M. A. Haque, B. Murali, E. Alarousu, O. F. Mohammed, T. Wu, and O. M. Bakr, "Ch3nh3pbcl3 Single Crystals: Inverse Temperature Crystallization and Visible-Blind UV-Photodetector," J. Phys. Chem. Lett., vol. 6, pp. 3781-3796, 2015.

[11] H. Chen, K. Liu, L. Hu, A. A. Al-Ghamdi and X. Fang, "New concept ultraviolet photodetectors," Materials Today, vol.18, pp.493-503, 2015.

[12] H. Shen, C. X. Shan, B. H. Li, B. Xuan, and D. Z. Shen, "Reliable self-powered highly spectrum-selective ZnO ultraviolet photodetectors," Applied Physics Letters, vol. 103, pp. 232112, 2013.

[13] J. Xu, Y. J. Song, J. H. Park, S. Lee, "Graphene/black phosphorus heterostructured photodetector," Solid-State Electronics, vol. 144, pp. 86-89, 2018.

[14] C. Persson, "Electronic and optical properties of Cu2ZnSnS4 and Cu2ZnSnSe4," Journal of Applied Physics, vol.107, pp.053710, 2010.

[15] S. Ahn, S. Jung, J. Gwak, A. Cho, K. Shin, K. Yoon, D. Park, H. Cheong and J. Hyun, "Determination of band gap energy (Eg) of Cu2ZnSnSe4 thin films: On the discrepancies of reported band gap values," Applied Physics Letters, vol. 97, pp. 021905, 2010.

[16] K. Ito and T. Nakazawa, "Electrical and optical properties of stannite-type quaternary semiconductor thin films," Japanese Journal of Applied Physics, vol.27, pp.2094, 1988.

[17] H, Katagiri, K. Jimbo, S. Yamada, T. Kamimura, W. S. Maw, T. Fukano, T. Ito and T. Motohiro, "Enhanced conversion efficiencies of Cu2ZnSnS4-based thin film solar cells by using preferential etching technique," Applied Physics Express, vol.1, pp.041201, 2008.

[18] B. Shin, O. Gunawan, Y. Zhu, N. A. Bojarczuk, S. J. Chey and S. Guha, "Thin film solar cell with 8.4% power conversion efficiency using an earth-abundant Cu2ZnSnS4 absorber," Prog. Photovolt: Res. Appl., vol. 21, pp. 72-76, 2011.

[19] W. Ki, H. W. Hillhouse, "Earth-Abundant Element Photovoltaics Directly from Soluble Precursors with High Yield Using a Non-Toxic Solvent," Adv. Energy Mater., vol. 1, pp. 732-735, 2011.

[20] H. Hiroi, N. Sakai, T. Kato, H. Sugimoto, "High Voltage Cu2ZnSnS4 Submodules by Hybrid Buffer Layer," In: Conference Record of the IEEE Photovoltaic Specialists Conference, 2013, Tampa, Florida, USA.

[21] G. E. Moore, "Cramming more components onto integrated circuits, Reprinted from Electronics, volume 38, number 8, April 19, 1965, pp.114 ff," IEEE Solid-State Circuits Newsletter, vol.11, pp. 33-35, 2006.

[22] International Technology Roadmap for Semiconductors (ITRS), published online at: http://itrs.net, 2013.

[23] D. A. B. Miller, "Rationale and challenges for optical interconnects to electronic chips," Proceedings of the IEEE, vol. 88, pp. 728-49, 2000.

[24] H. D. Thacker, X. Zheng, J. Lexau, R. Shafiiha, I. Shubin, S. Lin, S. Djordjevic, P. Amberg, E. Chang, F. Liu, J. Simons, J.-H. Lee, A. Abed, H. Liang, Y. Luo, J. Yao, D. Feng, M. Asghari, R. Ho, K. Raj, J. E. Cunningham, and A. V. Krishnamoorthy, "An all-solid-state, WDM silicon photonic digital link for chip-to-chip communications," Optics Express, vol. 23, pp. 12808, 2015.

[25] M. Huang, S. Li, P. Cai, G. Hou, Tzung-I. Su, W. Chen, C. Hong, and D. Pan "Germanium on Silicon Avalanche Photodiode" IEEE Journal of Selected Topics in Quantum Electronics, vol.24, pp. 3800911-1-3800911-11, 2018.

[26] D. Feng, S. Liao, P. Dong, N. Feng, H. Liang, D. Zheng, C. C. Kung, J. Fong, R. Shafiiha, J. Cunningham, A. V. Krishnamoorthy and M. Asghari, "High-Speed Ge Photodetector Monolithically Integrated with Large Cross-Section Silicon-on-Insulator Waveguide", Applied Physics Letters, vol. 95, pp. 261105, 2009.

[27] H. Xu, X. Xiao, X. Li, Y. Hu, Z. Li, T. Chu, Y. Yu, and J. Yu, "High speed silicon Mach-Zehnder modulator based on interleaved PN junctions," Optics express, vol. 20, pp. 93-99, 2012.

[28] M. Georgas, J. Leu, B. Moss, C. Sun, and V. Stojanovi, "Addressing link level design tradeoffs for integrated photonic interconnects," Custom Integrated Circuits Conference (CICC), 2011, San Jose, CA, USA.

[29] Y. Zhang, T. Liu, B. Meng, X. Li, G. Liang, X. Hu, Q.J. Wang, "Broadband high photoresponse from pure monolayer graphene photodetector," Nature communications, vol.4, pp.1811, 2013.

[30] F. Koppens, T. Mueller, P. Avouris, A. Ferrari, M. Vitiello, M. Polini, "Photodetectors based on graphene, other two-dimensional materials and hybrid systems," Nature nanotechnology, vol.9, pp.780-793, 2014.

[31] H. Xu, J. Wu, Q. Feng, N. Mao, C. Wang, J. Zhang, "High responsivity and gate tunable graphene MoS_2 hybrid phototransistor," Small, vol.10, pp.2300-2306, 2014.

[32] T. AlZoubi, H. Qutaish, E. Al-Shawwa and S. Hamzawy, "Enhanced UV-light detection based on ZnO nanowires/graphene oxide hybrid using cost-effective low temperature hydrothermal process," Optical Materials, vol.77, pp.226-232, 2018.

[33] F. Xia, H. Wang, Y. Jia, "Rediscovering black phosphorus as an anisotropic layered material for optoelectronics and electronics," Nature communications, vol.5 pp.4458, 2014.

[34] Z. Bai, X. Yan, X. Chen, H. Liu, Y. Shen, Y. Zhang, "ZnO nanowire array ultraviolet photodetectors with self-powered properties," Current Applied Physics, vol. 44, pp. 339-344, 2011.

[35] H. Y. Chen, K. W. Liu, X. Chen, Z. Z. Zhang, M. M. Fan, M. M. Jiang, X. H. Xie, H. F. Zhaoa and D. Z Shen, "Realization of a self-powered ZnO MSM UV photodetector with high responsivity using an asymmetric pair of Au electrodes," Journal of Materials Chemistry C, vol. 2, pp. 9689-9694, 2014.

[36] L. Duan, F. He, Y. Tian, B. Sun, J. Fan, X. Yu, L. Ni, Y. Zhang, Y. Chen and W. Zhang, "Fabrication of Self-Powered Fast-Response Ultraviolet Photodetectors Based on Graphene/ZnO:Al Nanorod-Array-Film Structure with Stable Schottky Barrier," Applied materials and interfaces, vol. 9, pp. 8161-8168, 2017.

[37] Z. Bai, X. Chen, X. Yan, X. Zheng, Z. Kanga and Y. Zhang, "Self-powered ultraviolet photodetectors based on selectively grown ZnO nanowire arrays with thermal tuning performance," Journal of Materials Chemistry C, vol.16, pp. 9525-9530, 2014.

[38] Q. Yang, Y. Liu, Z. Li, Z. Yang, X. Wang, Z. L. Wang, "Self-Powered Ultrasensitive Nanowire Photodetector Driven by a Hybridized Microbial Fuel Cell", Angewandte Chemie, vol. 51, pp. 6443-6446, 2012.

[39] X. Lia, C. Gao, H. Duan, B. Lu, X. Pan, E. Xie, "Nanocrystalline TiO_2 film based photoelectrochemical cell as self-powered UV-photodetector," Nano Energy, vol.1, pp.640-645, 2012.

[40] P. N. Ni, C. X. Shan, S. P. Wang, X. Y. Liua and D. Z. Shen, "Self-powered spectrum-selective photodetectors fabricated from n-ZnO/p-NiO core–shell nanowire arrays," J. Mater. Chem. C, vol.1, pp. 4445-4449, 2013.

[41] V. J. Sorger, R. F. Oulton, R. M. Ma and X. Zhang, "Toward integrated plasmonic circuits," MRS Bulletin, vol. 37, pp. 728-738, 2012.

[42] X. Fan, W. Zheng and D. J. Singh, "Light scattering and surface plasmons on small spherical particles," Light: Science & Applications, vol.3, pp. 179, 2014.

[43] C. F. Guo, T. Sun, F. Cao, Q. Liu and Z. Ren, "Metallic nanostructures for light trapping in energy-harvesting devices," Light: Science & Applications, vol.3, pp. 161, 2014.

[44] K. Liu, M. Sakurai, M. Liao, and M. Aono, "Giant Improvement of the Performance of ZnO Nanowire Photodetectors by Au Nanoparticles," J. Phys. Chem. C, vol.114, pp. 19835-19839, 2010.

[45] D. Li, X. Sun, H. Song, Z. Li, Y. Chen, H. Jiang, G. Miao, "Realization of a High-Performance GaN UV Detector by Nanoplasmonic Enhancement," Advenced Materials, vol.24, pp. 845-849, 2012.

[46] C. Sun, M. Wade, M. Georgas, S. Lin, L. Alloatti, B. Moss, R. Kumar, A. H. Atabaki, F. Pavanello, J. M. Shainline, J. S. Orcutt, R. J. Ram, M. Popovi, and V. Stojanovi, "A 45 nm CMOS-SOI monolithic photonics platform with bit-statistics-based resonant microring thermal tuning," IEEE Journal of Solid-State Circuits, vol. 51, pp. 893-907, 2016.

[47] C. L. Keraly et al. "Ultra-sensitive detector for Silicon Photonics; a photodiode incorporating integrated bipolar gain," In: 2015 IEEE Photonics Conference (IPC), 2015, Reston, VA, USA.

[48] C. L. Keraly et al. "Low capacitance, high speed phototransistors with a large absorption region," In: Energy Efficient Electronic Systems (E3S), 2015 Fourth Berkeley Symposium on. IEEE. 2015, Berkeley, CA, USA.

[49] J. W. et al. "Silicon waveguide integrated germanium JFET photodetector with improved speed performance," IEEE Photonics Technology Letters, vol.23, pp. 765-767, 2011.

[50] S. S. et al. "Junction field-effect-transistor-based germanium photodetector on silicon-on-insulator," Optics letters, vol.33, pp.1138-1140, 2008.

[51] A. K. Okyay et al. "Silicon germanium CMOS optoelectronic switching device: Bringing light to latch," IEEE Transactions on electron devices, vol.54, pp. 3252-3259, 2007.

[52] R. W. Going et al. "Germanium gate PhotoMOSFET integrated to silicon photonics," IEEE Journal of Selected Topics in Quantum Electronics, vol. 20, pp.1-7, 2014.

[53] K. W. Ang et al. "Low-voltage and high-responsivity germanium bipolar phototransistor for optical detections in the near-infrared regime," IEEE Electron Device Letters, vol.29, pp. 1124-1127, 2008.

[54] P. Kostov et al. "PNP PIN bipolar phototransistors for high-speed applications built in a 180nm CMOS process," Solid-state electronics, vol. 74, pp. 49-57, 2012.

[55] William Shockley, M. Sparks, and G. K. Teal, "p-n Junction Transistors," Physical Review, vol.83, pp. 151, 1951.

[56] J. N. Shive, "The properties of germanium phototransistors," Journal of the Optical Society of America, vol.43, pp. 239-244, 1953.

[57] H. Kroemer, "Theory of a wide-gap emitter for transistors," Proceedings of the IRE, vol.45, pp. 1535-1537, 1957.

[58] US Energy Information Administration. International energy outlook 2013. Technical report, US Energy Information Administration, 2013.

[59] M. A. Green, K. Emery, Y. Hishikawa, W. Warta, and E. D. Dunlop, "Solar cell efficiency tables (version 48)," Prog. Photovoltaics Res. Appl., vol. 24, pp. 905-913, 2016.

[60] J. G. J. Olivier, G. J. Maenhout, M. Muntean, and J. A. H. W Peters, "Trends In Global CO_2 Emissions," 2013.

[61] K. Yoshikawa, H. Kawasaki,W. Yoshida, T. Irie, K. Konishi, K. Nakano, T. Uto, D. Adachi, M. Kanematsu, H. Uzu and K. Yamamoto, "Silicon heterojunction solar cell with interdigitated back contacts for a photoconversion efficiencyover 26%," Nature energy, vol.2, pp. 1-8, 2017.

[62] A. D. Compaan, "Laser processing for thin-film photovoltaics," in Proc. SPIE, Laser-Induced Thin Film Process. (J. J. Dubowski, ed.), vol. 2403, p. 224, 1995.

[63] P. Jackson, D. Hariskos, E. Lotter, S. Paetel, R. Wuerz, R. Menner, W. Wischmann, M. Powalla, "New world record efficiency for Cu(In,Ga)Se2 thin-film solar cells beyond 20%," Comput. Prog. In Photovoltaics, vol. 19, pp 894-897, 2011.

[64] T. D. Leea and A. U. Ebong, "A review of thin film solar cell technologies and challenges," Renewable and Sustainable Energy Reviews, vol.70, pp. 1286-1297, 2017.

[65] X. Yang, Z. Bao, R. Luo, B. Liu, P. Tang, B. Li, J. Zhang, W. Li, L. Wu, and L. Feng, "Preparation and characterization of pulsed laser deposited CdS/CdSe bi-layer films for CdTe solar cell application," Mater. Sci. Semicond. Process., vol. 48, pp. 27-32, 2016.

[66] U. Saha and M. K. Alam, "Proposition and computational analysis of a kesterite/kesterite tandem solar cell with enhanced efficiency," RSC Adv., vol.7, pp. 4806, 2017.

[67] A. Luque and A. Marti, "Increasing the efficiency of ideal solar cells by photon induced transitions at intermediate levels," Phys. Rev. Lett., vol. 78, pp. 5014-5017, 1997.

[68] S. Kolodinski, J. H. Werner, T. Wittchen, and H. J. Queisser, "Quantum efficiencies exceeding unity due to impact ionization in silicon solar cells," Appl. Phys. Lett., vol. 63, pp. 2405-2407, 1993.

[69] T. Kato, H. Hiroi, N. Sakai, S. Muraoka, H. Sugimoto, "Characterization of Front and Back Interfaces on Cu2ZnSnS4 Thin-Film Solar Cells," In proceeding of 27th European Photovoltaic Solar Energy Conference and Exhibition, 2013, pp. 2236-2239.

[70] W. Wang, M. T. Winkler, O. Gunawan, T. Gokmen, T. K. Todorov, Y. Zhu, D. B. Mitzi, "Characteristics of CZTSSe Thin-Film Solar Cells with 12.6% Efficiency," Adv. Energy Mater., vol. 4, pp.1301465, 2014.

[71] P. Hansen, "P–N Junction Passivation in Kesterite Solar Cells by Use of Solution-Processed TiO_2 Layer," IEEE Journal of Photovoltaics, vol.99, pp.1-6, 2017.

[72] J. Kim, H. Hiroi, T. K. Todorov, O. Gunawan, M. Kuwahara, T. Gokmen, D. Nair, M. Hopstaken, B. Shin, Y. S. Lee, W. Wang, H. Sugimoto, D. B. Mitzi, "High Efficiency Cu2ZnSn(S,Se)4 Solar Cells by Applying a Double In_2S_3/CdS Emitter," Advanced Materials, vol. 26, pp. 7427-7431, 2014.

[73] M. Werner, D. Keller, S. G. Haass, C. Gretener, B. Bissig, P. Fuchs, F. L. Mattina, R. Erni, Y. E. Romanyuk, A. N. Tiwari, "Enhanced Carrier Collection from CdS Passivated Grains in Solution-Processed Cu2ZnSn(S,Se)4 Solar Cells," ACS Appl. Mater. Interfaces, vol. 22, pp. 12141, 2015.

[74] Y. S. Lee, T. Gershon, O. Gunawan, T. K. Todorov, T. Gokmen, Y. Virgus and S. Guha, "Cu2ZnSnSe4 Thin-Film Solar Cells by Thermal Co-evaporation with 11.6% Efficiency and Improved Minority Carrier Diffusion Length," Adv. Eng. Materials, vol.5, pp. 1401372, 2015.

[75] A. D. Collord, H. Xin, and H. W. Hillhouse, "Combinatorial Exploration of the Effects of Intrinsicand Extrinsic Defects in Cu2ZnSn(S,Se)," IEEE Journal of Photovoltaics, vol. 5, pp. 288-299, 2015.

[76] E. Aarts and J. K. Lenstra, editors. Local Search in Combinatorial Optimization. John Wiley & Sons, Inc., 1997.

[77] S. Al-Muhaideb, M. El B. Menai, "A new hybrid metaheuristic for medical data classification," Int. J. of Metaheuristics, vol.3, pp. 59-80, 2014.

[78] E. Alba. Parallel Metaheuristics: A New Class of Algorithms. Wiley-Inter science, 2005.

[79] E. Alba and M. Tomassini, "Parallelism and evolutionary algorithms," IEEE Transactions on Evolutionary Computation, vol.6, pp.443-462, 2002.

[80] I. Boussaïd, J. Lepagnot, P. Siarry, "A survey on optimization metaheuristics", Inf. Sci., vol. 237, pp. 82-117, 2013.

[81] J. Dréo, A. Pétrowski, P. Siarry, E. Taillard, "Metaheuristics for Hard Optimization," Berlin, Germany: Springer, 2006.

[82] J. Alves, P. Lucas, M. Thiago, F. Noronha and E. Figueiredo, "Heuristic and exact algorithms for product configuration in software product lines," International Transactions in Operational Research, vol.24, pp. 1285-1306, 2017.

[83] E. A. Silver, "An Overview of Heuristic Solution Methods," Journal of the operational research society, vol. 55, pp. 936-956, 2004.

[84] P. Festa, "A brief introduction to exact, approximation, and heuristic algorithms for solving hard combinatorial optimization problems," in: the 16th International Conference on Transparent Optical Networks (ICTON), pp. 936-956, pp.6-10, July 2014, Graz, Austria.

[85] C. Blum and A. Roli, "Metaheuristics in combinatorial optimization: Overview and conceptual comparison," ACM Computing Surveys, vol.35, pp.268-308, 2003.

[86] S. Fidanova and O. Roeva, "Metaheuristic techniques for optimization of an E. coli cultivation model," Biotechnology and Biotechnological Equipment, vol.27, pp.3870-3876, 2013.

[87] F. Glover, "Future paths for integer programming and links to artificial intelligence," Comput. Oper. Res., vol. 13, pp 533-549, 1986.

[88] J. H. Holland, "Adaptation in natural and artificial systems: an introductory analysis with applications to biology, control, and artificial intelligence," University of Michigan Press, 1975.

[89] M. Clerc and J. Kennedy, "The particle swarm - explosion, stability, and convergence in a multidimensional complex space," J. IEEE Trans. Evolut. Comput., vol. 73, pp. 58-73, 2002.

[90] S. Kirkpatrick, C. D. Gelatt and M. P. Vecchi, "Optimization by Simulated Annealing," Science, vol. 220, pp. 671-680, 1983.

[91] P. Hansen, "The Steepest Ascent Mildest Descent Heuristic for Combinatorial Programming," In Proceedings of the Congress on Numerical Methods in Combinatorial Optimization, Capri, Italy, 1986.

[92] J. D. Farmer, N. H. Packard and A. S. Perelson, "The immune system, adaptation, and machine learning," Phys. D, vol. 2, pp. 187-204, 1986.

[93] F. Glover, "Heuristics for integer programming using surrogate constraints," Decision Sciences, vol. 8, pp. 156-166, 1977.

[94] T. Weise, "Global Optimization Algorithms-Theory and Application" Second edition e-book, 2007.

[95] A. Kaveh and A. Zolghadr, "Comparison of nine meta-heuristic algorithms for optimal design of truss structures with frequency constraints," Adv. Eng. Software, vol.67, pp.9-30, 2014.

[96] C. Blum and A. Roli, "Metaheuristics in combinatorial optimization: Overview and conceptual comparison," ACM Computing Surveys, vol. 35, pp. 268-308, 2003.

[97] I. Boussaıd, J. Lepagnot and P. Siarry, "A survey on optimization metaheuristics," Information Sciences, vol.232, pp. 82-117, 2013.

[98] D. E. Goldberg, "Genetic algorithms in search, optimization, and machine learning," Addison-wesley Longman Publishing Co., Boston, MA, USA, 1989.

[99] M. Angelova, O. Roeva and T. Pencheva, "InterCriteria analysis of crossover and mutation rates relations in simple genetic algorithm," Annals of Computer Science and Information Systems, vol.5, pp.419-424, 2015.

[100] D.E. Goldberg, "Genetic Algorithms in Search, Optimization and Machine Learning," Addison Wesley Longman, London, 2006.

[101] I. Ono, H. Kita and S. Kobayashi, "A realcoded genetic algorithm using the unimodal normal distribution crossover," In Advances in evolutionary computing, pp. 213-237. Springer, 2003.

[102] M. T. McMahon and L. T. Watson, "A distributed genetic algorithm with migration for the design of composite laminate structures," Parallel algorithms and application, vol. 14, pp. 329-362, 2000.

[103] M. Mitchell, "An introduction to genetic algorithms," MIT press, 1998.

[104] T. Bendib and F. Djeffal, "Electrical Performance Optimization of Nanoscale Double-Gate MOSFETs Using Multi-objective Genetic Algorithms," IEEE Trans. on Electron Devices, vol. 58, pp. 3743-3750, 2011.

[105] F. Djeffal, N. Lakhdar, "An improved analog electrical performance of submicron Dual-Material gate (DM) GaAs-MESFETs using multi-objective computation", J. Comput. Electron. vol. 12, pp. 29-35, 2013.

[106] J. Horn, "Multicriterion decision making," In Handbook of evolutionary computation, IOP Publishing, Bristol, UK, 1997.

[107] A. L. Medaglia and S. C. Fang, "A genetic-based framework for solving (multi-criteria) weighted matching problems," European Journal of Operational Research, vol. 149, pp. 77-101, 2003.

[108] C. A. C. Coello, G.L. Lamont and D.A. van Veldhuizen, "Evolutionary Algorithms for Solving Multi-Objective Problems," In Genetic and Evolutionary Computation, Springer, Berlin, Heidelberg, 2007.

[109] F. Djeffal, N. Lakhdar, A. Yousfi, "An optimized design of 10-nm-scale dual-material surrounded gate MOSFETs for digital circuit applications," Physica E: Low-dimensional Systems and Nanostructures, vol. 44, pp. 339-344, 2011.

[110] F. Djeffal, T. Bendib, R. Benzid and A. Benhaya, "An approach based on particle swarm computation to study the nanoscale DG MOSFET-based circuits," Turk. J. Elec. Eng & Comp Sci., vol. 18, pp. 1131-1140, 2010.

[111] F. Djeffal, N. Lakhdar, M. Meguellati, A. Benhaya, "Particle swarm optimization versus genetic algorithms to study the electron mobility in wurtzite GaN-based devices," Solid-State Electronics, vol. 53, pp. 988-992, 2009.

[112] J. Sun, B. Feng and W. Xu, "Particle swarm optimization with particles having quantum behavior," In Proceedings of IEEE Congress on Evolutionary Computation, pp. 325-331, 2004.

[113] A. M. Selmana and Z. Hassana, "Fabrication and characterization of metal–semiconductor–metal ultraviolet photodetector based on rutile TiO_2 nanorod," Materials Research Bulletin, vol. 73, pp. 29-37, 2016.

[114] S. K. Singha, P. Hazrab, S. Tripathia, P. Chakrabartia, "Performance analysis of RF-sputtered ZnO/Si heterojunction UV photodetectors with high photo-responsivity," Superlattices and Microstructures, vol.91, pp. 62-69, 2016.

[115] H. Ferhati and F. Djeffal, "Role of gradual gate doping engineering in improving phototransistor performance for ultra-low power applications," Journal of Computational electronics, vol. 15, pp. 550-556, 2016.

[116] R. Wang, Y. Zhang, H. Wang, X. Song, L. Jin, and J. Yao, "Wide Spectral Response Field Effect Phototransistor Based on Graphene-Quantum Dot Hybrid", IEEE Photonics Journal, vol. 7, pp. 4500706-1- 4500706-6, 2015.

[117] L. Colace, V. Sorianello and S. Rajamani, "Investigation of Static and Dynamic Characteristics of Optically Controlled Field Effect Transistors," Journal of lightwave technology, vol. 32, pp. 2233-2239, 2014.

[118] S. Singh, S-H. Park, "Fabrication and characterization of Al:ZnO based MSM ultraviolet photodetectors", Superlattices and Microstructures, vol. 86, pp. 412-417, 2015.

[119] B. D. Boruah, A. Mukherjee, A. Misra, "Sandwiched Assembly of ZnO Nanowires between Graphene Layers for a Self-Powered and Fast Responsive Ultraviolet Photodetector," Nanotechnology, vol.27, pp.95205-95216, 2016.

[120] J. Xing, H. Wei1, E. J. Guo and F. Yang, "Highly sensitive fast-response UV photodetectors based on epitaxial TiO_2 films," J. Phys. D: Appl. Phys., vol.44, pp. 375104, 2011.

[121] H. Xue, X. Kong, Z. Liu, C. Liu, J. Zhou, W. Chen, S. Ruan, and Q. Xu, "TiO_2 based metal-semiconductor-metal ultraviolet photodetectors," Applied physics latters, vol. 90, pp. 201118, 2007.

[122] A. Lin, S. M. Fu, Y. K. Chung, S. Y. Lai, and C. W. Tseng, "An optimized surface plasmon photovoltaic structure using energy transfer between discrete nano-particles," Opt. Exp., vol. 21, pp. 132-145, 2013.

[123] Atlas User's manual, SILVACO TCAD, 2012.

[124] S. K. Singh, P. Hazra, S. Tripathi, and P. Chakrabarti, "Performance analysis of RF-sputtered ZnO/Si heterojunction UV photodetectors with high photo-responsivity," Superlattices Microstruct., vol. 91, pp. 62-69, 2016.

[125] S. M. Sze, Physics of Semiconductor Devices, 2nd ed. New York, NY, USA: Wiley, 1981.

[126] J. Schrier, D. O. Demchenko, and Li. Wang, "Optical Properties of ZnO/ZnS and ZnO/ZnTe Heterostructures for Photovoltaic Applications," Nano Lett., vol. 8, pp 2377-2382, 2007.

[127] H. Y. Chao, J. H. Cheng, J. Y. Lu, Y. H. Chang, C. L. Cheng, Y. F. Chen, "Growth and characterization of type-II ZnO/ZnTe core-shell nanowire arrays for solar cell applications," Physica E: Low-dimensional Systems and Nanostructures, vol. 47, pp. 160-164, 2010.

[128] P. I. Kuznetzov, S. V. Averin, V. A. Zhitov, L. Yu. Zakharov, V. M. Kotov, "MSM optical detector on the basis of II-type ZnSe/ZnTe superlattice," Semiconductors, vol. 51, pp. 249-253, 2017.

[129] H. Ferhati and F. Djeffal, "New high performance ultraviolet (MSM) TiO_2/glass photodetector based on diffraction grating for optoelectronic applications," Optik, vol. 127, pp.7202-7209, 2016.

[130] D. Prakash, A. M. Aboraia, M. El-Hagary, E. R. Shaaban, K. D. Verma, "Determination of the optical Constants and film thickness of ZnTe and ZnS thin films in terms of spectrophotometric and spectroscopic ellipsometry," Ceramics International, vol. 42, pp. 2676-2685, 2016.

[131] http://www.sspectra.com/sopra.html.

[132] F. Djeffal and H. Ferhati, "A new high-performance phototransistor design based on both surface texturization and graded gate doping engineering," Journal of Computational electronics, vol. 15, pp. 301-310, 2016.

[133] V. Sorianello, L. Colace, S. Rajamani, and G. Assanto "Design and simulation of optically controlled field effect transistors," Phys. Status Solidi C, vol.11, pp. 81-84, 2014.

[134] Y. Kang, H. D. Liu, M. Morse, M. J. Paniccia, M. Zadka, S. Litski, G. Sarid, A. Pauchard, Y. H. Kuo, H. W. Chen, W. S. Zaoui, J. E. Bowers, A. Beling, D. C. McIntosh, X. Zheng, and J. C. Campbell, "Monolithic germanium/silicon avalanche photodiodes with 340 GHz gain-bandwidth product," Nature Photonics, vol. 3, pp. 59–63, 2009.

[135] J. Michel, J. Liu, and L. C. Kimerling, "High-performance Ge-on-Si photodetectors," Nature Photon., vol. 4, pp. 527-534, 2010.

[136] J.P. Colinge, "Multi-gate SOI MOSFETs, Solid-State Electron," vol.48, pp. 897-905, 2004.

[137] J.P. Colinge, C.-W. Lee, A. Afzalian, N.D. Akhavan, et al, "Nanowire transistors without junctions," Nat. Nanotechnol, vol. 5, pp. 225-229, 2010.

[138] F. Djeffal, H. Ferhati and T. Bentrcia, "Improved analog and RF performances of gate-all-around junctionless MOSFET with drain and source extensions," Superlattices and Microstructures, vol.90, pp. 132-140, 2016.

[139] F. Lime, O. Moldovan and B. Iñiguez, "A Compact Explicit Model for Long-Channel Gate-All-Around Junctionless MOSFETs. Part I: DC Characteristics," IEEE Trans. Electron Devices, vol. 61, pp. 3036-3041, 2014.

[140] Sallese et. al. "Charge-Based Modeling of Junctionless Double-Gate Field-Effect Transistors," IEEE TED, vol.58, pp. 2628, 2011.

[141] M. Born, E. Wolf, Principles of Optics, seventh ed., Cambridge University Press, Cambridge, 1999, Section 1.6.

[142] S. Winitzki, Uniform Approximations for Transcendental Functions. Berlin, Germany: Springer-Verlag, 2003.

[143] H. Zimmermann, Integrated Silicon Optoelectronics. Springer, Second Edition, 2009.

[144] B. Van. Zeghbroeck, "Principles of Semiconductor Devices," ece.cololaro.edu/bart/book, Chapter 2, 2007.

[145] A. M. Ionescu and H. Riel, "Tunnel field-effect transistors as energy efficient electronic switches," Nature, vol.479, pp. 329-337, 2011.

[146] A. C. Seabaugh and Q. Zhang, "Low-voltage tunnel transistors for beyond CMOS logic," Proc. IEEE, vol.98, pp. 2095-2110, 2010.

[147] W. Y. Choi, B. G. Park, J. D. Lee, and T. J. K. Liu, "Tunneling field-effect transistors (TFETs) with subthreshold swing (SS) less than 60 mV/dec," IEEE Electron Device Lett., vol.28, pp. 743-745, 2007.

[148] D. B. Abdi and M. J. Kumar, "Controlling ambipolar current in tunneling FETs using overlapping gate-on-drain," J. Electron Device Soc., vol.2, pp.187-190, 2014.

[149] U. E. Avci, D. H. Morris and I. A. Young, "Tunnel field-effect transistors: Prospects and challenges," IEEE J. Electron Devices Soc., vol.3, pp.88-95, 2015.

[150] D. Esseni, M. Guglielmini, B. Kapidani, T. Rollo, and M. Alioto, "Tunnel FETs for ultralow voltage digital VLSI circuits: Part I Device-circuit interaction and evaluation at device level," IEEE Trans. Very Large Scale Integr. (VLSI) Syst., vol.22, pp. 2488-2498, 2014.

[151] U. E. Avci and I. A. Young, "Heterojunction TFET scaling and resonant-TFET for steep subthreshold slope at sub-9 nm gate-length," in IEDM Tech. Dig., Dec. 2013.

[152] K. Boucart and A. M. Ionescu, "Double-gate tunnel FET with High-κ gate dielectric," IEEE Trans. Electron Devices, vol.54, pp.1725-1733, 2007.

[153] W. Shockley and W. T. Read, "Statistics of the recombinations of holes and electrons," Phys. Rev., vol.87, pp.835, 1952.

[154] C. Lombardi, S. Manzini, A. Saporito and M. Vanzi, "A physically based mobility model for numerical simulation of nonplanar devices," IEEE Transactions on Computer-Aided Design of Integrated Circuits and Systems, vol.7, pp1164-1171, 1988.

[155] Konig, U. et al., "N- and p-type Si-SiGe hetero FETs," in: IEEE Int. Symp. on High Perf. Electron. Dev. for Microwave and Optoelectronic Appl., 2000, Glasgow, UK, UK.

[156] H. Ferhati and F. Djeffal, "Planar junctionless phototransistor: A potential high-performance and low-cost device for optical-communications," Optics & Laser Technology, vol.97, pp.29-35, 2017.

[157] International Energy Agency. Technology roadmap: Solar photovoltaic energy. Technical report, International Energy Agency, 2010.

[158] K. Kacha, F. Djeffal, H. Ferhati, D. Arar and M. Meguellati, "Numerical investigation of a double-junction a:SiGe thin-film solar cell including the multi-trench region," Journal of Semiconductors, vol.36, pp 1-5, 2015.

[159] F. Srairi, F. Djeffal and H. Ferhati," Efficiency increase of hybrid organic/inorganic solar cells with optimized interface grating morphology for improved light trapping," Optik, vol. 130, pp. 1092-1098, 2017.

[160] M. D. Kelzenberg, S. W. Boettcher, J. A. Petykiewicz, D. B. Turner-Evans, M. C. Putnam, E. L. Warren, J. M. Spurgeon, R. M. Briggs, N. S. Lewis, and H. A. Atwater, "Enhanced absorption and carrier collection in Si wire arrays for photovoltaic applications," Nature Materials, vol.9, pp.239-244, 2010.

[161] P. Reinhard et al., "Cu(In,Ga)Se2 thin-film solar cells and modules A boost in efficiency due to potassium," IEEE J. Photovoltaics, vol. 5, pp. 656–663, 2015.

[162] B. Vermang, V. Fjallstrom, X. Gao, and M. Edoff, "Improved rear surface passivation of Cu(In,Ga)Se_2 solar cells: A combination of an Al_2O_3 rear surface passivation layer and nanosized local rear point contacts," IEEE J. Photovoltaics, vol. 4, pp. 486-492, 2014.

[163] M. Suryawanshi, G. Agawane, S. Bhosale, S. Shin, P. Patil, L. Kim, A. Moholkar, "CZTS Based Thin Film Solar Cells," A Status Review. Materials Technology, vol.28, pp. 98-109, 2013.

[164] K. Sun, C. Yan, F. Liu, J. Huang, F. Zhou, J. A. Stride, M. Green, X. Hao, "Over 9% Efficient Kesterite Cu2znsns4 Solar Cell Fabricated by Using $Zn_{1-X}Cd_xS$ Buffer Layer," Advanced Energy Materials, vol.6, pp. 1600046, 2016.

[165] A. Chirila, et al., "Highly efficient Cu(In,Ga)Se_2 solar cells grown on flexible polymer films,". Nat. Mater., vol.10, pp.857–861, 2011.

[166] W. Wang, M. T. Winkler, O. Gunawan, T. Gokmen, T. K. Todorov, Y. Zhu, D. B. Mitzi, Device "Beyond 11% Efficient Sulfide Kesterite $Cu2Zn_xCd_{1-x}SnS_4$ Solar Cell: Effects of Cadmium Alloying," ACS Energy Lett., vol.2, pp.930-936, 2017.

[167] B. Vermang, Y. Ren, O. D. Gargand, C. Frisk, J. Joel, P. Salome, J. Borme, S. Sadewasser, C . P. Bjorkman, and Marika Edoff, "Rear Surface Optimization of CZTS Solar Cells by Use of a Passivation Layer With Nanosized Point Openings," IEEE Journal of Photovoltaic, vol. 6, pp.332-336, 2015.

[168] C. Yan, F. Liu a, K. Sun, N. Song, J. A. Stride, F. Zhou, X. Hao, M. Green," Boosting the efficiency of pure sulfide CZTS solar cells using the In/Cd-based hybrid buffers," Solar Energy Materials & Solar Cells, vol.144, pp.700-706, 2016.

[169] A. Crovetto, C. Yan, B. Iandolo, F. Zhou, J. Stride, J. Schou, X. Hao, and O. Hansen," Lattice-matched Cu_2ZnSnS_4/CeO_2 solar cell with open circuit voltage boost ," Appl. Phys. Lett., vol.109, pp. 233904, 2016.

[170] Chen, S.et al, "Compositional dependence of structural and electronic properties of Cu2ZnSn(S,Se)4 alloys for thin film solar cells," Phys. Rev. B, vol.83, pp. 125201, 2011.

[171] J. Tauc, A. Menth, "States in the gap," J. Non-Cryst. Solids, vol.8-10, pp.569-585, 1972.

[172] M. Courel, J. Arvizu and O. Galán, "The role of buffer/kesterite interface recombination and minority carrier lifetime on kesterite thin film solar cells," Mater. Res. Express, vol.3, pp. 095501, 2016.

[173] M. Murata, D. Hironiwa, N. Ashida, J. Chantana, K. Aoyagi, N. Kataoka, T. Minemoto, "Optimum band gap profile analysis of Cu(In,Ga)Se_2 solar cells with various defect densities by SCAPS," Jpn. J. Appl. Phys., vo.53, pp.4-14, 2014.

[174] A. Morales-Acevedo, "Analytical model for the photocurrent of solar cells based on graded band-gap CdZnTe thin films," Sol. Energy Mater. Sol. Cells, vol.95, pp.2837-2841, 2011.

[175] A. Morales-Acevedo, "Variable band-gap semiconductors as the basis of new solar cells," Solar Energy, vol.83, pp. 1466-1471, 2009.

[176] M. Krichen, A. B. Arab, "Analytical study of a-Si:H/c-Si thin heterojunction solar cells with back surface field," J. Comput. Electron., vol. 15, pp. 269-276, 2016.

[177] A. Benmir, M. S. Aida, "Analytical modeling and simulation of CIGS solar cells, Energy Procedia," vol. 36, pp. 618-627, 2013.

[178] A. H. Reshak, et al. "Structural, Electronic and Optical Properties in Earth-Abundant Photovoltaic Absorber of Cu_2ZnSnS_4 and $Cu_2ZnSnSe_4$ from DFT calculations," Int. J. Electrochem. Sci., vol. 9, pp.55-974, 2014.

[179] Z. Su, C. Yan, D. Tang, K. Sun, Z. Han, F. Liu, Y. Lai, J. Lia, Y. Liu, "Fabrication of Cu_2ZnSnS_4 nanowires and nanotubes based on AAO templates, " Cryst. Eng. Comm., vol.14, pp.782-785, 2012.

[180] P. Zhang, L. Gao, X. Song, J. Sun, "Micro and nanostructures of photoelectrodes for solar-driven water splitting, " Adv. Mater., vol.27, pp.562-568, 2015.

[181] O. A. M. Abdelraouf, N. K. Allam, "Nanostructuring for enhanced absorption and carrier collection in CZTS-based solar cells: Coupled optical and electrical modeling," Optical Materials, vol.54, pp.84-88, 2016.

[182] W. D. Park, "Optical constants and dispersion parameters of CdS thin film prepared by chemical bath deposition", Trans. Electr. Electron. Mater., vol.13, pp.196-200, 2012.

[183] S. Levcenko, G. Gurieva, M. Guc, A. Nateprov, "Optical constants of Cu_2ZnSnS_4 bulk crystals", Journal of Applied Physics, vol.108, pp.093502-093502-5, 2010.

[184] H. Guoa, C. Maa, K. Zhanga, X. Jiaa, X. Wanga, N. Yuana, J. Dinga, "Dual function of ultrathin Ti intermediate layers in CZTS solar cells: Sulfur blocking and charge enhancement", Solar Energy Materials and Solar Cells, vol.175, pp. 20-28, 2018.

[185] S. Hamwi, J. Meyer, M. Kroger, T. Winkler, M. Witte, T. Riedl, A. Kahn, W. Kowalsky, "The role of transition metal oxides in charge-generation layers for stacked organic light–emitting diodes, " Adv. Funct. Mater., vol.20, pp.1762-1766, 2010.

[186] W. Wu, J. Bao, X. Jia, Z. Liu, L. Cai, B. Liu, J. Song, H. Shen, "Dopant-free back contact silicon heterojunction solar cells employing transition metal oxide emitters," Phys. Status Solidi, vol.10, pp. 662-667, 2016.

[187] J. Geissbuhler, J. Werner, S.M. de Nicolas, L. Barraud, A.H. Wyser, M. Despeisse, S. Nicolay, A. Tomasi, B. Niesen, S. De Wolf, C. Ballif, "22.5% efficient silicon heterojunction solar cell with molybdenum oxide hole collector," Appl. Phys. Lett., vol.107, pp.081601, 2015.

[188] J. Meyer, S. Hamwi, M. Kreoger, W. Kowalsky, T. Riedl, A. Kahn, "Transition metal oxides for organic electronics: energetics, device physics and applications," Adv. Mater., vol. 24, pp. 5408-5427, 2012.

[189] A. H. Ali, Z. Hassan, A. Shuhaimi, "Enhancement of optical transmittance and electrical resistivity of post-annealed ITO thin films RF sputtered on Si," Applied Surface Science, vol. 443, pp. 544-547, 2018.

[190] B. Kınacı, S. S. Cetin, A. Bengi and S. ozcelik, "The temperature dependent analysis of Au/TiO_2 (rutile)/n-Si (MIS) SBDs using current–voltage–temperature (I–V–T) characteristics," Mater. Sci. Semicond. Process., vol.15, pp.531-535, 2012.

[191] A. D. Bartolomeo, "Graphene Schottky diodes: An experimental review of the rectifying graphene/semiconductor heterojunction," Physics Reports-Review Section of Physics Letters, vol. 606, pp.1-58, 2016.

[192] S. Shivaraman, L. H. Herman, F. Rana, J. Park, and M. G. Spencer, "Schottky barrier inhomogeneities at the interface of few layer epitaxial graphene and silicon carbide," Applied Physics Letters, vol.100, p.183112, 2012.

[193] M. Zhu, X. Li, Y. Guo, X. Li, P. Sun, X. Zang, K. Wang, M. Zhong ,D. Wud, and H. Zhu, "Vertical junction photodetectors based on reduced graphene oxide/silicon Schottky diodes, " Nanoscale, vol.6, pp.4909-4914, 2014.

[194] T. Tunc, S. Altindal, I. Uslu, I. Deokme and H. Uslu, "Temperature dependent current–voltage (I–V) characteristics of Au/n-Si (111) Schottky barrier diodes with PVA(Ni,Zn-doped) interfacial layer," Mater. Sci. Semicond. Process., vol.14, pp.139-145, 2011.

[195] I. Tasçıoglu, U. Aydemir, S. Altındal, "The explanation of barrier height inhomogeneities in Au/n-Si Schottky barrier diodes with organic thin interfacial layer," J. Appl. Phys., vol.108, pp.064506, 2010.

[196] J. Chen and J. Q. Lv "Wang, Electronic properties of Al/MoO3/p–InP enhanced Schottky barrier contacts," Thin Solid Films, vol.616, pp.145-150, 2016.

[197] O. F. Yuksel, M. Kus, N. Simsir, H. Safak, M. Sahin, E. Yenel, "A detailed analysis of current–voltage characteristics of Au/perylene-monoimide/n-Si Schottky barrier diodes over a wide temperature range," J. Appl. Phys., vol.110, pp.024507, 2011.

[198] P. P. Thapaswini, R. Padma, N. Balaram, B. Bindu, V. R. Reddy, "Modification of electrical properties of Au/n-type InP Schottky diode with a high-k Ba0.6Sr0.4TiO3 interlayer," Superlattices and Microstructures, vol. 93, pp. 82-91, 2016.

[199] V. Stranak, R. Bogdanowicz, P. Sezemsky, H. Wulff, A. Kruth, M. Smietana, J. Kratochvil, M. Cada, Z. Hubicka, "Towards high quality ITO coatings: The impact of nitrogen admixture in HiPIMS discharges," Surface and Coatings Technology, vol.335, pp.126-133, 2018.

[200] D. A. Álvarez, L. F. Llin, A. Mellor, D. J. Paul, N. J. Ekins-Daukes, "ITO and AZO films for low emissivity coatings in hybrid photovoltaic-thermal applications," Solar Energy, vol.155, pp.82-92, 2017.

[201] C. Manasterski, "La pulvérisation cathodique industrielle," PPUR polytechnics, 2005.

[202] F. Lapostolle, "Caractérisation de revêtements TiOx ($0 \leq x \leq 2$) élaborés sur métal ou sur verre par pulvérisation cathodique magnétron en condition réactive," Doctorat thesis, national institute of polytechnic of Lorraine, France, 2001.

[203] T. T. Mnatsakanov, M. E. Levinshtein, A. G. Tandoev, S. N. Yurkov and J. W. Palmour, "Minority carrier injection and current–voltage characteristics of Schottky diodes at high injection level," Solid-State Electronics, vol. 121, pp 41-46, 2016.

[204] A.H. Kacha, B. Akkal, Z. Benamara, M. Amrani, A. Rabhi, G. Monier, C. Robert-Goumet, L. Bideux and B. Gruzza, "Effects of the GaN layers and the annealing on the electrical properties in the Schottky diodes based on nitrated GaAs," Superlattices and Microstructures, vol.83, pp.827-833, 2015.

[205] S. Averine, Y. C. Chan, and Y. L. Lam, "Evaluation of Schottky contact parameters in metal–semiconductor–metal photodiode structures," Applied Physics Letters, vol.77, pp.274-276, 2000.